

**Combining Photocatalytic Water Treatment and Fuel  
Synthesis: Improving the Activity of TiO<sub>2</sub> by Cobalt -  
Doping and Ag/Ag<sub>2</sub>O - Deposition**

Von der Naturwissenschaftlichen Fakultät der  
Gottfried Wilhelm Leibniz Universität Hannover

zur Erlangung des Grades

**Doktorin der Naturwissenschaften (Dr. rer. nat.)**

genehmigte Dissertation

von

**Soukaina Boughaled El Lakhmissi, Master (Marokko)**

**2021**

Referent: Apl. Prof. Dr. rer. nat. habil. Detlef W. Bahnemann

Korreferentin: Prof. Dr. rer. nat. Nadja-Carola Bigall

Tag der Promotion: 18.08.2021

*Dedicated to My Family*





## Acknowledgments

First of all, I would like to express my deepest gratitude to my supervisor **Prof. Dr. Detlef Bahnemann** for accepting me as a Ph.D. student in his group. I also want to thank him for his continuous and strong support during my Ph.D. study, for his excellent academic guidance, and his inspiring scientific discussions throughout my work. Thank you for being such a great scientific mentor.

I would like to thank **Dr. Ralf Dillert**, who greatly enriched my knowledge with the many fruitful discussions and excellent ideas regarding my Ph.D. project. I am grateful to him for his critical reading of my research manuscripts, presentations, and my thesis.

I am also grateful to **Prof. Dr. Nadja-Carola Bigall** for kindly agreeing to be a co-referee of my thesis.

I am thankful to **Prof. Dr. Thomas Scheper** for giving me the opportunity to do my doctorate study at the institute of technical chemistry and for kindly accepting to become the head of my examination committee.

I would also like to thank all members of the Institute of Technical Chemistry, specifically the members of the Bahnemann research group (AK Bahnemann) for all the scientific discussions in our weekly seminars, the supportive atmosphere, and the fun time in the office. Special thanks go to my colleagues Dr. Wegdan Ramadan, Dr. Arsou Arimi, Dr. Lena Megatif, Dr. Hamza Belhadj, and Dr. Yamen AlSalka for their great help during my first months here in the Institute of Technical Chemistry.

I wish also to express my warmest gratitude to my close friends Dr. Narmina Balayeva and Dr. Samia Ben Hamouda who have been sisters for me here in Germany for encouraging me and making my Ph.D. life more pleasurable.

Last but by no means the least:

I would like to thank my parents, my father Ahmed Akel, and my mother Mahjouba Maagoul for their unconditional love, prayers, and for instilling in me the confidence that I am capable of doing anything I put in my mind to. To my sweet sister Aya, and brother Youssef I could just say that I love you as you are. My thanks also go to Eva-Maria Wanke who has always been like a member of my family.

I am the most grateful to my loving husband Dr. Redouan Boughaled who overflows me with affection and inspiration day by day. Thank you for your everlasting encouragement, moral support in all good and hard times, and patience during these years. Without your love, support and motivation, I would have never been able to achieve this Ph.D. degree.

## Zusammenfassung

Wasseraufbereitung und die Synthese von Brennstoffen unter Einsatz regenerativer Energiequellen werden heutzutage als zwei Hauptanliegen für ein nachhaltiges Lebensumfeld angesehen. Angesichts der wachsenden Nachfrage nach fortschrittlichen Techniken der Umweltsanierung für verschmutztes Wasser und steigenden Kosten für fossile Brennstoffe hat die Photokatalyse, in den letzten Jahren zunehmende Aufmerksamkeit erhalten. In der vorliegenden Arbeit werden modifizierte  $\text{TiO}_2$ -Photokatalysatoren für beide photokatalytischen Prozesse verwendet.

Anfänglich wird  $\text{TiO}_2$  (P25) mit unterschiedlichen Massenverhältnissen von selbst hergestelltem  $\text{Ag}/\text{Ag}_2\text{O}$  unter Verwendung von zwei Synthesemethoden modifiziert. Nach der Charakterisierung der sieben hergestellten Materialien, einschließlich  $\text{Ag}/\text{Ag}_2\text{O}$ ,  $\text{Ag}/\text{Ag}_2\text{O} // \text{TiO}_2$  Mischungen (TM) und  $\text{Ag} / \text{Ag}_2\text{O} // \text{TiO}_2$  Verbundwerkstoffen (TC), wird die photokatalytische Aktivität durch Bleichen von Methylenblau (MB) unter Bestrahlung mit UV-vis und sichtbarem Licht bewertet. Die Ergebnisse zeigen, dass das lichtinduzierte Bleichen von MB in Anwesenheit von TM und TC verbessert wird. Interessanterweise zeigt  $\text{Ag}/\text{Ag}_2\text{O}$  die beste photokatalytische Aktivität. Es wurde jedoch festgestellt, dass das Photobleichen von MB eher durch einen Grenzflächenelektronentransfer von dem photoangeregten MB, das an der Oberfläche von  $\text{Ag}_2\text{O}$  adsorbiert ist, zu seinem Leitungsband initiiert wird. Darüber hinaus bekräftigen XRD und XPS Daten, dass  $\text{Ag}_2\text{O}$  als Elektronenakzeptor bei der lichtinduzierten Reaktion von MB wirkt und  $\text{Ag}^+$  zu  $\text{Ag}(0)$  reduziert wird. Andererseits wird auch die photokatalytische  $\text{H}_2$  Erzeugung aus der Methanolreformierung unter Sonnenlicht, unter Verwendung dieser Photokatalysatoren untersucht. Die Ergebnisse zeigen, dass  $\text{Ag}/\text{Ag}_2\text{O}$  kein Elektron auf  $\text{H}^+$  übertragen kann, was auch durch die Messungen der Flachbandpotentiale bestätigt wird. Mit zunehmendem Massenanteil von  $\text{TiO}_2$  in den TC und TM wird jedoch beobachtet, dass die entwickelten Mengen an  $\text{H}_2$  zunehmen.  $\text{Ag} / \text{Ag}_2\text{O}$  ist damit kein (photo)stabiles Material soweit dass die Photoreduktion von  $\text{Ag}^+$  zu  $\text{Ag}$  führt.

Anschließend wird der photokatalytische Abbau von Oxytetracyclhydrochlorid (OTC HCl) in Gegenwart von mit Kobalt dotierten  $\text{TiO}_2$  ( $\text{Co-TiO}_2$ ) untersucht.  $\text{Co-TiO}_2$  wurden durch zwei Solvothermalverfahren synthetisiert, nämlich Rückflusssynthese ( $\text{Co-TiO}_2\text{-R}$ ) und hydrothermale Synthese ( $\text{Co-TiO}_2\text{-HT}$ ). Die Charakterisierung mittels XRD und Raman-Spektroskopie zeigt, dass  $\text{Ti}^{4+}$  in der  $\text{TiO}_2$  Kristallstruktur durch  $\text{Co}^{2+}$  substituiert wurde. Die beobachteten Reaktionsgeschwindigkeiten des lichtinduzierten Abbaus von OTC HCl über beide  $\text{Co-TiO}_2$  bei UV-vis-Licht sind höher als die von reinen  $\text{TiO}_2$  und dem kommerziellen P25. Die Photolyse von OTC HCl kann jedoch am Gesamtmechanismus teilnehmen.

Außerdem wird unter Verwendung der  $\text{Co-TiO}_2\text{-R}$  und  $\text{Co-TiO}_2\text{-HT}$  die photokatalytische  $\text{H}_2$  Bildung aus wässrigem Methanol unter Sonneneinstrahlung untersucht. Die Ergebnisse zeigen, dass die Kobaltdotierung keinen zusätzlichen Vorteil bei der photokatalytischen Aktivität hat. EPR Untersuchungen bestätigen die Rekombination photoerzeugter Ladungsträger. Um die schnelle Rekombination zwischen photoerzeugten Ladungsträgern zu unterdrücken, wird die Oberfläche von  $\text{Co-TiO}_2$  mit Pt modifiziert. Höhere Bildungsraten von  $\text{H}_2$  werden beobachtet. Dies scheint Pt die Abnahme der photokatalytischen Aktivität aufgrund der Co-Dotierung auszugleichen.

**Schlüsselwörter:** Photokatalyse, Titandioxid, Silber (I) -oxid,  $\text{Co-TiO}_2$ , Pt-beladenes Kobaltdotiertes Titandioxid, Methylenblau, Oxytetracyclhydrochlorid, UV-vis Licht, Wasseraufbereitung,  $\text{H}_2$ -Produktion.

## Abstract

Water treatment and solar fuel synthesis are nowadays considered to be the two major concerns for achieving a sustainable living environment. With the growing demand for advanced environmental remediation of polluted water and as the cost of fossil fuels increases, photocatalysis has received increasing attention in recent years. In the present work, modified  $\text{TiO}_2$  photocatalysts are used for both photocatalytic processes.

Initially,  $\text{TiO}_2$  (P25) is modified with different mass ratios of self-prepared  $\text{Ag}/\text{Ag}_2\text{O}$  employing two synthetic methods, namely, a mechanical mixture and a precipitation method. After the characterization, the photocatalytic activity of the seven prepared materials including  $\text{Ag}/\text{Ag}_2\text{O}$ ,  $\text{Ag}/\text{Ag}_2\text{O} // \text{TiO}_2$  mixtures (TM), and  $\text{Ag}/\text{Ag}_2\text{O} // \text{TiO}_2$  composites (TC) is evaluated by methylene blue (MB) bleaching under UV-vis and only visible light illumination. The results reveal that the light-induced bleaching of aqueous MB in the presence of TM and TC under both UV-vis and visible illumination is enhanced. Interestingly,  $\text{Ag}/\text{Ag}_2\text{O}$  shows the best photocatalytic activity under both illumination conditions. However, the observed photobleaching of MB is found to be rather initiated by an interfacial electron transfer from the photo-excited MB adsorbed at the surface of  $\text{Ag}_2\text{O}$  to the latter's conduction band. Moreover, XRD and XPS data confirm that  $\text{Ag}_2\text{O}$  performs as an electron acceptor in the light-induced reaction of MB, and  $\text{Ag}^+$  is reduced to  $\text{Ag}(0)$ . On the other hand, photocatalytic  $\text{H}_2$  generation from methanol reforming under solar light using all-synthesized photocatalysts is also studied. The experimental results indicate that bare  $\text{Ag}/\text{Ag}_2\text{O}$  is not able to transfer an electron to  $\text{H}^+$ , which is also confirmed by the flatband potentials measurements. Nevertheless, with increasing the mass fraction of  $\text{TiO}_2$  in the TC and TM, the evolved amounts of  $\text{H}_2$  are observed to increase implying that the fraction of photons absorbed by  $\text{Ag}_2\text{O}$  being inactive decreases. Hence, it is concluded that  $\text{Ag}/\text{Ag}_2\text{O}$  is not a (photo)stable material since the photoreduction of  $\text{Ag}^+$  is experimentally confirmed to proceed yielding Ag.

Afterward, the photocatalytic degradation of oxytetracycline hydrochloride (OTC HCl) is investigated in the presence of cobalt-doped  $\text{TiO}_2$  ( $\text{Co-TiO}_2$ ) photocatalysts.  $\text{Co-TiO}_2$  were synthesized by two different solvothermal methods, namely, reflux ( $\text{Co-TiO}_2$ -R) and hydrothermal ( $\text{Co-TiO}_2$ -HT) synthesis. The characterization of  $\text{Co-TiO}_2$ -R and  $\text{Co-TiO}_2$ -HT samples by means of XRD and Raman spectroscopy reveals that  $\text{Ti}^{4+}$  was substituted by  $\text{Co}^{2+}$  in the  $\text{TiO}_2$  crystal structure. The observed initial reaction rates of the light-induced degradation of OTC HCl over both Co-doped  $\text{TiO}_2$  upon UV-vis light are found to be higher than those of pure  $\text{TiO}_2$ , and the commercial P25. However, the photolysis of OTC HCl still can take part in the overall mechanism.

Besides, the photocatalytic  $\text{H}_2$  formation from aqueous methanol employing the  $\text{Co-TiO}_2$ -R and  $\text{Co-TiO}_2$ -HT under solar irradiation is studied. The experimental results evince that cobalt doping has no additional advantage regarding the photocatalytic activity since the evolved amounts of  $\text{H}_2$  are close to the detection limit. Mechanistic investigation using EPR confirms the recombination of photo-generated charge carriers. In order to suppress the fast charge carriers recombination, the surface of  $\text{Co-TiO}_2$  is modified with Pt. Higher formation rates of  $\text{H}_2$  are observed due to the improved electrons and holes separation. Therefore, Pt seems to compensate the decrease of the photocatalytic activity due to Co-doping.

**Keywords:** photocatalysis, titanium dioxide, silver (I) oxide,  $\text{Co-TiO}_2$ , Pt-loaded cobalt-doped titania, methylene blue, oxytetracycline hydrochloride, UV-vis light, water treatment,  $\text{H}_2$  evolution.

## Table of Content

Acknowledgments .....	III
Zusammenfassung .....	V
Abstract.....	VI
Table of Content .....	VII
Chapter 1. Background.....	1
1.1. Introduction.....	1
1.2. Water Treatment.....	2
1.2.1. Conventional Water Treatment.....	2
1.2.2. Heterogeneous Photocatalysis as an AOP.....	4
1.3. Combining Water Treatment and Fuel Production.....	5
1.4. Titanium Dioxide as a Photocatalyst.....	8
1.5. Improving the Activity of TiO <sub>2</sub> .....	11
1.5.1. Co-catalyst Deposition on TiO <sub>2</sub> .....	11
1.5.2. Coupling TiO <sub>2</sub> with Other Semiconductor Photocatalysts.....	14
1.5.3. Doping of TiO <sub>2</sub> .....	16
1.6. Aim of the Thesis.....	19
1.6.1. Thesis Objectives .....	19
1.6.2. Thesis Overview .....	21
1.7. References.....	24
Chapter 2. Ag/Ag <sub>2</sub> O as a Co-Catalyst in TiO <sub>2</sub> Photocatalysis: Effect of the Co-Catalyst/Photocatalyst Mass Ratio.....	38
2.1. Foreword .....	38
2.2. Abstract.....	39
2.3. Introduction.....	40
2.4. Results.....	43
2.4.1. Characterization of the Prepared Materials.....	43
2.4.2. Photocatalytic performance of the Materials.....	48
2.5. Discussion.....	51
2.5.1. The Photocatalytic Activity of Ag/Ag <sub>2</sub> O.....	51
2.5.2. The Photocatalytic Activity of Physical Ag/Ag <sub>2</sub> O// TiO <sub>2</sub> Mixtures.....	54
2.5.2.1. Bleaching of Methylene Blue .....	54

2.5.2.2. Light-Induced Hydrogen Evolution.....	57
2.5.3. The Photocatalytic Activity of Ag/Ag <sub>2</sub> O// TiO <sub>2</sub> Composites.....	58
2.5.3.1. Bleaching of Methylene Blue .....	58
2.5.3.2. Light-Induced Hydrogen Evolution.....	59
2.6. Experimental Section .....	61
2.6.1. Materials .....	61
2.6.2. Synthetic Methods.....	62
2.6.2.1. Preparation of Ag/Ag <sub>2</sub> O .....	62
2.6.2.2. Preparation of TM Mixtures .....	62
2.6.2.3. Preparation of TC Composites .....	62
2.6.3. Characterization of the Materials.....	63
2.6.4. Photocatalytic Measurements.....	64
2.6.4.1. Methylene Blue Degradation.....	64
2.6.4.2. Photocatalytic Hydrogen Formation.....	64
2.7. Conclusions .....	65
2.8. Supplementary Materials.....	66
2.9. Acknowledgments .....	74
2.10. References.....	74
Chapter 3. UV-vis Light Induced Degradation of Oxytetracycline Hydrochloride Mediated by Co-TiO <sub>2</sub> Nanoparticles .....	80
3.1. Foreword .....	80
3.2. Abstract.....	81
3.3. Introduction.....	82
3.4. Results .....	86
3.4.1. Photocatalysts Characterizations .....	86
3.4.2. Photocatalytic Activities of Co-TiO <sub>2</sub> -R and Co-TiO <sub>2</sub> -HT on UV-vis Light-Induced OTC HCl Degradation .....	91
3.5. Discussion.....	92
3.5.1. Characterization of Co-TiO <sub>2</sub> -R, and Co-TiO <sub>2</sub> -HT Composites.....	92
3.5.2. UV-vis Light-Induced Oxytetracycline Hydrochloride Degradation over Co-TiO <sub>2</sub> Composites .....	96
3.5.3. Proposed Mechanisms of UV-vis Light-Induced OTC HCl Degradation using Co-TiO <sub>2</sub> Catalysts.....	98

3.6. Materials and Methods.....	100
3.6.1. Materials Composites .....	100
3.6.2. Photocatalysts Synthesis.....	101
3.6.2.1. High-Temperature Synthesis of Cobalt-Doped TiO <sub>2</sub> .....	101
3.6.2.2. Reflux Synthesis of Cobalt-Doped TiO <sub>2</sub> .....	101
3.6.2.3. Photocatalysts Characterization.....	101
3.6.3. UV-vis Light-Induced Oxytetracycline Hydrochloride (OTC HCl) Degradation.....	102
3.7. Conclusions .....	104
3.8. Acknowledgments .....	104
3.9. References.....	104
Chapter 4. Photocatalytic Hydrogen Evolution over Pt/Co-TiO <sub>2</sub> Photocatalysts.....	114
4.1. Foreword .....	114
4.2. Abstract.....	115
4.3. Introduction.....	116
4.4. Experimental Section .....	120
4.4.1. Chemicals.....	120
4.4.2. Materials Preparation .....	120
4.4.2.1. Hydrothermal Synthesis (HT) .....	120
4.4.2.2. Reflux Synthesis (R) .....	121
4.4.2.3. Photoplatinization.....	121
4.4.3. Characterization of the Prepared Materials.....	122
4.4.4. Electrochemical Study .....	123
4.4.5. H <sub>2</sub> Evolution by Photocatalytic Reforming of CH <sub>3</sub> OH .....	123
4.5. Results and Discussion .....	124
4.5.1. Photocatalyst Characterization.....	124
4.5.2. XPS Analysis of Co-TiO <sub>2</sub> and TiO <sub>2</sub> Photocatalysts .....	128
4.5.3. EPR Analysis of Co-TiO <sub>2</sub> and TiO <sub>2</sub> Photocatalysts.....	130
4.5.4. Flatband Measurement of Co-TiO <sub>2</sub> and TiO <sub>2</sub> Photocatalysts.....	133
4.5.5. Photocatalytic Hydrogen Generation of Pt/(Co-TiO <sub>2</sub> ) and Pt/TiO <sub>2</sub> Composites.....	135
4.5.6. Mechanism of Photocatalytic Hydrogen Evolution from Water/ Methanol using Pt/(Co-TiO <sub>2</sub> ) and Pt/TiO <sub>2</sub> Catalysts .....	139

4.6. Conclusions .....	141
4.7. Supplementary Material.....	142
4.8. Acknowledgments .....	145
4.9. References.....	145
Chapter 5. Summarizing Discussion and Conclusions.....	153
5.1. Synthesis and Characterization of Photocatalysts.....	153
5.1.1. Ag/Ag <sub>2</sub> O// TiO <sub>2</sub> .....	153
5.1.2. Co-doped TiO <sub>2</sub> .....	157
5.1.3. Pt/Co-doped TiO <sub>2</sub> .....	160
5.2. Photocatalytic Oxidation of Organic Compounds .....	162
5.2.1. Methylene Blue Bleaching in the Presence of Ag/Ag <sub>2</sub> O// TiO <sub>2</sub> .....	162
5.2.2. Oxytetracycline Hydrochloride Oxidation in the presence of Co-doped TiO <sub>2</sub> .....	173
5.3. Photocatalytic Reforming of Methanol Yielding H <sub>2</sub> .....	180
5.3.1. H <sub>2</sub> Evolution in the Presence of Ag/Ag <sub>2</sub> O, Ag/Ag <sub>2</sub> O // TiO <sub>2</sub> Mixtures, and Ag/Ag <sub>2</sub> O// TiO <sub>2</sub> Composites .....	180
5.3.2. H <sub>2</sub> Evolution in the Presence of Co-TiO <sub>2</sub> .....	183
5.3.3. H <sub>2</sub> Evolution in the Presence of Pt loaded Co-TiO <sub>2</sub> .....	186
5.4. Conclusions .....	190
5.5. References.....	192
Publications .....	208
Curriculum Vitae.....	210



## Chapter 1. Background

### 1.1. Introduction

Water treatment and energy production are of great importance nowadays, due to the increasing demands for clean water and the extensive consumption of fossil fuels. In 2018, the worldwide energy demand grew by 2.3% which is almost twice the average rate of growth since 2010. Demand for all fuels soared, and fossil fuels represent almost 70% of the growth for the second year in a row. Consequently, carbon dioxide (CO<sub>2</sub>) emissions rose by 1.7% and reached a new record [1]. In addition to the increased energy demand, the world's water need according to the United Nations Educational, Scientific and Cultural Organization (UNESCO) is also expected to be growing by about 1% per year until 2050 to reach 20 to 30% above the current level of water use. Also, and as reported in the United Nation World Water Development Report (WWDR) 2019, more than 2 billion people are living in countries of severe water stress. Furthermore, about 4 billion people are experiencing a scarcity to access to water at least one month a year. For instance, in sub-Saharan Africa, six out of ten people lack access to a safe source of water and suffer from water contamination and inadequate sanitation [2]. Moreover, the bacteriological quality of drinking water is not imperiled just in urban or industrial areas, but also in developing countries. Significant contaminations by bacteria have been reported [3]. As an example, the recent epidemic outbreak of novel coronavirus pneumonia (COVID-19) caused by SARS-CoV-2 infection which was found to remain infectious in water and sewage for days to weeks [4, 5]. Conventional water treatment processes ought to inactivate the COVID-19 virus [6, 7]. However, the viral ribonucleic acid (RNA) may still be found in the treated wastewater [8].

Given these findings, approaches to the sustainable development of water resources are critical for assuring water quality and safety, and the treatment of wastewater is of worldwide concern since fresh water is indispensable for the existence of all living organisms on earth. On the other hand, the development of innovative and efficient processes to convert energy from a renewable resource is of huge importance.

Among various energy resources, hydrogen is of particular interest owing to its capacity to convert chemical energy into electrical energy using fuel cells.

## **1.2. Water Treatment**

### **1.2.1. Conventional Water Treatment**

Water is an absolute necessity for the survival of all forms of life on our planet. For humans, access to clean water is of major importance for maintaining acceptable living conditions, since clean and safe water is crucial for drinking, sanitation, hygiene services, along with other activities such as energy production and manufacturing processes, etc. Therefore, one of the biggest challenges nowadays is to provide access to affordable, clean, and safe water sources [2]. Due to the population growth together with socio-economic development, the demand for fresh water is increasing. However, water quality is affected by the discharge of large volumes of wastewater containing harmful and persistent pollutants which pose a threat to human health even at low concentrations [9].

Conventional wastewater treatment processes can be divided into mechanical, physico-chemical treatment, biological treatment, and advanced oxidation processes (AOP).

#### **a) Mechanical Treatment**

Screening is the preliminary unit operation used in wastewater treatment. Through the screening, items such as rags, paper, plastics, coarse solids, grit, and metals are removed to protect the downstream equipment, piping, and appurtenances [10]. Particles with a diameter greater than one millimeter, such as gravel and sand, are removed through the sedimentation process. Membrane filtration can also be used as a technique to remove pollutants of different origins with reduced cost and consumption of energy [11].

### **b) Physico-chemical Treatment**

Physico-chemical treatment methods usually utilized for wastewater treatment include processes such as reverse osmosis, electrodialysis, and adsorption techniques using organic and inorganic supports. Adsorption could be an economically efficient separation method in case of using inexpensive sorbents. A widely consumed adsorbent for the treatment of water and wastewater is activated carbon. However, its high cost, as well as the difficulty of its regeneration, are the two major drawbacks of using it at an industrial scale [12].

### **c) Biological Treatment**

The objective of the biological treatment is to convert the pollutants present in wastewater to bio-converted compounds which can be further mineralized. The biological process considered as the cheapest wastewater treatment method using microorganisms such as fungi, algae, bacteria, and so on, necessitates a large land area and is limited by the toxicity of the used chemicals, as well as it exhibits less flexibility in the design and performance [13]. Although biological treatment may degrade many organic compounds, non-bio-degradable molecules that have complex chemical structures and which are toxic to the aquatic environment such as pharmaceuticals, antibiotics, and pesticides are not converted.

### **d) Advanced Oxidation Processes (AOPs)**

Advanced oxidation processes are usually used to convert pollutants that are not amenable to biological treatment. Conventional processes are not very efficient for the treatment of persistent or emerging pollutants in water, since a large number of these compounds have complex structures with many aromatic cycles and, therefore, exhibit high chemical stability that inhibits their complete biological degradation. Hence, the goal of the AOPs as clean technologies is the complete mineralization of non-bio-convertible compounds to carbon dioxide and mineral acids or to transfer non-biodegradable pollutants into biodegradable [14]. Contaminants of emerging concerns (CEC), among all pollutants, come from a broad spectrum of sources such as

but not limited to pharmaceuticals, antibiotics, phthalates, disinfectants, pesticides, fragrances, etc., and their removal using conventional treatments methods is ineffective [15]. Also, several EU directives such as 85/337/EEC, 91/ 271/EEC, 76/464/EEC, 2006/118/EC, and 2010/75/EU restrict the use of conventional processes because of their effectiveness and incomplete biodegradation of the waste products. In this context, several research studies have been devoted to developing more powerful and promising processes of the so-called AOPs. These are clean techniques that involve the hydroxyl radical ( $\cdot\text{OH}$ ) generation for the treatment of contaminated waters with reaction rate constants of about  $10^9 \text{ L mol}^{-1}\text{s}^{-1}$  yielding carbon dioxide, water, and inorganic ions as final products [16]. However, AOPs are highly energy consuming, and therefore expensive.

### 1.2.2. Heterogeneous Photocatalysis as an AOP

The technology of semiconductor photocatalysis has seen growing interest by researchers all over the world and has rapidly expanded within the last four decades due to an assumed tremendous potential, particularly in the fields of water purification and simultaneous contaminant destruction. Unlike the abovementioned conventional AOPs, heterogeneous photocatalysis (as the term heterogeneous indicates) consists of two active phases in which the contaminants are present in the liquid phase and the semiconductor photocatalyst is in the solid phase.

Heterogeneous photocatalysis is based on the irradiation of a semiconductor acting as the photocatalyst using UV and/or vis-light to produce highly reactive species such as  $\cdot\text{OH}$  which can initiate the complete decomposition of toxic organic and inorganic pollutants at low levels [17, 18]. The main advantages of heterogeneous photocatalysis beyond other conventional methods are that the oxidation is powerful leading to the complete mineralization of most all-organic compounds. The process can be operated under ambient conditions along with the possibility of using sunlight as an irradiation source. The atmospheric oxygen is used as an oxidant and, therefore, the process does not require the addition of any other strong oxidant.

An ideal semiconductor photocatalyst should be easily available, inexpensive, non-toxic, chemically stable in wastewater over a high range of pH values, biologically and chemically inactive, and photostable [19]. However, the band edge positions of the semiconductor are of great importance since they control its ability to initiate photoinduced charge carrier transfer to the adsorbed species on its surface. From a thermodynamic point of view, the conduction band (CB) potential of the semiconductor has to be suitable to transfer an electron to molecular oxygen ( $O_2$ ) thus yielding the superoxide radical anion  $O_2^{\bullet-}$  ( $-0.33$  V vs. NHE), and the valence band (VB) potential of the semiconductor must be able to oxidize an adsorbed water molecule or a hydroxide ion to a hydroxyl radical ( $H_2O/\bullet OH$ ;  $2.8$  V vs. NHE, and  $OH^-/\bullet OH$ ;  $1.89$  V vs. NHE) which is capable to initiate the complete oxidation of an adsorbed organic pollutant yielding  $CO_2$  [17, 20, 21].

### 1.3. Combining Water Treatment and Fuel Production

Energy production and environmental remediation are the world's major concerns. Fossil fuels such as oil, natural gas, and coal play an important role to fulfill the worldwide energy requirements for industry, agriculture, transportation, and daily life. According to the BP Statistical Review of World Energy 2019, the energy consumption of fossil energy in 2018 was almost 36.44 billion barrels of oil, 3849 billion cubic meters of natural gas, and 3772 million tons oil equivalent. As a result, global challenges associated with rapid growth in  $CO_2$  emissions are confronted by a rise of 2.0 % recognized as the highest rate for seven years reaching 33,891 billion tons [22]. In this regard, a new form of clean, renewable, safe, cheap, and sustainable energy alternative to fossil fuels becomes mandatory. So far, diverse forms of sustainable energy such as wind, hydroelectric, geothermal, and solar energy have been exploited [23]. Solar energy as a primary energy source stands out as the solar energy radiation arriving at the earth's surface is estimated to be about 173,000 terawatts [24].

Molecular hydrogen ( $H_2$ ) as an ideal clean fuel has received much more attention in the past few decades. Nowadays,  $H_2$  is predominantly produced from fossil fuels by thermal methods such as steam methane reforming [25]. However, the

process is complicated requiring several catalytic steps. Therefore, hydrogen generation via the conversion of organic pollutants in wastewater, resulting mainly from industries, into  $H_2$  and valuable fuels with employing sunlight is a promising alternative to produce clean hydrogen using solar energy. Hence, simultaneous  $H_2$  evolution and degradation of organic contaminants are achieved in one reaction system supplying a clean environment and long-term solutions designed to meet the global energy demand.

Photocatalytic water treatment and  $H_2$  generation require photogeneration of electron/hole pairs. Nevertheless, in photocatalytic water treatment, the valence band holes ( $h_{VB}^+$ ) are the key elements that induce the decomposition of pollutants. In photocatalytic  $H_2$  generation, the conduction band electrons ( $e_{CB}^-$ ) play an important role in reducing protons to hydrogen molecules. Hence, the CB level of the semiconductor used must be more negative than the  $H_2$  production level  $E(H^+/H_2)$ . However, when molecular oxygen or other electron acceptors of suitable potential are available in the solution, the photo-generated electrons are transferred to the electron acceptors and subsequently initiate redox reactions. Thus, protons will not be reduced. These factors suggest that the conditions of photocatalytic water decontamination are not applied to photocatalytic  $H_2$  production as shown in **Figure 1.1**. The oxidation and reduction reactions are the basic mechanisms of photocatalytic water purification and photocatalytic hydrogen production, respectively.

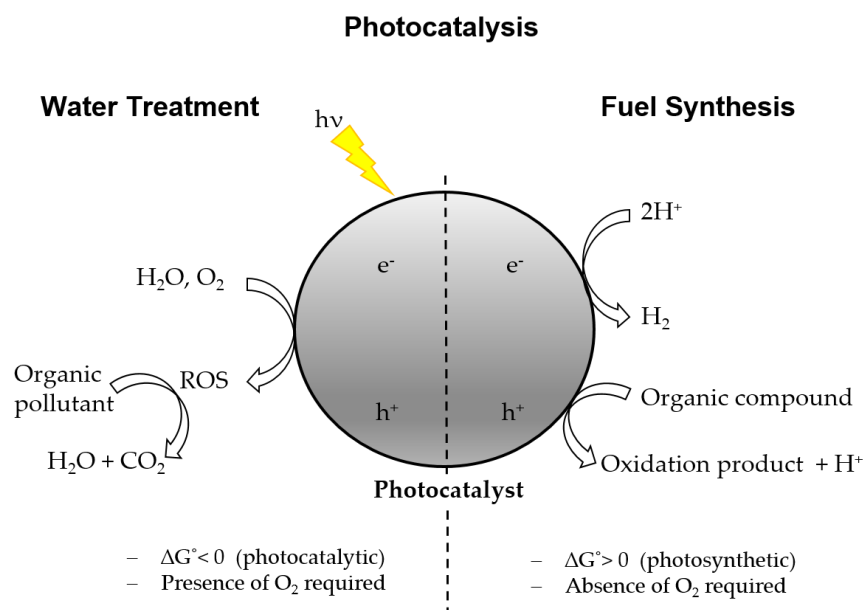


**Figure 1-1.** Schematic illustration comparing the photocatalytic reactions of water treatment and fuel synthesis.

In photocatalytic water splitting for  $H_2$  formation, the electronic structure of a semiconductor plays a key role in semiconductor photocatalysis. Upon illumination by photons with energy equal to or greater than the band gap energy of the semiconductor photocatalyst, electrons and holes are generated in the CB and VB of the semiconductor, respectively. These photo-generated charge carriers can either recombine readily in the bulk or on the semiconductor surface releasing energy in the form of heat, or they can migrate to the surface without recombination. The electrons and holes that migrate to the semiconductor surface reduce and oxidize water molecules to produce  $H_2$  and  $O_2$ , respectively. However, for the  $H_2$  production to proceed, the CB potential of the semiconductor photocatalyst have to be more negative than the potential of  $H_2$  generation ( $H^+/H_2$ ; 0.0 V vs NHE at pH 0) while the potential of the VB must be more positive than the oxidation potential of water ( $O_2/H_2O$ ; 1.23 V vs NHE at pH 0) [26]. Additionally, the backward reaction of hydrogen and oxygen recombination into water rapidly proceeds and ought to be inhibited, and the semiconductor photocatalyst itself has to be stable in the reaction, because even if the photogenerated electrons and holes have sufficient potential to split water, they may not do that if the semiconductor photocatalyst surface lacks from active sites.

To deal with the abovementioned difficulties, continuous efforts have been made for the promotion of photocatalytic hydrogen generation in the presence of organic pollutants which were found to prohibit the backward reaction. Methanol ( $\text{CH}_3\text{OH}$ ) as an organic pollutant present in wastewater was found to be the most widely studied to yield photocatalytic  $\text{H}_2$  evolution [27–39]. The deposition of a co-catalyst on the surface of the photocatalyst has been also reported to yield active sites for the photocatalytic  $\text{H}_2$  production [27, 40–42].

#### 1.4. Titanium Dioxide as a Photocatalyst

$\text{TiO}_2$  exists mainly in three different crystalline forms (**Figure 1-2**): tetragonal anatase, tetragonal rutile, and orthorhombic brookite [43]. Rutile is known to be thermodynamically the most stable form, while anatase and brookite are metastable and are consequently transformed to the rutile phase upon calcination at temperatures above  $\sim 600\text{ }^\circ\text{C}$  [44].

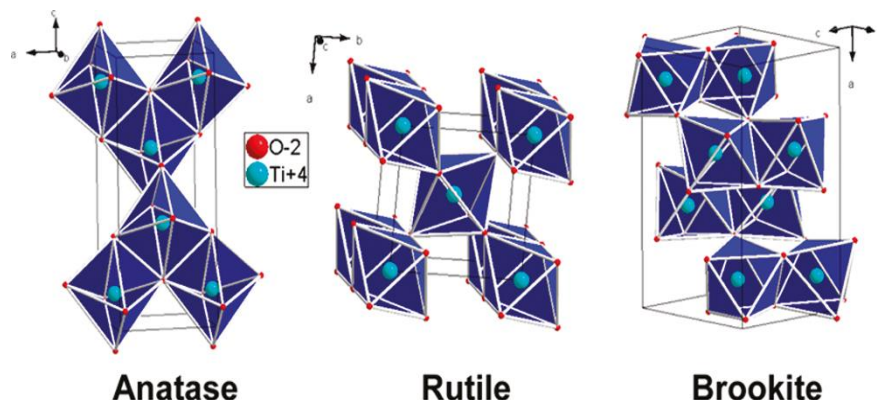
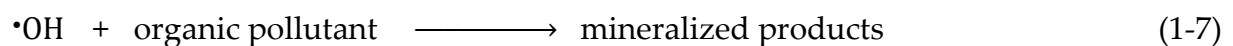
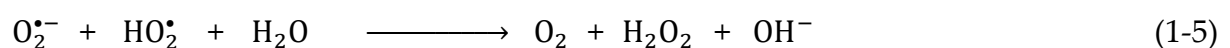


**Figure 1-2.** Crystal structures of  $\text{TiO}_2$  polymorphs: anatase, rutile, and brookite forms (reprinted with permission from ref. [45]).

Photocatalysis over  $\text{TiO}_2$  is initiated by the absorption of a photon with energy equivalent or superior to its band gap energy (ca. 3.2 eV for anatase). Thus electron-hole pairs ( $e^-/h^+$ ) are produced and electrons are transferred from the VB to the empty CB of the semiconductor particle forming an electron vacancy in the valence band described as a valence band hole ( $h_{\text{VB}}^+$ ) which acts as a strong oxidant with a redox potential of 2.7 V vs. NHE [46] (**Equation 1-1**). The conduction band electron ( $e_{\text{CB}}^-$ ) can recombine directly with the  $h_{\text{VB}}^+$  releasing the absorbed light energy as heat in the



system without any chemical reaction (**Equation 1-2**). On the other hand, the  $e_{CB}^-$  and the CB trapped electrons ( $Ti^{3+}$  centers) react with surface absorbed species such as  $O_2$  initiating a reduction reaction on the surface of the semiconductor yielding the superoxide radical anion  $O_2^{\bullet-}$  (-0.33 V vs. NHE) since the redox potential of the  $e_{CB}^-$  in  $TiO_2$  is negative enough (-0.52 V vs. NHE) [20] (**Equation 1-3**).  $O_2^{\bullet-}$  combines with  $H^+$  to form hydrogen peroxide  $H_2O_2$  (0.89 V vs. NHE) (**Equations 1-4** and **1-5**). Consequently,  $H_2O_2$  reacts with the  $e_{CB}^-$  generating  $\bullet OH$  (0.38 V vs. NHE) [47] (**Equation 1-6**), which further converts the organic pollutant to mineralized products (**Equation 1-7**). These reactions prevent the  $e_{CB}^-$  from recombining with the  $h_{VB}^+$  resulting in an accumulation of  $\bullet OH$  that participate in the degradation of the organic pollutants present in the solution. In fact, the charges can react directly with adsorbed contaminants, but reactions with water are predominant since water molecules are more abundant at the semiconductor surface than pollutant molecules [48]. Consequently, the charge transfer from either the adsorbed water molecule ( $H_2O$ ) or from hydroxide ion ( $OH^-$ ) to  $h_{VB}^+$  describes an oxidation process forming  $\bullet OH$  as a powerful oxidant; ( $H_2O/\bullet OH$ ; 2.8 V vs. NHE) (**Equation 1-8**) and ( $OH^-/\bullet OH$ ; 1.89 V vs. NHE) (**Equation 1-9**) as summarized in the following chemical equations [17, 21] and described in **Figure 1-3**.



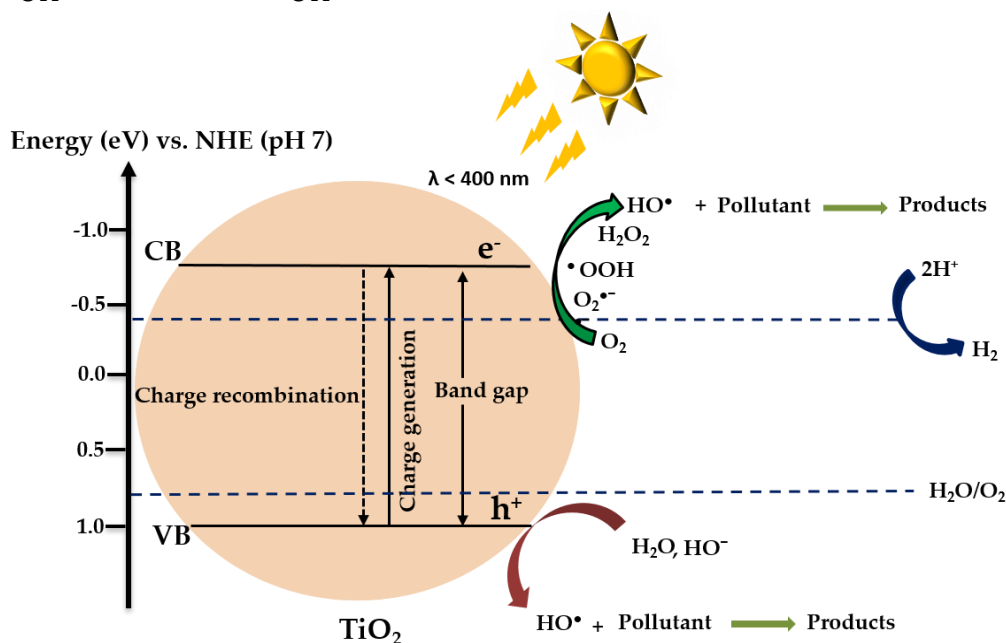


**Figure 1-3.** Schematic illustration of the charge transfer across the TiO<sub>2</sub> interface.

Compared to other semiconductor photocatalysts, TiO<sub>2</sub> remains one of the most promising materials for photocatalytic water treatment as it is non-corrosive, highly photostable, cost-effective, abundant, chemically inert, and has a high oxidation efficiency [19]. However, TiO<sub>2</sub> can be activated only under UV light due to its relatively wide band gap, which is equal to 3.2, 3.0, and 3.4 eV for anatase, rutile, and brookite phases, respectively [49, 50, 51]. UV photons constitute only about 5 % of the solar flux incident at the earth's surface which is of little practical use. They are expensive to produce when using UV lamps. In the case of using solar light irradiation, a huge light-harvesting area is required which is additionally expensive. Besides, the photocatalytic activity is limited by the recombination of the charge carrier since over 90 % of the charge carrier in TiO<sub>2</sub> recombine in the first nanoseconds and are not accessible for the photocatalytic reaction [52]. Furthermore, for the proton reduction reaction as shown in **Figure 1-3**, the potential of the TiO<sub>2</sub> CB is known to be only about equal or slightly above the potential of the redox couple H<sup>+</sup>/H<sub>2</sub>, which presents another disadvantage responsible for the low energy conversion efficiency of TiO<sub>2</sub> [53, 54]. These major drawbacks limit the TiO<sub>2</sub> application for a large scale.

## 1.5. Improving the Activity of TiO<sub>2</sub>

Recently, the design of new TiO<sub>2</sub> photocatalysts that can absorb visible light has been widely studied. Coupling TiO<sub>2</sub> with a wide or narrow band gap semiconductor [55, 56], doping it with metal ion/nonmetal ion [57, 58], using noble metal deposition on the surface [59], or with dye-sensitized TiO<sub>2</sub> [60] with modifying the electronic band structure result in higher photocatalytic reaction rates. The main goals of TiO<sub>2</sub> modification are: (i) to increase its specific surface area which results in more adsorption of organic compounds on the surface, (ii) to reduce its band gap so that it allows for more solar light absorption, and (iii) to minimize the electron-hole recombination.

### 1.5.1. Co-catalyst Deposition on TiO<sub>2</sub>

The fast recombination of the photogenerated charge carriers in a photocatalytic reaction is one of the major limitations in the photocatalytic H<sub>2</sub> generation. The role of a co-catalyst is to act as an electron sink and to host active sites for photocatalytic H<sub>2</sub> generation improving the photocatalytic activity. Noble metals including Pt, Au, Pd, Rh, Ni, Cu, and Ag, have been reported to be highly effective for the improvement of TiO<sub>2</sub> photocatalysis [27, 61–68]. Among these, Pt is well known as the best co-catalyst for the reduction of protons to generate H<sub>2</sub> [28, 69–74]. In addition, noble metal particles that absorb visible light via surface plasmon resonance (SPR) by the resonant oscillation of their conduction band electrons under visible light illumination can also accelerate the transfer of photogenerated electrons from plasmonic metal (e.g., Au, Ag) to the conduction band of TiO<sub>2</sub> and thus the photogenerated charge carriers are efficiently separated [75].

When a noble metal is loaded on a semiconductor surface, two types of metal/semiconductor contact can be formed (the Schottky barrier contact and the ohmic contact) depending only on the work function of the metal and the electron affinity of the semiconductor. An ideal ohmic contact is created if the barrier formed by the metal/semiconductor junction is zero, thus the electrons can easily flow in both directions between the metal and the semiconductor. For a metal/n-type

semiconductor heterojunction, an ohmic contact is created when the work function of the metal ( $\Phi_m$ ) is smaller than that of the semiconductor ( $\Phi_s$ ), whereas a Schottky barrier contact is formed when  $\Phi_m$  is larger than  $\Phi_s$  [76]. This Schottky barrier hinders the undesirable back oxidation of hydrogen [77–79]. Under these conditions, Pt nanoparticles (NPs) reveal more efficient electron-acceptor properties due to their high work function ( $\Phi_{Pt} = 5.65$  eV,  $\Phi_{Au} = 5.1$ ,  $\Phi_{Pd} = 5.12$  eV,  $\Phi_{Rh} = 4.98$  eV,  $\Phi_{Ag} = 4.26$ ) [80]. Indeed, noble metals have usually lower Fermi level ( $E_f$ ) positions than the CB energy of the semiconductor material (i.e;  $TiO_2$ ). Thus, photo-promoted electrons migrate from the  $TiO_2$  CB situated at more negative values to the relatively more positive CB of Pt. The two Fermi levels ( $E_f$ ) are then equal, and the metal surface gets saturated with electrons whereas the  $e_{CB}^-$  of the  $TiO_2$  decreased. Due to the electron's excess at the Pt/ $TiO_2$  interface, the bands of  $TiO_2$  bend upwards toward the surface establishing a Schottky barrier with a barrier height that equals the energy difference between the work function of Pt and the electron affinity of  $TiO_2$  as shown in **Figure 1-4** [81, 82]. Under illumination, the photogenerated  $e_{CB}^-$  continuously transfer across the Pt/ $TiO_2$  interface to Pt, and the photogenerated  $h_{VB}^+$  remains at the surface of  $TiO_2$ . Finally, the recombination of the electron-hole pairs is effectively suppressed, and the carrier transfer is enhanced leading to improved photocatalytic activity [64].

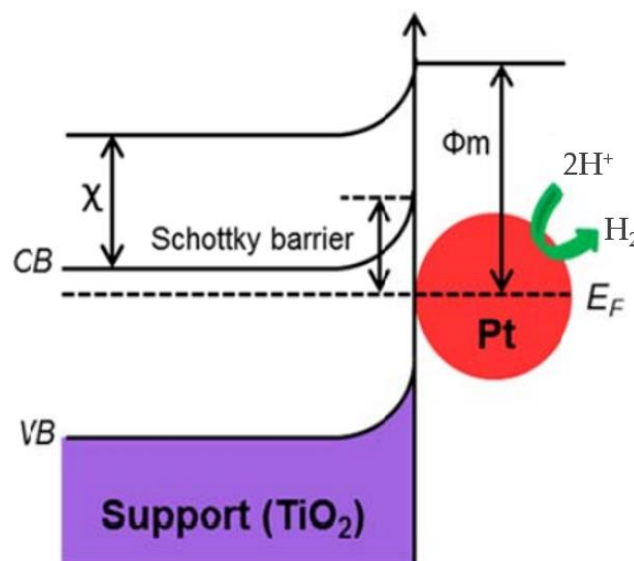


**Figure 1-4.** Formation of a Schottky barrier at the metal/semiconductor interface in the equilibrium.

$E_f$  = Fermi level of Pt,  $\Phi_m$  is the Pt work function and  $X$  is the electron affinity of  $TiO_2$ . Reproduced with permission from ref. [75].

Previous investigations have examined the influence of noble metals loading on TiO<sub>2</sub> for the degradation of wastewater pollutants and H<sub>2</sub> production. In water treatment application, Sakthivel *et al.* [62] investigated the photo-oxidation of acid green 16 in aqueous solution using Pt, Au, and Pd-deposited on TiO<sub>2</sub>. The highest photonic efficiency was observed with metal deposition of less than 1 wt%. Loadings of Pt and Au were more efficient than the loading of Pd due to their suitable electron affinity and work function. Mogyorsi *et al.* have compared the photocatalytic activity of Pt, Au, and Ag deposited on TiO<sub>2</sub> for the photocatalytic H<sub>2</sub> generation using different electron donors. The order of the photocatalytic activity was found to decrease in the following order Pt/TiO<sub>2</sub> > Au/TiO<sub>2</sub> > Ag/TiO<sub>2</sub> > P25 [68]. In an earlier study, Eastman *et al.* have also studied the effect of Pt, Au, and Ag loaded on the TiO<sub>2</sub> surface. Pt was the most active co-catalyst followed by Au then Ag because of its higher work function (i.e;  $\Phi_{Pt} = 5.65$  eV,  $\Phi_{Au} = 5.10$  eV, and  $\Phi_{Ag} = 4.00$  eV) [67]. Bamwenda *et al.* have compared the photocatalytic H<sub>2</sub> evolution from aqueous ethanol upon Pt-loaded TiO<sub>2</sub> and Au-loaded TiO<sub>2</sub>. Pt was found to be the best cocatalyst with optimum loading amounts of 0.3 - 1 wt% and the activity was found to decrease with a higher loading amount of the co-catalyst. This was explained by the fact that the metal particles might block the photo-absorption by TiO<sub>2</sub> decreasing the photogeneration of electron-holes pairs, or that the loaded metal particles may act as recombination centers. Furthermore, they have investigated the effect of the deposition methods on the activity using different metal particle deposition methods including deposition-precipitation, impregnation, and photodeposition. Au / TiO<sub>2</sub> synthesized by photodeposition was found to be the most active, while Pt/TiO<sub>2</sub> was less sensitive to the synthesis methods [63].

Since Pt is an expensive noble metal, low-cost metals suitable to improve the photocatalytic activity of a semiconductor are of great use. For instance, Wu and Lee deposited Cu particles on the surface of TiO<sub>2</sub> using methanol as a hole scavenger. They observed that the activity shows up to 10-fold enhancement at the optimum loading of about 1.2 wt% Cu [27]. Montoya and Gillan demonstrated an in-situ metal surface

deposition on  $\text{TiO}_2$  NPs using 3d transition metals (Co, Ni, Cu) to improve photocatalytic  $\text{H}_2$  evolution. The results have shown significant improvement (~ 5 times – 15 times) for UV photocatalytic  $\text{H}_2$  generation in comparison with  $\text{TiO}_2$  [30]. Other low-cost metals, such as Ag were also found to be efficient for the improvement of the photocatalytic hydrogen evolution activity enhancing the efficiency of the  $\text{TiO}_2$  by a factor of 5 for the photooxidation of oxalic acid [83], and 3.3 times as that of pure  $\text{TiO}_2$  [84]. In another study, Chen and co-workers have published a report comparing expensive metal (Au) and low-cost metallic nickel (Ni) NPs loaded on  $\text{TiO}_2$  for the photocatalytic  $\text{H}_2$  generation. They have found that the 0.5 wt.% Ni/ $\text{TiO}_2$  photocatalyst exhibited higher photocatalytic activity than the 2 wt.% Au/ $\text{TiO}_2$  which was associated with the high dispersion of Ni particles on the surface of  $\text{TiO}_2$ , and therefore can be efficiently used as a promising alternative to noble metal co-catalysts e. g., Pt, Au, or Pd. [85].

### 1.5.2. Coupling $\text{TiO}_2$ with Other Semiconductor Photocatalysts

Coupling  $\text{TiO}_2$  with another semiconductor that has a different band gap energy is an effective approach to promote better charge carrier separation and to improve the photostability of the materials [86–91]. According to the band positions of the two coupled semiconductors and the charge carrier transfer, the created heterostructure can be classified into three main types: straddling gap (type-I), staggered gap (type-II), and Z-scheme heterojunction [92, 93], as shown in **Figure 1-5**. Considering a type I heterojunction, the CB of semiconductor B is higher than the CB of semiconductor A and the VB of semiconductor B is lower than the VB of semiconductor A. Thus, the photoexcited electrons are transferred from the CB of the semiconductor with higher band edge (B) to the CB of the semiconductor with lower band edge (A), and the holes are transferred in the same direction. Therefore, charge carriers are accumulated on semiconductor A, yielding no enhancement for charge carrier separation, and subsequently no improvement in the photocatalytic activity. In type II heterojunction, the mechanism of the charge separation of the heterostructure photocatalysts is improved owing to the ideal band positions of the two

semiconductors. Upon irradiation, photoexcited electrons are injected from the CB of B to the CB of A. In turn, holes are transferred from VB of A to the VB of B increasing the rate of charge carrier separation and reducing the recombination of the electron-hole pairs [91]. Z-scheme heterojunction has the same band structure as type II heterojunction but a different charge carrier transfer mechanism as illustrated in **Figure 1-5**. In this type of heterojunction, electrons with lower reduction capacities of semiconductor A recombine with the holes with lower oxidation abilities of semiconductor B. Consequently, electrons with strong reduction potential in semiconductor B and holes with elevated oxidation efficiency in semiconductor A are maintained. Thus, not only an efficient separation of photogenerated carriers is achieved, but also their strong photoredox properties are preserved [93].

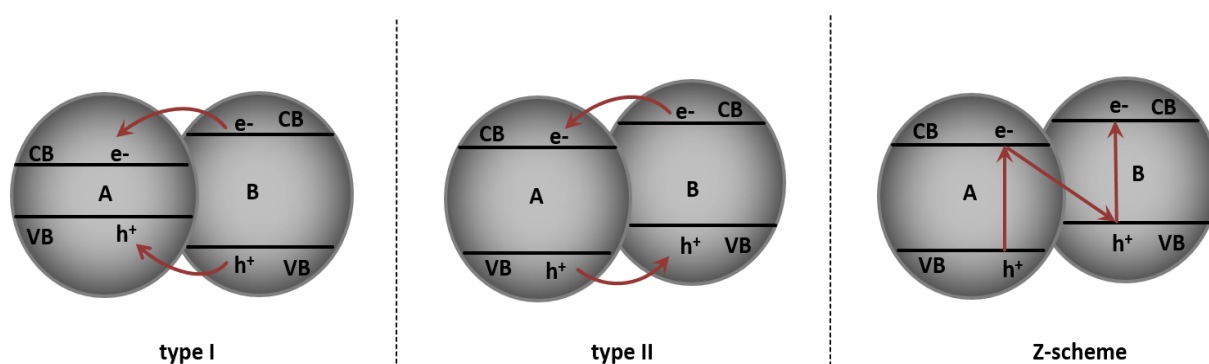


**Figure 1-5.** Schematic energy band diagram of different types of semiconductor heterojunctions.

In coupled semiconductors,  $M_xO_y/TiO_2$  and  $M_xS_y/TiO_2$  systems are the most broadly studied in photocatalytic water treatment [54, 94]. When  $TiO_2$  is coupled with a wide band gap semiconductor such as  $SnO_2$ ,  $ZnO$ , and  $WO_3$  (type II of semiconductor heterojunction), the photocatalytic activity was proven to enhance under UV light irradiation due to the improved charge separation [88, 95, 96]. For instance, in a study conducted by Zhou *et al.*,  $TiO_2/SnO_2$  composite has shown enhanced activity for the degradation of rhodamine B under UV irradiation [55]. Vinodgopal and Kamat have also reported higher efficiency of photocatalytic degradation of acid orange 7 over  $TiO_2/SnO_2$  composite under UV light [88]. A higher degradation rate of methyl orange employing the  $TiO_2/ZnO$  system using UV irradiation has been demonstrated by Wang and co-workers [97]. Besides coupling  $TiO_2$  with a large band gap semiconductor, the

formation of heterojunctions between  $\text{TiO}_2$  and a small band gap semiconductor has also been investigated [54]. When  $\text{TiO}_2$  is coupled with a small band gap semiconductor that has a more negative CB level, the CB electrons of the small band gap semiconductor used as a sensitizer can be injected into the CB of  $\text{TiO}_2$ . Hence, charge carrier transfer from one particle to another is ensured and electron-holes separation is achieved [86]. However, for the photocatalytic  $\text{H}_2$  evolution reaction to occur, the CB of the large band gap semiconductor ( $\text{TiO}_2$ ) should be more negative than the  $E(\text{H}^+/\text{H}_2)$ . In a study conducted by Jang and co-workers,  $\text{CdS}/\text{TiO}_2$  nano-bulk composite photocatalyst has shown a higher rate of  $\text{H}_2$  production from aqueous  $\text{H}_2\text{S}$  solution under visible light [98]. Zyoud *et al.* have reported 75 % of phenazopyridine degradation using  $\text{CdS}/\text{TiO}_2$  under solar simulated light. Under visible light,  $\text{CdS}$  act as a sensitizer and transfer electrons to the CB of  $\text{TiO}_2$ , and the formed hole in the VB of  $\text{CdS}$  undertake the oxidation reactions [99].  $\text{Ag}_2\text{O} / \text{TiO}_2$  materials (type I of semiconductor heterojunction) have been also reported for the degradation of pharmaceuticals [100-103], the inactivation of some pathogens presents in water [104, 105], and photocatalytic hydrogen generation [106–108]. In most of the cases, the outstanding photocatalytic activity of the  $\text{Ag}_2\text{O} / \text{TiO}_2$  NPs was explained by the electron trap effect exerted by  $\text{Ag}_2\text{O}$ , along with the appearance of  $\text{Ag}(0)$  throughout the photocatalytic degradation of organic pollutants, increasing the lifetime and the mobility of the charge carriers by impeding the recombination of the hole-electron pairs.

### 1.5.3. Doping of $\text{TiO}_2$

An effective way of modifying the electronic, optical, and structural properties of a semiconductor is doping. In silicon solar cells applied in photovoltaic, doping is commonly used for improving the conductivity with increasing the free charges. This can be through the donation of electrons for dopants that have a valency higher than that of the native material (n-type doping), or holes for dopants that have a lower valency (p-type doping) [109].



In TiO<sub>2</sub> photocatalysis, one of the conventional approaches that have been applied by numerous research groups to develop visible light-absorbing semiconductors is doping TiO<sub>2</sub> either by cations; including transition metal ions (Cr, Mn, Fe, Co, Ni, Cu, V, Zn) [57, 110–118], rare earth metal ions (Ce, Sc, Gd, Nd, Ho) [110, 119, 120], noble metal ions (Ru, Rh, Ir, Pt, Pd, Ag, Au) [110, 121, 122], post-transition metal ions (Bi, Al, Ga, Sn, Pb, Ti) [110, 123, 124], or anions (N, C, F, S, P, I,) [110, 125] extending the visible light response of TiO<sub>2</sub> and improving its photocatalytic activity [57, 58, 86]. With cation doping, impurity levels create either a donor level above the VB or an acceptor level below the CB in the forbidden band of the semiconductor photocatalyst decreasing its band gap as depicted in **Figure 1-6** [126]. Anions doping can result in the formation of a localized mid-gap state above the top of the semiconductor VB, resulting in narrowing the original band gap of the semiconductor to be activated under vis-light (**Figure 1-6**) [75].

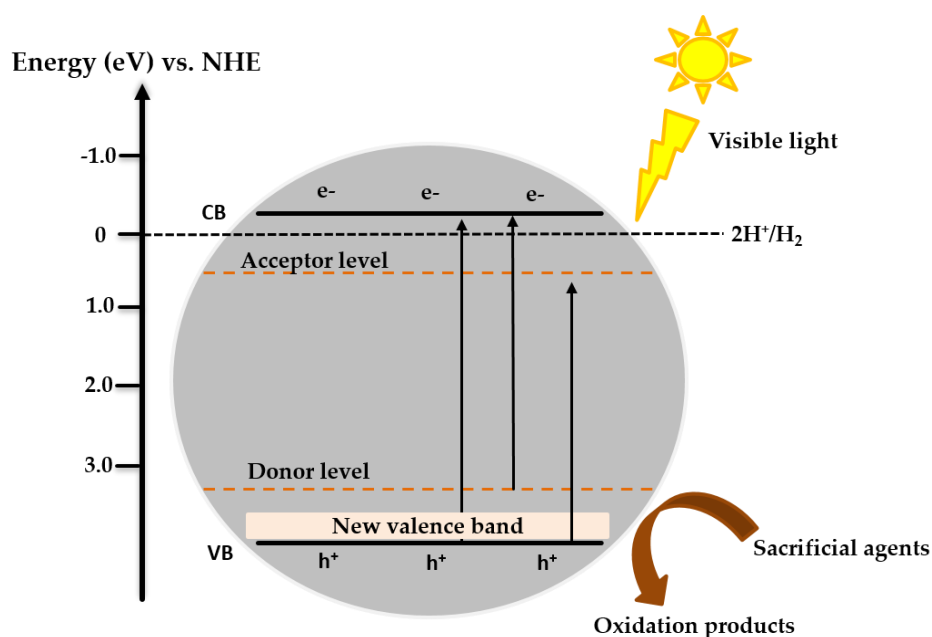


**Figure 1-6:** Schematic representation of donor, acceptor energy level formation by metal cation doping, and new valence band formation by non-metal ion doping.

In an early investigation, Choi *et al.* have performed a systematic study of metal ion doping employing quantum sized TiO<sub>2</sub> and 21 metal ions in terms of CHCl<sub>3</sub> oxidation and CCl<sub>4</sub> reduction. The dopants with closed-shell electronic configuration such as Li<sup>+</sup>, Mg<sup>2+</sup>, Zn<sup>2+</sup>, Ga<sup>3+</sup>, Al<sup>3+</sup>, Zr<sup>4+</sup>, Sn<sup>4+</sup>, Ta<sup>5+</sup>, and Sb<sup>5+</sup> have shown a slight

effect on the photoactivity. However,  $\text{Co}^{3+}$  was found to lower the photocatalytic activity, and  $\text{Fe}^{3+}$  resulted in improved activity compared to bare  $\text{TiO}_2$ . The relative photocatalytic efficiency of a metal-ion dopant was found to depend on whether the metal-ion serves as a mediator of interfacial charge transfer or acts as a recombination center [127]. A study on 13 different metal ions doped  $\text{TiO}_2$  employing a sol/gel process was conducted by the same group later. They have concluded that it is difficult to correlate between the physico-chemical properties such as light absorption and the visible light photocatalytic activities of the studied metal-doped  $\text{TiO}_2$  materials [57]. Karakitsou and Verykios have demonstrated that the concentration and the valence of the doping cations such as  $\text{Zn}^{2+}$ ,  $\text{W}^{6+}$ ,  $\text{Nb}^{5+}$ , etc., affected the improvement or the decrease of the photocatalytic activity [128]. Thereafter, a theoretical model that is applicable for all metal-doped photocatalysts and which describes the correlation between the photocatalytic activity, the doping ratio, and the particle size has been developed by Bahnemann and co-workers. This model assumes that at the optimum doping ratio two distinct criteria need to be satisfied. First, the doping ratio should not be too high to avoid recombination centers, and the second is that each particle should be doped. Moreover, it was shown that the stated controversy regarding transition metal doping in photocatalysis can be resolved by this model [129]. In a study conducted by Bloh *et al.*, it has been reported that tungsten–nitrogen-codoped titania featured both a reduced band gap and a positive shift of the conduction band edge. However, nitrogen doping is found to be responsible for the majority of the observed effects while tungsten contributes indirectly by stabilizing the nitrogen at higher temperatures [130].

As mentioned at the beginning of this sub-chapter, studies have been conducted on modified photocatalysts using cation [60, 131] and anion [132] doping for  $\text{H}_2$  evolution application. For instance, Peng *et al.* investigated the effect of  $\text{Be}^{2+}$  doped  $\text{TiO}_2$  on photocatalytic  $\text{H}_2$  production in the presence of ethanol [133]. They have revealed that when the doping ions were in the shallow surface, the doping was beneficial, while in the deep bulk, the doping had a detrimental effect. At the optimum

synthetic conditions, the photocatalytic H<sub>2</sub> evolution activity of the doped TiO<sub>2</sub> improved by 75% compared to undoped TiO<sub>2</sub>. Umebayashi *et al.* reported S doped TiO<sub>2</sub>. It was found that when TiO<sub>2</sub> was doped with S, the mixing of 3p states of S with the VB of TiO<sub>2</sub> increased the width of the VB resulting in narrowing the band gap. While the band gap narrowing was due to the VB upward shifting, the CB remained unaffected. Hence, the S-doped TiO<sub>2</sub> was able to generate molecular hydrogen under visible light [134]. In another study, Gao *et al.* have studied the effect of Mg doping on the inter-band defect states of anatase TiO<sub>2</sub> under UV irradiation using Pt as a co-catalyst and methanol as a sacrificial reagent. Using the transient infrared absorption excitation energy scanning spectroscopy, they have revealed that the shallow defect states are diminished, and the deep defect states are eliminated by 0.5 % of Mg doping resulting in higher H<sub>2</sub> efficiency [135]. Moreover, upon combining metal and non-metal dopants, it has been stated that the mobility, transfer, and consumption of photogenerated charge carriers are significantly enhanced by the introduction of new energy states, and therefore the hydrogen evolution efficiency was higher than the sum of the efficiencies of each dopant alone [136].

## 1.6. Aim of the Thesis

### 1.6.1. Thesis Objectives

This thesis aims to develop different TiO<sub>2</sub> based photocatalysts with enhanced photocatalytic activity under UV-visible light irradiation. Photocatalysis generally involves three processes comprising (1) the photon absorption, (2) the transfer, migration, and separation of the photogenerated electron/hole pairs, and (3) the photocatalytic reaction on the surface of the photocatalyst. Accordingly, photocatalytic activities can be improved at least by one of these features. In this doctoral research, TiO<sub>2</sub> has been modified employing three different approaches, that are: forming a heterojunction structure with a metal oxide (Ag<sub>2</sub>O), doping with a transition metal (Co), and surface modification with a noble metal (Pt). To evaluate the photocatalytic activity of the synthesized photocatalysts, organic pollutants, namely, methylene blue

(MB), oxytetracycline hydrochloride (OTC HCl), and methanol (CH<sub>3</sub>OH) were chosen as model compounds. Correspondingly, the photocatalytic degradation of these organic pollutants, as well as the photocatalytic hydrogen generation under UV-visible light irradiation, were investigated. Moreover, and to understand the key factors behind the enhanced photocatalytic activities, mechanistic studies have been performed within the frame of this work.

In detail, this doctoral research focuses on the following investigations:

- To develop heterojunction photocatalysts by combining physical mixtures of two different semiconducting metal oxides, namely TiO<sub>2</sub> (Degussa P25) and a self-prepared Ag/Ag<sub>2</sub>O.
- To synthesize in situ Ag/Ag<sub>2</sub>O // TiO<sub>2</sub> composites by a simple precipitation method employing TiO<sub>2</sub> and silver nitrate (AgNO<sub>3</sub>) to evaluate the effect of the synthesis method on the photocatalytic activity.
- To study the effect of the mass ratio of Ag/Ag<sub>2</sub>O on the structural, optical, morphological, and photocatalytic activity of the materials.
- To evaluate the photocatalytic activity of the prepared Ag/Ag<sub>2</sub>O // TiO<sub>2</sub> mixtures and composites under UV-vis-light and only under visible light irradiation for the methylene blue (MB) bleaching.
- To study the photocatalytic hydrogen generation under UV-vis-light irradiation using methanol as a sacrificial reagent. The stability and the recyclability of the prepared Ag/Ag<sub>2</sub>O // TiO<sub>2</sub> will also be studied.
- To explain the mechanism behind the high activity of the prepared mixtures and composites compared to the blank TiO<sub>2</sub>.
- To synthesize Co -doped TiO<sub>2</sub> using two solvothermal synthetic methods, namely, hydrothermal and reflux synthesis. Self-prepared TiO<sub>2</sub> and Evonik Degussa Aeroxide P25 modified with the same methods will be used for comparison purposes.

- To investigate the photocatalytic activity of the Co-doped materials for the UV-vis-light degradation of oxytetracycline hydrochloride (OTC HCl) as a model compound of emerging concern.
- To prepare Pt loaded on the Co-doped TiO<sub>2</sub> photocatalysts using a simple photodeposition method.
- To assess the rate of the photocatalytic hydrogen evolution from methanol under UV-vis-light irradiation.
- To understand and elucidate the mechanisms behind the UV-vis-light-induced photocatalytic degradation of OTC HCl, and methanol photoreforming.

### 1.6.2. Thesis Overview

The topics of this Ph.D. thesis are divided into five chapters:

**Chapter 1** is a general introduction to the topic of water treatment and fuel synthesis using TiO<sub>2</sub> photocatalysis. In this chapter, the background of this scientific research, and knowledge required to understand the chemistry behind TiO<sub>2</sub> and modified TiO<sub>2</sub> photocatalysts are given.

**Chapter 2** reports the synthesis of mixtures and composites of Ag/Ag<sub>2</sub>O// TiO<sub>2</sub> with different Ag/Ag<sub>2</sub>O mass ratio ranging from 20% to 80%. Conflicting reports exist in the literature while discussing the low stability of Ag<sub>2</sub>O containing materials due to the photo-induced reduction of Ag<sub>2</sub>O and Ag(0) formation. In this study, it was found that Ag/Ag<sub>2</sub>O enhances the rate of light-induced bleaching of aqueous MB under both UV-vis and vis illumination, in comparison to the bleaching in homogeneous solution. In suspensions containing mixtures and composites of Ag/Ag<sub>2</sub>O with TiO<sub>2</sub> (P25), having varying mass ratios of Ag/Ag<sub>2</sub>O (20%, 50%, and 80%), the reaction rate was slightly increased. It is therefore suggested that the bleaching of methylene blue is initiated by an interfacial electron transfer from the excited organic probe compound to Ag<sub>2</sub>O since TiO<sub>2</sub> layers covering the Ag<sub>2</sub>O seem to inhibit this electron transfer. Therefore, Ag<sub>2</sub>O cannot transfer an electron either to dissolved molecular oxygen nor to a proton for thermodynamic reasons. It is assumed that Ag<sup>+</sup> is reduced to Ag(0) in the processes investigated here. Results of XRD and XPS measurements also support

this assumption and indicate that Ag/Ag<sub>2</sub>O is not stable under the experimental conditions employed in this study. The often-reported stabilization of Ag<sub>2</sub>O by metallic silver was not observed. Hence, to address Ag/Ag<sub>2</sub>O as a (photo)catalytically active material does not seem appropriate. These findings were evaluated and discussed in detail in an article entitled “Ag/Ag<sub>2</sub>O as a Co-Catalyst in TiO<sub>2</sub> Photocatalysis: Effect of the Co-Catalyst/Photocatalyst Mass Ratio” by Soukaina Akel, Ralf Dillert, Narmina O. Balayeva, Redouan Boughaled, Julian Koch, Mohammed El Azzouzi, and Detlef W. Bahnemann, published in *Catalysts*, 2018, 8, 647; doi: 10.3390/catal8120647.

In **Chapter 3**, Co-doped TiO<sub>2</sub> was synthesized using two different solvothermal techniques to assess the removal of the pharmaceutical oxytetracycline hydrochloride (OTC HCl) upon UV-vis light irradiation. Although Co-doped TiO<sub>2</sub> NPs have been extensively studied previously, there are conflicting results on the effects of cobalt ion doping on the photocatalytic activity of TiO<sub>2</sub>. Also, the different synthesis methods employed to synthesize cobalt doped TiO<sub>2</sub> along with the different types of substrates utilized for photocatalytic degradation examinations create a varying set of data that can often create doubts about the influence of cobalt doping on the photocatalytic activity. Although OTC HCl is easily photolyzed under UV light irradiation, it was reported to be not significantly degradable upon visible light irradiation. Herein, it was observed that the initial reaction rate over Co-TiO<sub>2</sub> was higher compared with the pure TiO<sub>2</sub>, and the commercially available P25. This enhanced photocatalytic activity was attributed to the high surface area of the Co-doped materials along with the impurity levels within the band gap, promoting the charge separation and improving the charge transfer ability. Consequently, a mechanism including the processes of charge transfer during the degradation of OTC HCl over Co-TiO<sub>2</sub> upon UV-visible light was suggested in this Chapter (**Chapter 3**) which comprises the article entitled “UV/Vis Light Induced Degradation of Oxytetracycline Hydrochloride Mediated by Co-TiO<sub>2</sub> nanoparticles” by Soukaina Akel, Redouan Boughaled, Ralf Dillert, Mohamed



## 1.7. References

1. Global Energy and CO<sub>2</sub> Status Report. The Latest Trends in Energy and Emission in 2018. Internal Energy Agency. [www.iea.org](http://www.iea.org).
2. The United Nations World Water Development Report 2019: Leaving No One Behind. Paris, UNESCO. "WWAP (UNESCO World Water Assessment Programme) " 2019. ISBN 978-92-3-100309-7.
3. J. Wright, S. Gundry, R. Conroy. Household Drinking Water in Developing Countries: A Systematic Review of Microbiological Contamination Between Source and Point-of-Use. *Trop. Med. Int. Health* **2004**, 9, 106–117.
4. Water, Sanitation, Hygiene and Waste Management for the COVID-19: Technical Brief. 03 March 2020. World Health Organization & United Nations Children's Fund (UNICEF). <https://apps.who.int/iris/handle/10665/331305>.
5. L. Casanova, W.A. Rutala, D.J. Weber, M.D. Sobsey. Survival of Surrogate Coronaviruses in Water. *Water Res.* **2009**, 43(7), 1893–1898.
6. Guidelines for Drinking-water Quality, Fourth edition, Incorporating the First Addendum. Geneva: *World Health Organization* **2017**. ISBN: 978-92-4-154995-0.
7. SARS-CoV-2 – Water and Sanitation. Adelaide: *Water Research Australia* **2020**.
8. I.D. Amoah, S. Kumari, F. Bux. Coronaviruses in Wastewater Processes: Source, Fate and Potential Risks. *Environ. Int.* **2020**, 143, 105962.
9. Evaluation of the Council Directive 91/271/EEC of 21 May 1991, Concerning Urban Waste-water Treatment. **2019**.
10. Wastewater Technology Fact Sheet, Screening and Grit Removal. U.S. EPA. **2003**
11. H. Bessbousse, T. Rhlalou, J.F. Verchère, L. Lebrun. Removal of Heavy Metal Ions from Aqueous Solutions by Filtration with a Novel Complexing Membrane Containing Poly(ethyleneimine) in a Poly(vinyl alcohol) Matrix. *J. Membr. Sci.* **2008**, 307(2), 249–259.
12. T. Robinson, G. McMullan, R. Marchant, P. Nigam. Remediation of Dyes in Textile Effluent: A Critical Review on Current Treatment Technologies with a Proposed Alternative. *Bioresour. Technol.* **2001**, 77(3), 247–255.



13. K.G. Bhattacharyya, A. Sarma. Adsorption Characteristics of the Dye, Brilliant Green, on Neem Leaf Powder. *Dyes Pigm.* **2003**, 57(3), 211–222.
14. A.R. Ribeiro, O.C. Nunes, Manuel F.R. Pereira, Adrián M.T. Silva. An Overview on the Advanced Oxidation Processes Applied for the Treatment of Water Pollutants Defined in the Recently Launched Directive 2013/39/EU. *Environ. Int.* **2015**, 75, 33–51.
15. B. Kasprzyk-Hordern, M. Ziólek, J. Nawrocki. Catalytic Ozonation and Methods of Enhancing Molecular Ozone Reactions in Water Treatment. *Appl. Catal. B: Environ.* **2003**, 46, 639–669.
16. J. Hoigné. Inter-calibration of OH Radical Sources and Water Quality Parameters. *Water Sci. Technol.* **1997**, 35, 1–8.
17. M.R. Hoffmann, S.T. Martin, W. Choi, D.W. Bahnemann. Environmental Applications of Semiconductor Photocatalysis. *Chem. Rev.* **1995**, 95, 69–96.
18. US/EPA, Handbook of Advanced Photochemical Oxidation Processes, EPA/625/R-98/004, December **1998**.
19. D.W. Bahnemann. Mechanisms of Organic Transformations on Semiconductor Particles. In: E. Pelizzetti, M. Schiavello, editors. Photochemical Conversion and Storage of Solar Energy. Netherlands: Kluwer Academic Publishers; **1991**, 251–276.
20. A. Fujishima, T.N. Rao, D.A. Tryk. Titanium Dioxide Photocatalysis. *J. Photochem. Photobiol. C: Photochem. Rev.* **2000**, 1(1), 1–21.
21. D. Bahnemann. Photocatalytic Water Treatment: Solar Energy Applications. *Sol. Energy* **2004**, 77, 445–459.
22. BP Statistical Review of World Energy. Available online: <https://www.bp.com/content/dam/bp/businesssites/en/global/corporate/pdfs/energy-economics/statistical-review/bp-stats-review-2019-full-report.pdf>.
23. N.S. Lewis, G. Crabtree. Basic Research Needs for Solar Energy Utilization: report of the Basic Energy Sciences Workshop on Solar Energy Utilization, April 18-21, 2005. US Department of Energy, Office of Basic Energy Science, **2005**.

24. J.H. Kim, D. Hansora, P. Sharma, J.W. Jang, J.S. Lee. Toward Practical Solar Hydrogen Production—An Artificial Photosynthetic Leaf-to-farm Challenge. *Chem. Soc. Rev.* **2019**, 48, 1908–1971.
25. R.M. Navarro, M. Pena, J. Fierro, Hydrogen Production Reactions from Carbon Feedstocks: Fossil Fuels and Biomass. *Chem. Rev.* **2007**, 107, 3952–3991.
26. F.E. Osterloh. Inorganic Materials as Catalysts for Photochemical Splitting of Water. *Chem. Mater.* **2008**, 20, 35.
27. N.L. Wu, M.S. Lee. Enhanced  $\text{TiO}_2$  Photocatalysis by Cu in Hydrogen Production from Aqueous Methanol Solution. *Int. J. Hydrog. Energ.* **2004**, 29(15), 1601–5.
28. A. Galinska, J. Walendziewski. Photocatalytic Water Splitting over Pt– $\text{TiO}_2$  in the Presence of Sacrificial Reagents. *Energ. Fuel* **2005**, 19, 1143.
29. V. Subramanian, E.E. Wolf, P.V. Kamat. Catalysis with  $\text{TiO}_2$  /gold Nanocomposites. Effect of Metal Particle Size on the Fermi Level Equilibration, *J. Amer. Chem. Soc.* **2004**, 126, 4943–4950.
30. A.T. Montoya, E.G. Gillan. Enhanced Photocatalytic Hydrogen Evolution from Transition-metal Surface-modified  $\text{TiO}_2$ . *ACS Omega* **2018**, 3, 2947–2955.
31. X. Chen, S. Shen, L. Guo, S. S. Mao, Semiconductor-based Photocatalytic Hydrogen Generation. *Chem. Rev.* **2010**, 110, 6503–6570.
32. G.L. Chiarello, L. Forni, E. Selli. Photocatalytic Hydrogen Production by Liquid- and Gas-phase Reforming of  $\text{CH}_3\text{OH}$  over Flame-made C and Au/ C. *Catal. Today* **2009**, 144, 69.
33. G.L. Chiarello, D. Ferri, E. Selli. Effect of the  $\text{CH}_3\text{OH}/\text{H}_2\text{O}$  Ratio on the Mechanism of the Gas-phase Photocatalytic Reforming of Methanol on Noble Metal-modified  $\text{TiO}_2$ . *J. Catal.* **2011**, 280, 168–177.
34. H. Liu, J. Yuan, W. Shangguan. Photochemical Reduction and Oxidation of Water Including Sacrificial Reagents and Pt/ $\text{TiO}_2$  Catalyst. *Energy Fuels* **2006**, 20, 2289–2292.

35. J. J. Zou, C. J. Liu, K. L. Yu, D. G. Cheng, Y.P. Zhang, F. He, F. Du, L. Cui. Highly Efficient Pt/TiO<sub>2</sub> Photocatalyst Prepared by Plasma-enhanced Impregnation Method. *Chem. Phys. Lett.* **2004**, 400, 520–523.
36. A. Patsoura, D.I. Kondarides, X.E. Verykios. Photocatalytic Degradation of Organic Pollutants with Simultaneous Production of Hydrogen. *Catal. Today* **2007**, 124, 94–102.
37. A. Dickinson, D. James, N. Perkins, T. Cassidy, M. Bowker. The Photocatalytic Reforming of Methanol. *J. Mol. Catal. A: Chem.* **1999**, 146, 211–221.
38. C. Lee, J. Park, Y. Jeon, J.I. Park, H. Einaga, Y.B. Truong, I.L. Kyratzis, I. Mochida, J. Choi, Y.G. Shul. Phosphate-Modified TiO<sub>2</sub>/ZrO<sub>2</sub> Nanofibrous Web Composite Membrane for Enhanced Performance and Durability of High-temperature Proton Exchange Membrane Fuel Cells. *Energy Fuels* **2017**, 31, 7645–7652.
39. O. Ola, M.M. Maroto-Valer. Review of Material Design and Reactor Engineering on TiO<sub>2</sub> Photocatalysis for CO<sub>2</sub> Reduction. *J. Photochem. Photobiol. C: Photochem. Rev.* **2015**, 24, 16–42.
40. T.A. Kandiel, R. Dillert, A. Feldhoff, D.W. Bahnemann. Direct Synthesis of Photocatalytically Active Rutile TiO<sub>2</sub> Nanorods Partly Decorated with Anatase Nanoparticles. *J. Phys. Chem. C* **2010**, 114, 4909–4915.
41. T.A. Kandiel, R. Dillert, L. Robben, D.W. Bahnemann. Photonic Efficiency and Mechanism of Photocatalytic Molecular Hydrogen Production over Platinized Titanium Dioxide from Aqueous Methanol Solutions. *Catal. Today* **2011**, 161, 196–201.
42. T. Sakata, T. Kawai, K. Hashimoto. Heterogeneous Photocatalytic Reactions of Organic Acids and Water. New Reaction Paths Besides the Photo-kolbe Reaction. *J. Phys. Chem.* **1984**, 88, 2344–2350.
43. S.M. Gupta, M. Tripathi. A Review of TiO<sub>2</sub> Nanoparticles. *Chinese Sci. Bull.* **2011**, 56, 1639–1657.

44. A.A. Ismail, D.W. Bahnemann. Photochemical Splitting of Water for Hydrogen Production by Photocatalysis: A Review. *Sol. Energy Mater. Sol. Cells* **2014**, 128, 85–101.
45. D. Dambournet, I. Belharouak, K. Amine. Tailored Preparation Methods of TiO<sub>2</sub> Anatase, Rutile, Brookite: Mechanism of Formation and Electrochemical Properties. *Chem. Mater.* **2010**, 22(3), 1173–1179.
46. H. Hennig. Semiconductor Photocatalysis: Principles and Applications. *Angew. Chem. Int. Ed.* **2015**, 54(15), 4429.
47. P.M. Wood. The Potential Diagram for Oxygen at pH 7. *Biochem. J.* **1988**, 253(1), 287–289.
48. D.S. Bhatkhande, V.G. Pangarkar, A.A.C.M. Beenackers. Photocatalytic Degradation for Environmental Applications—A Review. *J. Chem. Technol. Biotechnol.* **2001**, 77, 102–116.
49. J. Zhang, P. Zhou, J. Liu, J. Yu. New Understanding of the Difference of Photocatalytic Activity Among Anatase, Rutile and Brookite TiO<sub>2</sub>. *Phys. Chem. Chem. Phys.* **2014**, 16, 20382–20386.
50. A. Di Paola, M. Bellardita, L. Palmisano. Brookite, the Least Known TiO<sub>2</sub> Photocatalyst. *Catalysts* **2013**, 3, 36–73.
51. N. Serpone, D. Lawless, J. Disdier, JM. Herrmann. Spectroscopic, Photoconductivity, and Photocatalytic Studies of TiO<sub>2</sub> Colloids: Naked and with the Lattice Doped with Cr<sup>3+</sup>, Fe<sup>3+</sup> and V<sup>5+</sup> Cations. *Langmuir* **1994**, 10, 643–52.
52. N. Serpone, D. Lawless, R. Khairutdinov, E. Pelizzetti. Subnanosecond Relaxation Dynamics in TiO<sub>2</sub> Colloidal Sols (Particle Sizes R<sub>p</sub> = 1.0–13.4 Nm). Relevance to Heterogeneous Photocatalysis. *J. Phys. Chem.* **1995**, 99(45), 16655–16661.
53. S. Girish Kumar, L. Gomathi Devi. Review on Modified TiO<sub>2</sub> Photocatalysis under UV/Visible Light: Selected Results and Related Mechanisms on Interfacial Charge Carrier Transfer Dynamics. *J. Phys. Chem. A* **2011**, 115, 13211–13241.

54. R. Dagherir, P. Drogui, D. Robert. Modified TiO<sub>2</sub> For Environmental Photocatalytic Applications: A Review. *Ind. Eng. Chem. Res.* **2013**, 52, 3581–3599.
55. M. Zhou, J. Yu, S. Liu, P. Zhai, L. Jiang. Effects of Calcination Temperatures on Photocatalytic Activity of SnO<sub>2</sub>/TiO<sub>2</sub> Composite Films Prepared by an EPD Method. *J. Hazard. Mater.* **2008**, 154, 1141–1148.
56. Y. Huo, X. Yang, J. Zhu, H. Li. Highly Active and Stable CdS-TiO<sub>2</sub> Visible Photocatalyst Prepared by in Situ Sulfurization under Supercritical Conditions. *Appl. Catal. B: Environ.* **2011**, 106, 69–75.
57. J. Choi, H. Park, M. Hoffman. Effects of Single Metal-ion Doping on the Visible-Light Photoreactivity of TiO<sub>2</sub>. *J. Phys. Chem. C* **2010**, 114, 2, 783–792.
58. Q. Guo, Y. Zhang, J. Qiu, G. Dong. Engineering the Electronic Structure and Optical Properties of g-C<sub>3</sub>N<sub>4</sub> by Non-metal Ion Doping. *J. Mater. Chem. C* **2016**, 4, 6839–6847.
59. J.A. Singh, N.F.W. Thissen, W.H. Kim, H. Johnson, W.M.M. Kessels, A.A. Bol, S. F. Bent, A.J.M. Mackus. Area-Selective Atomic Layer Deposition of Metal Oxides on Noble Metals through Catalytic Oxygen Activation. *Chem. Mater.* **2018**, 30, 3, 663–670.
60. H. Park, Y. Park, W. Kim, W. Choi. Surface Modification of TiO<sub>2</sub> Photocatalyst for Environmental Applications. *J. Photochem. Photobiol. C* **2013**, 15, 1–20.
61. M.R. John, A.J. Furgals, A.F. Sammells. Hydrogen Generation by Photocatalytic Oxidation of Glucose by Platinized n-TiO<sub>2</sub> Powder. *J. Phys. Chem.* **1983**, 87, 801–5.
62. S. Sakthivel, M.V. Shankar, M. Palanichamy, B. Arabindoo, D.W. Bahnemann, V. Murugesan. Enhancement of Photocatalytic Activity by Metal Deposition: Characterization and Photonic Efficiency of Pt, Au and Pd Deposited on TiO<sub>2</sub> Catalyst. *Water Res.* **2004**, 38, 3001–8.
63. G.R. Bamwenda, S. Tsubota, T. Nakamura, M. Haruta. Photoassisted Hydrogen Production from a Water Ethanol Solution: A Comparison of Activities of Au-TiO<sub>2</sub> and Pt-TiO<sub>2</sub>. *J. Photochem. Photobiol. A: Chem.* **1995**, 89, 177.

64. D. Hufschmidt, D. Bahnemann, J.J. Testa, C.A. Emilio, M.I. Litter. Enhancement of the Photocatalytic Activity of Various TiO<sub>2</sub> Materials by Platinization. *J. Photochem. Photobiol. A: Chem.* **2002**, 148, 223–231.
65. V. Subramanian, E.E. Wolf, P.V. Kamat. Catalysis with TiO<sub>2</sub> /gold Nanocomposites. Effect of Metal Particle Size on the Fermi Level Equilibration. *J. Amer. Chem. Soc.* **2004**, 126, 4943–4950.
66. J. Ran, J. Zhang, J. Yu, M. Jaroniec, S. Z. Qiao. Earth-abundant Cocatalysts for Semiconductor-based Photocatalytic Water Splitting. *Chem. Soc. Rev.* **2014**, 43, 7787–7812.
67. D. Eastman. Photoelectric Work Functions of Transition, Rare-earth, and Noble Metals. *Phys. Rev. B* **1970**, 2, 1.
68. K. Mogyorosi, A. Kmetyko, N. Czirbus, G. Vereb, A. Dombi. Comparison of the Substrate Dependent Performance of Pt-, Au- and Ag-doped TiO<sub>2</sub> Photocatalysts in H<sub>2</sub>-production and in Decomposition of Various Organics. *React. Kinet. Catal. Lett.* **2009**, 98, 215.
69. T. Chen, Z. Feng, G. Wu, J. Shi, G. Ma, P. Ying, C. Li. Mechanistic Studies of Photocatalytic Reaction of Methanol for Hydrogen Production on Pt/TiO<sub>2</sub> by in situ Fourier Transform IR and Time-resolved IR Spectroscopy. *J. Phys. Chem. C* **2007**, 111, 22, 8005–8014.
70. B. Kraeutler, A.J. Bard. Heterogeneous Photocatalytic Preparation of Supported Catalysts. Photodeposition of Platinum on Titanium Dioxide Powder and Other Substrates. *J. Am. Chem. Soc.* **1978**, 100, 4317–4318.
71. K. Matsubara, M. Inoue, H. Hagiwara, T. Abe. Photocatalytic Water Splitting over Pt-loaded TiO<sub>2</sub> (Pt/TiO<sub>2</sub>) Catalysts Prepared by the Polygonal Barrel-sputtering Method. *Appl. Catal. B: Environ.* **2019**, 254, 7–14.
72. B. Banerjee, V. Amoli, A. Maurya, A. K. Sinha, A. Bhaumik. Green Synthesis of Pt-doped TiO<sub>2</sub> Nanocrystals with Exposed (001) Facets and Mesoscopic Void Space for Photo-splitting of Water under Solar Irradiation. *Nanoscale* **2015**, 23.

73. O. Fontelles-Carceller, M.J. Muñoz-Batista, E. Rodríguez-Castellón, J.C. Conesa, M. Fernández-García, A. Kubacka. Measuring and Interpreting Quantum Efficiency for Hydrogen Photo-production using Pt-titania Catalysts. *J. Catal.* **2017**, 347, 157–169.
74. K. Hashimoto, T. Kawai, T. J. Sakata. Photocatalytic Reactions of Hydrocarbons and Fossil Fuels with Water. Hydrogen production and Oxidation. *Phys. Chem.* **1984**, 88, 4083.
75. S.Y. Moon, E.H. Gwag, J.Y. Park. Hydrogen Generation on Metal/Mesoporous Oxides: The Effects of Hierarchical Structure, Doping, and Co-catalysts. *Energy Technol.* **2018**, 6, 459–469.
76. S. M. Sze, K. K. Ng. *Physics of Semiconductor Devices*, 3rd Ed. Wiley, **2007**, 135.
77. A.L. Linsebigler, G. Lu, J.T. Yates Jr. Photocatalysis on TiO<sub>2</sub> Surfaces: Principles, Mechanisms, and Selected Results. *Chem. Rev.* **1995**, 95, 735–758.
78. R. Tung. Schottky-barrier Formation at Single-crystal Metal-semiconductor Interfaces. *Phy. Rev. Lett.* **1984**, 52, 461.
79. S.Y. Moon, B. Naik, K. An, S.M. Kim, J.Y. Park. Photocatalytic H<sub>2</sub> Generation on Macro-mesoporous Oxide-supported Pt Nanoparticles. *RSC Adv.* **2016**, 6, 18198.
80. B. Herbert, J. Michaelson. The Work Function of the Elements and its Periodicity. *J. Appl. Phys.* **1977**, 48, 4729–4733.
81. Y. H. Li, J. Xing, Z. J. Chen, Z. Li, F. Tian, L. R. Zheng, H. F. Wang, P. Hu, H. J. Zhao, H. G. Yang. Unidirectional Suppression of Hydrogen Oxidation on Oxidized Platinum Clusters. *Nat. Commun.* **2013**, 4, 2500.
82. J. Y. Park, J. R. Renzas, B. B. Hsu, G. A. Somorjai. Interfacial and Chemical Properties of Pt/TiO<sub>2</sub>, Pd/TiO<sub>2</sub>, and Pt/GaN Catalytic Nanodiodes Influencing Hot Electron Flow. *J. Phys. Chem. C* **2007**, 111, 15331–15336.
83. ES. Bardos, H. Czili, A. Horvath. Photocatalytic Oxidation of Oxalic Acid Enhanced by Silver Deposition on a TiO<sub>2</sub> Surface. *J. Photochem. Photobiol. A: Chem.* **2003**, 154, 195–201.

84. M. Anpo, M. Takeuchi. The Design and Development of Highly Reactive Titanium Oxide Photocatalysts Operating under Visible Light Irradiation. *J. Catal.* **2003**, 216, 505–516.
85. W. T. Chen, A. Chan, D. S. Waterhouse, T. Moriga, H. Idriss, G. I. Waterhouse, Ni/TiO<sub>2</sub>: A Promising Low-cost Photocatalytic System for Solar H<sub>2</sub> Production from Ethanol–water Mixtures. *J. Catal.* **2015**, 326, 43–53.
86. H. Zhang, G. Chen, D.W. Behnemann. Photo-electrocatalytic Materials for Environmental Applications. *J. Mater. Chem.* **2009**, 19, 5089–5121.
87. J. Ouyang, M. Chang, X. Li. CdS-sensitized ZnO Nanorod Arrays Coated with TiO<sub>2</sub> Layer for Visible Light Photo-electrocatalysis. *J. Mater. Sci.* **2012**, 47, 4187–4193.
88. K. Vinodgopal, P.V. Kamat. Enhanced Rates of Photocatalytic Degradation of an Azo Dye using SnO<sub>2</sub>/TiO<sub>2</sub> Coupled Semiconductor Thin Films. *Environ. Sci. Technol.* **1995**, 29, 841–845.
89. F. Riboni, L.G. Bettini, D.W. Bahnemann, E. Selli. WO<sub>3</sub> – TiO<sub>2</sub> vs. TiO<sub>2</sub> Photocatalysts: Effect of the W Precursor and Amount on the Photocatalytic Activity of Mixed Oxides. *Catal. Today* **2013**, 209, 28–34.
90. A. Hagfeldt, M. Graetzel. Light-induced Redox Reactions in Nanocrystalline Systems. *Chem. Rev.* **1995**, 95, 49–68.
91. W. Zhou, H. Liu, J. Wang, D. Liu, G. Du, J. Cui. Ag<sub>2</sub>O / TiO<sub>2</sub> Nanobelts Heterostructure with Enhanced Ultraviolet and Visible Photocatalytic Activity. *ACS Appl. Mater. Interfaces* **2010**, 2(8), 2385–2392.
92. R. Marschall. Semiconductor Composites: Strategies for Enhancing Charge Carrier Separation to Improve Photocatalytic Activity. *Adv. Funct. Mater.* **2014**, 24, 2421–2440.
93. P. Zhou, J. G. Yu, M. Jaroniec. All - Solid - State Z - Scheme Photocatalytic Systems. *Adv. Mater.* **2014**, 26, 4920–4935.
94. D. Robert. Photosensitization of TiO<sub>2</sub> by M<sub>x</sub>O<sub>y</sub> and M<sub>x</sub>S<sub>y</sub> Nanoparticles for Heterogeneous Photocatalysis Applications. *Catal. Today* **2007**, 122, 20–26.



95. V. Keller, F. Garin. Photocatalytic Behavior of a New Composite Ternary System:  $\text{WO}_3/\text{SiC} - \text{TiO}_2$ . Effect of the Coupling of Semiconductors and Oxides in Photocatalytic Oxidation of Methyl ethyl ketone in the Gas Phase. *Catal. Commun.* **2003**, 4, 377–83.
96. H. Wang, Z. Wu, Y. Liu, Z. J. Sheng. The Characterization of ZnO–anatase–rutile Three-component Semiconductor and Enhanced Photocatalytic Activity of Nitrogen Oxides. *Mol. Catal. A: Chem.* **2008**, 287, 176–181.
97. M. Ge, C. Guo, X. Zhu, L. Ma, Z. Han, W. Hu, Y. Wang. Photocatalytic Degradation of Methyl Orange using ZnO/TiO<sub>2</sub> Composites. *Front. Environ. Sci. Eng.* **2009**, 3, 271–280.
98. J. S. Jang, W. Li, S. H. Oh, J. S. Lee. Fabrication of CdS/TiO<sub>2</sub> Nano-bulk Composite Photocatalysts for Hydrogen Production from Aqueous H<sub>2</sub>S Solution under Visible Light. *Chem. Phys. Lett.* **2006**, 425, 278–282.
99. A.H. Zyoud, N. Zaatar, I. Saadeddin, C. Ali, D. Park, G. Campet, H.S. Hilal. CdS-sensitized TiO<sub>2</sub> in Phenazopyridine Photo-degradation: Catalyst Efficiency, Stability, and Feasibility Assessment. *J. Hazard. Mater.* **2010**, 173, 318–325.
100. H.T. Ren, Q. Yang. Fabrication of Ag<sub>2</sub>O/TiO<sub>2</sub> with Enhanced Photocatalytic Performances for Dye Pollutants Degradation by a pH-induced Method. *Appl. Surf. Sci.* **2017**, 396, 530–538.
101. X. Hu, X. Liu, J. Tian, Y. Li, H. Cui. Towards Full-Spectrum (UV, Visible, and Near-infrared) Photocatalysis: Achieving an All-solid-state Z-scheme between Ag<sub>2</sub>O and TiO<sub>2</sub> using Reduced Graphene Oxide as the Electron Mediator. *Catal. Sci. Technol.* **2017**, 7, 4193–4205.
102. J. Gou, Q. Ma, X. Deng, Y. Cui, H. Zhang, X. Cheng, X. Li, M. Xie, Q. Cheng. Fabrication of Ag<sub>2</sub>O/TiO<sub>2</sub>-Zeolite Composite and its Enhanced Solar Light Photocatalytic Performance and Mechanism for Degradation of Norfloxacin. *Chem. Eng. J.* **2017**, 308, 818–826.
103. A. Kaur, D.B. Salunke, A. Umar, S.K. Mehta, A.S.K. Sinha, S.K. Kansal. Visible Light Driven Photocatalytic Degradation of Fluoroquinolone Levofloxacin Drug

- using Ag<sub>2</sub>O / TiO<sub>2</sub> Quantum Dots: A Mechanistic Study and Degradation Pathway. *New J. Chem.* **2017**, 41, 12079–12090.
104. B. Liu, L. Mu, B. Han, J. Zhang, H. Shi. Fabrication of TiO<sub>2</sub>/Ag<sub>2</sub>O heterostructure with Enhanced Photocatalytic and Antibacterial Activities under Visible Light Irradiation. *Appl. Surf. Sci.* **2017**, 396, 1596–1603.
105. H. Hua, Y. Xi, Z. Zhao, X. Xie, C. Hu, H. Liu. Gram-scale Wet Chemical Synthesis of Ag<sub>2</sub>O / TiO<sub>2</sub> Aggregated Sphere Heterostructure with High Photocatalytic Activity. *Mater. Lett.* **2013**, 91, 81–83.
106. C. Wang, X. Cai, Y. Chen, Z. Cheng, X. Luo, S. Mo, L. Jia, R. Shu, P. Lin, Z. Yang. Efficient Hydrogen Production from Glycerol Photoreforming over Ag<sub>2</sub>O - TiO<sub>2</sub> Synthesized by a Sol-gel Method. *Int. J. Hydrog. Energy* **2017**, 42, 17063–17074.
107. K.K. Mandari, B.S. Kwak, A.K.R. Police, M. Kang. In-situ Photo-reduction of Silver Particles and their SPR Effect in Enhancing the Photocatalytic Water Splitting of Ag<sub>2</sub>O/TiO<sub>2</sub> Photocatalysts under Solar Light Irradiation: A Case Study. *Mater. Res. Bull.* **2017**, 95, 515–524.
108. C. Hao, W. Wang, R. Zhang, B. Zou, H. Shi. Enhanced Photoelectrochemical Water Splitting with TiO<sub>2</sub>@Ag<sub>2</sub>O Nanowire Arrays via p-n Heterojunction Formation. *Sol. Energy Mater. Sol. Cells* **2018**, 174, 132–139.
109. B. Roose, S. Pathak, U. Steiner. Doping of TiO<sub>2</sub> for Sensitized Solar Cells. *Chem. Soc. Rev.* **2015**, 44, 8326–8349.
110. C. M. Teh, A. R. Mohamed. Role of Titanium Dioxide and Ion Doped Titanium Dioxide on Photocatalytic Degradation of Organic Pollutants (Phenol Compounds and Dyes) in Aqueous Solutions: A Review. *J. Alloys Compd.* **2011**, 509, 1648–1660.
111. S. Kment, H. Kmentova, P. Kluson, J. Krysa, Z. Hubicka, V. Cirkva, I. Gregora, O. Solcova, L. Jastrabik. Notes on the Photoinduced Characteristics of Transition Metal-doped and Undoped Titanium Dioxide Thin Films. *J. Colloid Interface Sci.* **2010**, 348, 198–205.

- 112.A. Di Paola, E. Garcia-Lopez, S. Ikeda, G. Marc, B. Ohtani, L. Palmisano, Photocatalytic Degradation of Organic Compounds in Aqueous Systems by Transition Metal-doped Polycrystalline TiO<sub>2</sub>. *Catal. Today* **2002**, 75, 87–93.
- 113.MI. Litter. Heterogeneous Photocatalysis Transition Metal Ions in Photocatalytic Systems. *Appl. Catal. B: Environ.* **1999**, 23, 89–114.
- 114.D. Dvoranova, V. Brezova, M. Mazur, M. Malati. Investigations of Metal-doped Titanium Dioxide Photocatalysts. *Appl. Catal. B: Environ.* **2002**, 37, 91–105.
- 115.H. Kisch, L. Zang, C. Lange, W. F. Maier, C. Antonius, D. Meissner. Modified Amorphous Titania. A Hybrid Semiconductor for Detoxification and Current Generation by Visible Light. *Angew. Chem. Int. Ed.* **1998**, 37, 3034–3036.
- 116.A. Hameed, MA. Gondal, ZH. Yamani. Effect of Transition Metal Doping on Photocatalytic Activity of WO<sub>3</sub> for Water Splitting under Laser Illumination: Role of 3d-orbitals. *Catal. Commun.* **2004**, 5, 715–719.
- 117.A. Di Paola, G. Marci, L. Palmisano, M. Schiavello, K. Uosaki, S. Ikeda, *et al.* Preparation of Polycrystalline TiO<sub>2</sub> Photocatalysts Impregnated with Various Transition Metal Ions: Characterization and Photocatalytic Activity for Degradation of 4-nitrophenol. *J. Phys. Chem. B* **2002**, 106, 637–645.
- 118.K. Wilke, HD. Breuer. The Influence of Transition Metal Doping on the Physical and Photocatalytic Properties of Titania. *J. Photochem. Photobiol. A: Chem.* **1999**, 121(1), 49–53.
- 119.A.W. Xu, Y. Gao, HQ. Liu. The Preparation Characterization and their Photocatalytic Activities of Rare Earth Doped TiO<sub>2</sub> Nanoparticles. *J. Catal.* **2002**, 207, 151–157.
- 120.Z.M. El-Bahy, A.A. Ismail, R.M. Mohamed. Enhancement of Titania by Doping Rare Earth for Photodegradation of Organic Dye (Direct Blue). *J. Hazard. Mater.* **2009**, 166, 138–143.
- 121.R. Wang, J.H. Xin, Y. Yang, H. Liu, L. Xu, J. Hu. The Characteristics and Photocatalytic Activities of Silver Doped ZnO Nanocrystallites. *Appl. Surf. Sci.* **2004**, 227, 312–317.

122. J.W. Yoon, T. Sasaki, N. Koshizaki. Dispersion of Nanosized Noble Metals in TiO<sub>2</sub> Matrix and their Photoelectrode Properties. *Thin Solid Films* **2005**, 483, 276–282.
123. Y. J. Choi, Z. Seeley, A. Bandyopadhyay, S. Bose, S.A. Akbar. Aluminium-doped TiO<sub>2</sub> Nano-powders for Gas Sensors. *Sens. Actuators B. Chem.* **2007**, 124, 111–117.
124. L.E. Depero, A. Marino, B. Allieri, E. Bontempi, L. Sangaletti, C. Casale, M. Notaro. Morphology and Microstructural Properties of TiO<sub>2</sub> Nanopowders Doped with Trivalent Al and Ga Cations. *J. Mater. Res.* **2000**, 15, 2080–2086.
125. S. Sakthivel, M. Janczarek, H. Kisch. Visible Light Activity and Photoelectrochemical Properties of Nitrogen-doped TiO<sub>2</sub>. *J. Phys. Chem. B* **2004**, 108, 19384–19387.
126. S. Martha, P.C. Sahoo, K. Parida. An overview on Visible Light Responsive Metal Oxide Based Photocatalysts for Hydrogen Energy Production. *RSC Adv.* **2015**, 5, 61535–61553.
127. W. Choi, A. Termin, M. R. Hoffmann. Effects of Metal Ion Dopants on the Photocatalytic Reactivity of Quantum Sized TiO<sub>2</sub> Particles. *Angew. Chem. Int. Ed.* **1994**, 33(10), 1091–1092.
128. K.E. Karakitsou, X.E. Verykios. Effects of Altrivalent Cation Doping of TiO<sub>2</sub> on its Performance as a Photocatalyst for Water Cleavage. *J. Phys. Chem.* **1993**, 97, 1184–1189.
129. J.Z. Bloh, R. Dillert, D.W. Bahnemann. Designing Optimal Metal-doped Photocatalysts: Correlation between Photocatalytic Activity, Doping Ratio, and Particle Size. *J. Phys. Chem. C* **2012**, 116(48), 25558–25562.
130. J. Z. Bloh, A. Folli. D. E. Macphee. Adjusting Nitrogen Doping Level in Titanium Dioxide by Codoping with Tungsten: Properties and Band Structure of the Resulting Materials. *J. Phys. Chem. C.* **2014**, 118, 36, 21281–21292.
131. G. Blasse, G. J. Dirksen, P. H. M. Dekorte. Materials with Cationic Valence and Conduction Bands for Photoelectrolysis of Water. *Mater. Res. Bull.* **1981**, 16, 991–998.

132. B. Naik, K.M. Parida, C.S. Gopinath. Facile Synthesis of N- and S-incorporated Nanocrystalline TiO<sub>2</sub> and Direct Solar-light-driven Photocatalytic Activity. *J. Phys. Chem. C* **2010**, 114, 19473–19482.
133. S. Peng, Y. Li, F. Jiang, G. Lu, S. Li. Effect of Be<sup>2p</sup> Doping TiO<sub>2</sub> on its Photocatalytic Activity. *Chem. Phys. Lett.* **2004**, 398(1–3), 235–239.
134. T. Umebayashi, T. Yamaki, H. Itoh, K. Asai. Band Gap Narrowing of Titanium Dioxide by Sulfur Doping. *Appl. Phys. Lett.* **2002**, 81(3), 454–456.
135. L. Gao, Y. Li, J. Ren, S. Wang, R. Wang, G. Fu, Y. Hu. Passivation of Defect States in Anatase TiO<sub>2</sub> Hollow Spheres with Mg Doping: Realizing Efficient Photocatalytic Overall Water Splitting. *Appl. Catal. B: Environ.* **2017**, 202, 127–133.
136. L. Clarizia, I. Di Somma, L. Onotri, R. Andreozzi, R. Marotta. Kinetic Modeling of Hydrogen Generation over Nano- Cu<sub>(s)</sub> / TiO<sub>2</sub> Catalyst through Photoreforming of Alcohols. *Catal. Today* **2017**, 281, 117–123.

## Chapter 2. Ag/Ag<sub>2</sub>O as a Co-Catalyst in TiO<sub>2</sub> Photocatalysis: Effect of the Co-Catalyst/Photocatalyst Mass Ratio

### 2.1. Foreword

Nanostructured oxides have been widely used in many industrial fields. Amongst these oxides silver oxide, Ag<sub>2</sub>O NPs, have drawn recently momentous attention owing to their unique properties such as their excellent visible-light absorption ability, innocuous nature, high abundance, and low cost. However, due to its photosensitive nature and instability under light irradiation, Ag<sub>2</sub>O is often employed as the main photocatalytic material besides acting as a co-catalyst. Nevertheless, Ag<sub>2</sub>O as a co-catalyst has shown high potential to promote the reduction reaction forming metallic silver Ag(0) on its surface. Accordingly, several reports have suggested a self-stabilization of Ag<sub>2</sub>O by the electron transfer from the excited Ag<sub>2</sub>O to Ag(0). Besides, the photoactivity of Ag<sub>2</sub>O comprising materials has been found to reduce after recycling. Thus, in this Chapter, the stability of Ag<sub>2</sub>O was investigated using X-ray powder diffraction (XRD) and X-ray photoelectron spectroscopy (XPS) before and after the photocatalytic degradation of MB used as a probe compound, along with the H<sub>2</sub> evolution using methanol as a sacrificial reagent.

This Chapter covers the article entitled “Ag/Ag<sub>2</sub>O as a Co-Catalyst in TiO<sub>2</sub> Photocatalysis: Effect of the Co-Catalyst/Photocatalyst Mass Ratio” by Soukaina Akel, Ralf Dillert, Narmina O. Balayeva, Redouan Boughaled, Julian Koch, Mohammed El Azzouzi, and Detlef W. Bahnemann, published in *Catalysts*, 2018, 8, 647; doi: 10.3390/catal8120647. Herein, pure Ag/Ag<sub>2</sub>O was synthesized through a precipitation method using AgNO<sub>3</sub> and NaOH. Mixtures of Ag/Ag<sub>2</sub>O // TiO<sub>2</sub>, and composites of Ag/Ag<sub>2</sub>O // TiO<sub>2</sub> were prepared with mixing solutions of TiO<sub>2</sub> (P25) and Ag/Ag<sub>2</sub>O by sonication, and using an in-situ precipitation method, respectively to evaluate the effect of the synthetic method on the photocatalytic activity of the samples. The effect of the mass ratio of Ag/Ag<sub>2</sub>O in Ag/Ag<sub>2</sub>O // TiO<sub>2</sub> mixtures (TM) and composites (TC) was also studied by changing the calculated amount of AgNO<sub>3</sub> corresponding to 20%, 50%,

and 80% of Ag/Ag<sub>2</sub>O. XRD and XPS investigations conducted on the fresh mechanically and chemically prepared materials and of those taken after 2 runs of the bleaching of MB revealed that the Ag(I) was reduced during the light-induced bleaching reaction of MB in the presence of mixtures and composites yielding Ag(0). A self-stabilization of Ag<sub>2</sub>O by metallic silver, as claimed by some authors, was not observed in this study. The as-prepared mixtures and composites showed enhanced visible light activity for MB bleaching, compared to bare TiO<sub>2</sub>, and high photocatalytic H<sub>2</sub> generation from methanol oxidation under artificial solar light illumination. However, the MB bleaching rate was lower over the composites and mixtures than that calculated for pure Ag/Ag<sub>2</sub>O. This was due to the electron transfer inhibition from the excited MB to Ag/Ag<sub>2</sub>O caused by TiO<sub>2</sub> layers. Flatband potential measurements confirm that Ag<sub>2</sub>O was not able to transfer an electron neither to dissolved O<sub>2</sub> nor to H<sup>+</sup>. Thus, Ag<sup>+</sup> is reduced to Ag(0) in the current investigation.

## 2.2. Abstract

Mixtures and composites of Ag/Ag<sub>2</sub>O and TiO<sub>2</sub> (P25) with varying mass ratios of Ag/Ag<sub>2</sub>O were prepared, employing two methods. Mechanical mixtures (TM) were obtained by the sonication of a suspension containing TiO<sub>2</sub> and Ag/Ag<sub>2</sub>O. Composites (TC) were prepared by a precipitation method employing TiO<sub>2</sub> and AgNO<sub>3</sub>. XRD and XPS confirmed the presence of Ag(0) and Ag<sub>2</sub>O. The activity of the materials was determined by employing MB as the probe compound. Bleaching of MB was observed in the presence of all materials. The bleaching rate was found to increase with increasing amounts of TiO<sub>2</sub> under UV-vis-light. In contrast, the MB bleaching rate decreased with increasing TiO<sub>2</sub> content upon visible light illumination. XRD and XPS data indicate that Ag<sub>2</sub>O acts as an electron acceptor in the light-induced reaction of MB and is transformed by the reduction of Ag<sup>+</sup>, yielding Ag(0). As a second light-induced reaction, the evolution of molecular hydrogen from aqueous methanol was investigated. Significant H<sub>2</sub> evolution rates were only determined in the presence of materials containing more than 50 mass% of TiO<sub>2</sub>. The experimental results suggest

that Ag/Ag<sub>2</sub>O is not stable under the experimental conditions. Therefore, to address Ag/Ag<sub>2</sub>O as a (photo)catalytically active material does not seem appropriate.

**Keywords:** photocatalysis; silver (II) oxide; titanium dioxide; mechanical mixture; in situ deposition; hydrogen evolution.

### 2.3. Introduction

Environmental problems related to water and air contamination, due to the increasing world population and the resulting tremendous growth of industry and fuel combustion, have become a major concern of advanced science. In order to deal with this important problem, photocatalytic processes with employment of semiconductors are the most conventional approaches for water and air purification, along with alternative energy storage (e.g., H<sub>2</sub>) [1–4].

To date, different semiconductor NPs such as TiO<sub>2</sub>, ZnO, Fe<sub>2</sub>O<sub>3</sub>, niobates, tantalates, and metal sulfides, and their underlying working mechanisms, have been investigated with the aim of increasing their photocatalytic activity. It is well known that, besides the ability to decontaminate polluted air and water, a photocatalyst should meet certain requirements such as cost efficiency, stability, non-toxicity, and broad range response towards incident light. TiO<sub>2</sub> is reported as the most durable photocatalyst, responding to all the above-mentioned requirements apart from broad range response to incident solar light due to its wide bandgap energy, (3.2 eV for anatase, 3.0 eV for rutile) which accounts for no more than 5% of the entire solar spectrum [1]. This lack of photocatalytic activity under visible light illumination allows the use of TiO<sub>2</sub> as a UV blocker in sunscreens [5]. The tremendous interest in modification of titanium dioxide with different metals and oxides, to enable absorption of lower energy states and increase stability, has been rising over the last 20 years. Nonetheless, the range of visible-light photocatalysts is still restricted. Thus, it is essential to discover new and efficient photocatalytic materials that are sensitive to visible light.



Ag<sub>2</sub>O NPs have been broadly utilized in various manufacturing areas as stabilizers, cleaning agents, electrode supplies, dyes, antioxidants, and catalysts for alkane activation and olefin [6, 7]. Several papers have been published reporting the photocatalytic activity of Ag<sub>2</sub>O, Ag / Ag<sub>2</sub>O, Ag<sub>2</sub>O /semiconductors, and Ag/Ag<sub>2</sub>O/semiconductor composites, and some reviews are available [8–33]. Ag<sub>2</sub>O is reported to be a visible light active photocatalyst. However, due to its photosensitive and labile properties under incident light illumination, Ag<sub>2</sub>O is infrequently employed alone as a main photocatalyst rather than as a co-catalyst [8].

Wang *et al.* investigated the photocatalytic performance of Ag<sub>2</sub>O on the photocatalytic decolorization of methyl orange, rhodamine B, and phenol solution under fluorescent light irradiation, and concluded that the stability and high photocatalytic activity of Ag<sub>2</sub>O are maintained by the partial formation of metallic Ag on its surface during the photodecomposition of organic compounds [9]. Jiang *et al.* also reported the decomposition of methyl orange under visible light, ultraviolet light, near-infrared (NIR) light, and sunlight irradiation, using silver oxide nanoparticle aggregation. The superb photo-oxidation performance of Ag<sub>2</sub>O is kept almost constant after repeated exposure to light due to its narrow band gap, high surface area, and numerous crystal boundaries supplied by Ag<sub>2</sub>O quantum dots [13]. Several authors have claimed that an Ag/Ag<sub>2</sub>O structure exhibits ‘self-stability’ [9, 10] during a photocatalytic run, due to rapid electron transfer from the excited Ag<sub>2</sub>O to Ag(0) [12, 20].

Visible light active nanocomposites of Ag/Ag<sub>2</sub>O/TiO<sub>2</sub> have been synthesized using different methods, such as a microwave-assisted method [28], a low-temperature hydrothermal method [32], a one-step solution reduction process in the presence of potassium borohydride [22], a simple pH-mediated precipitation [23], and a sol-gel method [27]. Moreover, Su *et al.* developed a novel multilayer photocatalytic membrane, consisting of an Ag<sub>2</sub>O / TiO<sub>2</sub> layer stacked on a chitosan sub-layer immobilized onto a polypropylene [31]. Light-induced hydrogen production via photoreforming of aqueous glycerol has been scrutinized, employing Ag<sub>2</sub>O/TiO<sub>2</sub>

catalysts prepared by a sol-gel method with varying content of Ag<sub>2</sub>O (0.72 – 6.75 wt %) [30]. Hao *et al.* have reported that TiO<sub>2</sub>/Ag<sub>2</sub>O nanowire arrays forming a p-n heterojunction are applicable for enhanced photo-electrochemical water splitting [33]. Hu *et al.* reported the photocatalytic degradation of tetracycline under UV, visible, NIR, and simulated solar light irradiation with the Z-scheme between visible/NIR light activated Ag<sub>2</sub>O and UV light activated TiO<sub>2</sub>, using reduced graphene oxide as the electron mediator. They also investigated the stability of Ag<sub>2</sub>O, Ag<sub>2</sub>O/TiO<sub>2</sub>, and Ag<sub>2</sub>O/TiO<sub>2</sub> in combination with reduced graphene oxide as an electron mediator. A large amount of Ag(0) was formed into Ag<sub>2</sub>O and Ag<sub>2</sub>O/TiO<sub>2</sub> after four cycles of tetracycline photodegradation under UV, visible, and NIR illumination [23]. Ren *et al.* also observed the light-induced reduction of Ag<sub>2</sub>O during dye degradation in Ag<sub>2</sub>O/TiO<sub>2</sub> suspensions. The authors suggested that the formation of Ag(0) contributed to the high stability of their photocatalyst [29]. The stabilization of Ag<sub>2</sub>O/TiO<sub>2</sub> photocatalysts by Ag(0) formed at an initial stage of an experimental run has already been proposed earlier [11]. The photocatalytic stability of Ag-bridged Ag<sub>2</sub>O nanowire networks/ TiO<sub>2</sub> nanotubes, which were fabricated by a simple electrochemical method, revealed only an insignificant loss in performance, with respect to photocatalytic degradation of the dye acid orange 7, under simulated solar light [15]. On the other hand, Kaur *et al.* reported a decrease in the degradation efficiency from 81% to 54%, after the third experimental run employing Ag<sub>2</sub>O/TiO<sub>2</sub> as the photocatalyst and the drug levofloxacin as the probe compound [24]. Very recently, Mandari *et al.* synthesized plasmonic Ag<sub>2</sub>O/TiO<sub>2</sub> photocatalysts, which could absorb visible light by the resonant oscillation of the conduction band electrons under visible light illumination. With this method, they were able to improve the efficiency of TiO<sub>2</sub> as a photocatalyst for hydrogen production by H<sub>2</sub>O splitting under natural solar light. The authors observed the formation of Ag(0) by light-induced reduction of Ag<sub>2</sub>O [26]. Light-induced reduction of Ag(I) to Ag(0) has also been reported for an Ag(0)/ Ag(I) co-doped TiO<sub>2</sub> photocatalyst [34].

The preceding discussion of published experimental results provoked doubt on the stability of Ag<sub>2</sub>O-containing photocatalysts under UV-vis illumination. Therefore, visible light-harvesting Ag/Ag<sub>2</sub>O // TiO<sub>2</sub> photocatalysts for water treatment and photocatalytic hydrogen generation were synthesized. To the best of our knowledge, physical Ag/Ag<sub>2</sub>O // TiO<sub>2</sub> mixtures synthesized by the sonication of a suspension containing TiO<sub>2</sub> (P25) and a self-prepared Ag/Ag<sub>2</sub>O were investigated for the first time. Ag/Ag<sub>2</sub>O // TiO<sub>2</sub> composites, prepared in situ by a simple precipitation method employing TiO<sub>2</sub> and AgNO<sub>3</sub>, were also prepared, in order to evaluate the effect of the synthesis method on the photocatalytic activity. Additionally, the effect of the mass ratio of Ag/Ag<sub>2</sub>O was studied. The as-prepared mixtures and composites showed improved visible light activity for MB bleaching, compared to blank TiO<sub>2</sub>, and high photocatalytic H<sub>2</sub> production from a methanol-water mixture under artificial solar light illumination.

## 2.4. Results

### 2.4.1. Characterization of the Prepared Materials

The XRD patterns of Ag/Ag<sub>2</sub>O, physical mixtures of Ag/Ag<sub>2</sub>O // TiO<sub>2</sub> with increasing amounts of TiO<sub>2</sub> (20 mass% (TM 41), 50% (TM 11), and 80% (TM 14)), and in situ prepared Ag/Ag<sub>2</sub>O // TiO<sub>2</sub> composites (20 mass% TiO<sub>2</sub> (TC 41), 50% (TC 11), and 80% (TC 14)) are shown in **Figure 2-1**. The XRD peaks for Ag/Ag<sub>2</sub>O at 26.7°, 32.8°, 38.1°, 54.9°, 65.4°, and 68.8° perfectly correlate to the (110), (111), (200), (220), (311), and (222) crystal planes of cubic Ag<sub>2</sub>O (JCPDS 41–1104). The three peaks at 44.3°, 64.7°, and 77.5° are indexed to the (200), (200), and (311) crystal planes of cubic Ag(0), respectively (JCPDS 04–0783) [35, 36].

The TiO<sub>2</sub> containing mixtures (TM) and composites (TC) exhibit diffraction peaks at 25°, 38°, 48°, 54°, 55°, 63°, 69°, 71°, 75°, and 83°, which are attributed to the tetragonal phase of anatase TiO<sub>2</sub>, whereas one peak at 27.8° corresponds to the tetragonal phase of rutile TiO<sub>2</sub>. **Figure 2-1 (a)** presents the patterns of the TM mixtures, where two phases of titania were present. The two strongest peaks of Ag<sub>2</sub>O become more prominent, with the Ag<sub>2</sub>O mass ratio increasing from TM 14 to TM 41. The small

diffraction peaks situated at 44.4°, 64.2°, and 77.5° are indexed to the (200), (200), and (311) plane of metallic Ag(0) (JCPDS 04–0783) [20]. The strongest peak of Ag(111) might likely be masked by the TiO<sub>2</sub> peak at 2 $\theta$  = 38°. The diffraction peaks in the TM mixture patterns correspond to the cubic structure of Ag<sub>2</sub>O and the cubic structure of Ag [35, 36]. **Figure 2-1 (b)** illustrates the XRD patterns of the TC composites. As the figure shows, no significant difference between the two preparations methods was observed, except that in TiO<sub>2</sub>-rich composites TC 11 and TC 14 no Ag<sub>2</sub>O diffraction peaks were observed, suggesting a complete reduction of Ag<sub>2</sub>O to metallic silver Ag(0) during the preparation of these composites. The XRD pattern of TiO<sub>2</sub> is presented for comparison. The diffractogram clearly indicates the presence of two TiO<sub>2</sub> phases with the predominance of the anatase phase (JCPDS 21–1272).

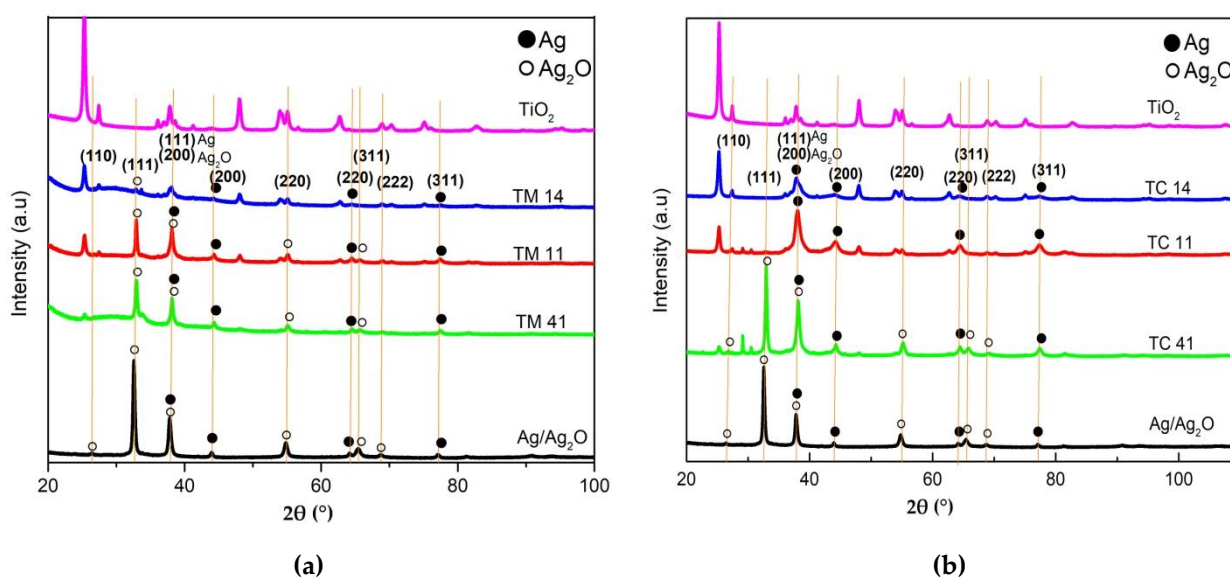


**Figure 2-1.** XRD patterns of (a) TiO<sub>2</sub> containing mixtures (TM), and (b) TiO<sub>2</sub> containing composites (TC). The diffractograms of Ag/Ag<sub>2</sub>O and TiO<sub>2</sub> are included in both figures.

In order to investigate the oxidation states of the silver species present on the materials, XPS analysis was performed and the results are shown in **Figure S2-3**. The deconvolution of the high-resolution spectra for Ag 3d reveals that silver was present in more than one oxidation state in all samples. The binding energies of Ag 3d at 367.5 and 373.5 eV are assigned to the Ag 3d<sub>5/2</sub> and Ag 3d<sub>3/2</sub> photoelectrons respectively, indicating the presence of silver in the +1 oxidation state. The other two peaks of Ag

3d<sub>5/2</sub> and Ag 3d<sub>3/2</sub>, at 368.3 and 374.3 eV respectively, confirm the existence of silver in the Ag(0) state. These binding energies are in good agreement with the values reported for Ag(I) in Ag<sub>2</sub>O and Ag(0) [16, 37, 38]. The peaks for O 1s, located in the ranges of 528.9–530.1 eV and 530.5–531.2 eV, are ascribed to O<sup>2-</sup> in Ag<sub>2</sub>O and TiO<sub>2</sub> respectively (**Figure S2-3**). From the Ti 2p core-level spectrum, two peaks at about 464.3 and 458.7 eV can be assigned to the Ti 2p<sub>1/2</sub> and Ti 2p<sub>3/2</sub> spin-orbital components respectively, which correspond to the characteristic peaks of Ti<sup>4+</sup>.

The scanning electron microscopy (SEM) images of blank TiO<sub>2</sub>, Ag/Ag<sub>2</sub>O, TM mixtures, and TC composites are presented in **Figure 2-2**. Ag/Ag<sub>2</sub>O showed well-defined particles with particle sizes ranging from 100 nm to 500 nm (**Figure 2-2 a**). The small particles that contrast as white spots correspond to the metallic silver Ag(0) distributed on the surface of silver oxide, which is in agreement with the XRD results. The energy dispersive X-ray analysis (EDX) reveals that the sample contained Ag and O without any other impurities (**Figure S2-1**).

**Figure 2-2 (b-d)** shows SEM images of the physical mixtures of Ag/Ag<sub>2</sub>O with TiO<sub>2</sub>. It becomes obvious from these images that Ag/Ag<sub>2</sub>O changed its shape during the preparation of the mixtures by sonification of aqueous suspensions of the oxides. The increasing loading of the Ag<sub>2</sub>O platelets with TiO<sub>2</sub> is also clearly recognizable in these figures. In the Ag/Ag<sub>2</sub>O//TiO<sub>2</sub> mixture with the highest mass fraction of TiO<sub>2</sub> (TM 14), the appearance was apparently determined by the titanium dioxide distributed over the underlying surface of the Ag<sub>2</sub>O platelets (**Figure 2-2 (d)**). This was also reflected in the specific surface area (SSA) of the materials. The TiO<sub>2</sub> (P25) used in this work is known to have an average diameter and specific surface area of 21 nm and about 50 m<sup>2</sup>g<sup>-1</sup>, respectively [39]. The SSA of the Ag/Ag<sub>2</sub>O synthesized in this work was determined to be 2.7 m<sup>2</sup>g<sup>-1</sup>. As expected, the SSA of the Ag/Ag<sub>2</sub>O//TiO<sub>2</sub> mixtures was found to increase with increasing TiO<sub>2</sub> content (**Table 2-1**), resulting in a SSA of 38.5 m<sup>2</sup>g<sup>-1</sup> for TM 14.

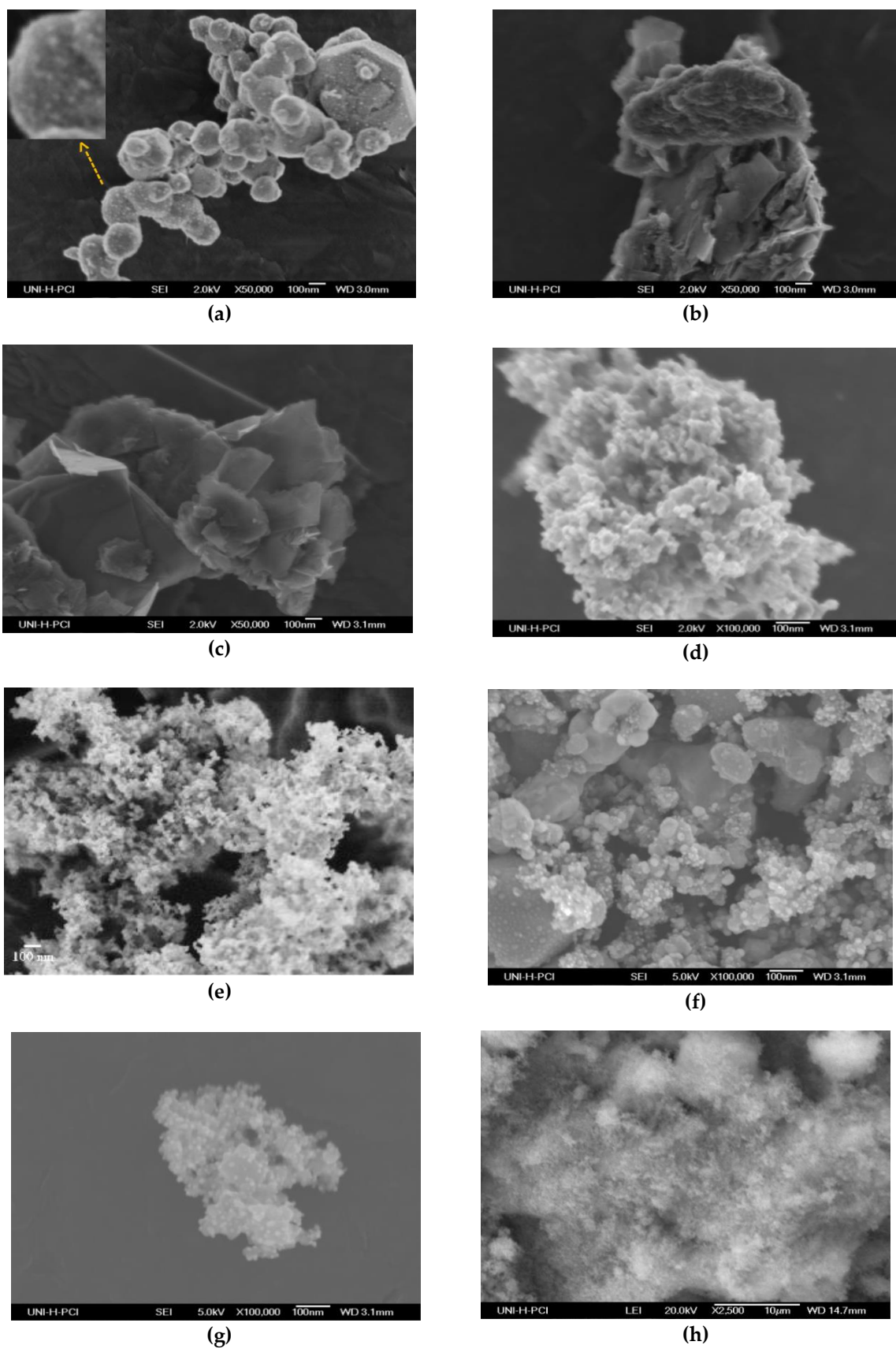


**Figure 2-2.** SEM pictures of (a) Ag/Ag<sub>2</sub>O, (b) TM 41, (c) TM 11, (d) TM 14, (e) TiO<sub>2</sub> (P25), (f) TC 41, (g) TC 11, and (h) TC 14.

SEM images of the TC composites are presented in **Figure 2 (f-h)**. The image of the TiO<sub>2</sub>-poor composite TC 41 clearly shows the large Ag/Ag<sub>2</sub>O particles covered with TiO<sub>2</sub> (**Figure 2-2 (f)**). The SSA of this composite was determined to be 8.4 m<sup>2</sup>g<sup>-1</sup>, thus being equal within the limits of the experimental error to the surface area of the corresponding physical mixture TC 41 (SSA = 9.7 m<sup>2</sup>g<sup>-1</sup>). The images of the composites richer in TiO<sub>2</sub> (TC 11 and TC 14) seemed to be dominated by aggregates or agglomerates of small TiO<sub>2</sub> particles.

The optical properties of TiO<sub>2</sub> and the as-prepared Ag-containing mixtures and composites were investigated by UV-vis diffuse reflectance spectroscopy (UV-vis DRS) (**Figure 2-3**). Ag/Ag<sub>2</sub>O, as well as the TM, and TC materials, had a dark brown to black color. They displayed strong absorption over the whole UV and visible range (200 nm – 800 nm). TiO<sub>2</sub> showed only the absorption band below 405 nm, which matches the band gap energy of 3.06 eV calculated from the formula  $\lambda = 1239.8/E_g$  due to the charge transfer from O (VB) to Ti (CB).

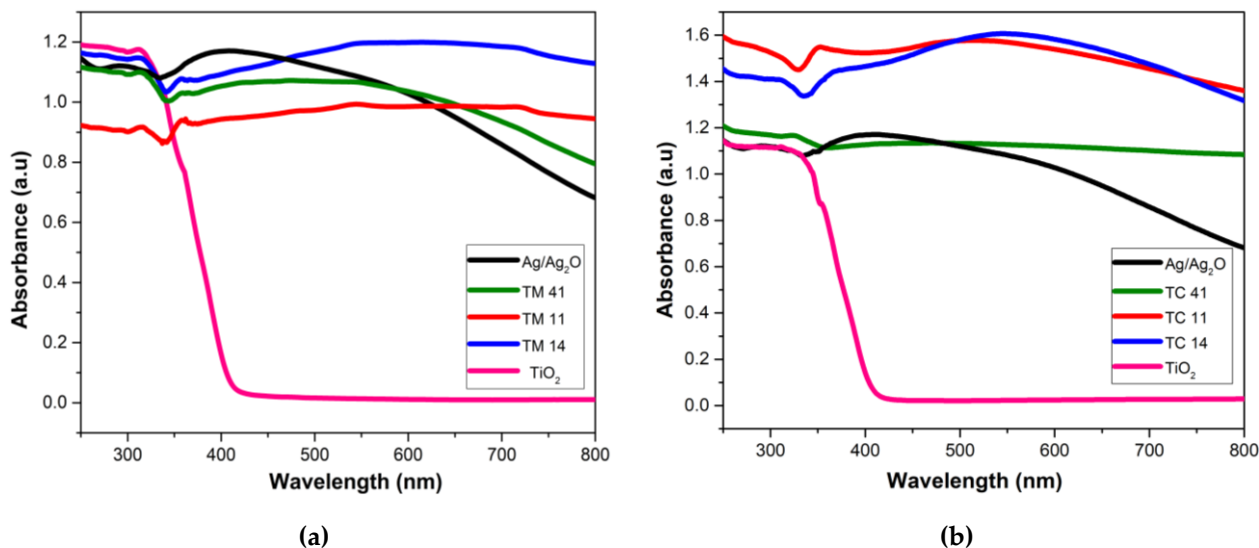


**Figure 2-3.** UV-vis diffuse reflectance spectra of (a) TiO<sub>2</sub>, Ag/Ag<sub>2</sub>O, TM mixtures, and (b) TC composites.

Ag/Ag<sub>2</sub>O exhibited a band gap energy < 1.5 eV, which is in agreement with the reported value of  $1.3 \pm 0.3$  eV [40]. The scattering of the reported values might be due to different particle diameters, as shown for TiO<sub>2</sub> [41]. Electrochemical measurements in suspensions yielded flatband potentials of -0.4 V and +0.3 V vs. NHE for TiO<sub>2</sub> and

Ag<sub>2</sub>O, respectively. The value measured here for the flatband potential of Ag<sub>2</sub>O is also in reasonably good agreement with published values [42, 43].

#### 2.4.2. Photocatalytic performance of the Materials

The photocatalytic activity of all materials described above was investigated, employing MB as the probe compound. The materials in aqueous suspensions were excited by the full output of a xenon lamp (UV-vis illumination), and by Xe light after passing a UV cut-off filter ( $\geq 410$  nm, vis illumination). **Figure 2-4** illustrates the bleaching of an aqueous solution of MB and the MB-containing suspensions. Photolysis of MB (initiated by the direct excitation of the probe compound) was observed under both UV-vis and vis-light illumination. The bleaching of MB was significantly accelerated by the presence of Ag/Ag<sub>2</sub>O. Under UV-vis illumination, Ag/Ag<sub>2</sub>O was found to be nearly as active as TiO<sub>2</sub> (P25), which is well known to be a very efficient photocatalyst suitable to degrade MB [44] (**Figure 2-4 (a)**). In the presence of Ag/Ag<sub>2</sub>O, MB was bleached very rapidly even when exposed to visible light. As expected, TiO<sub>2</sub>, having a band gap energy of 3.1 eV, was found to be inactive under vis illumination (**Figure 2-4 (c)**).

In the presence of mixtures of Ag/Ag<sub>2</sub>O with TiO<sub>2</sub>, MB was bleached under UV-vis illumination only in the presence of the TiO<sub>2</sub>-rich TM 14, with a significantly increased rate compared to the rate of MB photolysis. In suspensions containing TM 41 and TM 11, the rate of bleaching was almost the same as the rate of photolysis (**Figure 2-4 a**). Exposure to visible light in the presence of the Ag/Ag<sub>2</sub>O-rich TM 41 resulted in bleaching of MB with a slightly increased rate. In contrast, the TiO<sub>2</sub>-rich mixtures TM 11 and TM 14 were virtually inactive under this illumination condition (**Figure 2-4 (c)**).



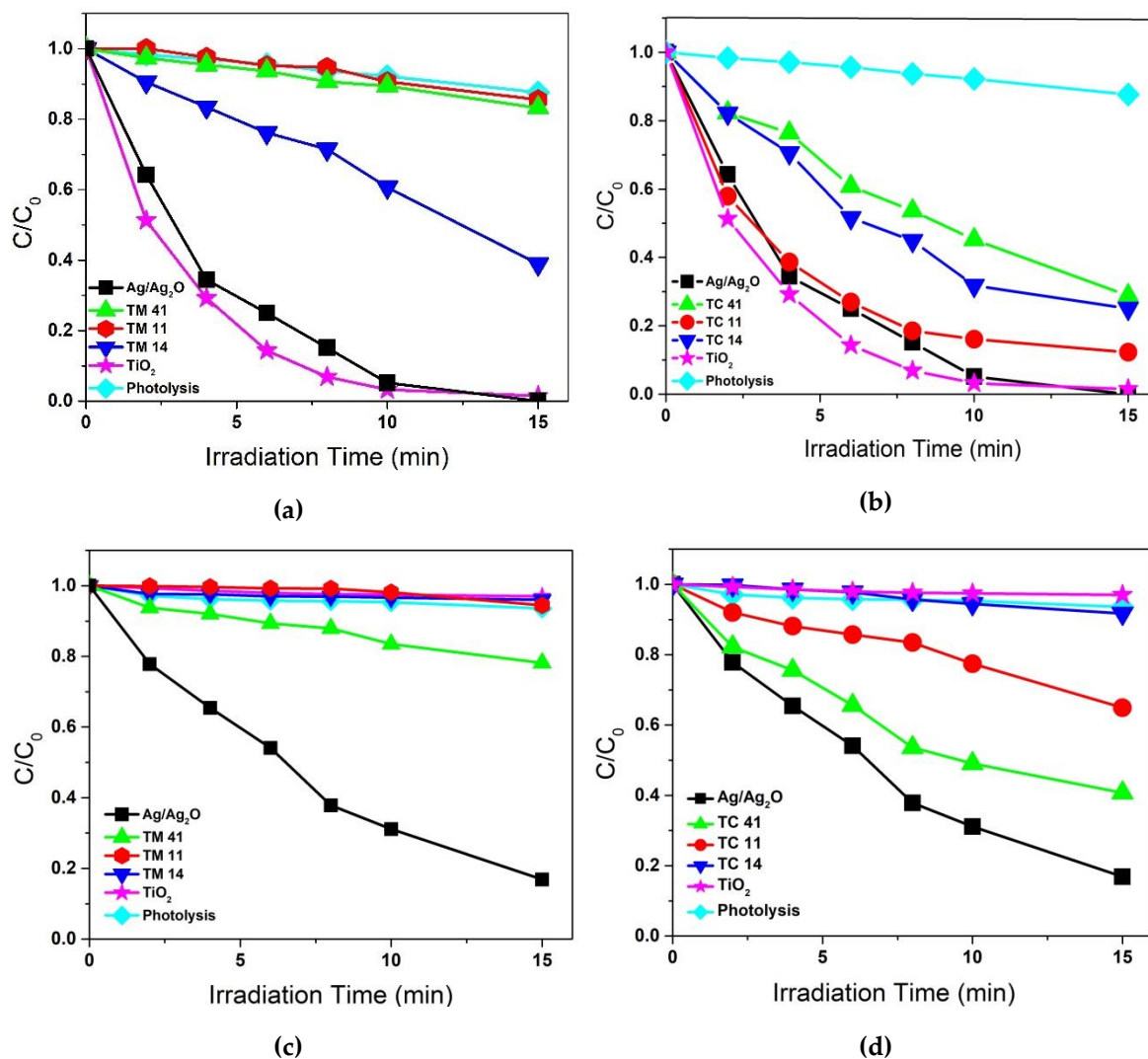


**Figure 2-4.** Bleaching of MB in the presence of Ag/Ag<sub>2</sub>O, TiO<sub>2</sub>, the TM mixtures and the TC composites under UV-vis (a,b) and under vis light only (c,d).

In the presence of the composites TC, MB was bleached with significantly faster reaction rates than the rate of photolysis when exposed to UV-vis and visible light. The rates were, however, lower than the rate of bleaching in the presence of the bare TiO<sub>2</sub> (Figure 2-4 (b, d)). Interestingly, while increasing the amount of TiO<sub>2</sub> in the TC composites, the visible light activity of the materials seemed to decrease, thus confirming the essential influence of Ag/Ag<sub>2</sub>O on MB bleaching under illumination with wavelengths  $\geq 410$  nm.

As a second test reaction for the activity of the materials, the UV-vis-light induced evolution of molecular hydrogen by reforming of aqueous methanol was used. Figure 2-5 shows the amount of H<sub>2</sub> vs. illumination time in the presence of TiO<sub>2</sub>,

Ag/Ag<sub>2</sub>O, and the prepared mixtures and composites. No H<sub>2</sub> evolution was observed in the presence of Ag/Ag<sub>2</sub>O and the Ag/Ag<sub>2</sub>O-rich TM 41. In the presence of all other materials, the evolution of H<sub>2</sub> was detected. However, large amounts of H<sub>2</sub> were only evolved with the materials TM 14 (104 μmol/6 h) and TC 11 (174 μmol/6 h).

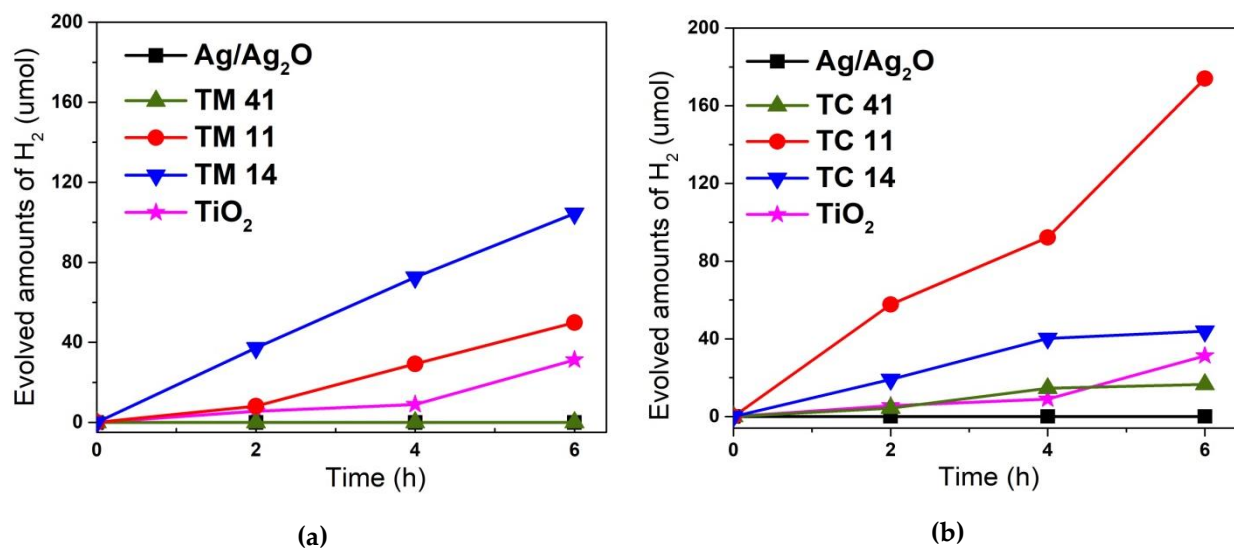


**Figure 2-5.** The amount of H<sub>2</sub> evolved from aqueous CH<sub>3</sub>OH under UV-vis illumination of Ag/Ag<sub>2</sub>O, TiO<sub>2</sub>, (a) TM mixtures, and (b) TC composites vs. illumination time.

Many authors have reported that the kinetic behavior of photocatalytic reactions can be described by a Langmuir–Hinshelwood rate law, with the two limiting cases of zero-order and first-order kinetics [45, 46]. To calculate the initial rates  $r_0$  of the bleaching of methylene blue, first-order kinetics have been assumed ( $r_0 = k C_0$ ). To determine the rate constant  $k$ , the data given in **Figure 2-4** have therefore been fitted with  $C = C_0 \exp(-kt)$ . The initial rates are given in **Table 2-1**.

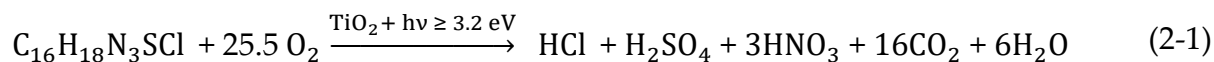
**Table 2-1.** Brunauer-Emmet-Teller (BET) surface area, initial rates of methylene blue (MB) bleaching, and H<sub>2</sub> generation in the presence of Ag/Ag<sub>2</sub>O, TiO<sub>2</sub>, the TM mixtures, and the TC composites.

Sample	Preparation Method	Composition	SSA	r <sub>0</sub> (MB)	r <sub>0</sub> (MB)	r (H <sub>2</sub> )
			m <sup>2</sup> g <sup>-1</sup>	UV-vis mg L <sup>-1</sup> min <sup>-1</sup>	vis mg L <sup>-1</sup> min <sup>-1</sup>	UV-vis μmol h <sup>-1</sup>
Photolysis	-	-	-	0.08	0.05	-
Ag/Ag <sub>2</sub> O	in situ	Ag/Ag <sub>2</sub> O	2.7	2.64	1.17	-
TM 41	mechanical mixture	Ag/Ag <sub>2</sub> O//TiO <sub>2</sub> (20% TiO <sub>2</sub> )	9.7	0.12	0.17	-
TM 11	mechanical mixture	Ag/Ag <sub>2</sub> O//TiO <sub>2</sub> (50% TiO <sub>2</sub> )	22.6	0.09	0.03	9
TM 14	mechanical mixture	Ag/Ag <sub>2</sub> O//TiO <sub>2</sub> (80% TiO <sub>2</sub> )	38.5	0.55	0.03	17
TiO <sub>2</sub>	-	TiO <sub>2</sub>	50	3.08	0.03	5
TC 41	in situ	Ag/Ag <sub>2</sub> O//TiO <sub>2</sub> (20% TiO <sub>2</sub> )	8.4	0.81	0.61	3
TC 11	in situ	Ag/Ag <sub>2</sub> O//TiO <sub>2</sub> (50% TiO <sub>2</sub> )	20.1	2.03	0.27	28
TC 14	in situ	Ag/Ag <sub>2</sub> O//TiO <sub>2</sub> (80% TiO <sub>2</sub> )	22.1	1.00	0.05	8

## 2.5. Discussion

### 2.5.1. The Photocatalytic Activity of Ag/Ag<sub>2</sub>O

It is well known that MB is photocatalytically oxidized in the presence of TiO<sub>2</sub> under illumination with photons having an energy equal to or larger than the bandgap energy of the semiconductor. The photocatalytic degradation of MB in the presence of molecular oxygen is reported to follow **Equation (2-1)** [44].



The energetic positions of the valence and conduction bands of TiO<sub>2</sub> and Ag<sub>2</sub>O, and the reduction potentials of some species (possibly) present in the surrounding electrolyte are shown in **Figure 2-6**. As becomes obvious from this Figure, the conduction band electrons generated by UV illumination of TiO<sub>2</sub> are able to reduce O<sub>2</sub> adsorbed at the semiconductor surface. From a thermodynamic point of view, valence band holes at the TiO<sub>2</sub> surface have energy suitable to oxidize H<sub>2</sub>O/OH<sup>-</sup>, yielding •OH.

These •OH are generally assumed to be the oxidizing species in photocatalytic MB degradation.

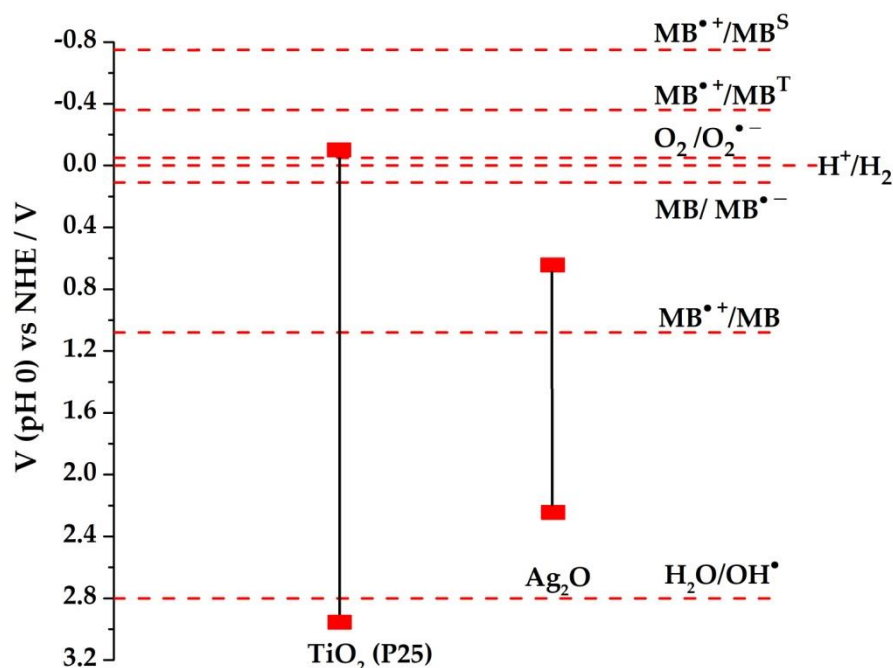


**Figure 2-6.** The electrochemical potentials (vs. NHE) of the valence and conduction bands of TiO<sub>2</sub> and Ag<sub>2</sub>O, and the reduction potentials of some species (possibly) present in the surrounding electrolyte. MB, MB<sup>•-</sup>, MB<sup>•+</sup>, MB<sup>T</sup>, and MB<sup>S</sup> denote the MB ground state, the semi-reduced MB, the oxidized MB, the excited triplet state, and the excited singlet state of MB, respectively. The one electron reduction potentials have been calculated with data given in References [44, 47, 48].

With the assumption that the flatband potential of Ag<sub>2</sub>O, which has been determined to be +0.3 V vs. NHE at pH 7, was equal to the conduction band edge of this semiconductor and a bandgap energy  $E_g = 1.5$  eV, the valence band position was calculated to be +2.0 V vs. NHE. Xu and Schoonen reported a value of +0.2 V vs. NHE for the energy of the Ag<sub>2</sub>O conduction band [49]. As becomes obvious from **Figure 2-6**, excited Ag<sub>2</sub>O was neither able to reduce O<sub>2</sub> nor to oxidize H<sub>2</sub>O/OH<sup>-</sup>. Consequently, the mechanism of MB bleaching observed in the presence of Ag/Ag<sub>2</sub>O (**Figure 2-4** and **Table 2-1**) was different from the MB degradation mechanism in the presence of TiO<sub>2</sub>. A possible explanation for the decolorization of MB in the presence of Ag/Ag<sub>2</sub>O is that MB is excited by light of suitable wavelength (Equation (2-2), MB\* = MB<sup>S</sup> and or MB<sup>T</sup>),

which is subsequently followed by electron injection into the conduction band of Ag<sub>2</sub>O (**Equation (2-3)**).



As an alternative to these reactions, the direct oxidation of MB by valence band holes according to



has to be considered. Both mechanisms require an electron transfer between Ag<sub>2</sub>O and MB. Despite the low surface area available for this reaction, the electron transfer between the solid and the probe compound appears to be very efficient.

It is well known that Ag<sub>2</sub>O is sensitive to light and decomposes under illumination. However, it has been suggested that Ag(0) being present in Ag/Ag<sub>2</sub>O acts as an electron sink and accepts the conduction band electron of Ag<sub>2</sub>O, thus inhibiting the reduction of Ag<sup>+</sup> and stabilizing the Ag<sub>2</sub>O [9, 10, 12, 20]. However, the possibility cannot be excluded that Ag<sup>+</sup> is reduced during the processes given in the **Equations (2-2) – (2-5)**, yielding Ag(0), since no other suitable electron acceptor is available. Regardless of whether the electrons reduce Ag<sup>+</sup> or become stored in Ag(0), Ag/Ag<sub>2</sub>O is not acting as a photocatalyst, because the material changes irreversibly during the reaction.

The potential of the Ag<sub>2</sub>O conduction band electron is more positive than the reduction potential of the H<sup>+</sup>/H<sub>2</sub> couple (**Figure 2-6**). Consequently, light-induced proton reduction yielding H<sub>2</sub> is thermodynamically impossible in suspensions containing only Ag/Ag<sub>2</sub>O. This is in accordance with the experimental results reported in **Section 2.4.2**.

## 2.5.2. The Photocatalytic Activity of Physical Ag/Ag<sub>2</sub>O//TiO<sub>2</sub> Mixtures

### 2.5.2.1. Bleaching of Methylene Blue

When irradiated with light at wavelengths  $\geq 410$  nm, methylene blue was found to be bleached in the presence of Ag/Ag<sub>2</sub>O, and mixtures of this material with TiO<sub>2</sub>. The rate of MB bleaching decreased with increasing amounts of TiO<sub>2</sub>. Of course, TiO<sub>2</sub> itself was found to be photocatalytically inactive, since it was not excited under this illumination condition (**Figure 2-4 (c)** and **Table 2-1**). The electron transfer reaction resulting in the observed bleaching of the MB solution occurred at the surface of the Ag<sub>2</sub>O, as discussed in **Section 2.5.1**. According to the SEM images (**Figure 2-2 (a–d)**), the surface of the Ag<sub>2</sub>O was increasingly covered by TiO<sub>2</sub> as the content of this oxide in the mixture increased. The interfacial electron transfer was inhibited by this TiO<sub>2</sub> layer (**Figure 2-7**). The reaction rates suggest that this inhibition increased with increasing amounts of TiO<sub>2</sub> on the Ag/Ag<sub>2</sub>O surface. Consequently, the TiO<sub>2</sub>-rich mixtures TM 11 and TM 14 exhibited rates of bleaching almost the same as the rate of photolysis in homogeneous solution (**Table 2-1**). Interfacial electron transfer from excited MB to TiO<sub>2</sub> (which is thermodynamically possible; cf. **Figure 2-6**) obviously did not contribute significantly, since no MB bleaching was observed under visible light illumination of suspensions containing only this photocatalyst.



**Figure 2-7.** Possible mechanism of MB bleaching by Ag<sub>2</sub>O and Ag<sub>2</sub>O-containing mixtures and composites under visible light illumination.

The situation was different when the TM mixtures were illuminated with UV-vis-light. The rate of MB bleaching in the presence of the Ag/Ag<sub>2</sub>O//TiO<sub>2</sub> mixtures was found to increase with increasing TiO<sub>2</sub> content. However, the rates were always lower than the rates determined for suspensions containing only Ag/Ag<sub>2</sub>O or bare TiO<sub>2</sub>

(**Figure 2-4 (a)** and **Table 2-1**). These rates cannot be explained solely by the optical properties of the suspensions. Of course, as the Ag/Ag<sub>2</sub>O content increases, more UV photons are absorbed by Ag<sub>2</sub>O. They are thus no longer available for the excitation of the TiO<sub>2</sub> that results in decreasing amounts of charge carriers in the TiO<sub>2</sub> and, consequently, decreasing rates of MB degradation. However, the MB bleaching rate calculated for the TiO<sub>2</sub>-rich TM 14 mixture suggests that not all photogenerated charge carriers were used in the desired MB bleaching reaction, but some were lost by reactions between excited TiO<sub>2</sub> and Ag/Ag<sub>2</sub>O, resulting in the reduction of Ag<sup>+</sup>.

XRD measurements revealed the reduction of Ag<sup>+</sup> during the light-induced bleaching of MB under UV-vis illumination. The ratios of the peak intensities corresponding to Ag<sub>2</sub>O and TiO<sub>2</sub> of the mixture TM 41 and the composite TC 41 were significantly lower after two experimental runs than before illumination (**Figure 2-8**). On the other hand, the ratios of the peak intensities attributed to metallic Ag and TiO<sub>2</sub> obviously increased. In the case of the Ag/Ag<sub>2</sub>O//TiO<sub>2</sub> mixture TM 11, apart from the TiO<sub>2</sub> peaks, the only visible XRD peaks could be assigned to AgCl and Ag(0) after illumination of a suspension containing MB (**Figure S2-2**). The new peaks in the diffractogram, which are indexed to AgCl, were possibly formed by a reaction between Ag<sup>+</sup> and Cl<sup>-</sup> known to be present at the surface of TiO<sub>2</sub> P25 [39]. This reaction certainly explains the decrease of the Ag<sub>2</sub>O peaks in the diffractogram. However, this explanation does not exclude that Ag<sub>2</sub>O is also transformed by a light-induced reduction reaction, yielding Ag(0).

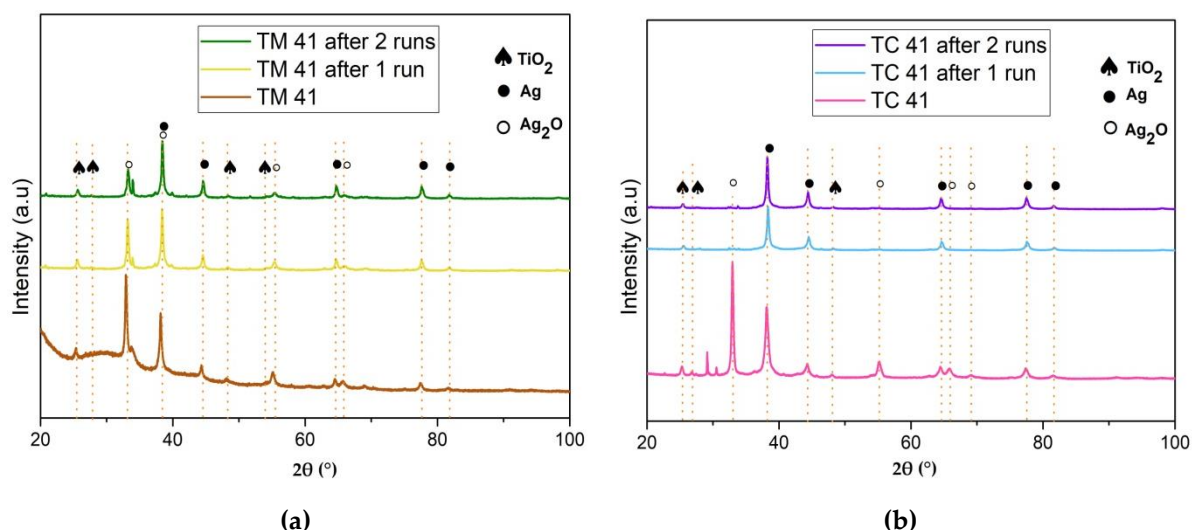


**Figure 2-8.** XRD patterns of (a) TM 41 and (b) TC 41 after two cycles of MB bleaching employing UV-vis light.

The conclusion from the XRD data, that Ag(I) was reduced yielding Ag(0) during the light-induced bleaching of MB in the presence of the mixture TM 41, is supported by the results of the analysis of XPS data taken before and after two experimental runs (**Figures 2-9 (a, b)** and **S2-3**). It becomes obvious from **Figure 2-9 (a)** that the Ag 3d<sub>5/2</sub> and Ag 3d<sub>3/2</sub> peaks of Ag<sub>2</sub>O in the mixture TM 41 decreased in intensity and broadened, while the Ag(0) 3d<sub>5/2</sub> and Ag(0) 3d<sub>3/2</sub> peaks increased in intensity after two photocatalytic reactions. Furthermore, the deconvolution of the O 1s peaks denotes that the peak corresponding to the Ag-O bond had a lower intensity compared to the same peak observed before the reaction, indicating significant changes occurred during the light-induced MB bleaching reaction (**Figure 2-9 (b)**). These changes were mainly due to the light-induced reduction of Ag<sup>+</sup> yielding Ag(0). Again, the condition of stability of a catalyst was not satisfied.



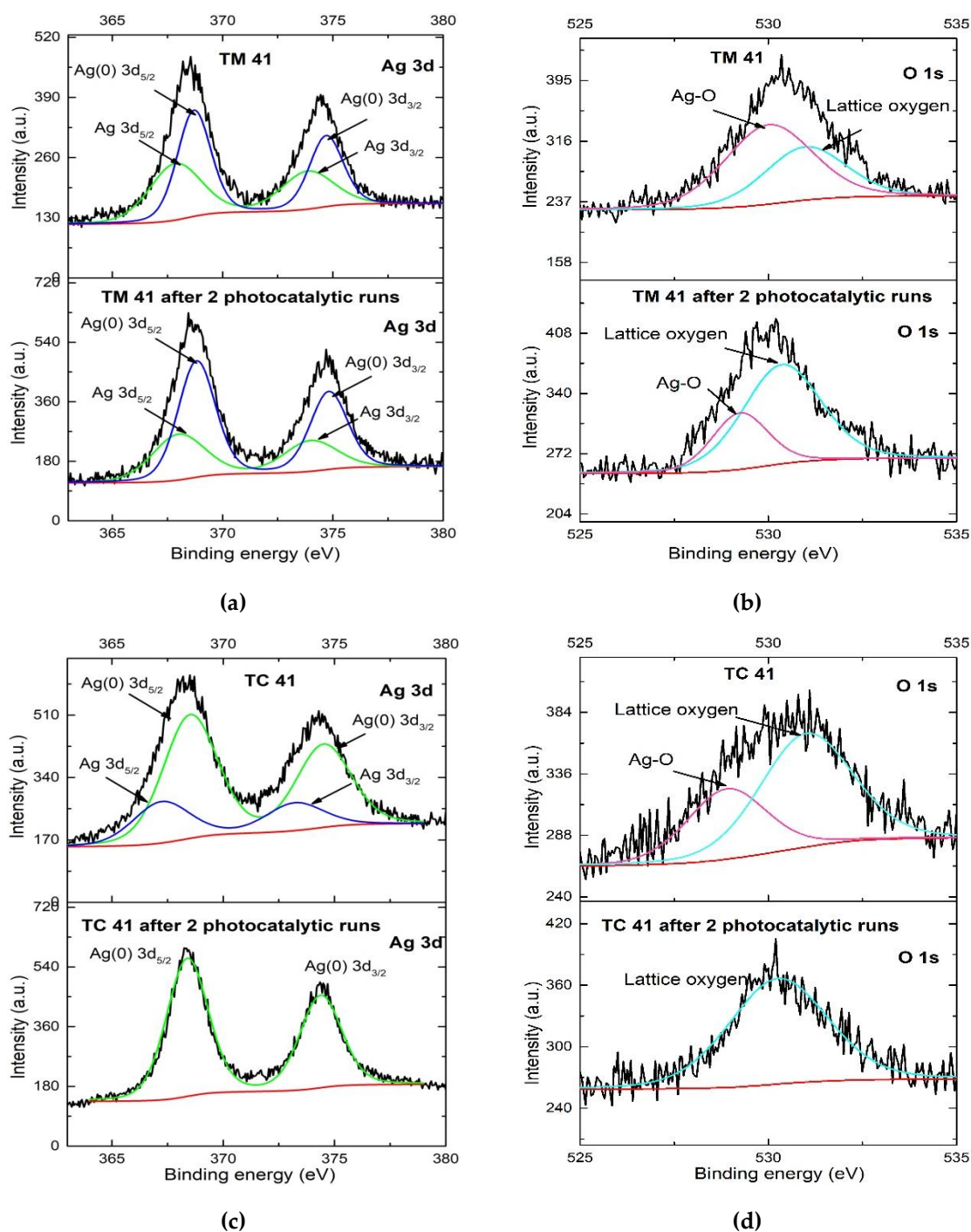


**Figure 2-9.** High-resolution XPS spectra of the Ag 3d and O 1s signals of TM 41 (a,b) and TC 41 (c,d) before and after two experimental runs.

### 2.5.2.2. Light-Induced Hydrogen Evolution

From a thermodynamic point of view, excited TiO<sub>2</sub> is able to transfer a conduction band electron to a proton present at the photocatalyst surface (Figure 2-6). This electron transfer is, however, known to be a kinetically inhibited process. Therefore, it is necessary to deposit an electrocatalyst at the TiO<sub>2</sub> surface, which

accelerates the interfacial electron transfer. Ag(0) is known to be a suitable, though relatively inactive, electrocatalyst [50, 51]. In this work as well, pure TiO<sub>2</sub> showed only a very low photocatalytic activity with regard to H<sub>2</sub> evolution from aqueous methanol. When using the TM materials, a significant increase in the amount of H<sub>2</sub> evolved (consequently corresponding with an increase in the reaction rate) during six hours of illumination of the mixture was observed with increasing TiO<sub>2</sub> content (**Figure 2-5 (a)** and **Table 2-1**). On the one hand, this can be explained by the fact that a significant portion of the UV photons was absorbed by Ag<sub>2</sub>O being inactive under this illumination condition, and thus was not available for the desired H<sub>2</sub> evolution reaction. However, this portion decreased with increasing TiO<sub>2</sub> amount of the mixture. On the other hand, some of the TiO<sub>2</sub> conduction band electrons were transferred to the Ag<sub>2</sub>O, where they were consumed to reduce Ag<sup>+</sup> to Ag(0). These electrons were therefore also not available for the desired reaction. Obviously, these undesired electron losses are lower the higher the mass fraction of TiO<sub>2</sub> in the physical mixture, resulting in increasing H<sub>2</sub> evolution rates with increasing mass fraction of TiO<sub>2</sub>.

### 2.5.3. The Photocatalytic Activity of Ag /Ag<sub>2</sub>O //TiO<sub>2</sub> Composites

#### 2.5.3.1. Bleaching of Methylene Blue

When irradiated with light at wavelengths  $\geq 410$  nm, methylene blue was found to be bleached in the presence of the three TC composites (**Figure 2-4 d** and **Table 2-1**). All TC composites exhibited a higher activity than the corresponding TM mixtures. As in the case of the TM materials, the rate of MB bleaching decreased with increasing amounts of TiO<sub>2</sub>. The increased reaction rates for MB bleaching in the presence of Ag<sub>2</sub>O containing solids, compared to the rate of photolysis under visible light illumination, were explained in **Section 2.5.2.1.** with an interfacial electron transfer from (excited) MB to Ag<sub>2</sub>O (cf. **Figure 2-7**). However, the experimental result is surprising when it is considered that the surfaces of the composites were smaller than the surfaces of the corresponding TM mixtures. A possible explanation may be due to the preparation method. For the TC materials, the Ag/Ag<sub>2</sub>O was prepared in a TiO<sub>2</sub> suspension. Therefore, the Ag/Ag<sub>2</sub>O was attached on the surface of the TiO<sub>2</sub> particles. In contrast,

in the TM mixtures large Ag/Ag<sub>2</sub>O particles were covered by TiO<sub>2</sub>, hindering the electron transfer from excited MB to the Ag<sub>2</sub>O, as discussed in **Section 2.5.2.1**.

The rate of MB bleaching in the presence of TC composite was significantly higher under UV-vis than under visible light illumination. As observed for the TM materials, the bleaching rates were lower in suspensions containing the composites than in suspensions containing only Ag/Ag<sub>2</sub>O or TiO<sub>2</sub> (**Figure 2.4 (b)** and **Table 2.1**).

XRD and XPS data indicate that Ag(I) was reduced, yielding Ag(0), during the light-induced bleaching reaction of MB in the presence of the composite TC 41. A stabilization of Ag<sub>2</sub>O by metallic silver, as claimed by several authors [9–12, 20, 29], was not observed. No XRD peaks that can be attributed to Ag<sub>2</sub>O, were observed after two experimental runs of the composite. However, the ratios of the peak intensities due to metallic Ag and TiO<sub>2</sub> obviously increased (**Figure 2-8 (b)**). No Ag 3d<sub>5/2</sub> and Ag 3d<sub>3/2</sub> peaks, which can be attributed to Ag(I), were present either in the deconvoluted XPS spectra obtained after two experimental runs (**Figures 2-9 c** and **S2-3**). The XPS peak, which was attributed to the presence of Ag<sub>2</sub>O, also disappeared during the light-induced reaction (**Figures 2-9 d** and **S2-3**).

These observations support the statement made above that Ag/Ag<sub>2</sub>O cannot be called a photocatalyst. The XRD pattern shown in **Figure 2-8 (b)** as well as the XPS data presented in **Figure 2-9 (c, d)** clearly evince that the Ag: Ag<sub>2</sub>O ratio changed during the light-induced bleaching of MB. Thus, the condition for a catalyst to exit a chemical reaction unchanged is not satisfied.

### 2.5.3.2. Light-Induced Hydrogen Evolution

The three TC composites were found to be able to promote light-induced H<sub>2</sub> evolution from aqueous methanol. The calculated reaction rates were significantly larger than those of the corresponding TM mixtures. The highest H<sub>2</sub> evolution rate was observed in the presence of TC 11 (**Figure 2-5 (b)** and **Table 2-1**), which was also characterized by a high MB bleaching rate under UV-vis illumination. A possible mechanistic explanation for the high activity of the TC 11 composite is based on the assumption of synergistic effects, due to the presence of both Ag(0) and Ag<sub>2</sub>O at the

TiO<sub>2</sub> surface (**Figure 2-10**). TiO<sub>2</sub> is excited by UV photons. The photogenerated conduction band electrons migrated to the Ag(0) attached to the TiO<sub>2</sub> surface. In a subsequent step, interfacial electron transfer from Ag(0) to protons present in the surrounding electrolyte occurred, thus yielding molecular hydrogen. The valence band hole inside the TiO<sub>2</sub> particle was filled by an electron from an attached Ag<sub>2</sub>O particle. Methanol was oxidized by this hole in the valence band of the Ag<sub>2</sub>O. According to this mechanism, Ag(0) acts as an electron sink, thus decreasing the electron-hole recombination, and as electrocatalyst for the hydrogen evolution reaction, while Ag<sub>2</sub>O is an electrocatalyst for the oxidation reaction of methanol yielding methanal. The supposition made here, that the methanol oxidation occurs at the Ag<sub>2</sub>O surface via electron transfer to the valence band of the excited TiO<sub>2</sub>, has already been proclaimed earlier [16, 19, 23, 26]. It should be emphasized again that the energy of an electron in the conduction band of the Ag<sub>2</sub>O employed in this study is insufficient to reduce a proton (**Figure 2-6**). Consequently, excitation of TiO<sub>2</sub> is a prerequisite for photocatalytic reforming of methanol. TiO<sub>2</sub> is known to be a relatively inactive material for the photocatalytic reduction of protons. High evolution rates of molecular hydrogen are observed only in the presence of a co-catalyst. Ag<sub>2</sub>O was found here to be an unsuitable co-catalyst for the hydrogen evolution reaction, since electron transfer from the excited TiO<sub>2</sub> can only occur into the conduction band of this material. The photocatalytic activities of the composites and mixtures discussed here are thus determined to a considerable extent by the competition between interfacial electron transfer to protons in the surrounding electrolyte, and to silver ions in Ag<sub>2</sub>O. The mechanism of the photocatalytic hydrogen evolution by reforming of organic compounds in the presence of the mixtures and composites employed in this study does not contradict the mechanism discussed for Ag/Ag<sub>2</sub>O // TiO<sub>2</sub> samples, which contain Ag<sub>2</sub>O with a significantly more negative conduction band energy than TiO<sub>2</sub> [17, 24, 26, 33].

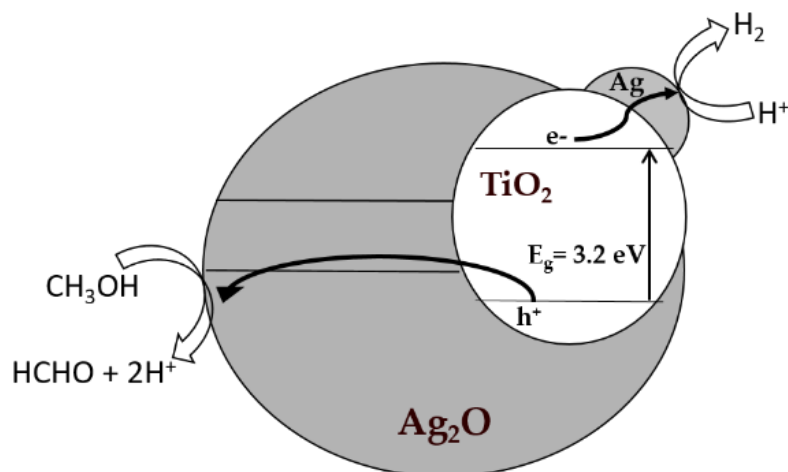


**Figure 2-10.** Mechanism of hydrogen evolution from aqueous CH<sub>3</sub>OH under UV-vis illumination.

Changes in the respective mass fractions of TiO<sub>2</sub>, Ag, and Ag<sub>2</sub>O at constant total mass of the solid in suspension may have several impacts on the rate of hydrogen evolution. Increasing mass fractions of UV absorbing and scattering Ag and Ag<sub>2</sub>O reduces the number of photons to be absorbed by the TiO<sub>2</sub>, thus reducing the H<sub>2</sub> evolution rate. A reduction of the mass fraction of metallic Ag may possibly slow down the interfacial electron transfer to the proton, while a reduction of the mass fraction of Ag<sub>2</sub>O might negatively affect the oxidation reaction. It should also be noted that Ag<sub>2</sub>O can act as a sink for a TiO<sub>2</sub> conduction band electron (cf. **Figure 2-6**). These partially opposing effects may be responsible for the observed differences in the H<sub>2</sub> evolution rates in the presence of the various TC composites (and TM mixtures).

## 2.6. Experimental Section

### 2.6.1. Materials

Titania P25 (TiO<sub>2</sub>) with a mixture of anatase (80%) and rutile (20%) crystal phase, and a specific surface area of 50.1 m<sup>2</sup>g<sup>-1</sup>, was kindly provided by Evonik, Essen, Germany. Silver nitrate (99%, Sigma Aldrich Chemie GmbH, München, Germany), sodium hydroxide pellets (99%, Carl Roth, Karlsruhe, Germany), methanol (99.9%, Carl Roth), and methylene blue (Sigma Aldrich) were used without further purification. Deionized water with a resistivity of 18.2 MΩ cm was obtained from a

Sartorius Arium 611 device (Sartorius Göttingen, Germany) and used for the preparation of all aqueous solutions and suspensions.

## 2.6.2. Synthetic Methods

### 2.6.2.1. Preparation of Ag /Ag<sub>2</sub>O

An amount of AgNO<sub>3</sub> was dissolved in 50 mL of distilled water. The obtained solution was stirred for 30 min. Subsequently, 50 mL NaOH (0.2 M) was added dropwise. The resulting suspension was stirred for another 30 min to promote hydrolysis, and centrifuged, washed with distilled water three times, and dried at 70°C for 24 h.

### 2.6.2.2. Preparation of TM Mixtures

The samples were obtained by mixing the self-prepared Ag<sub>2</sub>O with TiO<sub>2</sub> at mass ratios of 4:1 (20 mass% TiO<sub>2</sub>), 1:1 (50 mass% TiO<sub>2</sub>), and 1:4 (20 mass% TiO<sub>2</sub>) with water. The suspensions were sonicated for 1.5 h and dried at 70 °C for 24 h. The Ag/Ag<sub>2</sub>O//TiO<sub>2</sub> with 20%, 50%, and 80% of TiO<sub>2</sub> were nominated as TM 41, TM 11, and TM 14, respectively. For purpose of comparison, a TiO<sub>2</sub> sample was prepared by the same procedure without the addition of Ag/Ag<sub>2</sub>O.

### 2.6.2.3. Preparation of TC Composites

The TC composites were prepared by a published precipitation method [25,29]. A measured amount of TiO<sub>2</sub> was suspended in 50 mL of distilled water, and the calculated amount of AgNO<sub>3</sub> corresponding to the desired mass ratio of Ag<sub>2</sub>O was added to the solution. The obtained suspension was stirred for 30 min. A volume of 50 mL 0.2 M NaOH was added dropwise. The resulting suspension was stirred for another 30 min to promote hydrolysis and centrifuged, washed with distilled water three times, and dried at 70 °C for 24 h. The Ag/Ag<sub>2</sub>O//TiO<sub>2</sub> with 20 mass%, 50 mass%, and 80 mass% of TiO<sub>2</sub> were denoted as TC 41, TC 11, and TC 14, respectively.

### 2.6.3. Characterization of the Materials

The crystalline structure of the catalysts was measured by powder X-ray diffraction XRD (D8 Advance system, Bruker, Billerica, MA, USA), using a Cu K $\alpha$  radiation source with a wavelength of  $\lambda = 0.154178 \text{ \AA}$  over a  $2\theta$  range from  $20^\circ$  to  $100^\circ$ , with a  $0.011^\circ$  step width. The morphology of the prepared materials was determined using a scanning electron microscope (SEM), employing a JEOL JSM-6700F field emission instrument (Tokyo, Japan) with a resolution of 100 nm and 1  $\mu\text{m}$  using an EDXS detector. Measurements of X-ray photoelectron spectra were carried out using a Leybold Heraeus (Cologne, Germany) with X-ray source, Mg & Al anode, nonmonochromatic, hemispherical analyzer, 100 mm radius. Data analysis was performed using XPSPEAK 4.1 software (Hong Kong, China). The energy of the C 1s-line was set to 284.8 eV and used as a reference for the data correction. Diffuse reflectance UV-vis spectroscopy was employed using a spectrophotometer (Varian Spectrophotometer Cary-100 Bio, Agilent technologies, Santa Clara, CA, USA) at room temperature. Barium sulfate was used as a standard for 100% reflection. The specific surface area (SSA) of the samples was calculated by N<sub>2</sub> adsorption-desorption measurements, employing the Brunauer-Emmet-Teller (BET) method using a FlowSorb II 2300 apparatus from Micromeritics Instrument Company (Corp., Norcross, GA, USA). Prior to these measurements, the samples were evacuated at  $180^\circ\text{C}$  for 1 h. Measurements of photocurrents and flatband potentials were performed with an electrochemical analyzer using three electrodes employing an Iviumstat potentiostat (Ivium Technologies bv, Eindhoven, The Netherlands). Films of the samples were used as the working electrode, after being coated on cleaned fluorine-doped tin oxide (FTO) coated glass using the doctor blade method and calcinated at  $400^\circ\text{C}$  for 2 h. These working electrodes were prepared by grinding 100 mg of the photocatalysts and 50 mg polyethylene glycol with one drop of Triton, followed by the addition of 200  $\mu\text{L}$  of deionized water and a sufficient amount of ethanol. An Ag/AgCl electrode (3 M NaCl, +209 mV vs. NHE) and a platinum coil were used as the reference electrode and the counter electrode, respectively. Potassium nitrate aqueous solution

(0.1 M) was used as the electrolyte. The impedance spectra were recorded in the range between the chosen potential from -1 V to +1 V at frequencies of 10, 100, and 1000 Hz with 20 mV amplitude vs. Ag/AgCl. The capacitance was plotted against  $V$ , and the flatband was calculated from the intercept of the plot. (i.e., a plot of  $C^{-2}$  vs.  $V$ , where  $C$  was the capacitance and  $V$  was the potential across the space charge layer).

## 2.6.4. Photocatalytic Measurements

### 2.6.4.1. Methylene Blue Degradation

The apparatus used for carrying out of the photocatalytic degradation reactions consisted of a double jacket cylindrical reactor with a 230 mL volume, which circulated with cold water to maintain the ambient reaction. A volume of 200 mL of aqueous solution of methylene blue (MB, 10 mg L<sup>-1</sup>) and 200 mg of photocatalysts were used for each reaction experiment. A 300 W Xenon arc lamp (Müller Elektronik-Optik, Moosinning, Germany) was used both as the UV-vis light source and as the vis light source by placing a UV cut-off filter ( $\geq 410$  nm) in the light path. The lamp was started 30 min before the degradation experiments to ensure maximum emission. Aliquots (1.5 mL) of the suspensions were collected at given time intervals (0, 2, 4, 6, 8, 10, 15, and 30 min), centrifuged to remove the solid, and analyzed immediately with the UV-vis spectrophotometer.

### 2.6.4.2. Photocatalytic Hydrogen Formation

The photocatalytic H<sub>2</sub> generation experiments were conducted in quartz vials (capacity of 10 mL) under illumination with a 1000 W Xenon lamp (Hönle UV Technology, Gräfelfing, Germany; Sol 1200 solar). An amount of 6 mg of the photocatalyst was suspended in 6 mL aqueous methanol (10 vol%). The suspension was purged with argon for 20 min to remove the air, and the quartz vial was sealed with a specially made rubber septum degassed for sampling. The amount of H<sub>2</sub> gas evolved during the photocatalytic reaction was quantified every two hours using a gas chromatograph (Shimadzu GC-8A, Shimadzu Deutschland GmbH, Duisburg,



Germany) equipped with a thermal conductivity detector (TCD) and 60/80 molecular sieve 5 Å column.

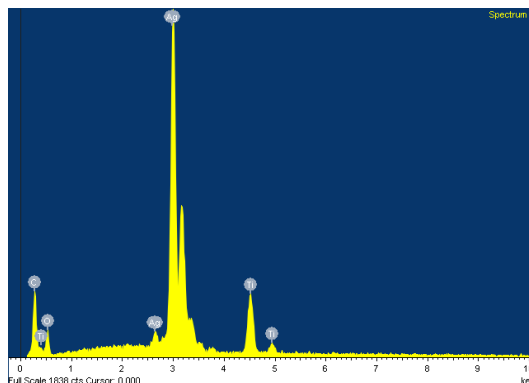
## 2.7. Conclusions

Ag/Ag<sub>2</sub>O was found to enhance the rate of light-induced bleaching of aqueous MB under both UV-vis and vis illumination, in comparison to the bleaching in homogeneous solution. Even in suspensions containing mixtures and composites of Ag/Ag<sub>2</sub>O with TiO<sub>2</sub> (P25), with varying mass ratios of Ag/Ag<sub>2</sub>O (20%, 50%, and 80%), the reaction rate was slightly increased under these illumination conditions. However, the bleaching rate of MB was lower in the presence of the composites and mixtures than the rate measured for bare Ag/Ag<sub>2</sub>O. It is therefore suggested that the bleaching of MB is initiated by an interfacial electron transfer from the excited organic probe compound to Ag<sub>2</sub>O. TiO<sub>2</sub> layers covering the Ag<sub>2</sub>O seem to inhibit this electron transfer. Since Ag<sub>2</sub>O can transfer an electron neither to dissolved molecular oxygen nor to a proton for thermodynamic reasons, it is assumed that Ag<sup>+</sup> is reduced to Ag(0) in the processes investigated here. Results of XRD and XPS measurements support this assumption and indicate that Ag/Ag<sub>2</sub>O is not stable under the experimental conditions employed in this study. A stabilization of Ag<sub>2</sub>O by metallic silver, as occasionally claimed, was not observed. Therefore, to address Ag/Ag<sub>2</sub>O as a (photo)catalytically active material does not seem appropriate.

## 2.8. Supplementary Materials

### Ag/Ag<sub>2</sub>O

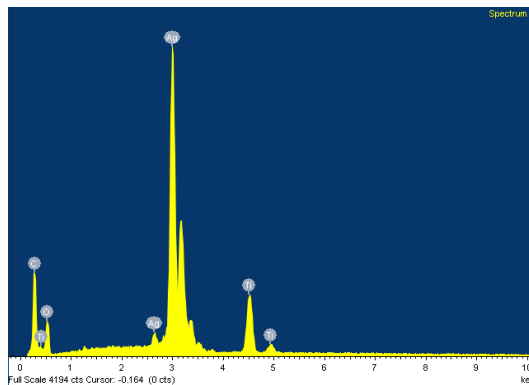
Element	App	Intensity	Weight%	Weight%	Atomic%
	Conc.	Corrn.		Sigma	
C K	4.12	1.3816	3.05	0.31	15.09
O K	2.69	0.2766	9.92	0.85	36.88
Ag L	82.86	0.9721	87.04	0.87	48.02
Totals			100.00		



### Ag/Ag<sub>2</sub>O // TiO<sub>2</sub> Mixtures (TM):

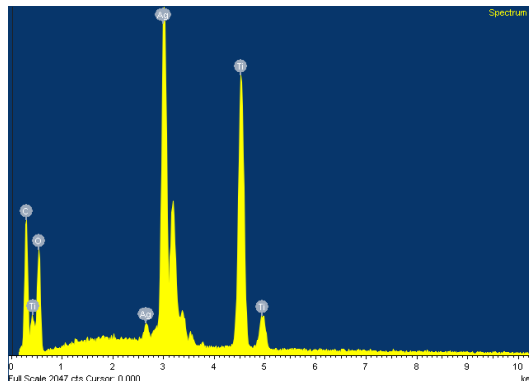
#### TM 41

Element	App	Intensity	Weight%	Weight%	Atomic%
	Conc.	Corrn.		Sigma	
C K	25.22	1.2513	14.45	0.39	36.34
O K	9.51	0.3007	22.70	0.75	42.84
Ti K	9.83	0.7639	9.23	0.19	5.82
Ag L	69.39	0.9279	53.62	0.61	15.01
Totals			100.00		



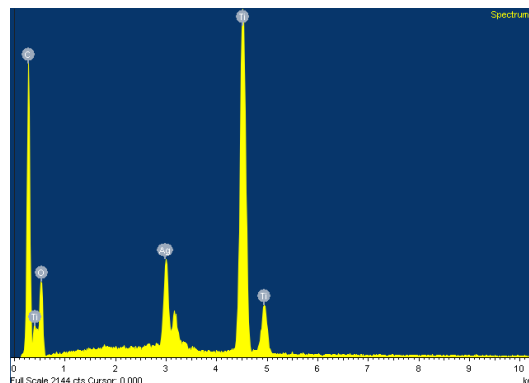
#### TM 11

Element	App	Intensity	Weight%	Weight%	Atomic%
	Conc.	Corrn.		Sigma	
C K	25.52	1.0672	14.39	0.43	29.89
O K	17.42	0.3139	33.40	0.78	52.08
Ti K	27.43	0.8024	20.57	0.33	10.71
Ag L	47.95	0.9123	31.63	0.48	7.32
Totals			100.00		



**TM 14**

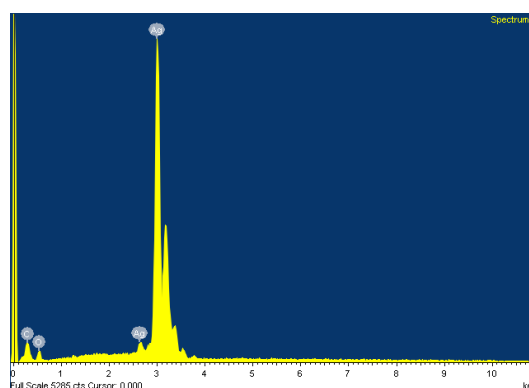
Element	App	Intensity	Weight%	Weight%	Atomic%
	Conc.	Corrn.		Sigma	
C K	81.93	1.0428	34.68	0.57	54.02
O K	18.65	0.2861	28.77	0.80	33.64
Ti K	52.56	0.8386	27.67	0.40	10.80
Ag L	18.07	0.8986	8.88	0.25	1.54
Totals			100.00		



**Ag/Ag<sub>2</sub>O//TiO<sub>2</sub> Composites (TC):**

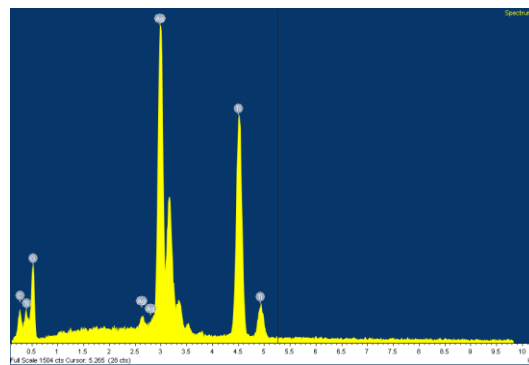
**TC 41**

Element	App	Intensity	Weight%	Weight%	Atomic%
	Conc.	Corrn.		Sigma	
C K	16.91	1.2750	11.03	0.56	33.55
O K	5.62	0.2828	16.53	1.21	37.75
Ti K	8.99	0.7587	9.86	0.32	7.52
Ag L	70.99	0.9439	62.57	1.04	21.19
Totals			100.00		



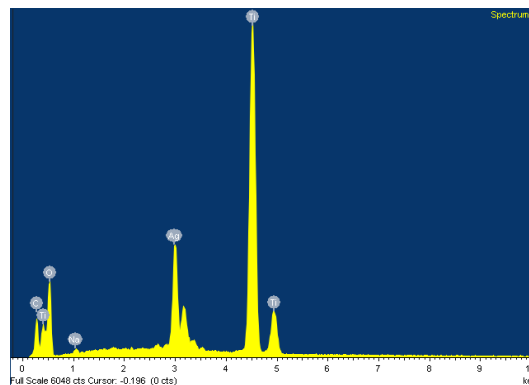
**TC 11**

Element	App	Intensity	Weight%	Weight%	Atomic%
	Conc.	Corrn.		Sigma	
C K	3.29	1.0249	3.28	0.31	8.36
O K	10.33	0.3084	34.19	0.88	65.50
Ti K	18.21	0.8019	23.17	0.38	14.83
Ag L	35.39	0.9264	38.98	0.60	11.08
Totals			100.00		

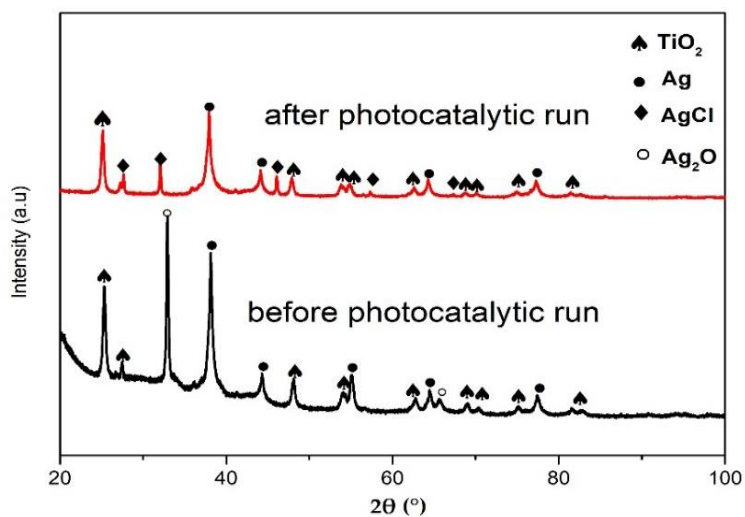


**TC 14**

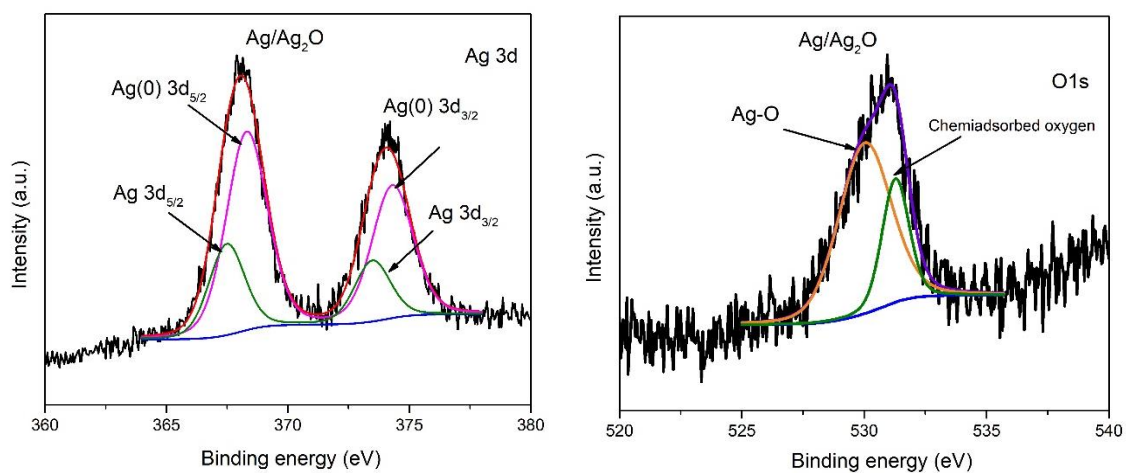
Element	App	Intensity	Weight%	Weight%	Atomic%
	Conc.	Corrn.		Sigma	
C K	10.84	0.8727	7.10	0.28	14.81
O K	20.51	0.2994	39.16	0.57	61.30
Na K	0.42	0.5372	0.45	0.08	0.49
Ti K	56.66	0.8535	37.94	0.39	19.84
Ag L	24.65	0.9179	15.35	0.24	3.56
Totals			100.00		

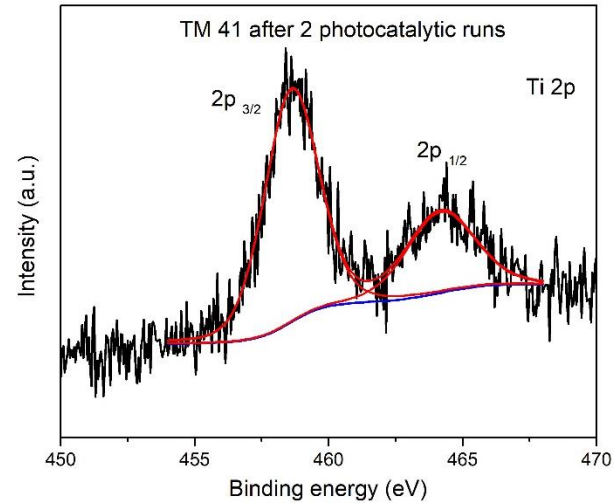
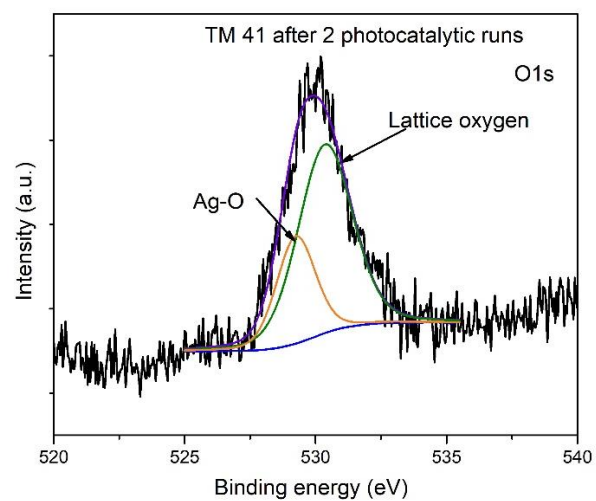
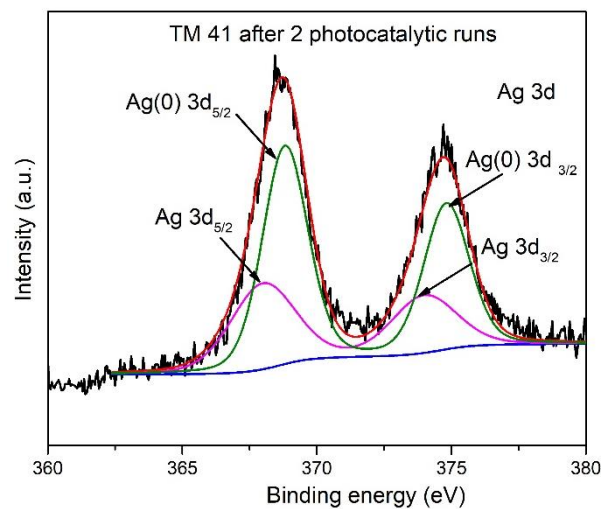
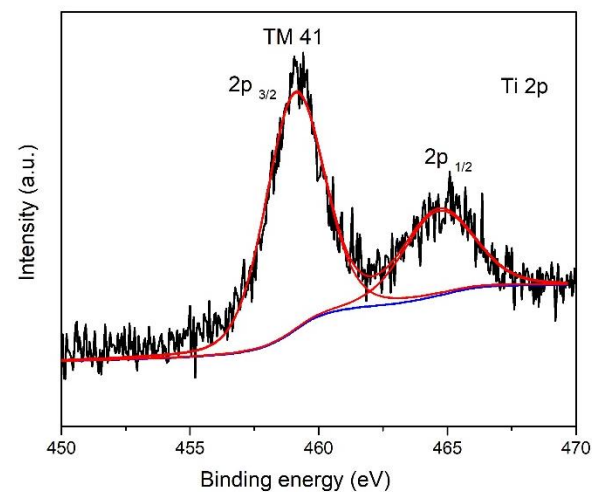
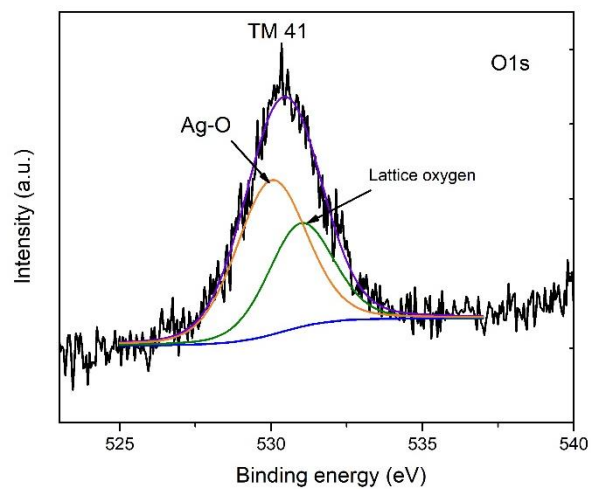
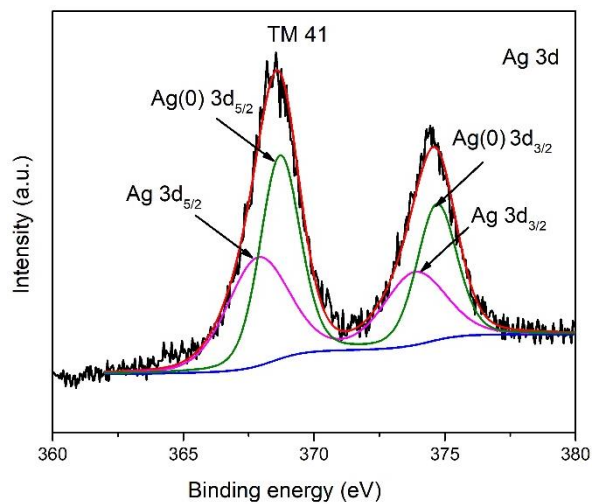


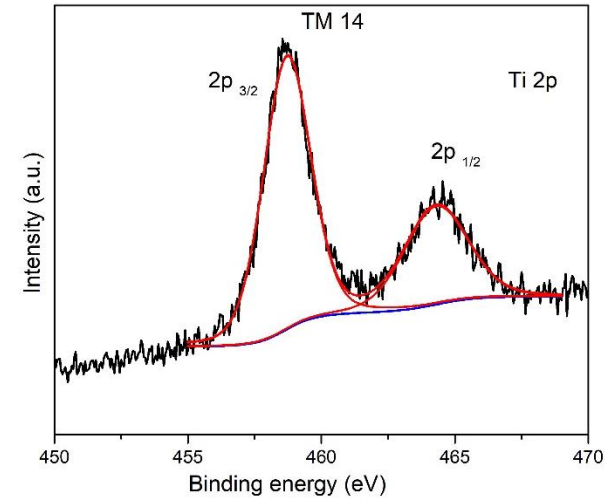
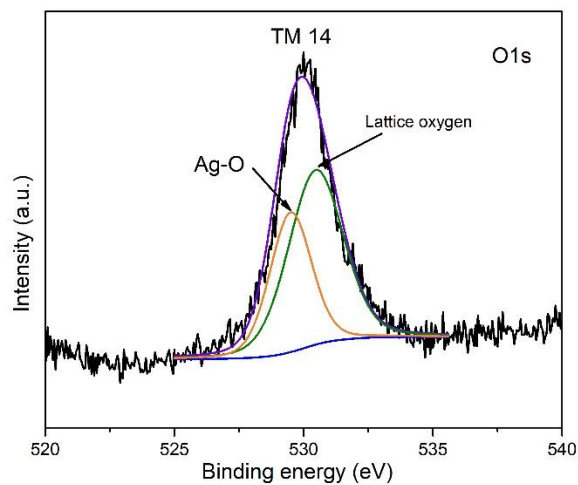
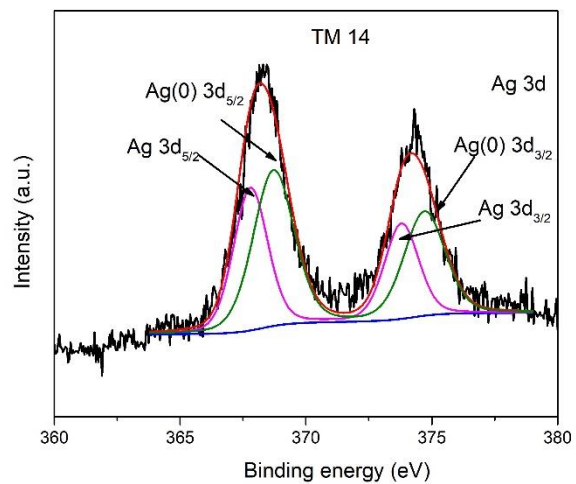
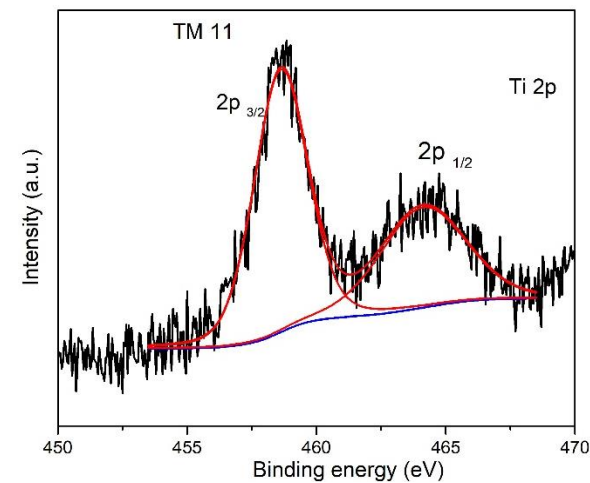
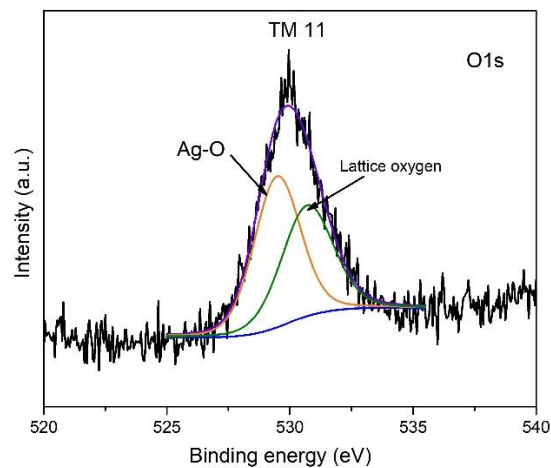
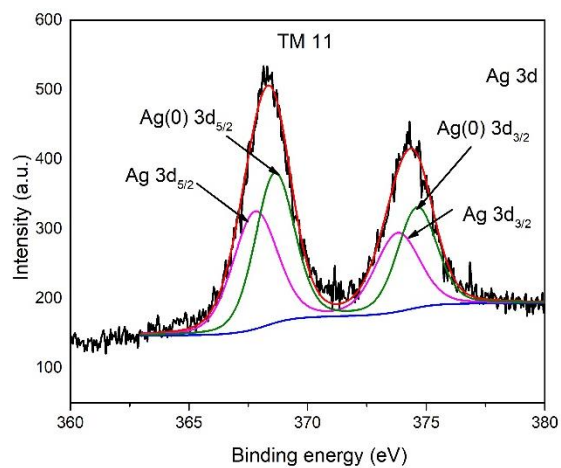
**Figure S2-1.** EDX diagrams of all prepared photocatalysts.

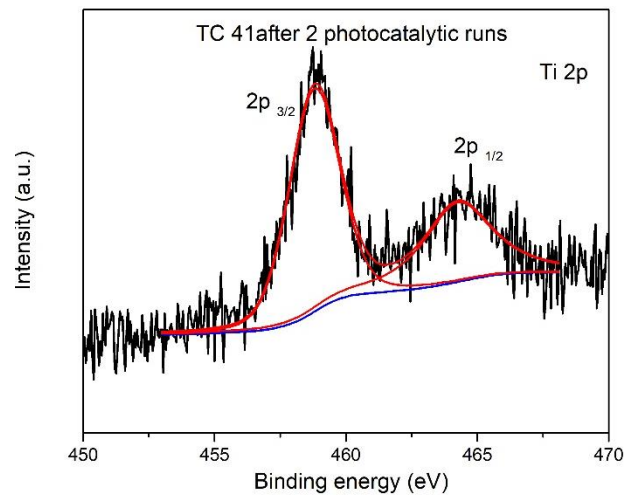
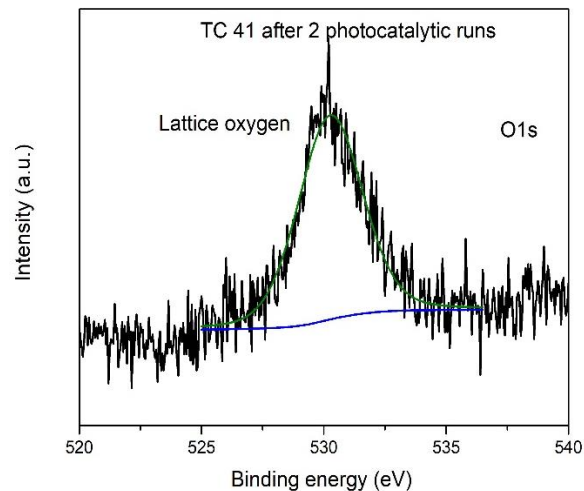
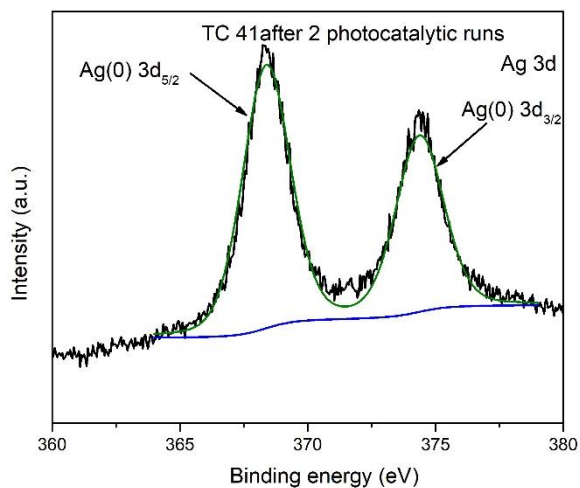
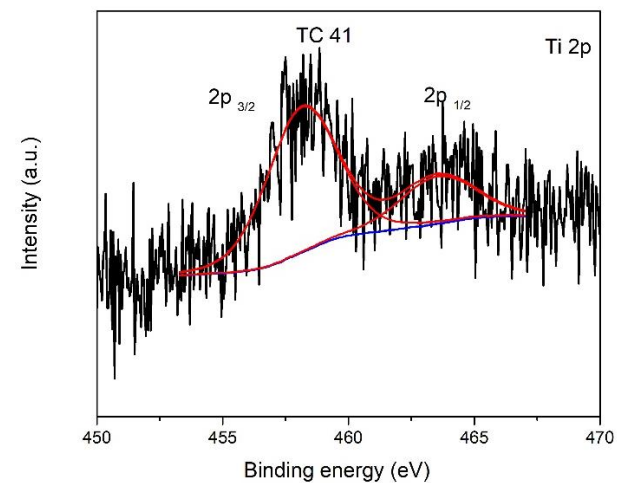
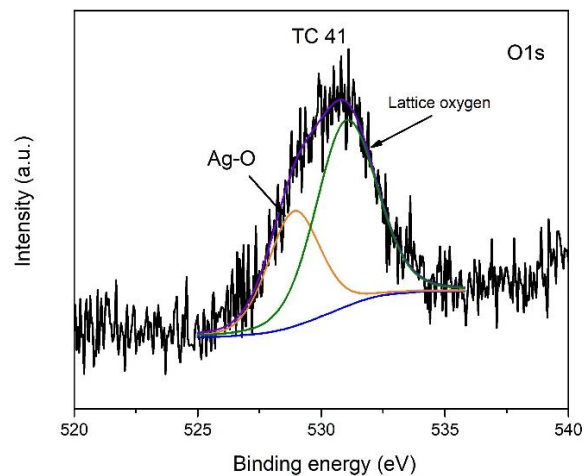
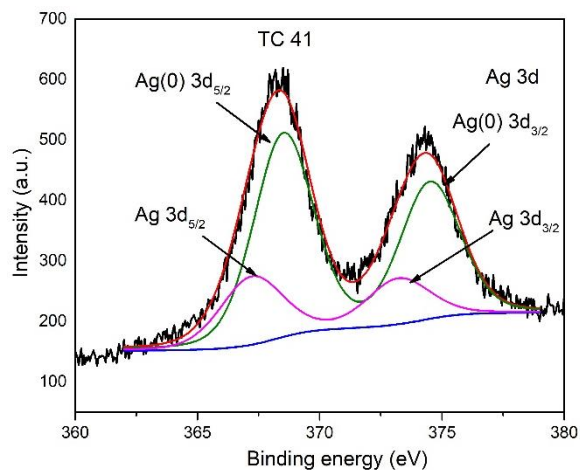


**Figure S2-2.** XRD patterns of TM 11 photocatalyst after one cycle of MB bleaching employing UV-vis light.











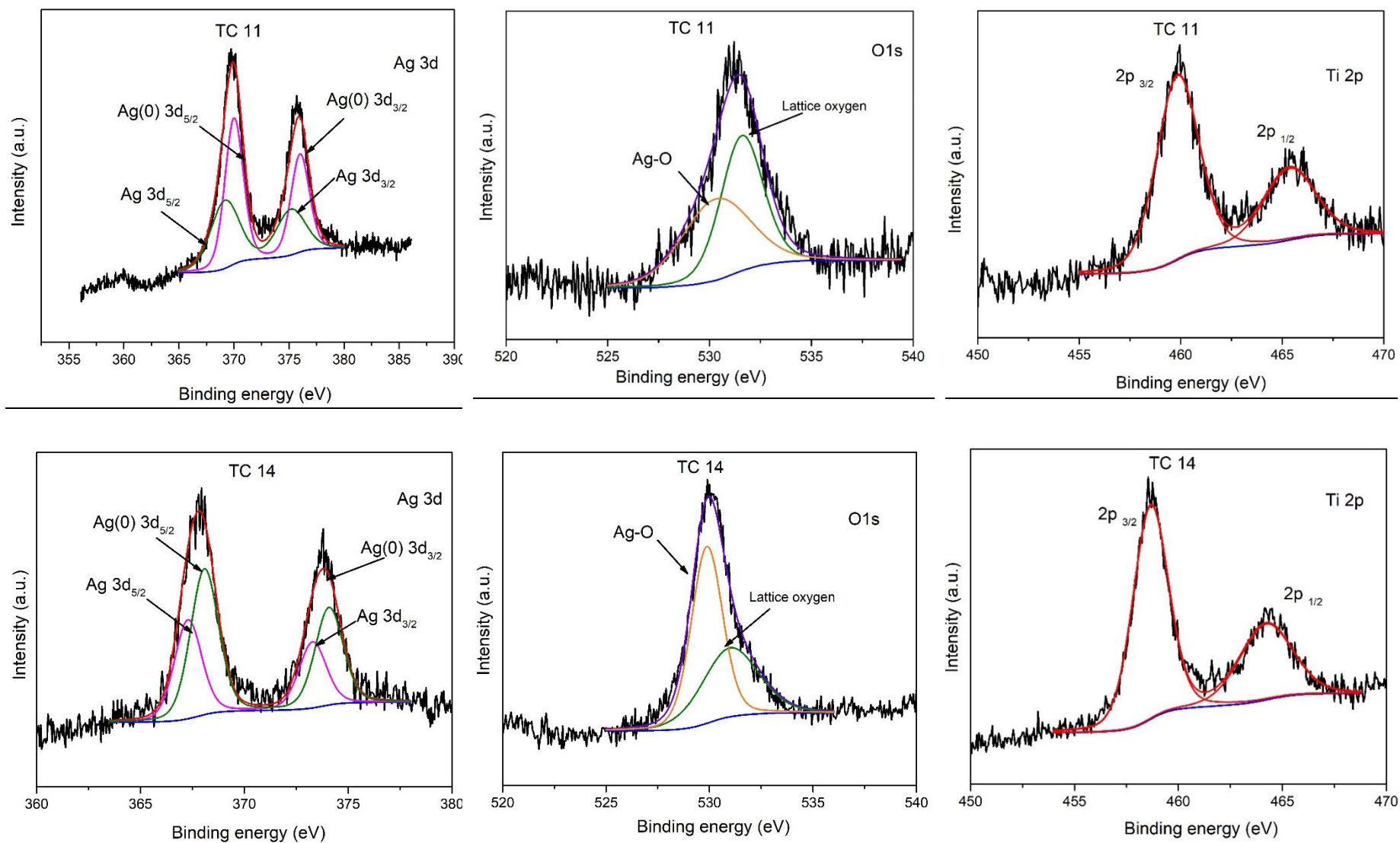


Figure S2-3. XPS spectra of Ag 3d, O 1s, and Ti 2p in the Ag/Ag<sub>2</sub>O, TM, and TC materials.



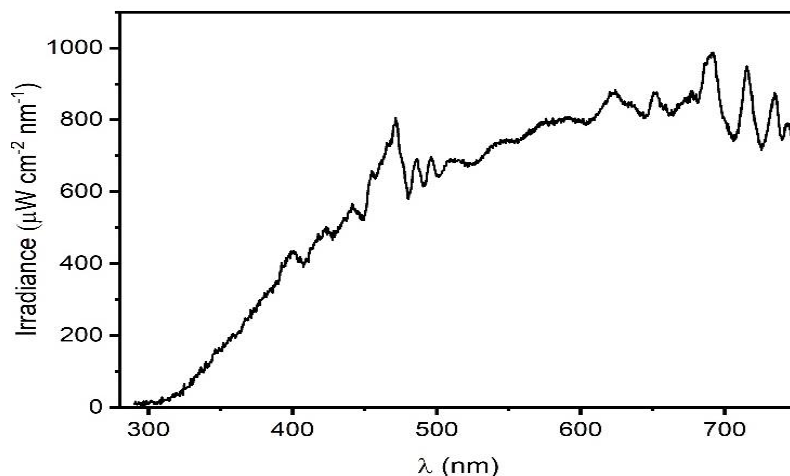


Figure S2-4. The emission spectrum of the used Xenon lamp.

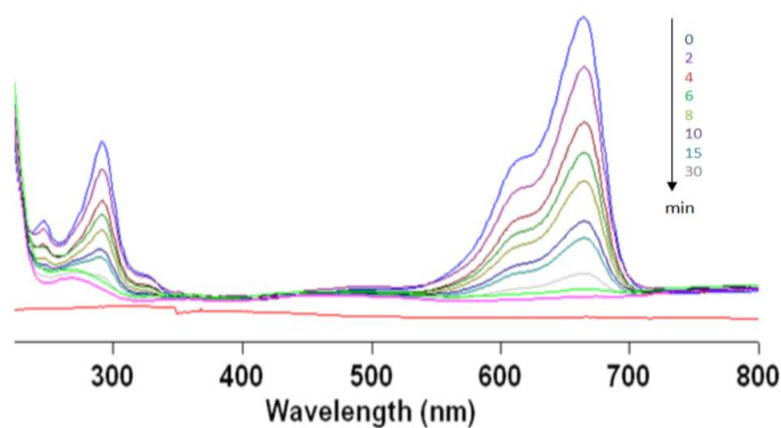


Figure S2-5. UV-vis spectra of aqueous methylene blue solutions obtained during illumination with visible light in the presence of Ag/Ag<sub>2</sub>O.

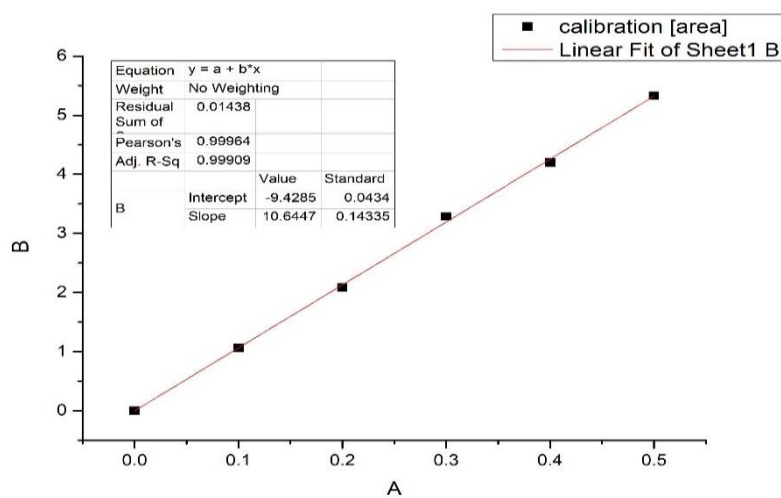


Figure S2-6. Calibration curve for H<sub>2</sub> experiment.

## 2.9. Acknowledgments

The authors wish to thank Luis Granone for XRD measurements and Stephanie Melchers for SEM/EDAX images. The publication of this article was funded by the Open Access Fund of the Gottfried Wilhelm Leibniz Universität Hannover.

## 2.10. References

1. D.W. Bahnemann. Mechanisms of Organic Transformations on Semiconductor Particles. In Photochemical Conversion and Storage of Solar Energy; Proceedings of the Eighth International Conference on Photochemical Conversion and Storage of Solar Energy, IPS-8, Palermo, Italy, 15–20 July 1990; Pelizzetti, E., Schiavello, M., Eds.; Springer Science/Kluwer Academic Publishers: Dordrecht, The Netherlands; Boston, MA, USA, **1991**, 251–276.
2. M.R. Hoffmann, S.T. Martin, W. Choi, D.W. Bahnemann. Environmental Applications of Semiconductor Photocatalysis. *Chem. Rev.* **1995**, 95, 69–96.
3. D.W. Bahnemann. Photocatalytic Detoxification of Polluted Waters. In *Environmental Photochemistry*. Boule, P., Ed.; Springer: Berlin/Heidelberg, Germany, **1999**, 285–351.
4. A. Fujishima, T.N. Rao, D.A. Tryk. Titanium Dioxide Photocatalysis. *J. Photochem. Photobiol. C: Photochem. Rev.* **2000**, 1, 1–21.
5. J.J. Reinoso, C.M. Álvarez-Docio, V.Z. Ramírez, J.F. Fernández. Hierarchical Nano ZnO -micro TiO<sub>2</sub> Composites: High UV Protection Yield Lowering Photodegradation in Sunscreens. *Ceram. Int.* **2018**, 44, 2827–2834.
6. X. Wang, H.F. Wu, Q. Kuang, R.B. Huang, Z.X. Xie, L.S. Zheng. Shape-dependent Antibacterial Activities of Ag<sub>2</sub>O Polyhedral Particles. *Langmuir* **2010**, 26, 2774–2778.
7. J. Zou, Y. Xu, B. Hou, D. Wu, Y. Sun. Self-assembly Ag<sub>2</sub>O Nanoparticles into Nanowires with the Aid of Amino-Functionalized Silica Nanoparticles. *Powder Technol.* **2008**, 183, 122–126.

8. K. Lalitha, J.K. Reddy, M.V. Phanikrishna Sharma, V.D. Kumari, M. Subrahmanyam. Continuous Hydrogen Production Activity over Finely Dispersed Ag<sub>2</sub>O / TiO<sub>2</sub> Catalysts from Methanol:Water Mixtures under Solar Irradiation: A Structure-Activity Correlation. *Int. J. Hydrog. Energy* **2010**, 35, 3991–4001.
9. X. Wang, S. Li, H. Yu, J. Yu, S. Liu. Ag<sub>2</sub>O as a New Visible-Light Photocatalyst: Self-Stability and High Photocatalytic Activity. *Chem. Eur. J.* **2011**, 17, 7777–7780.
10. G. Wang, X. Ma, B. Huang, H. Cheng, Z. Wang, J. Zhan, X. Qin, X. Zhang, Y. Dai. Controlled Synthesis of Ag<sub>2</sub>O Microcrystals with Facet-dependent Photocatalytic Activities. *J. Mater. Chem.* **2012**, 22, 21189–21194.
11. F. Chen, Z. Liu, Y. Liu, P. Fang, Y. Dai. Enhanced Adsorption and Photocatalytic Degradation of High-concentration Methylene Blue on Ag<sub>2</sub>O-modified TiO<sub>2</sub>-based Nanosheet. *Chem. Eng. J.* **2013**, 221, 283–291.
12. X. Hu, C. Hu, R. Wang. Enhanced Solar Photodegradation of Toxic Pollutants by Long-Lived Electrons in Ag–Ag<sub>2</sub>O Nanocomposites. *Appl. Catal. B: Environ.* **2015**, 176–177, 637–645.
13. W. Jiang, X. Wang, Z. Wu, X. Yue, S. Yuan, H. Lu, B. Liang. Silver Oxide as Superb and Stable Photocatalyst under Visible and Near-infrared Light Irradiation and its Photocatalytic Mechanism. *Ind. Eng. Chem. Res.* **2015**, 54, 832–841.
14. J. Li, W. Fang, C. Yu, W. Zhou, L. Zhu, Y. Xie. Ag-based Semiconductor Photocatalysts in Environmental Purification. *Appl. Surf. Sci.* **2015**, 358, 46–56.
15. C. Liu, C. Cao, X. Luo, S. Luo. Ag-bridged Ag<sub>2</sub>O Nanowire Network/ TiO<sub>2</sub> Nanotube Array p–n Heterojunction as a Highly Efficient and Stable Visible Light Photocatalyst. *J. Hazard. Mater.* **2015**, 285, 319–324.
16. H.-T. Ren, S.-Y. Jia, J.-J. Zou, S.-H. Wu, X. Han. A facile Preparation of Ag<sub>2</sub>O/P25 Photocatalyst for Selective Reduction of Nitrate. *Appl. Catal. B: Environ.* **2015**, 176–177, 53–61.
17. D.P. Kumar, N.L. Reddy, M. Karthik, B. Neppolian, J. Madhavan, M.V. Shankar, Solar Light Sensitized p-Ag<sub>2</sub>O/n-TiO<sub>2</sub> Nanotubes Heterojunction Photocatalysts

- for Enhanced Hydrogen Production in Aqueous-Glycerol Solution. *Sol. Energy Mater. Sol. Cells* **2016**, 154, 78–87.
18. R. Kumar, R.M. El-Shishtawy, M.A. Barakat. Synthesis and Characterization of Ag-Ag<sub>2</sub>O/TiO<sub>2</sub>@polypyrrole Heterojunction for Enhanced Photocatalytic Degradation of Methylene Blue. *Catalysts* **2016**, 6, 76.
  19. N. Wei, H. Cui, Q. Song, L. Zhang, X. Song, K. Wang, Y. Zhang, J. Li, J. Wen, J. Tian. Ag<sub>2</sub>O Nanoparticle/TiO<sub>2</sub> Nanobelt Heterostructures with Remarkable Photo-Response and Photocatalytic Properties under UV, Visible and Near-infrared Irradiation. *Appl. Catal. B: Environ.* **2016**, 198, 83–90.
  20. H. Yang, J. Tian, T. Li, H. Cui. Synthesis of Novel Ag/Ag<sub>2</sub>O Heterostructures with Solar Full Spectrum (UV, Visible and Near-Infrared) Light-driven Photocatalytic Activity and Enhanced Photoelectrochemical Performance. *Catal. Commun.* **2016**, 87, 82–85.
  21. J. Zhang, H. Liu, Z. Ma. Flower-Like Ag<sub>2</sub>O/Bi<sub>2</sub>MoO<sub>6</sub> p-n Heterojunction with Enhanced Photocatalytic Activity under Visible Light Irradiation. *J. Molec. Catal. A: Chem.* **2016**, 424, 37–44.
  22. Y. Cui, Q. Ma, X. Deng, Q. Meng, X. Cheng, M. Xie, X. Li, Q. Cheng, H. Liu. Fabrication of Ag - Ag<sub>2</sub>O /Reduced TiO<sub>2</sub> Nanophotocatalyst and its Enhanced Visible Light Driven Photocatalytic Performance for Degradation of Diclofenac Solution. *Appl. Catal. B: Environ.* **2017**, 206, 136–145.
  23. X. Hu, X. Liu, J. Tian, Y. Li, H. Cui. Towards Full-Spectrum (UV, Visible, and Near-Infrared) Photocatalysis: Achieving an All-Solid-State Z-scheme between Ag<sub>2</sub>O and TiO<sub>2</sub> using Reduced Graphene Oxide as the Electron Mediator. *Catal. Sci. Technol.* **2017**, 7, 4193–4205.
  24. A. Kaur, D.B. Salunke, A. Umar, S.K. Mehta, A.S.K. Sinha, S.K. Kansal. Visible Light Driven Photocatalytic Degradation of Fluoroquinolone Levofloxacin Drug using Ag<sub>2</sub>O/ TiO<sub>2</sub> Quantum Dots: A Mechanistic Study and Degradation Pathway. *New J. Chem.* **2017**, 41, 12079–12090.

25. B. Liu, L. Mu, B. Han, J. Zhang, H. Shi. Fabrication of TiO<sub>2</sub>/Ag<sub>2</sub>O Heterostructure with Enhanced Photocatalytic and Antibacterial Activities under Visible Light Irradiation. *Appl. Surf. Sci.* **2017**, 396, 1596–1603.
26. K.K. Mandari, B.S. Kwak, A.K.R. Police, M. Kang. In-situ Photo-Reduction of Silver Particles and their SPR Effect in Enhancing the Photocatalytic Water Splitting of Ag<sub>2</sub>O/TiO<sub>2</sub> Photocatalysts under Solar Light Irradiation: A Case Study. *Mater. Res. Bull.* **2017**, 95, 515–524.
27. M.E. Olya, M. Vafaei, M. Jahangiri. Modeling of Acid Dye Decolorization by TiO<sub>2</sub>–Ag<sub>2</sub>O Nano-photocatalytic Process using Response Surface Methodology. *J. Saudi Chem. Soc.* **2017**, 21, 633–642.
28. S.P. Prakoso, A. Taufik, R. Saleh. Ag/Ag<sub>2</sub>O/TiO<sub>2</sub> Nanocomposites: Microwave-Assisted Synthesis, Characterization, and Photosonocatalytic Activities. *IOP Conf. Ser. Mater. Sci. Eng.* **2017**, 188, 012029.
29. H.T. Ren, Q. Yang. Fabrication of Ag<sub>2</sub>O / TiO<sub>2</sub> with Enhanced Photocatalytic Performances for Dye Pollutants Degradation by a pH-induced Method. *Appl. Surf. Sci.* **2017**, 396, 530–538.
30. C. Wang, X. Cai, Y. Chen, Z. Cheng, X. Luo, S. Mo, L. Jia, R. Shu, P. Lin, Z. Yang, *et al.* Efficient Hydrogen Production from Glycerol Photoreforming over Ag<sub>2</sub>O–TiO<sub>2</sub> Synthesized by a Sol–Gel Method. *Int. J. Hydrog. Energy.* **2017**, 42, 17063–17074.
31. Y. Zhao, C. Tao, G. Xiao, H. Su. Controlled Synthesis and Wastewater Treatment of Ag<sub>2</sub>O/TiO<sub>2</sub> Modified Chitosan-based Photocatalytic Film. *RSC Adv.* **2017**, 7, 11211–11221.
32. A. Deng, Y. Zhu. Synthesis of TiO<sub>2</sub> / SiO<sub>2</sub> / Ag / Ag<sub>2</sub>O and TiO<sub>2</sub> / Ag / Ag<sub>2</sub>O Nanocomposite Spheres with Photocatalytic Performance. *Res. Chem. Intermed.* **2018**, 44, 4227–4243.
33. C. Hao, W. Wang, R. Zhang, B. Zou, H. Shi. Enhanced Photoelectrochemical Water Splitting with TiO<sub>2</sub>@Ag<sub>2</sub>O Nanowire Arrays via p-n Heterojunction Formation. *Sol. Energy Mater. Sol. Cells* **2018**, 174, 132–139.

34. R. Liu, P. Wang, X. Wang, H. Yu, J. Yu. UV- and Visible-light Photocatalytic Activity of Simultaneously Deposited and Doped Ag/ Ag(I)- TiO<sub>2</sub> Photocatalyst. *J. Phys. Chem. C* **2012**, 116, 17721–17728.
35. J.G. Kang, Y. Sohn. Interfacial Nature of Ag Nanoparticles Supported on TiO<sub>2</sub> Photocatalysts. *J. Mater. Sci.* **2012**, 47, 824–832.
36. B. Jiang, Z. Hou, C. Tian, W. Zhou, X. Zhang, A. Wu, G. Tian, K. Pan, Z. Ren, H. Fu. A Facile and Green Synthesis Route Towards Two-dimensional TiO<sub>2</sub>@ Ag Heterojunction Structure with Enhanced Visible Light Photocatalytic Activity. *CrystEngComm*. **2013**, 15, 5821–5827.
37. J.S. Hammond, S.W. Gaarenstroom, N. Winograd. X-ray Photoelectron Spectroscopic Studies of Cadmium- and Silver-oxygen Surfaces. *Anal. Chem.* **1975**, 47, 2193–2199.
38. B.A. Zaccheo, R.M. Crooks. Stabilization of Alkaline Phosphatase with Au@Ag<sub>2</sub>O Nanoparticles. *Langmuir* **2011**, 27, 11591–11596.
39. Aeroxide, Aerodisp and Aeroperl. Titanium Dioxide as Photocatalyst. Technical Information.
40. L.H. Tjeng, M.B.J. Meinders, J. van Elp, J. Ghijsen, G.A. Sawatzky, R.L. Johnson. Electronic Structure of Ag<sub>2</sub>O. *Phys. Rev. B.* **1990**, 41, 3190–3199.
41. J.J. Reinoso, P. Leret, C.M. Álvarez-Docio, A. Del Campo, J.F. Fernández. Enhancement of UV Absorption Behavior in ZnO-TiO<sub>2</sub> Composites. *Bol. Soc. Esp. Ceram. Vidr.* **2016**, 55, 55–62.
42. Z. Jiang, S. Huang, B. Quian. Semiconductor Properties of Ag<sub>2</sub>O Film Formed on the Silver Electrode in 1 M NaOH Solution. *Electrochim. Acta.* **1994**, 39, 2465–2470.
43. A. Vvedenskii, S. Grushevskaya, D. Kudryashov, S. Ganzha. The Influence of the Conditions of the Anodic Formation and the Thickness of Ag(I) Oxide Nanofilm on its Semiconductor Properties. *J. Solid State Electrochem.* **2010**, 14, 1401–1413.
44. A. Mills, J. Wang. Photobleaching of Methylene Blue Sensitised by TiO<sub>2</sub>: An Ambiguous System? *J. Photochem. Photobiol. A: Chem.* **1999**, 127, 123–134.

45. J.-M. Herrmann. Fundamentals and Misconceptions in Photocatalysis. *J. Photochem. Photobiol. A: Chem.* **2010**, 216, 85–93.
46. J.-M. Herrmann. Photocatalysis Fundamentals Revisited to Avoid Several Misconceptions. *Appl. Catal. B: Environ.* **2010**, 99, 461–468.
47. S.G. Bratsch. Standard Electrode Potentials and Temperature Coefficients in Water at 298.15 K. *J. Phys. Chem. Ref. Data* **1989**, 18, 1–21.
48. A. Arimi, L. Megatiff, L.I. Granone, R. Dillert, D.W. Bahnemann. Visible-light Photocatalytic Activity of Zinc Ferrites. *J. Photochem. Photobiol. A: Chem.* **2018**, 366, 118–126.
49. Y. Xu, M.A.A. Schoonen. The Absolute Energy Positions of Conduction and Valence Bands of Selected Semiconducting Minerals. *Am. Mineral.* **2000**, 85, 543–556.
50. T. Harifi, M. Montazer, R. Dillert, D.W. Bahnemann. TiO<sub>2</sub> / Fe<sub>3</sub>O<sub>4</sub> / Ag Nanophotocatalysts in Solar Fuel Production: New Approach to using a Flexible Lightweight Sustainable Textile Fabric. *J. Clean. Prod.* **2018**, 196, 688–697.
51. S. Hamid, R. Dillert, D.W. Bahnemann. Photocatalytic Reforming of Aqueous Acetic Acid into Molecular Hydrogen and Hydrocarbons over Co-catalyst-loaded TiO<sub>2</sub>: Shifting the Product Distribution. *J. Phys. Chem. C* **2018**, 122, 12792–12809.

## **Chapter 3. UV-vis Light Induced Degradation of Oxytetracycline Hydrochloride Mediated by Co - TiO<sub>2</sub> Nanoparticles**

### **3.1. Foreword**

Besides methylene blue (MB) used as an antipsychotic drug and discussed in Chapter 2, oxytetracycline hydrochloride (OTC HCl) is one of the most frequently detected antibiotics in water. However, OTC HCl is confirmed to undergo direct photolysis under UV and solar light illumination, its photolytic byproducts may be more toxic than the organic molecule itself, and therefore the degradation of OTC HCl by the photolytic process is not a safe path to mineralize this pharmaceutical of emerging concern. Photocatalytic degradation of OTC HCl was chosen in this study to assess the photoactivity of cobalt-doped TiO<sub>2</sub> (Co-TiO<sub>2</sub>) materials under UV-vis light irradiation. As an interesting low-cost and earth-abundant mineral, cobalt as a transition metal dopant has drawn a great deal of interest and has been exceedingly investigated for the development of visible-light-driven TiO<sub>2</sub> photocatalysts. However, the various preparation procedures used to synthesize Co-TiO<sub>2</sub> seems to influence its physico-chemical properties and thus the photoactivity of the material. Additionally, distinct types of substrates are employed to evaluate the photocatalytic degradation providing deviating results between groups that affirm the positive influence of Co ions, others that observed a slight improvement, and those who reported a detrimental effect on the photocatalytic activity. These varying findings can create misgivings about the factual effect of the cobalt doping on the photocatalytic activity.

Accordingly, it was of high interest to synthesize Co-TiO<sub>2</sub> with two different solvothermal methods, namely reflux and hydrothermal, to investigate the impact of the synthetic method in the physico-chemical properties of Co-TiO<sub>2</sub> and consequently on its photoactivity under UV-vis light irradiation.

This chapter encloses the article “UV-vis Light Induced Degradation of Oxytetracycline Hydrochloride Mediated by Co - TiO<sub>2</sub> Nanoparticles” by Soukaina



Akel, Redouan Boughaled, Ralf Dillert, Mohamed El Azzouzi, and Detlef W. Bahnemann, published in *Molecules*, 2020, 25, 249; doi: 10.3390/molecules25020249. In this study, 0.5 wt.% Co-TiO<sub>2</sub> catalysts were prepared using a common preparation method, which is hydrothermal, and a simple reflux synthesis that is less reported in the literature. The crystalline size, the SSA, and the band gap energies of the as-synthesized Co-TiO<sub>2</sub> and bare TiO<sub>2</sub> photocatalysts were determined to comprehend the effect of the synthetic method on the photocatalytic activity of the materials. In this regard, the UV-vis light-induced photocatalytic degradation of OTC HCl in the presence of Co-TiO<sub>2</sub>NPs was studied. The high specific surface area along with the defect levels formed within the band gap of Co-TiO<sub>2</sub> NPs have been found to enhance the photocatalytic activity. Moreover, Co-TiO<sub>2</sub>-assisted photodegradation of OTC HCl took place by two competitive processes, i.e., photocatalytic process and photosensitized process of the OTC HCl under light irradiation.

### 3.2. Abstract

Pharmaceuticals, especially antibiotics, constitute an important group of aquatic contaminants given their environmental impact. Specifically, tetracycline antibiotics are produced in great amounts for the treatment of bacterial infections in both human and veterinary medicine. Several studies have shown that among all antibiotics, oxytetracycline hydrochloride (OTC HCl) is one of the most frequently detected TCs in soil and surface water. Results of the photocatalytic degradation of OTC HCl in aqueous suspensions (30 mg L<sup>-1</sup>) of 0.5 wt.% cobalt doped TiO<sub>2</sub> catalysts are reported in this study. The heterogeneous Co - TiO<sub>2</sub> photocatalysts were synthesized by two different solvothermal methods. Evonik Degussa Aevoxide P25 and self-prepared TiO<sub>2</sub> modified by the same methods were used for comparison. The synthesized photocatalysts were characterized by XRD, Raman spectroscopy, transmission electron microscopy (TEM), UV-vis DRS, and N<sub>2</sub> adsorption (BET) for SSA determination. The XRD and Raman results suggest that Ti<sup>4+</sup> was substituted by Co<sup>2+</sup> in the TiO<sub>2</sub> crystal structure. UV-visible spectroscopy of Co-TiO<sub>2</sub>-R showed a substantial redshift in comparison with bare TiO<sub>2</sub>-R. The photocatalytic performance

of the prepared photocatalysts in OTC HCl degradation was investigated employing UV-vis spectroscopy and high-performance liquid chromatography (HPLC). The observed initial reaction rates over Co-TiO<sub>2</sub>-R was higher compared with that of Co-TiO<sub>2</sub>-HT, self-prepared TiO<sub>2</sub>, and the commercial P25. The high surface area (153 m<sup>2</sup>g<sup>-1</sup>) which forms conducive conditions for the adsorption of the OTC HCl on the surface of the catalyst along with the impurity levels within the band gap (2.93 eV) play a pivotal role in the photocatalytic reactions by promoting the charge separation and improving the charge transfer ability. From these experimental results, it can be concluded that Co -doping under reflux demonstrates better photocatalytic performances than with the hydrothermal treatment.

**Keywords:** Photocatalysis, Co - TiO<sub>2</sub> catalyst, oxytetracycline hydrochloride, solvothermal synthesis, water treatment.

### 3.3. Introduction

The growing demand for clean water sources has become an important issue worldwide owing to increasing water pollution by, for example, pharmaceuticals, personal care products, and endocrine disruptors. Among a wide variety of pharmaceutical compounds, antibiotics, owing to their extensive use in human and veterinary medicine, may cause environmental impacts, disturbing the function of the ecosystem by developing antibiotic-resistant pathogens that are of potential risk for human health after incorporation with drinking water, and vegetables or fruits irrigated with contaminated water [1–3].

Tetracyclines (TCs), as the second most commonly known antibiotic in production and use, have been used as bacteriostatic agents for treating infections in both humans and animals, and as fungicides in fruit tree [4, 5]. Oxytetracycline hydrochloride (OTC HCl), a common member of tetracyclines TCs, is a broad-spectrum antibiotic frequently employed in veterinary medicine and agriculture. Although the concentrations of the antibiotics released from the environmental matrix to aquatic

systems are extremely low ( $\mu\text{g L}^{-1}$  to  $\text{mg L}^{-1}$ ), OTC HCl recognized as an emerging pollutant may cause serious risks to human health and ecosystems [6].

Owing to its chemical stability and antibiotic property, residues of OTC HCl released in the aquatic environment cannot be removed by conventional water treatment processes [7]. Therefore, AOPs have been considered as one of the most effective technologies to clean of the aquatic environment from this contaminant of emerging concern [2, 8]. So far, the photodegradation of tetracycline hydrochloride (TC HCl) has been reported using the photo-Fenton process [4, 9] and ozonation [10, 11]. Degradation of OTC has also been studied by the action of UV light, UV/H<sub>2</sub>O<sub>2</sub>, and UV activation of persulfate (UV/PS) [6, 12, 13]. However, there are numerous limitations such as the formation of byproducts, selective functional, photosensitive groups, and contact time [3]. Therefore, treatment processes using heterogeneous photocatalysis with TiO<sub>2</sub> have received enormous attention in recent years and have been employed in water treatment as a promising method for removal and mineralization of organic contaminants such as tetracyclines that are present in the aquatic environment [5, 14–18].

Photocatalysis using semiconductors has gained an important place among the AOPs. Notably, TiO<sub>2</sub> has received much more attention thanks to the high oxidizing power of its holes, as well as its photostability, non-toxicity, and low cost [19]. However, TiO<sub>2</sub>, owing to its intrinsic wide band gap (3.2 eV for anatase, 3.0 eV for rutile), can be only activated under UV light. Moreover, 90% of the photogenerated electrons and holes recombine in 10 ns [20]. These drawbacks are still a major limitation for the widespread application of TiO<sub>2</sub>.

In this respect, investigations of the visible light responsivity of TiO<sub>2</sub> have been developed via TiO<sub>2</sub> doping by low amounts of cations [21]; anions [22, 23]; and transition metals such as Fe, Cu, Mn, Ni, Cr, Zn, and Co [21–27]. Among various transition metals (i.e., Pt, Ag, Au, Ru, and Pd) [28–31] and transition metal oxides (i.e., Cu<sub>2</sub>O,  $\alpha$ -Fe<sub>2</sub>O<sub>3</sub>) [32–34], cobalt [35, 36] and cobalt oxides [37–40] as an interesting low-cost and earth-abundant mineral have attracted tremendous attention for the

development of visible light active TiO<sub>2</sub> materials. Cobalt-doped TiO<sub>2</sub> photocatalysts have been synthesized by various methods, such as the sol/gel technique [36, 41–50], hydrothermal treatment [51–54], impregnation method [55, 56], precipitation process [57] for the photocatalytic degradation of methylene blue [57,58], rhodamine B [58], methylene orange [57], phenol [41], 2-chlorophenol [41], and so on.

Among these preparation methods, hydrothermal synthesis as a well-known preparation method is environmentally friendly because the reaction proceeds in a closed system; the composition of the products is well controlled; and the materials prepared with this method are well crystallized and have a smaller particle size, positively affecting the thermal stability and the photocatalytic activity. For example, Jiang *et al.* [59] synthesized cobalt-doped TiO<sub>2</sub> by a one-step hydrothermal method for the photodegradation of phenol under visible light. They found that the catalyst doped with 0.3 wt.% shows the highest photocatalytic activity, and they contributed that to the high visible light response by inducing impurity states within its band gap. Rashad *et al.* [60] reported the photocatalytic degradation of methylene blue under UV light in the presence of cobalt-doped TiO<sub>2</sub> prepared using a hydrothermal treatment with a post-annealing temperature process at 500 °C. They observed a decrease in the surface area, a blue shift of the band gap with a slight enhancement in the photocatalytic activity by adding Co ions. Controversially, Castro *et al.* [51] synthesized Co-doped TiO<sub>2</sub> powders using hydrothermal synthesis. A mixed oxidation state of cobalt ions, that is, Co<sup>3+</sup> and Co<sup>4+</sup>, was deduced. Even if a decrease in the band gap was observed, no photocatalytic degradation of diquat under UV light was detected. They concluded that both the doped-metal content and valence of the doping ions are crucial factors that strongly determine the photocatalytic activity of the materials.

Reflux synthesis as an alternative low-temperature process is much more beneficial because of the lower equipment cost and simplicity. However, the doping of TiO<sub>2</sub> with cobalt using this method had just a few reports [61].

Although Co-doped TiO<sub>2</sub> NPs have been extensively studied previously, there are conflicting results on the effects of cobalt ion doping on the photoactivity of TiO<sub>2</sub>.

For example, Choi *et al.* reported that doping with Co<sup>3+</sup>, among various transition metals using the sol/gel method, decreased the photoactivity for the degradation of CHCl<sub>3</sub> under UV irradiation [21]. In 2010, the same group conducted a study on 13 different metal ions-doped TiO<sub>2</sub> with a sol/gel procedure and indicated that Co-TiO<sub>2</sub> material had a slight increase in the observed rate constant of methylene blue degradation. They also concluded that it is difficult to correlate between the physico-chemical properties such as light absorption and the visible light photocatalytic activities of the studied metal-doped TiO<sub>2</sub> materials [43]. The investigation of Bouras *et al.* indicated that Co-doping applying a sol/gel synthesis had a detrimental effect on the photocatalytic behavior of TiO<sub>2</sub> for the photocatalytic degradation of basic blue [44]. In contrast, other scientific groups reported that cobalt-modified TiO<sub>2</sub> synthesized by wet impregnation methods seems to increase the photocatalytic activity [55, 56]. Additionally, earlier studies have been mostly done on Co-doped TiO<sub>2</sub> thin films, and the main focus has commonly been made on the ferromagnetic properties of these catalysts [45, 53, 62–64].

The different synthesis methods employed to synthesize cobalt-doped TiO<sub>2</sub> along with the different types of substrates utilized for photocatalytic degradation examinations create a varying set of data that can often become controversial. These diverging results create doubts about the factual influence of cobalt doping on the photocatalytic activity. Therefore, Co-doped TiO<sub>2</sub> materials have been synthesized through two different methods, namely reflux and hydrothermal, to investigate the effect of incorporating cobalt cations in the TiO<sub>2</sub> matrix, as well as their photocatalytic activity under UV-visible irradiation. Although Co-doped TiO<sub>2</sub> NPs can be synthesized easily employing the reflux method, hardly any reports discussing its photocatalytic activity have been published. Until now, and to the best of the authors' knowledge, the UV-vis light-induced photocatalytic degradation of OTC HCl in the presence of Co-doped TiO<sub>2</sub> NPs has not been studied.

## 3.4. Results

### 3.4.1. Photocatalysts Characterizations

TiO<sub>2</sub> and Co-doped TiO<sub>2</sub> NPs were synthesized by thermal treatment of solutions of the Ti-and Co-precursors in propanol/water in an open system at the boiling point (reflux) and in a closed autoclave at 200 °C. The NPs obtained by the reflux method were labeled as TiO<sub>2</sub>-R and Co-TiO<sub>2</sub>-R, while the materials obtained at 200 °C were labeled as TiO<sub>2</sub>-HT and Co-TiO<sub>2</sub>-HT. The structural parameters and the phase purity of Co-TiO<sub>2</sub>-R, Co-TiO<sub>2</sub>-HT, TiO<sub>2</sub>-R, and TiO<sub>2</sub>-HT were investigated by means of XRD and the results are plotted in **Figure 3-1 (a)**.

All materials exhibit diffraction peaks occurring at  $2\theta = 25.42^\circ$ ,  $38.18^\circ$ ,  $48.24^\circ$ ,  $55.30^\circ$ ,  $63.12^\circ$ , and  $69.41^\circ$ , characteristic of the (101), (004), (200), (211), (204), and (116) planes of anatase TiO<sub>2</sub> (JCPDS 01-072-4820), respectively. Only trace amounts of brookite TiO<sub>2</sub> were detected at  $2\theta = 30.83^\circ$  in all NPs (JCPDS 01-076-1934). The XRD patterns of pure TiO<sub>2</sub>-HT show weak peaks at  $2\theta = 27.39^\circ$  and  $2\theta = 36.08^\circ$ , which were attributed to the (110) and (101) planes of the rutile phase (JCPDS 01-089-0552), respectively. There were no other TiO<sub>2</sub> peaks or any peaks that could be ascribed to Co, CoO, or CoTiO<sub>3</sub>, which is consistent with highly orientated Co-TiO<sub>2</sub> without any impurity phase. The particle sizes were calculated from the XRD data using the Debye Scherrer equation, and the calculated values are shown in **Table 3-1**. The cobalt doping seems to decrease the particle size of the Co-TiO<sub>2</sub>-HT, whereas it does not affect the particle size of the Co-TiO<sub>2</sub>-R.

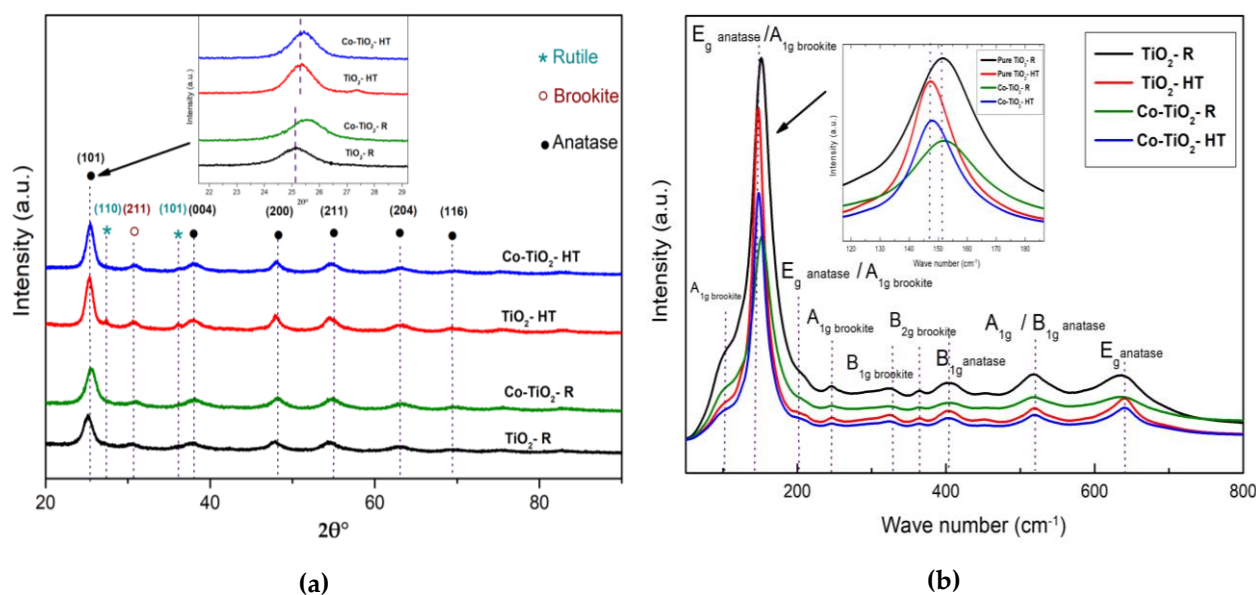


**Figure 3-1.** (a) X-ray diffraction (XRD) patterns, and (b) Raman spectra of TiO<sub>2</sub>-R, Co-TiO<sub>2</sub>-R, TiO<sub>2</sub>-HT, and Co-TiO<sub>2</sub>-HT composites.

**Table 3-1.** The crystal size, SSA, apparent band gap, and initial rates ( $r_0$ ) of OTC HCl degradation in the presence of TiO<sub>2</sub>-R, Co-TiO<sub>2</sub>-R, TiO<sub>2</sub>-HT, Co-TiO<sub>2</sub>-HT, and commercial P25.

Catalysts	XRD Size (nm)	TEM Size (nm)	SSA (m <sup>2</sup> g <sup>-1</sup> )	Band gap (eV)	$r_0$ [OTC HCl] UV-vis (mg L <sup>-1</sup> min <sup>-1</sup> )
TiO <sub>2</sub> -R	9.5	9.8 ± 0.2	160 ± 5	3.06	3.45
Co-TiO <sub>2</sub> -R	9.2	9.5 ± 0.2	153 ± 5	2.93	8.83
TiO <sub>2</sub> -HT	9.9	10.5 ± 0.2	109 ± 5	3.10	3.87
Co-TiO <sub>2</sub> -HT	8.4	9.7 ± 0.2	126 ± 5	3.03	4.05
P25	21	20 ± 0.2	50 ± 5	3.06	3.34
Photolysis	-	-	-	-	1.26

The Raman spectra of Co-TiO<sub>2</sub>-R, Co-TiO<sub>2</sub>-HT, TiO<sub>2</sub>-R, and TiO<sub>2</sub>-HT composites measured at room temperature in the range between 80 cm<sup>-1</sup> and 800 cm<sup>-1</sup> are shown in **Figure 3-1 (b)**. All samples reveal Raman bands at around 148, 402, 519, and 639 cm<sup>-1</sup> associated with E<sub>g</sub>, B<sub>1g</sub>, A<sub>1g</sub> or B<sub>1g</sub>, and E<sub>g</sub> vibrations of anatase TiO<sub>2</sub>, respectively. The additional very weak signal at 197 (sh) cm<sup>-1</sup> was also resolved and assigned to anatase TiO<sub>2</sub>. Characteristic peaks of brookite titania at 245, 324, and 364 cm<sup>-1</sup> were also observed. In order to see the changes associated with cobalt doping,

the full widths at half-maximum (FWHM) of the bands were calculated and given in **Table 3-2**. A slight change in the E<sub>g</sub> signals of anatase phase in all FWHM Raman signal values towards higher values indicates deviations in the local structure around Ti<sup>4+</sup> after cobalt modification, thus indicating the incorporation of cobalt ions in the TiO<sub>2</sub> lattice.

**Table 3-2.** The FWHM of TiO<sub>2</sub>-R, Co-TiO<sub>2</sub>-R, TiO<sub>2</sub>-HT, and Co-TiO<sub>2</sub>-HT composites.

Catalysts	E <sub>g</sub>	A <sub>1g</sub>	B <sub>1g</sub>	B <sub>2g</sub>	B <sub>1g</sub>	A <sub>1g</sub> /B <sub>1g</sub>	E <sub>g</sub>
	anatase	brookite	brookite	brookite	anatase	anatase	anatase
TiO <sub>2</sub> -R	32.8	41	75.5	26	93.5	96.5	129.2
Co-TiO <sub>2</sub> -R	34.8	46.5	71	23.5	96	94.5	172
TiO <sub>2</sub> -HT	19.5	33.5	83	27	97	94.5	84.8
Co-TiO <sub>2</sub> -HT	20.5	31.5	82	28	96.5	92.5	91.3

Morphological and detailed structural features of Co-TiO<sub>2</sub> and TiO<sub>2</sub> NPs were further explored using transmission electron microscopy (TEM) and high-resolution transmission electron microscopy (HRTEM). **Figure 3-2 (a, c, e, g)** show TEM images of Co-TiO<sub>2</sub> and bare TiO<sub>2</sub>. The TiO<sub>2</sub> NPs appear transparent and dense when the particles are in layers. The HRTEM images in **Figure 3-2 (b, d, f, h)** show that all materials are well crystallized, as indicated by the spacing of 0.35 nm, which corresponds to the (101) plane of anatase TiO<sub>2</sub>. The crystallite sizes of TiO<sub>2</sub>-R, Co-TiO<sub>2</sub>-R, TiO<sub>2</sub>-HT, and Co-TiO<sub>2</sub>-HT derived from the TEM images are in good agreement with the sizes calculated from the XRD data with the Scherrer equation (**Table 3-1**).



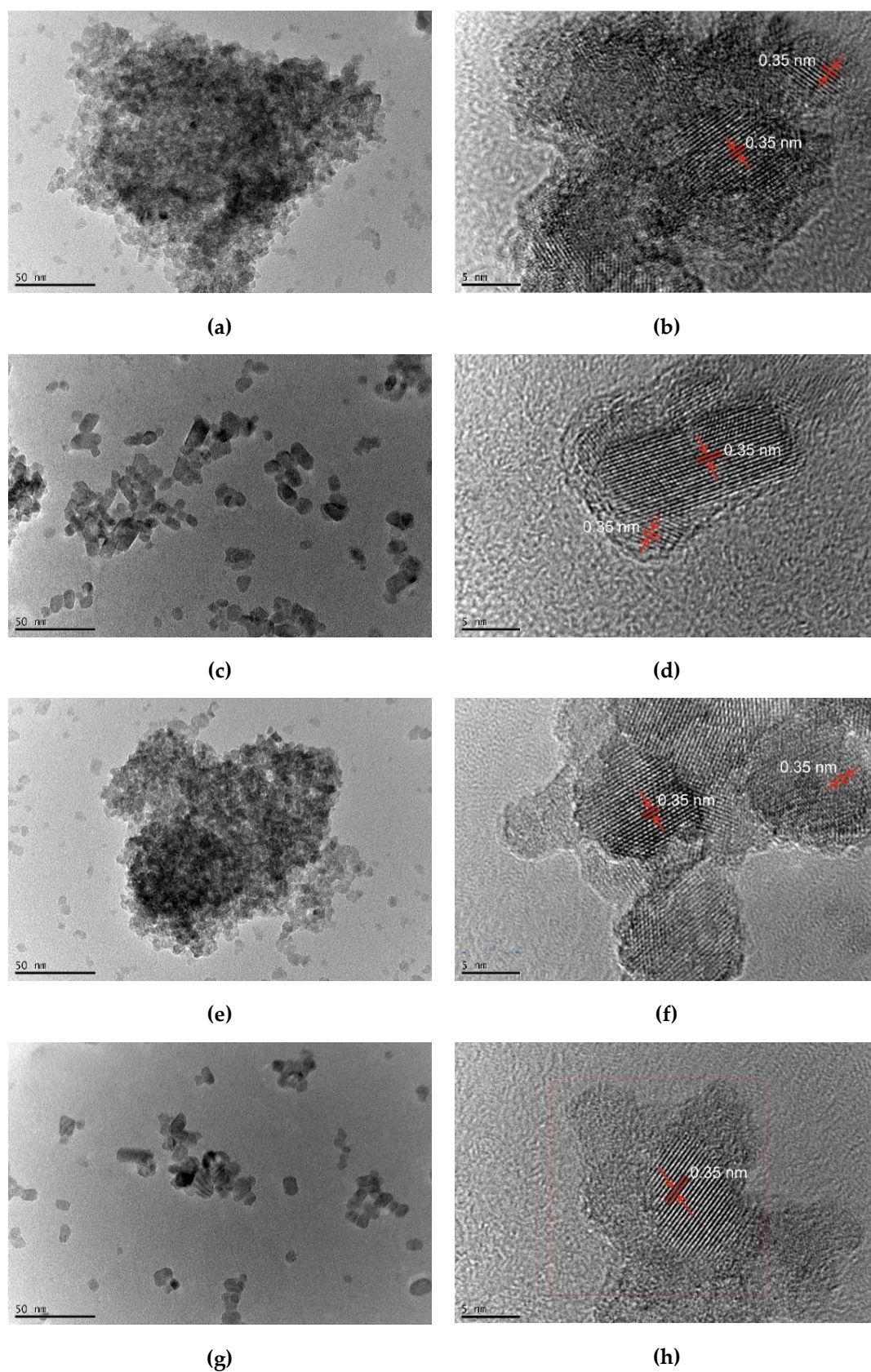


**Figure 3-2.** TEM and HRTEM images of (a,b) TiO<sub>2</sub>-R, (c,d) TiO<sub>2</sub>-HT, (e,f) Co-TiO<sub>2</sub>-R, and (g,h) Co-TiO<sub>2</sub>-HT composites.

The light absorption property of the as-prepared photocatalysts was explored through UV-vis DRS measurements. The corresponding results are depicted in **Figure 3-3 (a)**. The weak peak around 350 nm is the result of the switching in the absorption of the lamp. TiO<sub>2</sub>-HT and TiO<sub>2</sub>-R exhibit no optical response in the visible region. Cobalt doping into the TiO<sub>2</sub> lattice resulted in a significant absorption in the visible region (400 – 700 nm) of the spectrum. The band gap energies are obtained by converting the UV-vis absorbance spectra into Tauc plots using the equation  $(\alpha h\nu)^{1/n} = A(h\nu - E_g)$ , where  $h$  is Planck's constant,  $\nu$  is the frequency,  $\alpha$  is the absorption coefficient, and  $A$  is a proportionality constant. The value of the exponent  $n$  denotes the nature of the transition, which is equal to 1/2 for a direct band gap or equal to 2 for an indirect band gap transition. The plots shown in **Figure 3-3 (b)** indicate indirect allowed transitions in all four NPs, with band gap energies as given by the intercept of the tangent lines with the abscissa in **Figure 3-3 (b)** of 2.93–3.03 eV and 3.06–3.10 eV for the Co-doped and the bare TiO<sub>2</sub> NPs, respectively (**Table 3-1**).

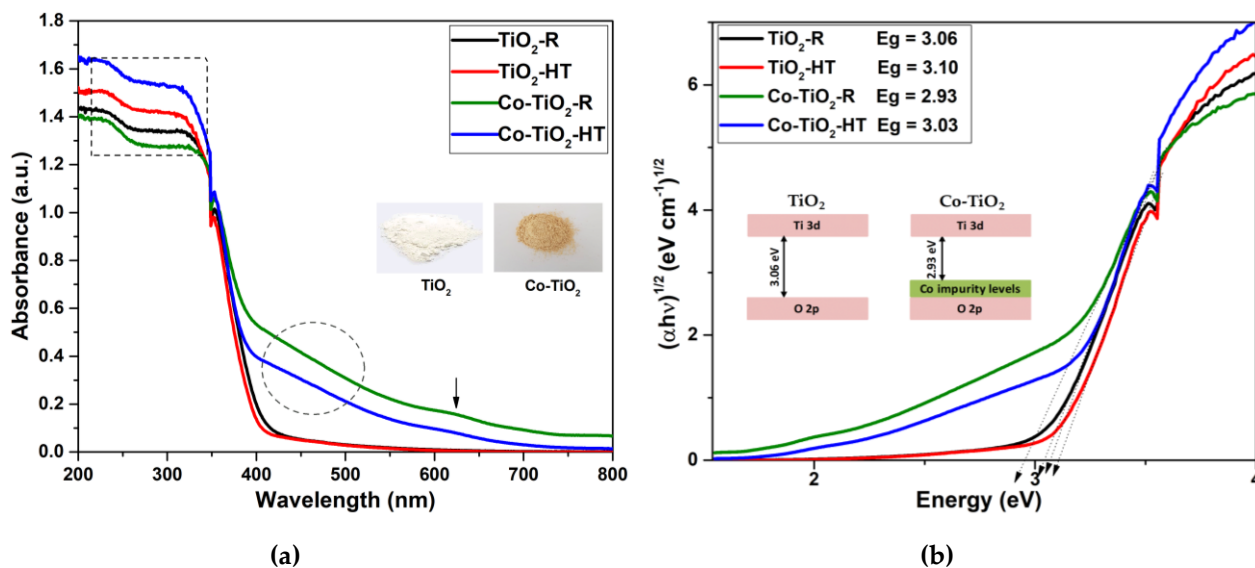


**Figure 3-3.** (a) UV-vis DRS and (b) the corresponding indirect band gap energies of TiO<sub>2</sub>-R, Co-TiO<sub>2</sub>-R, TiO<sub>2</sub>-HT, and Co-TiO<sub>2</sub>-HT NPs.

### 3.4.2. Photocatalytic Activities of Co-TiO<sub>2</sub>-R and Co-TiO<sub>2</sub>-HT on UV-vis Light-Induced OTC HCl Degradation

The photocatalytic ability of the synthesized photocatalysts was evaluated in the aqueous phase at constant pH (pH 5) by the photodegradation of OTC HCl as the target pollutant under the full output of a xenon arc lamp (UV-vis illumination). The intensity of the OTC HCl characteristic peak decreased with increasing the UV-vis irradiation time, as shown in the time-dependent UV-vis absorbance spectra in **Figure 3-4 (a)**. The experimental results of the photocatalytic degradation over all samples are depicted in **Figure 3-4 (b)**. To further compare the photocatalytic activities of the doped and bare materials, kinetic analysis of OTC HCl photodegradation was carried out by assuming first-order kinetics;  $\ln(C_t/C_0) = -kt$ . The corresponding initial reaction rates were calculated ( $r_0 = k \cdot C_0$ ) and are shown in **Table 3-1**. Among all prepared composites, the catalyst prepared by the reflux synthesis showed a higher initial rate of OTC degradation ( $8.83 \text{ mg L}^{-1} \text{ min}^{-1}$ ). As depicted in the table, the observed initial reaction rates for the bare TiO<sub>2</sub> and Co-doped TiO<sub>2</sub> materials were found to decrease in the following order: Co-TiO<sub>2</sub>-R > Co-TiO<sub>2</sub>-HT > TiO<sub>2</sub>-HT > TiO<sub>2</sub>-R > P25.

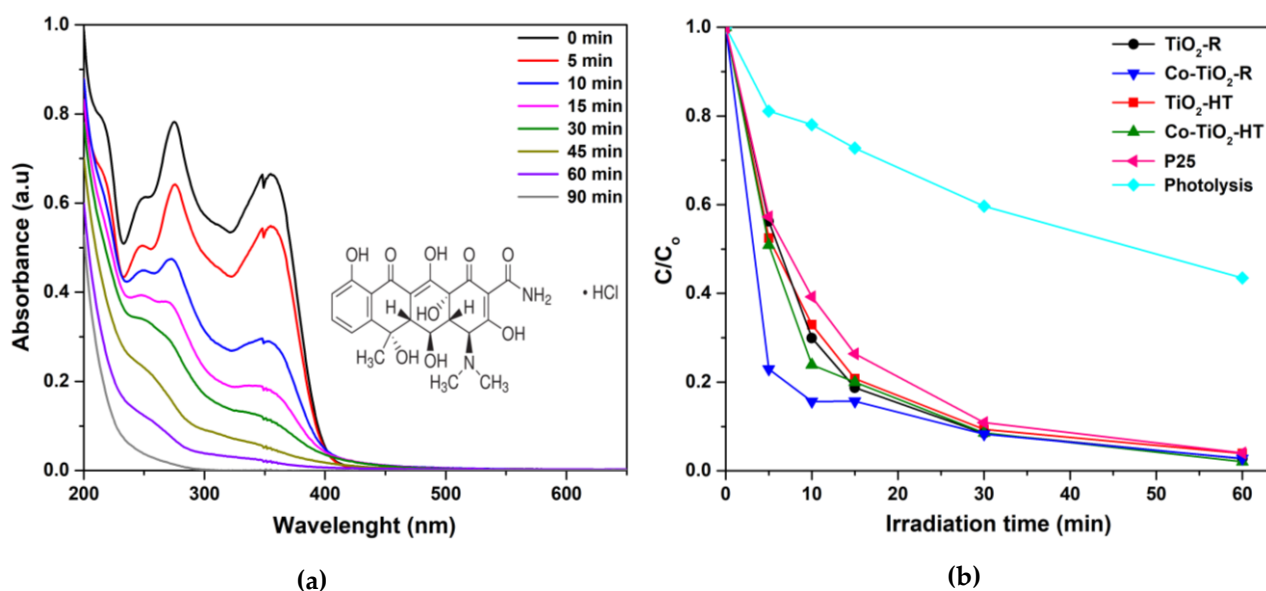


**Figure 3-4.** (a) Time-dependent UV-vis spectra of OTC HCl solution at pH=5, and (b) kinetics of OTC HCl ( $30 \text{ mg L}^{-1}$ ; pH=5) photodegradation using Co-TiO<sub>2</sub> and TiO<sub>2</sub> photocatalysts upon UV-vis illumination.

## 3.5. Discussion

### 3.5.1. Characterization of Co-TiO<sub>2</sub>-R, and Co-TiO<sub>2</sub>-HT Composites

The effect of the preparation method as well as the effect of cobalt ions doping on TiO<sub>2</sub> for the photodegradation of OTC HCl pharmaceutical was investigated in this study. The highest photocatalytic activity was achieved for the catalyst modified with 0.5 wt.% cobalt and prepared in reflux (i.e., Co-TiO<sub>2</sub>-R; **Figure 3-4 (b)**). It is known that dopant atoms may be introduced in TiO<sub>2</sub> either substitutionally or interstitially depending on the ionic radius of the dopant. As previously reported by Rodríguez-Talavera *et al.* [65], the substitution of high spin Co<sup>2+</sup> with the ionic radius R(Co<sup>2+</sup>) = 0.885 Å for the octahedral Ti<sup>4+</sup> with the ionic radius R(Ti<sup>4+</sup>) = 0.745 Å in the TiO<sub>6</sub> octahedra of the anatase structure induces O<sup>2-</sup> vacancies and might cause the lattice distortion to rise. The XRD patterns of the Co-TiO<sub>2</sub> resemble those of the bare TiO<sub>2</sub> without any peaks associated with metallic Co or cobalt oxides, confirming that cobalt is present as Co(II) ions. The structural characteristic of Co-TiO<sub>2</sub> and bare TiO<sub>2</sub>, as displayed in **Figure 3-1 (a)**, are mainly composed of the anatase phase. The presence of small contamination of the brookite phase is evidenced in all samples at 2θ = 30.83°, with a possible overlapping of the (120) and (111) peaks of brookite at 2θ = 25.34° and 25.69° with the (101) diffraction peak of anatase at 2θ = 25.28°. The appearance of brookite was further confirmed by the analysis of Raman spectra (**Figure 3-1 (b)**). This observation of the brookite phase is probably because of the acidic conditions in which the synthesis was performed, as seen in the work of [66], and since, it has been reported by the authors of [67] that the synthesis in ammonia limits the brookite formation. In the TiO<sub>2</sub> prepared under hydrothermal conditions, two small diffraction peaks characteristic of the rutile phase were evidenced at 2θ = 27.39° and 2θ = 36.08°, indicating lower stability of this sample, which was not seen in the case of bare TiO<sub>2</sub>-R. No rutile phase was detected for Co-TiO<sub>2</sub>-R and Co-TiO<sub>2</sub>-HT, which can be explained by the stabilizing effect of Co ions on the crystalline structure of anatase TiO<sub>2</sub>, preventing the formation of the rutile phase. This observation was also previously reported in Co-doped TiO<sub>2</sub> [46]. Additionally, the position of the most intense peak and

the lattice parameters of anatase phase (101) for the Co-TiO<sub>2</sub>-R and Co-TiO<sub>2</sub>-HT samples are significantly shifted towards a higher angle, as shown in **Figure 3-1 (a inset)**, supporting the substitution of some Co into the Ti lattice site. This Co substitution has also been described by Le *et al.* [68]. The particle sizes of the synthesized photocatalysts as listed in **Table 3-1** remain almost unchanged for the catalysts prepared in reflux ( $9.5 \pm 0.2$  nm and  $9.2 \pm 0.2$  nm), whereas the crystallite size of Co-TiO<sub>2</sub>-HT is slightly smaller than that of the TiO<sub>2</sub>-HT sample ( $9.9 \pm 0.2$  nm and  $8.4 \pm 0.2$  nm). It is generally expected that the crystallite size decreases after metal doping, which may be explained by the Co-O bond formation on the surface of the modified titania, which might be responsible for the non-growth of TiO<sub>2</sub> crystallite.

The Co-induced structural modification of TiO<sub>2</sub> NPs was further analyzed with micro Raman spectroscopy, which is shown in **Figure 3-1 (b)**. In addition to the common anatase vibrations, a weak sub-band at  $197\text{ cm}^{-1}$ , which may coincide with the brookite band ( $A_{1g}$ ), and a very weak signal at  $447\text{ cm}^{-1}$ , characteristic of the rutile phase, was observed in all materials. The reason for not detecting the brookite characteristic peak at  $151\text{ cm}^{-1}$  could be because of the overlapping with the anatase intense band ( $E_g$ ), which is also observed at about  $148\text{ cm}^{-1}$ . These results are in good agreement with the XRD data and match well with those reported for anatase and brookite phases of titania [69]. As is well known, doping TiO<sub>2</sub> with Co<sup>2+</sup> induces the formation of oxygen vacancies, because substitution of Ti<sup>4+</sup> by Co<sup>2+</sup> demands oxygen vacancy to balance the charges [65]. A very close look into the spectra in **Figure 3-1 (b inset)** reveals a small shift in the most intense Raman band ( $E_g$ ) at  $148\text{ cm}^{-1}$ . This result suggests that Co<sup>2+</sup> has been inserted into the anatase structure and substituted the Ti ions in the crystal lattice. Moreover, the intensity of the signals in the Co-doped samples has decreased, indicating the effect of the cobalt atoms on the lattice vibration of titania. Similar behavior has been reported by Huang *et al.* for the 5 at.% Co-doped TiO<sub>2</sub> nanotubes prepared by sol/gel [47]. This shift in the anatase/brookite peak position ( $E_g$ ) with the decrease of the peak intensity and the change in FWHM values of Co-TiO<sub>2</sub>-R and Co-TiO<sub>2</sub>-HT endorse the incorporation of cobalt ions in the TiO<sub>2</sub>



matrix. No vibration modes for cobalt clusters or cobalt oxides were observed, which additionally supports the presence of dopant cation in the substitutional positions of the titania host lattice in the Co-TiO<sub>2</sub> NPs. These outcomes are well consistent with the XRD results.

To further elucidate the size and the structure of the Co-doped TiO<sub>2</sub> NPs, TEM measurements were carried out and are presented in **Figure 3-2**. Owing to the low amount of the dopant (0.5 wt.%), defects in the lattice structures do not become observable. As revealed by the HRTEM results in **Figure 3-2 (b, d, f, h)**, the interlayer distance of the NPs is about 0.35 nm for TiO<sub>2</sub>-R, Co-TiO<sub>2</sub>-R, TiO<sub>2</sub>-HT, and Co-TiO<sub>2</sub>-HT, which is assigned to the crystal plane (101) of anatase TiO<sub>2</sub>. As indicated in **Figure 3-2 (c, g)** using the hydrothermal method, TiO<sub>2</sub> was transformed and appears as well-defined multilayer spherical and pseudo-cubic in shape, which could be probably due to the small amount of brookite phase present in the titania [70]. The lattice fringes obtained with an interval of 0.35 nm, thus corresponding to the (101) plane of anatase and the (210) plane of brookite [52, 70], imply that the NPs are highly crystalline, which is in accordance with the XRD patterns and Raman shifts shown in **Figure 3-1**. From these TEM images, the average particle size of the as-synthesized NPs is found to be about 9.8, 9.5, 10.5, and 9.7 nm, and almost independent from the synthetic method within the limit of the experimental error ( $\pm 0.2$  nm) for the TiO<sub>2</sub>-R, Co-TiO<sub>2</sub>-R, TiO<sub>2</sub>-HT, and Co-TiO<sub>2</sub>-HT, respectively. These particle sizes are in good agreement with published data [59], and approximately in the same range as the particle sizes calculated from XRD data using Scherrer's formula (**Table 3-1**).

The SSA is assumed to play a crucial role in photocatalytic reactions. The SSA of all synthesized photocatalysts was measured via BET adsorption analysis and the values obtained for the Co-doped TiO<sub>2</sub> and bare TiO<sub>2</sub> samples are summarized in **Table 3-1**. The surface areas of the synthesized TiO<sub>2</sub>-R and Co-TiO<sub>2</sub>-R composites are almost identical considering the experimental error of the device, giving the values of  $(160 \pm 5)$  and  $(153 \pm 5)$  m<sup>2</sup>g<sup>-1</sup> for TiO<sub>2</sub>-R and Co-TiO<sub>2</sub>-R, respectively. However, doping TiO<sub>2</sub> with cobalt using the hydrothermal route resulted in a slight increase of the

surface area from  $(109 \pm 5)$  up to  $(126 \pm 5)$  m<sup>2</sup>g<sup>-1</sup>, which was also reported in the work of [71]. It is reasonable to assume that Co doping affects the TiO<sub>2</sub> unit cell parameters, resulting in a distortion of the crystal lattice, which may increase the surface area of the doped material, reflecting a loss of the crystallinity. However, the surface area of Co-TiO<sub>2</sub>-R remains greater than that of Co-TiO<sub>2</sub>-HT, allowing the assumption that Co-TiO<sub>2</sub>-R adsorbs more substrate than Co-TiO<sub>2</sub>-HT.

The optical properties of pure TiO<sub>2</sub> and Co-TiO<sub>2</sub> prepared by hydrothermal and reflux methods were investigated. The results depicted in **Figure 3-3 (a)** indicate that doping TiO<sub>2</sub> with cobalt significantly increases the light absorbance of the materials. The diffuse reflectance spectra of pure TiO<sub>2</sub> consist of a sharp absorption edge around 400 and 407 nm for TiO<sub>2</sub>-HT and TiO<sub>2</sub>-R, which is attributed to the electron transition from the valence band to the conduction band O<sub>2p</sub>-to-Ti<sub>3d</sub>, whereas the Co-doped samples have an extended visible light absorption range with absorption bands up to 410 and 423 nm for Co-TiO<sub>2</sub>-HT and Co-TiO<sub>2</sub>-R, respectively. It is also worth noting that Co-TiO<sub>2</sub>-HT, as seen from the framed region in the UV region of **Figure 3-3 (a)**, has the highest absorbance intensity in the UV spectrum, followed immediately by bare TiO<sub>2</sub>-HT. Furthermore, the UV-vis absorbance spectra of the Co-doped materials exhibit a tail in the visible range from 400 nm to 700 nm. The additional broad absorption band in the region between 420 and 520 nm (marked with a circle) may be assigned to the <sup>4</sup>T<sub>1g</sub>-to-<sup>4</sup>T<sub>1g</sub> (P) transition, and the weak peak at 620 nm (marked with an arrow) can be attributed to the <sup>4</sup>T<sub>1g</sub>-to-<sup>4</sup>A<sub>2g</sub> transition for high spin Co<sup>2+</sup> (3d<sup>7</sup>) incorporated into the TiO<sub>2</sub> framework, as previously reported in the literature [27, 59, 72, 73]. From the photocatalysis viewpoint, this sub-band level within the band gap is of great use, as it can be possible to tune the absorption onset to the higher visible wavelength by Co-doping and improve the photocatalytic activity.

The determination of the corresponding band gaps of the pure TiO<sub>2</sub> and Co-doped TiO<sub>2</sub> samples was evaluated using the Tauc plot method. The  $(\alpha\hbar\nu)^{1/n}$  versus  $(\hbar\nu)$  plots of the catalysts are presented in **Figure 3-3 (b)**. Plotting  $(\alpha\hbar\nu)^{1/n}$  versus  $(\hbar\nu)$  is a matter of testing n=1/2 or n=2 to compare which gives the better fit, and thus

identifies the correct electron transition type occurring in Co-TiO<sub>2</sub> powders. In TiO<sub>2</sub>-R and TiO<sub>2</sub>-HT materials, the square power  $(\alpha h\nu)^{1/2}$  used as titanium dioxide is well known to have an indirect allowed transition. Thus, the optical absorption band gaps ( $E_g$ ) for TiO<sub>2</sub>-R and TiO<sub>2</sub>-HT were estimated to be 3.06 and 3.10 eV, respectively. To find out the effect of the cobalt ion doping on the TiO<sub>2</sub> band gap, the Tauc plots of the Co-TiO<sub>2</sub> samples were also analyzed and depicted in **Figure 3-3 (b)**. As could be seen, Co-TiO<sub>2</sub>-R exhibited band gap energy, which decreased up to 2.93 eV, possibly because of the generation of Co-3d defect states near the valence band maximum of TiO<sub>2</sub>-R, as shown in the inset of **Figure 3-3 (b)**, whereas the cobalt doping using hydrothermal synthesis does not affect significantly the band gap of TiO<sub>2</sub>-HT with a value of 3.03 eV for Co-TiO<sub>2</sub>-HT. This narrowing of the energy band gap of Co-TiO<sub>2</sub> has been also observed by the authors of [59], Choudhury [48], and Khurana *et al.* [49], and was explained by the introduction of new impurity states near the valence band edge of TiO<sub>2</sub>. It can be concluded from these results that Co<sup>2+</sup> doping employing reflux synthesis results in a remarkable decrease in the band gap of TiO<sub>2</sub> and a red shift of the absorption onset within the visible spectrum, leading to much greater electrons and holes generation, which could migrate to the surface to drive redox reactions with the adsorbed pharmaceutical.

### 3.5.2. UV-vis Light-Induced Oxytetracycline Hydrochloride Degradation over Co-TiO<sub>2</sub> Composites

The solar light-induced photocatalytic ability of the synthesized Co-doped TiO<sub>2</sub> system was evaluated through the degradation of OTC HCl in aqueous suspension at constant pH. A comparison of the activity was made with undoped TiO<sub>2</sub> and the commercial Degussa P25. The UV-vis-light-induced degradation profile of OTC HCl using pure TiO<sub>2</sub> and Co-doped TiO<sub>2</sub> is given in **Figure 3-4 (b)**. As previously reported [74, 75], OTC HCl has four species at different pH ranges, and each species has a unique electric charge state, which may have an influence on the photolytic and photocatalytic degradation under both UV and visible light. To avoid any possible changes in the form of OTC HCl, it was chosen to maintain the pH at 5, which corresponds to the



neutral zwitterions form (H<sub>2</sub>OTC<sup>±</sup>). Under UV-vis irradiation, the light-induced degradation of OTC HCl in terms of initial reaction rates was found to increase drastically from 3.45 to 8.83 mg L<sup>-1</sup>min<sup>-1</sup> for the Co-TiO<sub>2</sub>-R composite. A negligible increase in the initial rates from 3.87 to 4.05 mg L<sup>-1</sup>min<sup>-1</sup> was also observed for the Co-TiO<sub>2</sub>-HT. Furthermore, the observed initial reaction rate for all composites was higher than that of the commercially available P25. These experimental results agree well with the BET surface area results and the UV-vis absorption data, suggesting that the high surface area along with the reduced band gap of the Co-TiO<sub>2</sub>-R have a major influence on the kinetics of the photocatalytic performance of this material (**Table 3-1**). It is also worth noting that all samples led finally to complete mineralization of OTC HCl, even bare TiO<sub>2</sub>. This may be because of the mixed brookite with anatase phases leading to an occurrence of junctions among different polymorphic TiO<sub>2</sub> phases that enhance the separation of the photogenerated electron-hole pairs under UV light. It is also expected that, with UV-vis, excitation of TiO<sub>2</sub> using a xenon arc lamp suggests that photocatalysis acts by direct near-UV excitation of TiO<sub>2</sub>. Additionally, and owing to the photosensitization reaction, bare TiO<sub>2</sub> could be rather activated under visible irradiation.

Comparing the photocatalytic results obtained with the composites prepared by the two synthesis methods, the UV-vis-light-induced degradation of OTC HCl mediated by Co-TiO<sub>2</sub> and TiO<sub>2</sub> using the hydrothermal synthesis seems to have an increasing function with the BET surface area. Compared with TiO<sub>2</sub>-HT, Co-TiO<sub>2</sub>-HT has a significantly larger specific surface area and smaller particle size, which indicates that the Co species decelerates the crystal-growth rate of the anatase phase. This result suggests that cobalt doping can significantly increase the SSA for the Co-TiO<sub>2</sub>-HT sample and prevent the phase transformation of anatase to rutile phase, which was evidenced by the absence of the two main peaks of rutile at 2θ = 27.39° (110) and 2θ = 36.08° (101) observed in the XRD patterns of TiO<sub>2</sub>-HT, resulting in the stability of the material with a slight enhancement of the photocatalytic activity of the light-induced degradation of OTC HCl using Co-TiO<sub>2</sub>-HT. Controversially, the Co-doping did not

significantly affect the SSA of Co-TiO<sub>2</sub> synthesized under reflux. However, the surface area of Co-TiO<sub>2</sub>-R stayed larger than that of Co-TiO<sub>2</sub>-HT. On the other hand, Co-TiO<sub>2</sub>-R showed the highest UV-vis light absorption, resulting in efficient UV-vis-light-induced degradation of the target pollutant. This high enhancement seen in the case of the co-doped sample prepared by the reflux method could be attributed in part to its high surface area, which allows adsorbing more substrate (OTC HCl) on the surface of the catalyst, and in another part to the high ability of this catalyst to absorb UV-vis-light, which facilitates the electron-hole pair generation participating in the photocatalytic reactions in the system.

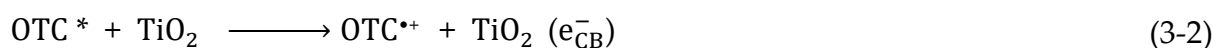
The blank experiment indicates that the direct photolysis of OTC HCl cannot be ignored, because around 38% was decayed without a photocatalyst within 30 min of UV-vis irradiation. This result suggests the responsible mechanism for the photolytic degradation of OTC HCl at pH 5, which may involve the excitation of OTC HCl to singlet (S<sub>1</sub>) or triplet (T<sub>1</sub>) states (OTC\*) under UV light.

### 3.5.3. Proposed Mechanisms of UV-vis Light-Induced OTC HCl Degradation using Co-TiO<sub>2</sub> Catalysts

In general, the photocatalytic oxidation of organic compounds mainly involves the photoabsorption of the photocatalyst, the generation of photogenerated electron-hole, the transfer of charge carriers, and the consumption of the charge carriers by the targets [76]. Co-doped TiO<sub>2</sub> materials showed the ability to absorb visible light, affecting the transition of the electrons from the VB (O 2p) to CB (Ti 4d) in the photocatalysts. **Figure 3-3 (a)** showed that the light absorption by the Co-doped TiO<sub>2</sub> samples occurred mainly when  $\lambda < 400$  nm. As shown in **Figure 3-4 (a)**, OTC HCl has no light absorption characteristics in the visible region (wavelengths longer than 400 nm) and was degraded within a certain wavelength range of the UV light. However, it was found that OTC HCl was decayed by Co-TiO<sub>2</sub> materials upon UV-vis-light irradiation. Thus, the materials absorbing light irradiation in the present study are supposed to be Co-TiO<sub>2</sub> catalyst and OTC HCl. Therefore, both photocatalytic and

photosensitized process would work simultaneously under these experimental conditions.

As bare TiO<sub>2</sub> absorbs only UV light, the degradation of OTC HCl can be induced indirectly by the absorption of the TiO<sub>2</sub> conduction band electron acting as an electron scavenger on the TiO<sub>2</sub> surface. In addition to the photocatalytic oxidation mechanism, which is thermodynamically possible, the photosensitizing oxidation mechanism of OTC HCl can also occur, suggesting that the electron from the excited OTC HCl molecule is injected into the CB of the TiO<sub>2</sub>, and the radical formed at the surface rapidly undergoes degradation to yield products (**Equations (3-1) and (3-2)**) [74, 77]. The photocatalytic degradation of OTC HCl over bare TiO<sub>2</sub> might also occur by the combined action of holes and •OH yielding products.



Considering the present results, a mechanism of the light-induced charge transfer behaviors during the degradation of OTC HCl and using the Co-doped TiO<sub>2</sub> is illustrated in **Figure 3-5**. Accordingly, the cobalt would introduce a new energy level (3d orbit) just above the valence band of TiO<sub>2</sub> and decreases the band gap, as shown in **Figure 3-3 (b)**. Hence, Co-TiO<sub>2</sub>-R and Co-TiO<sub>2</sub>-HT can be activated under visible light. Therefore, more electrons from the visible region are used to produce photogenerated electrons and holes. The photogenerated electrons accumulated in the Co-TiO<sub>2</sub> conduction band could easily transfer to the adsorbed oxygen O<sub>2</sub>, forming a superoxide radical anion O<sub>2</sub><sup>•-</sup> (-0.13 V vs. NHE), which combines with H<sup>+</sup> to form hydrogen peroxide H<sub>2</sub>O<sub>2</sub> (0.89 V vs. NHE). Consequently, O<sub>2</sub><sup>•-</sup> reacts with H<sub>2</sub>O<sub>2</sub>, generating •OH (0.38 V vs. NHE), which further converts OTC HCl to mineralized products. On another hand, the photogenerated holes (h<sub>VB</sub><sup>+</sup>) accumulate in the valence band of Co-TiO<sub>2</sub> and either oxidize directly the pollutant, or they are consumed by participating in the oxidation of water yielding •OH (1.89 V vs. NHE), which further oxidizes OTC HCl. The Co species could trap the part of photogenerated holes. Thus,

the recombination rate of photogenerated electrons and holes might be decreased. Consequently, the photocatalytic degradation efficiency of OTC HCl over Co-TiO<sub>2</sub> catalysts is improved (**Figure 3-5**).

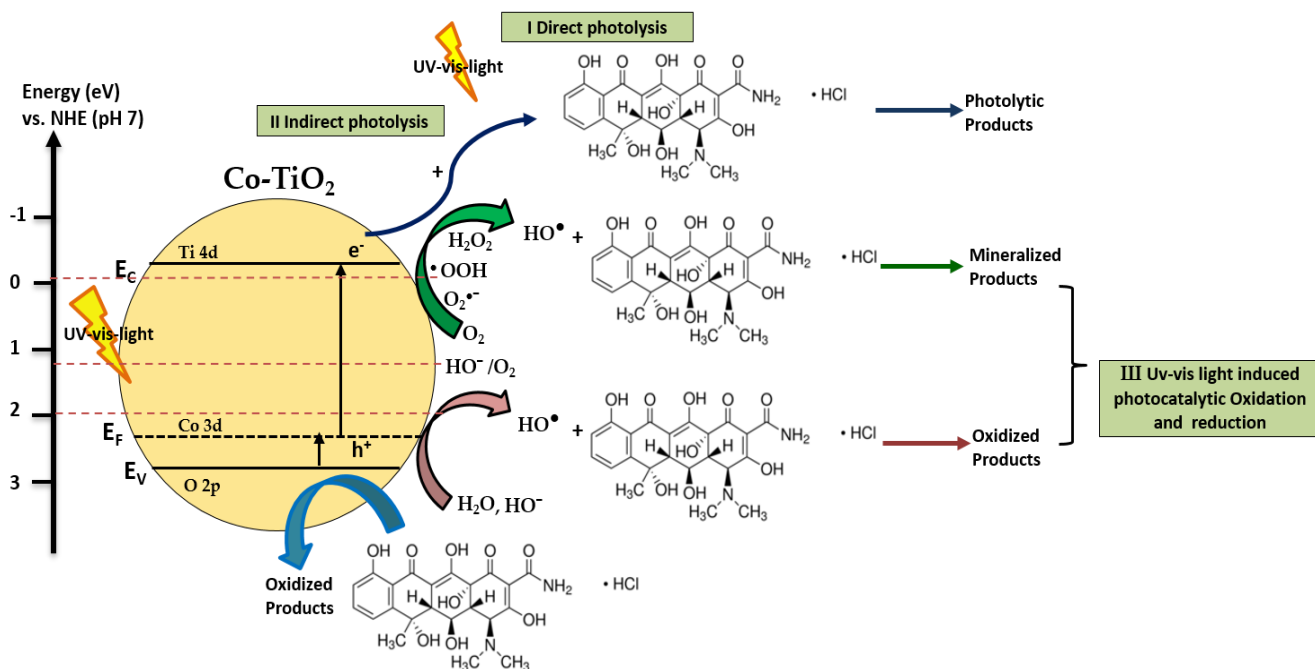


**Figure 3-5.** Illustration of the mechanism of UV-vis light-induced OTC HCl degradation using Co-TiO<sub>2</sub> NPs.

## 3.6. Materials and Methods

### 3.6.1. Materials Composites

Titanium (IV) isopropoxide (Ti(OPri)<sub>4</sub> (97%)), cobalt (II) acetate tetrahydrate (Co(Ac)<sub>2</sub>·4H<sub>2</sub>O (99.99%)), oxytetracycline hydrochloride (OTC HCl, 95%), and hydrochloric acid (HCl, 37%) were purchased from Sigma Aldrich Chemie GmbH, München, Germany, 2-propanol anhydrous (99.5%, Carl Roth GmbH, Karlsruhe, Germany) and methanol (99.9%, Carl Roth GmbH, Karlsruhe, Germany) were used of analytical grade and used without further purification. Aeroxide TiO<sub>2</sub> P25 with a mixture of anatase (80%) and rutile (20%) crystal phase and a specific surface area of 50.1 m<sup>2</sup>g<sup>-1</sup> was kindly provided by Evonik Industries AG, Essen, Germany. Deionized water from a Sartorius Arium 611 device (Sartorius AG, Göttingen, Germany) with a resistivity of 18.2 MΩ·cm was used for the preparation of all aqueous solutions.

### 3.6.2. Photocatalysts Synthesis

#### 3.6.2.1. High-Temperature Synthesis of Cobalt-Doped TiO<sub>2</sub>

Two solutions were prepared: solution A containing a prescribed amount of titanium isopropoxide (Ti(OPri)<sub>4</sub>) as the TiO<sub>2</sub> precursor dissolved in anhydrous propanol with vigorous stirring. Solution B was prepared by adding 0.5 g (Co(Ac)<sub>2</sub>·4H<sub>2</sub>O to 50 mL of 2-propanol, 10 mL of distilled water, and 0.5 mL of 1M HCl in a 500 mL flask and stirring for 20 min. Solution A was then added dropwise to solution B with continuous stirring. The formed gel was aged for 24 h to ensure complete hydrolysis. The obtained mixture was transformed into a stainless-steel autoclave and hydrothermally heated to 200 °C for 10 h. After the autoclave was cooled to room temperature, the yellow precipitate at the bottom of the autoclave was separated, washed with ethanol and deionized water several times, and dried at 70 °C overnight. The obtained residue was calcined at 500 °C for 5 h and denoted as Co-TiO<sub>2</sub>-HT. For comparison purposes, the pure TiO<sub>2</sub> was synthesized using the same procedure without adding the Co precursor. Bare TiO<sub>2</sub> catalyst was denoted as TiO<sub>2</sub>-HT.

#### 3.6.2.2. Reflux Synthesis of Cobalt-Doped TiO<sub>2</sub>

To synthesize the same photocatalysts by the reflux method, the mixture of solutions A and B were refluxed for 6 h. The obtained residue was calcined at 500 °C for 5 h and denoted as Co-TiO<sub>2</sub>-R. The pure TiO<sub>2</sub> was prepared using the same procedure without adding the cobalt precursor. The pure TiO<sub>2</sub> catalyst was denoted as TiO<sub>2</sub>-R.

#### 3.6.2.3. Photocatalysts Characterization

The crystalline structure of the Co-TiO<sub>2</sub>-R, Co-TiO<sub>2</sub>-HT, TiO<sub>2</sub>-R, and TiO<sub>2</sub>-HT catalysts was measured by powder X-ray diffraction (XRD) (D8 Advance system, Bruker, Billerica, MA, USA), using a Cu K $\alpha$  radiation source with a wavelength of  $\lambda = 1.54178 \text{ \AA}$  over a  $2\theta$  range from 20° to 100°, with a 0.011° step width. The average crystal sizes of the synthesized Co-TiO<sub>2</sub> and pure TiO<sub>2</sub> samples were calculated by

applying the scattering characteristic of the anatase structure to the Scherrer equation. Raman measurements were made employing a confocal micro-Raman spectrometer (Senterra Bruker Optik GmbH, Ettlingen, Germany). All depolarized spectra were obtained at ambient conditions in backscattering geometry using an Olympus BX 51 microscope (Olympus Corp., Tokyo, Japan) that allows the incident 532 nm laser beam to be focused on the sample as a spot of about 2 μm in diameter. An integration time of 1 s, 50 co-additions, and a power of 2 mW was used. The instrumental precision was within ± 3 cm<sup>-1</sup>. Diffuse reflectance (DR) UV-vis spectroscopy was employed using a spectrophotometer (Varian Spectrophotometer Cary-100 Bio, Agilent Technologies, Santa Clara, CA, USA) at room temperature. Barium sulfate (BaSO<sub>4</sub>) was used as a standard for 100% reflectance measurement. Reflectance was converted by the instrument software to F[R] values according to the Kubelka-Munk theory. The specific surface area (SSA) of the investigated materials was determined according to the multi-layer adsorption model by the BET method using a FlowSorb II 2300 apparatus from Micromeritics Instrument Company (Norcross, GA, USA). Before all measurements, the samples were evacuated at 180 °C for 1 h. Transmission electron micrographs (TEMs) of the catalysts were taken using a TEM Tecnai G2 F20 TMP device (FEI Company, Hillsboro, OR, USA) operated at an acceleration potential of 200 kV with a FEG field effect, objective lenses TWIN, and point resolution of 0.27 nm.

### 3.6.3. UV-vis Light-Induced Oxytetracycline Hydrochloride (OTC HCl) Degradation

Photocatalytic efficiencies of the commercial Degussa P25, pure TiO<sub>2</sub>, and Co-TiO<sub>2</sub> photocatalysts were measured for OTC HCl photodegradation as a model compound. The photocatalytic degradation experiments were carried out using a 300 W Xenon arc lamp (Müller Elektronik-Optik, Moosinning, Germany) as the UV-vis light source. The experiments were conducted on a Pyrex glass reactor with a capacity of 230 mL and equipped with a cooling jacket. The temperature was maintained constant at 25 °C using a thermostatic bath (Julabo GmbH, Seelbach, Germany). An aqueous solution of OTC HCl (230 mL, 30 mg L<sup>-1</sup>) and 0.5 g L<sup>-1</sup> of the catalyst were added to the Pyrex reactor and stirred for 30 minutes before starting the degradation

experiment to reach maximum output. The pH of the solution was adjusted to pH = 5 by adding solutions of HNO<sub>3</sub> and NaOH using a pH-stat technique. This technique consists of an automatic dosing unit (Basic Titrino 794 from Metrohm AG, Herisau, Switzerland) with a high-performance titrimetric pipette able to add drops of 0.5 μL, a highly sensitive semi-micro pH electrode combined with an Ag/AgCl reference electrode (Thermo-Orion Ross 8115, Chelmsford, UK) with pH accuracy up to the third decimal, and a computer to control and register the results. The system was then irradiated by a 300 W Xenon arc lamp for 90min. The entire experimental set-up is shown in **Figure 3-6**. Aliquots (1.5 mL) were withdrawn periodically, centrifuged to remove the catalyst, and analyzed immediately. Two independent analytical methods were used, that is, UV-vis analysis and high-performance liquid chromatography HPLC (Ecom System Inc, Sarasota, FL, USA) equipped with UV-vis detectors operated at 355 nm and a Knauer Vertex plus column packed with Eurospher II 100-5 C18 A material (L x I.D. = 150 cm x 4 mm) with precolumn. The oven temperature was 30 °C and the mobile phase was a mixture of methanol / acetonitrile/ (0.01 mol/L) oxalic acid solution (20/20/60, v/v%).

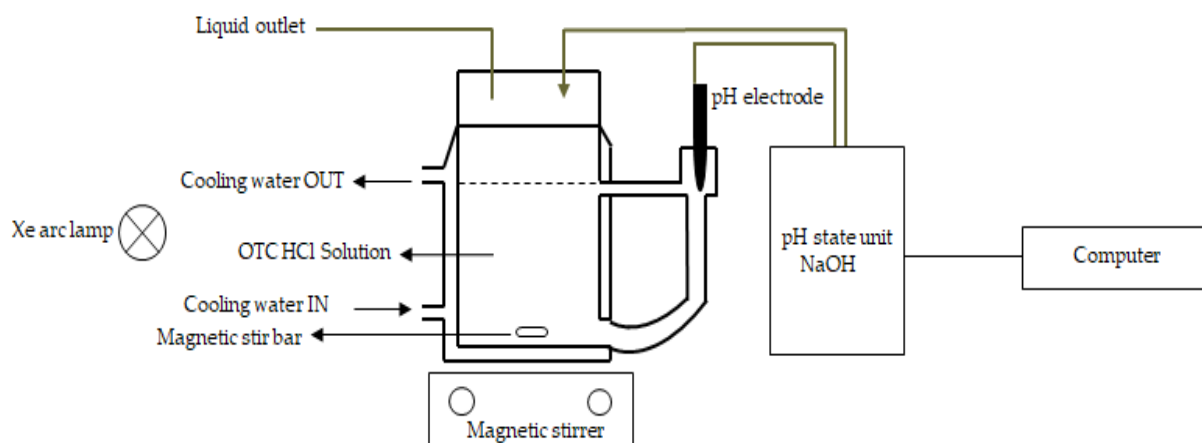


**Figure 3-6.** Scheme of the experimental set-up used for the photocatalytic degradation experiments.

### 3.7. Conclusions

To summarize, Co - TiO<sub>2</sub> composites synthesized through reflux and hydrothermal methods were found to enhance the light-induced degradation rate of OTC HCl under UV-vis irradiation. Significant differences in the structural analysis were observed between the materials prepared by the two preparation methods. Co-doping through the hydrothermal synthesis resulted in preventing the rutile phase formation with an increase in the surface area, while the doping using the reflux method does not affect the specific surface area. The Co-doped TiO<sub>2</sub> NPs prepared by reflux showed enhanced UV-vis-light-induced OTC HCl degradation with an initial rate of 8.83 mg L<sup>-1</sup> min<sup>-1</sup>, which was higher than the degradation rate of the all prepared catalysts and commercial P25. The high photocatalytic activity of the Co-TiO<sub>2</sub>-R was attributed to its high surface area, which serves as a good absorber for the substrate molecule, and to the defect levels created below the valence band of TiO<sub>2</sub>-R, which lead to better charge separation and improve the kinetic properties of this material. Co-TiO<sub>2</sub>-assisted photodegradation of OTC HCl was found to occur via two competitive processes: a photocatalytic process and a photosensitized process. In the photocatalytic process, direct hole transfers, O<sub>2</sub><sup>•-</sup>, and •OH could take part in the Co-TiO<sub>2</sub> photocatalysis.

### 3.8. Acknowledgments

The authors wish to thank Luis Granone for XRD and Raman measurements, Barbara Nunes for TEM measurements, and Narmina Balayeva for the valuable discussions. The publication of this article was funded by the Open Access Fund of the Gottfried Wilhelm Leibniz Universität Hannover.

### 3.9. References

1. T. Heberer, Occurrence, Fate, and Removal of Pharmaceutical Residues in The Aquatic Environment: A review of Recent Research Data. *Toxicol. Lett.* **2002**, 131, 5–17.



2. M.M. Huber, S. Canonica, G. Park, U. Gunten. Oxidation of Pharmaceuticals during Ozonation and Advanced Oxidation Processes. *Environ. Sci. Technol.* **2003**, 37, 1016–1024.
3. V. Homem, L. Santos. Degradation and Removal Methods of Antibiotics from Aqueous Matrices—A review. *J. Environ. Manage.* **2011**, 92, 2304–2347.
4. I.R. Bautitz, R.F. Pupo Nogueira. Degradation of Tetracycline by Photo-fenton Process—solar Irradiation and Matrix Effects. *J.Photochem. Photobiol. A: Chem.* **2007**, 187, 33–39.
5. C. Reyes, J. Fernández, J. Freer, M.A. Mondaca, C. Zaror, S. Malato, H.D. Mansilla. Degradation and Inactivation of Tetracycline by TiO<sub>2</sub> Photocatalysis. *J. Photochem. Photobiol. A: Chem.* **2006**, 184, 141–146.
6. Y. Liu, X. He, Y. Fu, D.D. Dionysiou. Kinetics and Mechanism Investigation on The Destruction of Oxytetracycline by UV-254 nm Activation of Persulfate. *J. Hazard. Mater.* **2016**, 305, 229–239.
7. C. Zhao, H. Deng, Y. Li, Z. Li. Photodegradation of Oxytetracycline in Aqueous by 5A and 13X Loaded with TiO<sub>2</sub> Under UV Irradiation. *J. Hazard. Mater.* **2010**, 176, 884–892.
8. Y. Liu, X. He, X. Duan, Y. Fu, D.D. Dionysiou. Photochemical Degradation of Oxytetracycline: Influence of pH and Role of Carbonate Radical. *Chem. Eng. J.* **2015**, 276, 113–121.
9. J.H. Pereira, D.B. Queirós, A.C. Reis, O.C. Nunes, M.T. Borges, R.A. Boaventura, V.J. Vilar. Process. Enhancement at Near Neutral pH of a Homogeneous Photo-Fenton Reaction using Ferricarboxylate Complexes: Application to Oxytetracycline Degradation. *Chem. Eng. J.* **2014**, 253, 217–228.
10. M.H. Khan, H. Bae, J. Jung. Tetracycline Degradation by Ozonation in The Aqueous Phase: Proposed Degradation Intermediates and Pathway. *J. Hazard. Mater.* **2010**, 181, 659–665.

11. M.C. Dodd, H.E. Kohler, U. Gunten. Oxidation of Antibacterial Compounds by Ozone and Hydroxyl Radical: Elimination of Biological Activity during Aqueous Ozonation Processes. *Environ. Sci. Technol.* **2009**, 43, 2498–2504.
12. C.V. Gomez-Pacheco, M. Sanchez-Polo, J. Rivera-Utrilla, J.J. Lopez-Peñalver. Tetracycline Degradation in Aqueous Phase by Ultraviolet Radiation. *Chem. Eng. J.* **2012**, 187, 89–95.
13. Y. Liu, X. He, X. Duan, Y. Fu, D. Fatta-Kassinos, D.D. Dionysiou. Significant Role of UV and Carbonate Radical on the Degradation of Oxytetracycline in UV-AOPs: Kinetics and Mechanism. *Water Res.* **2016**, 95, 195–204.
14. R.A. Palominos, M.A. Mondaca, A. Giraldo, G. Penñela, M. Pérez-Moya, H. D. Mansilla. Photocatalytic Oxidation of the Antibiotic Tetracycline on TiO<sub>2</sub> and ZnO Suspensions. *Catal. Today* **2009**, 144, 100–105.
15. J. H.O.S. Pereira, A.C. Reis, D. Queirós, O.C. Nunes, M.T. Borges, V.J.P. Vilar, R. A.R. Boaventura. Insights into Solar TiO<sub>2</sub> -assisted Photocatalytic Oxidation of Two Antibiotics Employed in Aquatic Animal Production, Oxolinic Acid and Oxytetracycline. *Sci. Total Environ.* **2013**, 463–464, 274–283.
16. L. Rimoldi, D. Meroni, G. Cappelletti, S. Ardizzone. Green and Low Cost Tetracycline Degradation Processes by Nanometric and Immobilized TiO<sub>2</sub> Systems. *Catal. Today* **2017**, 281, 38–44.
17. S. Yahiat, F. Fourcade, S. Brosillon, A. Amrane. Removal of Antibiotics by An Integrated Process Coupling Photocatalysis and Biological Treatment-case of Tetracycline and Tylosin. *Inter. Biodeterior. Biodegrad.* **2011**, 65, 997–1003.
18. X-D. Zhu, Y-J. Wang, R-J. Sun, D.-M. Zhou. Photocatalytic Degradation of Tetracycline in Aqueous Solution by Nanosized TiO<sub>2</sub>. *Chemosphere* **2013**, 92, 925–932.
19. M.R. Hoffmann, Scot T. Martin, W. Choi, D.W. Bahnemann. Environmental Applications of Semiconductor Photocatalysis. *Chem. Rev.* **1995**, 95, 1, 69–96.

20. N. Serpone, D. Lawless, R. Khairutdinov, E. Pelizzetti. Subnanosecond Relaxation Dynamics in TiO<sub>2</sub> Colloidal Sols (Particle Sizes  $R_p = 1.0\text{-}13.4$  Nm). Relevance to Heterogeneous Photocatalysis. *J. Phys. Chem.* **1995**, *99*, 16655–16661.
21. W. Y. Choi, A. Termin, M. R. Hoffmann. The Role of Metal Ion Dopants in Quantum-Sized TiO<sub>2</sub> : Correlation between Photoreactivity and Charge Carrier Recombination Dynamics. *J. Phys. Chem.* **1994**, *98*, 13669–13679.
22. B. Naik, K. M. Parida, C. S. Gopinath. Facile Synthesis of N- and S-incorporated Nanocrystalline TiO<sub>2</sub> and Direct Solar-light-driven Photocatalytic Activity. *J. Phys. Chem. C* **2010**, *114*, 19473–19482.
23. P. Wang, P-S. Yap, T-T. Lim. C-N-S Tridoped TiO<sub>2</sub> for Photocatalytic Degradation of Tetracycline under Visible-light Irradiation. *Appl. Catal. A.* **2011**, *399*, 252–261.
24. W. Jo, S. Kumar, M.A. Isaacs, A.F. Lee, S. Karthikeyan. Cobalt Promoted TiO<sub>2</sub>/GO for the Photocatalytic Degradation of Oxytetracycline and Congo Red. *Appl. Catal. B: Environ.* **2017**, *201*, 159–168.
25. M. I. Litter. Heterogeneous Photocatalysis Transition Metal Ions in Photocatalytic Systems. *Appl Catal B: Environ.* **1999**, *23*, 89–114.
26. D. Dvoranova, V. Brezova, M. Mazur, M. Malati. Investigations of Metal-doped Titanium Dioxide Photocatalysts. *Appl Catal B: Environ.* **2002**, *37*, 91–105.
27. Y. Lu, Y. Lin, D. Wang, L. Wang, T. Xie, T. Jiang. A High Performance Cobalt-doped ZnO Visible Light Photocatalyst and its Photogenerated Charge Transfer Properties. *Nano Res.* **2011**, *4*, 1144–1152.
28. S.T. Kochuveedu, Y.H. Jang, D.H. Kim. A Study on The Mechanism for The Interaction of Light with Noble Metal-metal Oxide Semiconductor Nanostructures for Various Photophysical Applications. *Chem. Soc. Rev.* **2013**, *42*, 8467–8493.
29. A. Iwase, Y.H. Ng, Y. Ishiguro, A. Kudo, R. Amal. Reduced Graphene Oxide as a Solid-State Electron Mediator in Z-scheme Photocatalytic Water Splitting under Visible Light. *J. Am. Chem. Soc.* **2011**, *133*, 11054–11057.
30. L.L. Tan, W.J. Ong, S.P. Chai, A.R. Mohamed. Noble Metal Modified Reduced Graphene Oxide/TiO<sub>2</sub> Ternary Nanostructures for Efficient Visible Light-driven

- Photoreduction of Carbon Dioxide into Methane. *Appl. Catal. B: Environ.* **2014**, 166–167, 251–259.
31. Q. Chen, S. Wu, Y. Xin. Synthesis of Au–CuS–TiO<sub>2</sub> Nanobelts Photocatalyst for Efficient Photocatalytic Degradation of Antibiotic Oxytetracycline. *Chem. Eng. J.* **2016**, 302, 377–387.
  32. M. Wang, J. Ioccozia, L. Sun, C. Lin, Z. Lin. Inorganic-modified Semiconductor TiO<sub>2</sub> Nanotube Arrays for Photocatalysis. *Energy Environ. Sci.* **2014**, 7, 2182–2202.
  33. M. Liu, R. Inde, M. Nishikawa, X. Qiu, D. Atarashi, E. Sakai, Y. Nosaka, K. Hashimoto, M. Miyauchi. Enhanced Photoactivity with Nanocluster-grafted Titanium Dioxide Photocatalysts. *ACS Nano.* **2014**, 8, 7229–7238.
  34. Li, R.; Jia, Y.; Wu, J.; Zhen, Q. Photocatalytic Degradation and Pathway of Oxytetracycline in Aqueous Solution by Fe<sub>2</sub>O<sub>3</sub>–TiO<sub>2</sub> Nanopowder. *RSC Adv.* **2015**, 5, 40764–40771.
  35. J. Ran, J. Zhang, J. Yu, M. Jaroniec, S.Z. Qiao. Earth-abundant Cocatalysts for Semiconductor Based Photocatalytic Water Splitting. *Chem. Soc. Rev.* **2014**, 43, 7787–7812.
  36. W. Alamgir, S. Khan, M.M. Ahmad, A.H. Naqvi Hassan. Structural Phase Analysis, Band Gap Tuning and Fluorescence Properties of Co Doped TiO<sub>2</sub> Nanoparticles. *Opt. Mater.* **2014**, 38, 278–285.
  37. F. Zhang, A. Yamakata, K. Maeda, Y. Moriya, T. Takata, J. Kubota, K. Teshima, S. Oishi, K. Domen. Cobalt-modified Porous Single-Crystalline LaTiO<sub>2</sub>N for Highly Efficient Water Oxidation under Visible Light. *J. Am. Chem. Soc.* **2012**, 134, 8348–8351.
  38. J. Lee, D.H.K. Jackson, T. Li, R.E. Winans, J.A. Dumesic, T.F. Kuech, G.W. Huber. Enhanced Stability of Cobalt Catalysts by Atomic Layer Deposition for Aqueous-Phase Reactions. *Energy Environ. Sci.* **2014**, 7, 1657–1660.
  39. M. Dahl, Y. Liu, Y. Yin. Composite Titanium Dioxide Nanomaterials. *Chem. Rev.* **2014**, 114, 9853–9889.

40. R.P. Marin, S.A. Kondrat, J.R. Gallagher, D.I. Enache, P. Smith, P. Boldrin, T.E. Davies, J.K. Bartley, G.B. Combes, P.B. Williams, *et al.* Preparation of Fischer–Tropsch Supported Cobalt Catalysts using a New Gas Anti-solvent Process. *ACS Catal.* **2013**, 3, 764–772.
41. A. Siddiqa, D. Masih, D. Anjum, M. Siddiq. Cobalt and Sulfur Co-doped Nano-Size TiO<sub>2</sub> for Photodegradation of Various Dyes and Phenol. *J. Environ. Sci.* **2015**, 37, 100–109.
42. M.A. Barakat, H. Schaeffer, G. Hayes, S. Ismat-Shah. Photocatalytic Degradation of 2-chlorophenol by Co-doped TiO<sub>2</sub> Nanoparticles. *Appl. Catal. B: Environ.* **2005**, 57, 23–30.
43. J. Choi, H. Park, M.R. Hoffmann. Effects of Single Metal-ion Doping on The Visible-light Photoreactivity of TiO<sub>2</sub>. *J. Phys. Chem. C* **2010**, 114, 783–792.
44. P. Bouras, E. Stathatos, P. Lianos. Pure Versus Metal-ion-doped Nanocrystalline Titania for Photocatalysis. *Appl. Catal. B: Environ.* **2007**, 73, 51–59.
45. K. Karthik, P.S. Kesava, K. Suresh Kumar, N. Victor Jaya. Influence of Dopant Level on Structural, Optical and Magnetic Properties of Co-doped Anatase TiO<sub>2</sub> Nanoparticles. *Appl. Surf. Sci.* **2010**, 256, 4757–4760.
46. L. Samet, J.B. Nasseur, R. Chtourou, K. March, O. Stephan. Heat Treatment Effect on The Physical Properties of Cobalt Doped TiO<sub>2</sub> Sol-gel Materials. *Mater. Charact.* **2013**, 85, 1–12.
47. C. Huang, X. Liu, Y. Liu, Y. Wang. Room Temperature Ferromagnetism of Co-Doped TiO<sub>2</sub> Nanotube Arrays Prepared by Sol-gel Template Synthesis. *Chem. Phys. Lett.* **2006**, 432, 468–472.
48. B. Choudhury, A. Choudhury. Luminescence Characteristics of Cobalt Doped TiO<sub>2</sub> Nanoparticles. *J. Lumin.* **2012**, 132, 178–184.
49. C. Khurana, O.P. Pandey, B. Chudasama. Synthesis of Visible Light-Responsive Cobalt-Doped TiO<sub>2</sub> Nanoparticles with Tunable Optical Band Gap. *J. Sol-Gel Sci. Technol.* **2015**, 75, 424–435.

50. A. Hamadani, A. Reisi-Vanani, A. Majedi. Sol-gel Preparation and Characterization of Co/TiO<sub>2</sub> Nanoparticles: Application to the Degradation of Methyl Orange. *J. Iran. Chem. Soc.* **2010**, 7, 52–58.
51. A.L. Castro, M.R. Nunes, M.D. Carvalho, L.P. Ferreira, J.-C. Jumes, F.M. Costa, M.H. Florencio. Doped Titanium Dioxide Nanocrystalline Powders with High Photocatalytic Activity. *J. Solid State Chem.* **2009**, 182, 1838–1845.
52. H. Zhang, T. Ji, Y. Liu, J. Cai. Preparation and Characterization of Room Temperature Ferromagnetic Co-doped Anatase TiO<sub>2</sub> Nanobelts. *J. Phys. Chem. C* **2008**, 112, 8604–8608.
53. A.Y. Yermakov, G.S. Zakharova, M.A. Uimin, M.V. Kuznetsov, L.S. Molochnikov, S.F. Konev, A.S. Konev, A.S. Minin, V.V. Mesilov, V.R. Galakhov, *et al.* Surface Magnetism of Cobalt-doped Anatase TiO<sub>2</sub> Nanopowders. *J. Phys. Chem. C* **2016**, 120, 28857–28866.
54. V.V. Mesilov, V.R. Galakhov, A.F. Gubkin, E.A. Sherstobitova, G.S. Zakharova, M.A. Uimin, A.Y.e. Yermakov, K.O. Kvashnina, D.A. Smirnov. X-ray Diffraction and X-ray Spectroscopy Studies of Cobalt-doped Anatase TiO<sub>2</sub> : Co Nanopowders. *J. Phys. Chem. C* **2017**, 121, 24235–24244.
55. R.J. Tayade, R.G. Kulkarni, R.V. Jasra. Transition metal Ion Impregnated Mesoporous TiO<sub>2</sub> for Photocatalytic Degradation of Organic Contaminants in Water. *Ind. Eng. Chem. Res.* **2006**, 45, 5231–5238.
56. A. Di Paola, E. García-López, S. Ikeda, G. Marci, B. Ohtani, L. Palmisano. Photocatalytic Degradation of Organic Compounds in Aqueous Systems by Transition Metal Doped Polycrystalline TiO<sub>2</sub>. *Catal. Today* **2002**, 75, 87–93.
57. Ö. Kerkez-Kuyumcu, E. Kibar, K. Dayıoglu, F. Gedik, A.N. Akın, S. Özkara-Aydınoglu. A Comparative Study for Removal of Different Dyes over M/TiO<sub>2</sub> (M = Cu, Ni, Co, Fe, Mn, and Cr) Photocatalysts under Visible Light Irradiation. *J. Photochem. Photobiol. A* **2015**, 311, 176–185.

58. Y. Miao, Z. Zhai, L. Jiang, Y. Shi, Z. Yan, D. Duana, K. Zhen, J. Wang. Facile and New Synthesis of Cobalt Doped Mesoporous TiO<sub>2</sub> with High Visible-light Performance. *Powder Technol.* **2014**, 266, 365–371.
59. P. Jiang, W. Xiang, J. Kuang, W. Liu, W. Cao. Effect of Cobalt Doping on the Electronic, Optical and Photocatalytic Properties of TiO<sub>2</sub>. *Solid State Sci.* **2015**, 46, 27–32.
60. M.M. Rashad, E.M. Elsayed, M.S. Al-Kotb, A.E. Shalan. The Structural, Optical, Magnetic and Photocatalytic Properties of Transition Metal Ions Doped TiO<sub>2</sub> Nanoparticles. *J. Alloys Compd.* **2013**, 581, 71–78.
61. M. Iwasaki, M. Hara, H. Kawada, H. Taday, S. Ito. Cobalt Ion-doped TiO<sub>2</sub> Photocatalyst Response to Visible Light. *J. Colloid Interface Sci.* **2000**, 224, 202–204.
62. Y. Matsumoto, M. Murakami, T. Shono, T. Hasegawa, T. Fukumura, M. Kawasaki, P. Ahmet, T. Chikyow, S. Koshihara, H. Koinuma. Room-temperature Ferromagnetism in Transparent Transition Metal-doped Titanium Dioxide. *Science* **2001**, 291, 854–856.
63. H. Toyosaki, T. Fukumura, Y. Yamada, K. Nakajima, T. Chikyow, T. Hasegawa, H. Koinuma, M. Kawasaki. Anomalous Hall Effect Governed by Electron Doping in a Room-temperature Transparent Ferromagnetic Semiconductor. *Nature* **2004**, 3, 221–224.
64. K.A. Griffin, A.B. Pakhomov, C.M. Wang, S.M. Heald, K.M. Krishnan. Intrinsic Ferromagnetism in Insulating Cobalt Doped Anatase TiO<sub>2</sub>. *Phys. Rev. Lett.* **2005**, 94, 157204.
65. R. Rodríguez-Talavera, S. Vargas, R. Arroyo-Murillo, R. Montiel-Campos, E. Haro-Poniatowski. Modification of the Phase Transition Temperatures in Titania Doped with Various Cations. *J. Mater. Res.* **1997**, 12, 439–443.
66. C. Zhao, X. Shu, D. Zhu, S. Wei, Y. Wang, M. Tu, W. Gao. High Visible Light Photocatalytic Property of Co<sup>2+</sup>-doped TiO<sub>2</sub> Nanoparticles with Mixed Phases. *Superlattice Microst.* **2015**, 88, 32–42.

67. A. Martinelli, S. Alberti, V. Caratto, P. Lova, F. Locardi, G. Pampararo, S. Villa, M. Ferretti. Structural Studies on Copper and Nitrogen-doped Nanosized Anatase. *Z. Kristallogr.* **2018**, 233, 867–876.
68. T.T. Le, M.S. Akhtar, D.M. Park, J.C. Lee, O.B. Yang. Water Splitting on Rhodamine-B Dye-sensitized Co-doped TiO<sub>2</sub> Catalyst under Visible Light. *Appl. Catal. B: Environ.* **2012**, 111–112, 397–401.
69. M. Qiu, Y. Tian, Z. Chen, Z. Yang, W. Li, K. Wang, L. Wang, K. Wang, W. Zhang. Synthesis of Ti<sup>3+</sup> Self-doped TiO<sub>2</sub> Nanocrystals Based on Le Chatelier's Principle and their Application in Solar Light Photocatalysis. *RSC Adv.* **2016**, 6, 74376–74383.
70. Y. Ohno, K. Tomita, Y. Komatsubara, T. Taniguchi, K. Katsumata, N. Matsushita, T. Kogure, K. Okada. Pseudo-cube Shaped Brookite (TiO<sub>2</sub>) Nanocrystals Synthesized by an Oleate-modified Hydrothermal Growth Method. *Cryst. Growth Des.* **2011**, 11, 4831–4836.
71. C.T. Hsieh, W.S. Fan, W.Y. Chen, J.Y. Lin. Adsorption and Visible-light-derived Photocatalytic Kinetics of Organic Dye on Co-doped Titania Nanotubes Prepared by Hydrothermal Synthesis. *Sep. Purif. Technol.* **2009**, 67, 312–318.
72. J.D. Lee. *Concise Inorganic Chemistry*. 5th ed.; Blackwell Science: Hoboken, NJ, USA, **1996**.
73. L. Jing, B. Xin, F. Yuan, L. Xue, B. Wang, H. Fu. Effects of Surface Oxygen Vacancies on Photophysical and Photochemical Processes of Zn-doped TiO<sub>2</sub> Nanoparticles and their Relationships. *J. Phys. Chem. B* **2006**, 110, 17860–17865.
74. C. Zhao, M. Pelaez, X. Duan, H. Deng, K. O'Shea, D. Fatta-Kassinos, D.D. Dionysiou. Role of pH on Photolytic and Photocatalytic Degradation of Antibiotic Oxytetracycline in Aqueous Solution under Visible/Solar Light: Kinetics and Mechanism Studies. *Appl. Catal. B: Environ.* **2013**, 134–135, 83–92.
75. S.A. Sassman, L.S. Lee. Sorption of Three Tetracyclines by Several Soils: Assessing the Role of pH and Cation Exchange. *Environ. Sci. Technol.* **2005**, 39, 7452–7459.
76. C.C. Wong, W. Chu. The Hydrogen Peroxide-assisted Photocatalytic Degradation of Alachlor in TiO<sub>2</sub> Suspensions. *Environ. Sci. Technol.* **2003**, 37, 2310–2316.



77. K. Hara, T. Sato, R. Katoh, A. Furube, Y. Ohga, A. Shinpo, S. Suga, K. Sayama, H. Sugihara, H. Arakawa. Molecular Design of Coumarin Dyes for Efficient Dye-sensitized Solar Cells. *J. Phys. Chem. B* **2003**, 107, 597–606.

## Chapter 4. Photocatalytic Hydrogen Evolution over Pt / Co - TiO<sub>2</sub> Photocatalysts

### 4.1. Foreword

Following the previous chapter, Co -doped TiO<sub>2</sub> materials have shown enhanced photocatalytic activity for OTC HCl degradation under UV-vis illumination owing to their large surface area and improved visible light absorption. Therefore, it has been suggested to examine their photoactivity for the photocatalytic decomposition of methanol under simulated solar light. Mainly, methanol is known to be one of the most efficient sacrificial reagents to yield H<sub>2</sub>. Thus, the investigation of the cobalt doping effect for the photocatalytic H<sub>2</sub> generation was the main objective of this study. A literature survey has led to the conclusion that some scientific studies have shown enhanced H<sub>2</sub> generation on the Co<sup>2+</sup> doped TiO<sub>2</sub>, while other groups observed a decrease in the H<sub>2</sub> production activity. In this regard, it was of great importance to investigate the physico-chemical and the paramagnetic properties of Co-TiO<sub>2</sub> prepared in different solvothermal ways, and their influence on the photocatalytic H<sub>2</sub> production. Moreover, as Pt is reported to exhibit the highest quantum efficiency for H<sub>2</sub> evolution, Pt islands are deposited on the surface of the Co-TiO<sub>2</sub> photocatalysts to ensure a high and stable activity.

This chapter contains the article “Photocatalytic Hydrogen Evolution over Pt/Co-TiO<sub>2</sub> Photocatalysts” by Soukaina Akel, Ralf Dillert, and Detlef W Bahnemann, published in the *Journal of Photocatalysis*, 2021, 2, 35–48; doi: 10.2174/2665976x01999200718010443. The present study considers the use of Co-doped TiO<sub>2</sub> materials prepared within the procedures described in **chapter 3** for the photocatalytic H<sub>2</sub> generation activity since they exhibit a high surface area and light absorbance. The photocatalytic hydrogen generation from methanol-reforming revealed that the Co-doping does not affect the photocatalytic activity of both Pt/Co-TiO<sub>2</sub> catalysts, which was afterward confirmed with the flatband potential measurements showing that the conduction band of the Co-doped TiO<sub>2</sub> materials was

slightly more negative than hydrogen production potential H<sup>+</sup>/H<sub>2</sub> (− 0.41 V vs NHE at pH = 7), which suggest an insignificant amount of photogenerated H<sub>2</sub>.

## 4.2. Abstract

**Aims:** In this study, the photocatalytic hydrogen evolution reaction from aqueous methanol was investigated upon simulated solar light using platinum loaded on cobalt doped TiO<sub>2</sub> (Pt/Co-TiO<sub>2</sub>) composites.

**Background:** Controversial results of cobalt-based composites create doubts about their photocatalytic activity. Thus, cobalt doped TiO<sub>2</sub> composites were synthesized differently, and the photocatalytic activity was examined for the photocatalytic hydrogen generation.

**Objective:** The current study aims to investigate the influence of cobalt doping and platinum loading on the photocatalytic activities of TiO<sub>2</sub> nanoparticles for the photocatalytic H<sub>2</sub> generation.

**Methods:** The 0.5 wt.% Co-TiO<sub>2</sub> and bare TiO<sub>2</sub> photocatalysts were synthesized using two different methods, namely, reflux and hydrothermal synthesis. Additionally, the Pt deposition on the prepared Co-TiO<sub>2</sub> and TiO<sub>2</sub> catalysts (1 wt.% Pt) was performed using a photo-platinization method. The as-prepared catalysts were characterized by X-ray diffraction (XRD), scanning electron microscopy/energy dispersive X-ray analysis (SEM/EDX), transmission electron microscopy (TEM), ultra-violet-visible spectroscopy (UV-vis), X-ray photoelectron spectroscopy (XPS), electron paramagnetic resonance (EPR), and electrochemical impedance spectroscopy (EIS).

**Results:** The XRD and EPR studies clearly indicated that the Co was incorporated into the titanium dioxide lattice. The EIS results suggested that the reduction of protons over Co-TiO<sub>2</sub> and bare TiO<sub>2</sub> materials was possible from a thermodynamic point of view. However, the photocatalytic results revealed that the formed amount of H<sub>2</sub> was extremely low and close to the detection limit. The evolution of H<sub>2</sub> from aqueous methanol (10 vol%) showed higher rates when employing 1 wt.% Pt loaded on 0.5

wt.% Co-TiO<sub>2</sub> photocatalysts under simulated solar light irradiation. A maximum of  $317 \pm 44 \mu\text{mol h}^{-1}$  was observed over the Pt/Co-TiO<sub>2</sub>-HT photocatalyst.

**Conclusion:** EPR results confirmed that the cobalt ions were introduced into the TiO<sub>2</sub> lattice by trapping the photogenerated conduction band electrons and decreasing the defects in the crystal cell. The Mott–Schottky analysis of electrochemical impedance measurements showed that all catalysts were n-type semiconductors and that cobalt doping induces impurity level within the band gap of TiO<sub>2</sub>. The experimental results of photocatalytic H<sub>2</sub> generation from methanol-reforming demonstrated that no significant impact of Co-doping on the photocatalytic H<sub>2</sub> formation was observed neither for bare TiO<sub>2</sub> samples nor for the platinized materials. Based on these experimental findings, a possible mechanism for the continuous photocatalytic activity of Pt/Co-TiO<sub>2</sub> photocatalysts under simulated solar light was proposed.

**Keywords:** Photocatalysis, cobalt-doped titania, H<sub>2</sub> evolution, simulated solar light, EPR spectroscopy, Mott–Schottky method.

### 4.3. Introduction

Meeting the demands of an energy-thirsty world without environmental pollution is one of the key challenges nowadays. Molecular hydrogen is considered a major source of energy that can be produced from environment-friendly, abundant, and renewable energy sources such as biomass and water [1].

For about 50 years since the discovery of photoelectrochemical water splitting on a TiO<sub>2</sub> electrode by Fujishima and Honda [2], various types of photoelectrodes and photocatalysts have been developed to improve the efficiency of light-driven hydrogen generation from water [3, 4]. However, the hydrogen evolution yield is still quite low [5]. Higher efficiencies for the photocatalytic hydrogen evolution can be achieved with the use of electron donors as sacrificial reagents (e.g., alcohol, sulfide ion, or organic contaminants) which react irreversibly with the photoinduced holes

thus suppressing the recombination with electrons [6]. Efficient photocatalytic hydrogen evolution requires semiconducting materials of high photochemical stability having, in particular, a conduction band position ( $E_{CB}$ ) that is lower than the  $H_2/H_2O$  level  $E(H^+/H_2)$  ( $-0.413$  V at pH 7). The production of molecular oxygen could take place only if the potential of the valence band ( $E_{VB}$ ) is higher than the  $O_2/H_2O$  level  $E(O_2/H_2O)$  ( $0.817$  V at pH 7) [7]. Therefore, semiconductors with band energy levels that involve the hydrogen and oxygen evolution potentials are, theoretically, able to split water. Among various semiconductors which have been studied for the photocatalytic water splitting, TiO<sub>2</sub> is considered as the most promising photocatalyst because of its favorable bandgap energy, the positions of the conduction and valence bands, and due to its exceptional properties such as photostability and chemical stability, long-term corrosion resistance, and nontoxicity [8].

However, its larger band gap energy (3.2 eV) restricts the application in the photocatalytic hydrogen production under visible light irradiation [9]. One strategy to enhance the photoproduction of H<sub>2</sub> from an aqueous suspension containing TiO<sub>2</sub> is to increase its photoactivity in the near-UV region of the solar spectrum by retarding the recombination of the photogenerated charge carrier, i.e., conduction-band electrons and valence-band holes which occurs in nanoseconds. For this aim, NPs cocatalysts in the form of metal (Pt, Au, Pd, Rh, Co, Ni) or metal oxide (RuO<sub>2</sub>, Co<sub>3</sub>O<sub>4</sub>) have been deposited on the surface [10–17]. Recently, Moon *et al.* [18] investigated the effects of macro-mesoporous oxides (i.e. Pt–TiO<sub>2</sub>, Pt–Ta<sub>2</sub>O<sub>5</sub>, Pt–Nb<sub>2</sub>O<sub>5</sub>, Pt–ZrO<sub>2</sub>, and Pt–Al<sub>2</sub>O<sub>3</sub>) on photocatalytic H<sub>2</sub> generation from aqueous methanol. They observed that among all oxide-supported Pt nanoparticle photocatalysts, Pt–TiO<sub>2</sub> exhibits the highest photocatalytic H<sub>2</sub> production activity. It has been shown that the Pt deposition onto the TiO<sub>2</sub> surface resulted in the formation of a Schottky barrier at the interface of the metal/semiconductor retarding the electron/hole recombination [19]. Amongst all noble metals, Pt particularly has competed for an important role in the photocatalytic hydrogen production system [20]. According to the Schottky barriers, platinization of semiconductor photocatalysts such as TiO<sub>2</sub> promotes the transfer of the

photogenerated holes in the surface which allow the accumulation of the trapped electron in the Pt NPs enhancing the molecular hydrogen formation by reducing the reduction potential of protons [21, 22].

Over the past few years, cobalt-based complexes as more earth-abundant metal have been reported as alternative systems to catalyze the reduction of protons in aqueous solution [23, 24]. Recently, Rodenberg *et al.* investigated the mechanism of the photocatalytic hydrogen generation using a polypyridyl-based cobalt complex in aqueous solution [25]. Eisenberg and co-workers applied the cobalt–dithiolene complex to catalyze the photocatalytic proton reduction with very high activity, achieving >2700 turnovers when paired with Ru(bpy<sub>3</sub>)<sup>2+</sup> as a photosensitizer and ascorbic acid as the sacrificial donor [26]. Although these complexes generally perform remarkably, the stability under the turnover conditions was identified as one of the major drawbacks of such compounds.

Cobalt oxide (CoO<sub>x</sub>) based catalysts have been extensively examined for photocatalytic water oxidation [27, 28]. In the recent past, enormous attention has been paid to cobalt oxide-based TiO<sub>2</sub> photocatalysts for photocatalytic hydrogen generation. A nonaqueous sol-gel preparation of CoO<sub>x</sub>/TiO<sub>2</sub> nanocomposites for photocatalytic hydrogen generation has been described by Wang *et al.*, who showed the capability of the composites with the optimum Co/Ti ratio for photocatalytic hydrogen generation with methanol or ethanol as a sacrificial agent under UV irradiation [29]. A new Co<sub>3</sub>O<sub>4</sub>/TiO<sub>2</sub> system with a p–n heterojunction for photocatalytic hydrogen evolution has been synthesized by Bala *et al.* showing a maximum of photocatalytic hydrogen evolution rate of ~7 mmol g<sup>-1</sup> h<sup>-1</sup> at optimized Co loading [16]. Also, Yan *et al.* have prepared cobalt oxide loaded titanium dioxide/cadmium sulfide semiconductor composites using an aqueous solution containing sodium sulfide/sodium sulfite as hole scavengers under visible light irradiation, and they reported an average rate of hydrogen evolution of 7 times higher than titanium dioxide/cadmium sulfide composite [30]. Mahoney *et al.* have found that the cobalt

oxide nanoclusters minimize the charge-carrier recombination and hence enhance the hydrogen production under solar simulated irradiation [31].

Extensive researches have been carried out to decrease the TiO<sub>2</sub> band-gap energy or to introduce intra-bandgap states without changing the conduction band level, which may improve the efficiency within the visible wavelength. Doping a wide band gap metal oxide such as TiO<sub>2</sub> is one of the most effective methods that have been widely studied for the development of visible light-responsive photocatalysts. So far, continuous hydrogen production from glycerol aqueous solution under solar light has been investigated through Co<sup>2+</sup> doped TiO<sub>2</sub>, and maximum hydrogen production of 11021 μmol h<sup>-1</sup>g<sup>-1</sup> was attained over 1 wt.% cobalt doped TiO<sub>2</sub> in 5% glycerol aqueous solutions [32]. In another work reported by Shi *et al.* a maximum of 2499 μmol of molecular hydrogen has been obtained on only 0.3 % of Co-TiO<sub>2</sub> [33]. Conversely, a non-enhancement of the photoactivity on the cobalt-doped materials has been reported. For instance, Wu *et al.* [34] have doped commercial P25 with 0.4 wt.% Co<sup>2+</sup> for hydrogen production from aqueous ethanol solution. They have observed that after a long-term photoreaction, the photocatalytic hydrogen production activities of Co<sup>2+</sup> modified P25 have decreased by a factor of 2. Wang *et al.* have synthesized CoO<sub>x</sub>/TiO<sub>2</sub> nanocomposites which were only UV-active and exhibited no activity in the visible light despite that the nanocomposites were colored [29]. In an early paper, Hoffman and co-workers have reported a detrimental effect of Co<sup>3+</sup> doped TiO<sub>2</sub> for the photocatalytic degradation of CHCl<sub>3</sub> under UV irradiation [35]. In another study of the same group, they have demonstrated that Co<sup>2+</sup> doped TiO<sub>2</sub> material had a slight increase in the observed rate constant of the visible light photocatalytic degradation of methylene blue [36].

In view of the reported results above, doubts about the photocatalytic activity of the cobalt doped TiO<sub>2</sub> materials are created. Thus, cobalt doped TiO<sub>2</sub> composites were synthesized with the aim to decrease the TiO<sub>2</sub> band gap which results in enhanced visible absorption, and then loaded with 1 wt.% of Pt for promoting the formation of molecular hydrogen. To the best of our knowledge, the influence of Pt

loaded on cobalt doped TiO<sub>2</sub> catalysts prepared by two different solvothermal methods for the photocatalytic hydrogen generation has never been developed before. Therefore, it is the purpose of this work to investigate the influence of the synthesis conditions on the structural, paramagnetic, and photocatalytic properties of the platinumized Co-TiO<sub>2</sub> photocatalysts. The synthesized materials were characterized by means of XRD, TEM, UV-vis, XPS, EPR, and EIS, then evaluated by the photocatalytic hydrogen generation from aqueous methanol. Based on the experimental results, the possible mechanism for H<sub>2</sub> evolution over Pt/Co-TiO<sub>2</sub> is proposed.

## 4.4. Experimental Section

### 4.4.1. Chemicals

Titanium (IV) isopropoxide (Ti(OPri)<sub>4</sub> (97%)), cobalt (II) acetate tetrahydrate (Co(Ac)<sub>2</sub>·4H<sub>2</sub>O (99.99%)), hydrochloric acid (HCl), and hexachloroplatinic acid (H<sub>2</sub>PtCl<sub>6</sub>·6H<sub>2</sub>O) were purchased from Sigma Aldrich Chemie GmbH, München, Germany. 2-propanol anhydrous (99.5%), and methanol (99.9%), Carl Roth GmbH, Karlsruhe, Germany, were used for analytical grade and without further purification. Aeroxide TiO<sub>2</sub> P25 with a mixture of anatase (80%) and rutile (20%) crystal phase and a specific surface area of 50.1 m<sup>2</sup> g<sup>-1</sup> was kindly provided by Evonik Industries AG, Essen, Germany. Hombikat UV 100 with a SSA superior to 250 m<sup>2</sup> g<sup>-1</sup> provided from Sachtleben Chemie GmbH, Duisburg, Germany. Deionized water from a Sartorius Arium 611 device (Sartorius AG, Göttingen, Germany) with a resistivity of 18.2 MΩ·cm at 298 K was used for the preparation of all aqueous solutions, and suspensions.

### 4.4.2. Materials Preparation

#### 4.4.2.1. Hydrothermal Synthesis (HT)

In a typical reaction, a prescribed amount of titanium isopropoxide was dissolved in anhydrous propanol. After that, a second solution containing 0.5 g Co(Ac)<sub>2</sub>·4H<sub>2</sub>O dissolved in 50 mL of propanol, 10 mL distilled water and 0.5 mL HCl was added dropwise to the first solution containing TiO<sub>2</sub> precursor under magnetic stirring. The same procedures were followed for the synthesis of bare TiO<sub>2</sub> in the



absence of the cobalt salt. The resultant sol was then aged for 1 day and then hydrothermally treated at 473 K for 10 h. The gained precipitate was washed by distilled water, dried at 343 K for 24 h and then placed in a muffle furnace for annealing at 773 K for 5 h.

#### 4.4.2.2. Reflux Synthesis (R)

Synthesis of Pt/Co-TiO<sub>2</sub> and Pt/TiO<sub>2</sub> NPs in reflux was also carried out using the same TiO<sub>2</sub> and Co precursors as used in the hydrothermal synthesis. Briefly, titanium isopropoxide dissolved in anhydrous propanol solution was mixed with the solution of Co(Ac)<sub>2</sub>·4H<sub>2</sub>O dissolved in propanol, distilled water, and HCl as described in the hydrothermal synthesis. The mixture was maintained in a closed system heated to boiling under reflux and stirring for 6 h to promote further hydrolysis and crystallization of the product. The reaction was stopped by removing the heat source, the residue was washed thoroughly with distilled water, centrifuged, dried at 343 K in an oven for 24 h, and then calcined at 773 K for 5 h. The bare TiO<sub>2</sub> was prepared in the absence of Co(Ac)<sub>2</sub>·4H<sub>2</sub>O under the same conditions.

#### 4.4.2.3. Photoplatinization

The Pt deposition on the prepared TiO<sub>2</sub> and Co-TiO<sub>2</sub> catalysts (1 wt.% Pt) was performed by the photoplatinization method using the appropriate volume of H<sub>2</sub>PtHCl<sub>6</sub>·6H<sub>2</sub>O as the platinum precursor. A pre-determined amount of TiO<sub>2</sub> or Co-TiO<sub>2</sub> was suspended in a solution containing 5.13 mL of H<sub>2</sub>PtHCl<sub>6</sub>·6H<sub>2</sub>O, a 30% volume of methanol used as the sacrificial hole scavenger during the photodeposition of platinum, and 70% volume of distilled water. The suspension was kept in a cylindrical glass reactor of 50 mL volume then irradiated for 24 h under UV light irradiation (1 mW cm<sup>-2</sup>) with continuous stirring (400 rpm). The milky white (bare TiO<sub>2</sub>) and yellow (Co-TiO<sub>2</sub>) suspensions turn to a pale grey color. The suspensions were then centrifuged, washed repeatedly with distilled water, and dried at 343 K for 12 h. The two catalysts synthesized under hydrothermal conditions were denoted as Pt/Co-TiO<sub>2</sub>-HT and Pt/TiO<sub>2</sub>-HT. The two materials synthesized within the reflux method were

represented as Pt/Co-TiO<sub>2</sub>-R and Pt/TiO<sub>2</sub>-R. Titanium dioxide Evonik P25 with a mixture of anatase (80%) and rutile (20%) crystal phase and a specific surface area of 50.1 m<sup>2</sup>g<sup>-1</sup> kindly provided by Evonik Industries AG, Essen, Germany, and Hombikat UV 100 with a specific surface area of 250 m<sup>2</sup>g<sup>-1</sup> provided from Sachtleben Chemie GmbH, Duisburg, Germany, were also modified with 1 wt.% Pt and used for comparison.

#### 4.4.3. Characterization of the Prepared Materials

XRD measurements were determined using a D8 Advance system (Bruker, Billerica, MA, USA) using a Cu K $\alpha$  radiation source with a wavelength of  $\lambda = 0.0154178$  nm over a  $2\theta$  range from 20 to 80 with a 0.011 step width. The morphology of the prepared photocatalysts was determined using SEM, employing a JEOL JSM-6700F field emission instrument (Tokyo, Japan) with a resolution of 100 nm and 1  $\mu$ m using an EDXS detector. The nanoparticle size was determined using a TEM Tecnai G2 F20 TMP device (FEI Company, Hillsboro, OR, USA) conducted at an acceleration potential of 200kV with a FEG field effect, objective lenses TWIN, and point resolution of 0.27 nm. The full Co-TiO<sub>2</sub> and TiO<sub>2</sub> materials characterizations have been reported in our previous work [33]. Diffuse reflectance UV-vis spectroscopy was employed using a spectrophotometer (Varian Spectrophotometer Cary-100 Bio, Agilent technologies, Santa Clara, CA, USA) at room temperature. Barium sulfate was used as a standard for 100% reflection. The SSA of the investigated materials was determined according to the multi-layer adsorption model by the BET method using a FlowSorb II 2300 apparatus from Micromeritics Instrument Company (Norcross, GA, USA).

Measurements of XPS were carried out using a Leybold Heraeus (Cologne, Germany) with X-ray source, Mg & Al anode, nonmonochromatic, hemispherical analyzer, 100 mm radius. Data analysis was performed using XPSPEAK 4.1 software (Hong Kong, China). The energy of the C 1s-line was set to 284.8 eV and used as a reference for the data correction.

The EPR spin trapping experiments were performed with a MiniScope X-band EPR spectrometer (MS400 Magnetech GmbH) at 77 K operating at about 9.47 - 9.51

GHz field frequency. The acquisition parameters were; center field: 337 mT, sweep time 60 s, modulation amplitude: 0.15 mT, number of points: 4096, number of scans: 1, microwave power: 10 mW, gain 5. All the measurements were recorded at 77 K with nitrogen cooling at a normal air atmosphere in order to avert the fast recombination of electron-hole pairs. Initially, bare TiO<sub>2</sub> and Co-TiO<sub>2</sub> photocatalysts were studied in the dark and then under illumination. Irradiation experiments were performed irradiating the samples with a 200 W xenon lamp with the wavelength from 250 - 450 nm equipped with an IR water filter.

#### 4.4.4. Electrochemical Study

Electrochemical impedance spectroscopy (EIS) was conducted using a ZENNIUM potentiostat and a PECC-2 photoelectrochemical cell (ZAHNER-Elektrik GmbH & Co. KG). Films of the samples were used as the working electrode, after being coated on cleaned FTO coated glass and calcinated at 673 K for 2 h. An Ag/AgCl electrode (3 M NaCl, +209 mV vs. NHE) and a platinum coil were used as the reference electrode and the counter electrode, respectively. KNO<sub>3</sub> aqueous solution (0.1 M) was used as the electrolyte. The impedance spectra were recorded in the range between the chosen potential from -1 V to +1 V at frequencies of 10, 100, and 1000 Hz with 20 mV amplitude vs. Ag/AgCl. The capacitance was plotted against V, and the flatband was calculated from the intercept of the plot. (i.e., a plot of C<sup>-2</sup> vs. V, where C was the capacitance and V was the potential across the space charge layer).

#### 4.4.5. H<sub>2</sub> Evolution by Photocatalytic Reforming of CH<sub>3</sub>OH

Measurements of photocatalytic H<sub>2</sub> formation activities were performed in sealed glass vials (capacity of 10 mL) under illumination with a 1000 W Xenon lamp, (Hönle UV Technology, Gräfelfing, Germany; Sol 1200 solar). The full emission spectrum of the Xenon lamp is given in **Figure S4-1**. Typically, an amount of 6 mg of the photocatalyst (TiO<sub>2</sub>, Co-TiO<sub>2</sub>, Pt/TiO<sub>2</sub>, Pt/Co-TiO<sub>2</sub>, as well as Pt-loaded P25 and Pt-loaded UV100) was suspended in 6 mL aqueous methanol (10 vol%). The solution was purged with argon for 30 min to remove the air. The amount of H<sub>2</sub> gas evolved via the

photocatalytic reaction was quantified every two hours using a gas chromatograph (Shimadzu GC-8A, Shimadzu Deutschland GmbH, Duisburg, Germany) equipped with TCD and 60/80 molecular sieve 0.5 nm column.

## 4.5. Results and Discussion

### 4.5.1. Photocatalyst Characterization

The XRD patterns of different platinum loaded samples are shown in **Figure 4-1**. The XRD patterns of the bare TiO<sub>2</sub> and Co-TiO<sub>2</sub> samples were investigated in our previous study [37]. All the synthesized samples exhibited the characteristic peaks of anatase TiO<sub>2</sub> at  $2\theta = 25^\circ$  (major),  $38^\circ$ ,  $48^\circ$ ,  $55^\circ$ ,  $63^\circ$ ,  $69^\circ$ , and  $75^\circ$ . Small peaks of the rutile phase at  $2\theta = 28^\circ$  and  $36^\circ$  were also observed on the Pt/TiO<sub>2</sub>-HT, Pt/Co-TiO<sub>2</sub>-HT, and the Pt/P25. Contaminations of the brookite phase at  $2\theta = 31^\circ$  and  $40^\circ$  were also detected in the Pt/TiO<sub>2</sub>-HT, Pt/Co-TiO<sub>2</sub>-HT, Pt/TiO<sub>2</sub>-R, and Pt/Co-TiO<sub>2</sub>-R. According to the literature, anatase to rutile transformation in the titania system occurs when the temperature is increased above 450 °C [38]. However, Castro *et al.* have reported that mild hydrothermal synthesis enables one to obtain pure and stable anatase TiO<sub>2</sub> until 800 °C [39]. In a study conducted by Zhao *et al.*, the presence of three titania polymorphs was demonstrated for Co-doped TiO<sub>2</sub> using combined sol-gel and hydrothermal methods [40]. As shown in **Figure 4-1**, The XRD patterns of the Co-TiO<sub>2</sub> did not exhibit any peaks related to metallic Co or cobalt oxides, proving that cobalt is well incorporated in the TiO<sub>2</sub> crystal cell. The characteristic peak platinum was not detected for all the photocatalysts probably due to the low amount of the metals or to the high dispersion of these metals on the TiO<sub>2</sub> supports [41]. The addition of platinum resulted in an increase of brookite content for the refluxed and hydrothermally prepared catalysts. This was evidenced in the peak that occurred at  $2\theta = 40^\circ$  which was not existing in the absence of Pt loading [37].

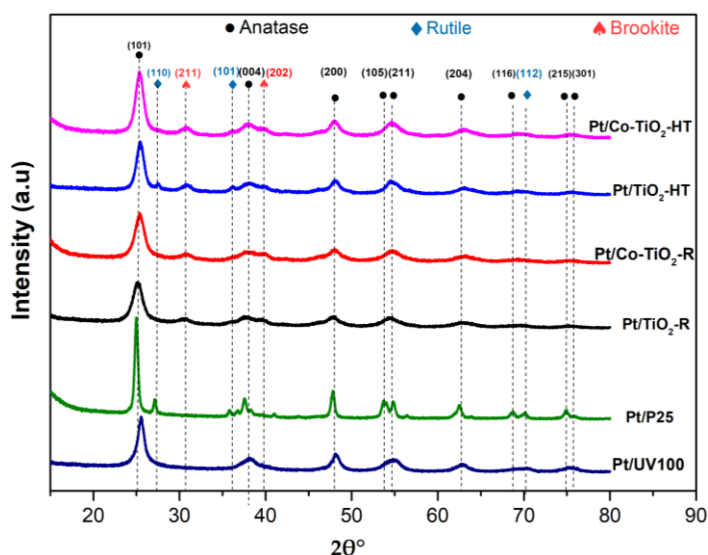


**Figure 4-1.** X-ray diffraction patterns of Pt/Co-TiO<sub>2</sub>-R, Pt/Co-TiO<sub>2</sub>-HT, Pt/TiO<sub>2</sub>-R, Pt/TiO<sub>2</sub>-HT, Pt/UV100, and Pt/P25.

The SEM analysis of the synthesized cobalt-doped TiO<sub>2</sub> and pure TiO<sub>2</sub> were studied for the investigation of the surface morphology and characteristics. **Figures S4-2** and **S4-3** present the SEM and the corresponding EDX images of the TiO<sub>2</sub> and Co-TiO<sub>2</sub> catalysts, respectively. The samples display a spherical structure, nevertheless, most of them are in agglomerated form. The EDX elemental analysis shown in **Figure S4-3 (a, c)** endorse the presence of Ti, O, and Cl. The existence of chlorine as an impurity is due to the HCl used to prepare the catalysts as observed by [42]. Very weak peaks of cobalt are additionally seen in **Figure S4-3 (b, d)**, which can be explained by the low amount of Co-doping (ca. 0.5 wt.%) and its good dispersion over Co-TiO<sub>2</sub>-HT and in Co-TiO<sub>2</sub>-R. This has been also reported in previous studies [43, 44].

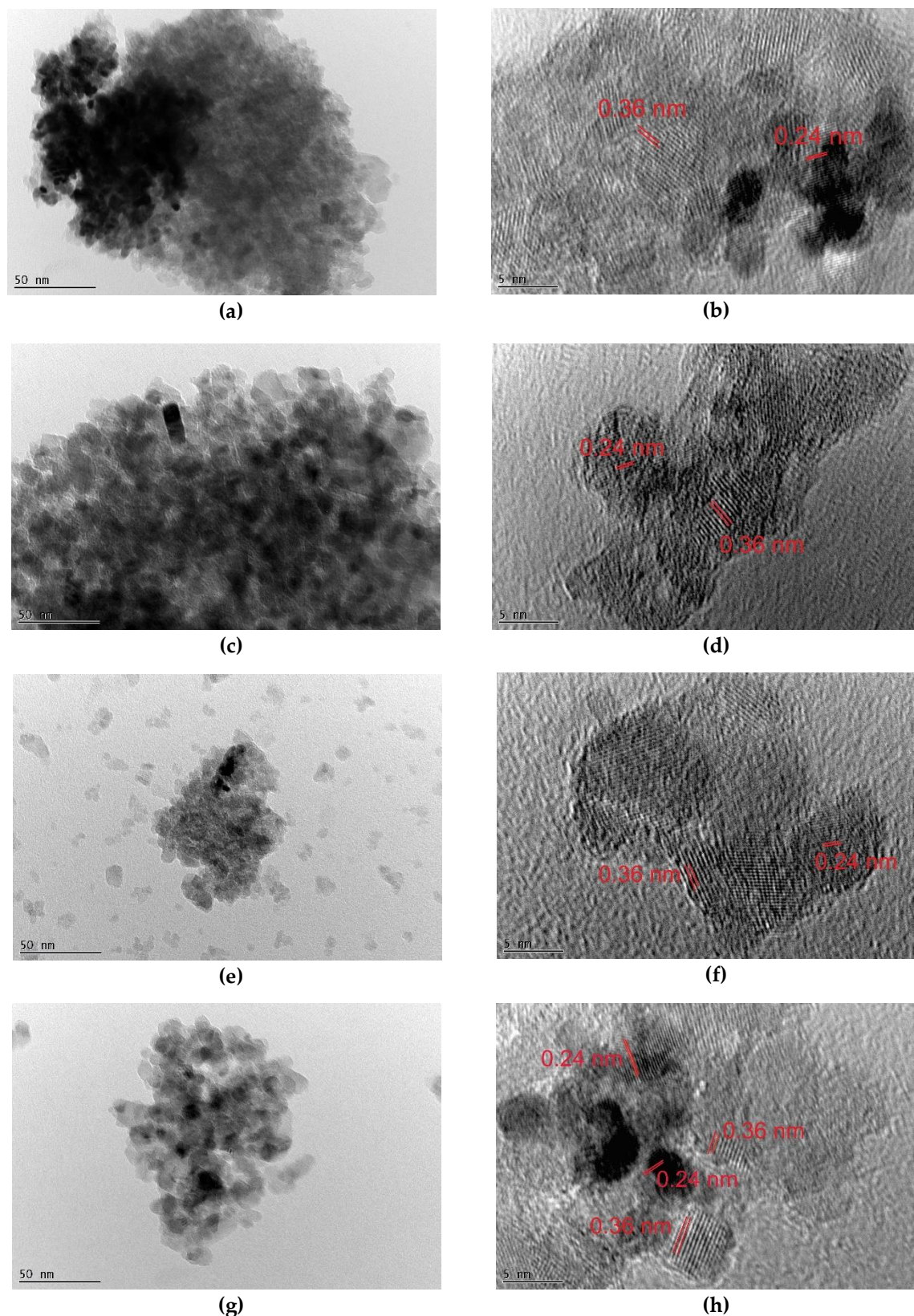


**Figure 4-2.** TEM images of (a) Pt/TiO<sub>2</sub>-R, (c) Pt/TiO<sub>2</sub>-HT, (e) Pt/Co-TiO<sub>2</sub>-R, and (g) Pt/Co-TiO<sub>2</sub>-HT, and HRTEM images of (b) Pt/TiO<sub>2</sub>-R, (d) Pt/TiO<sub>2</sub>-HT, (f) Pt/Co-TiO<sub>2</sub>-R, and (h) Pt/Co-TiO<sub>2</sub>-HT.

Complementary morphological amplification can be achieved with the TEM study. **Figure 4-2** shows the TEM/HRTEM images of the Pt/TiO<sub>2</sub> and the Pt/Co-TiO<sub>2</sub>

powders. The NPs have an almost spherical shape and they are bigger in size in the case of Pt/TiO<sub>2</sub>-HT and Pt/Co-TiO<sub>2</sub>-HT, and much more porous and agglomerated in Pt/TiO<sub>2</sub>-R and Pt/Co-TiO<sub>2</sub>-R. The particle size determined from TEM images ranged between  $7 \pm 0.5$  nm and  $9 \pm 0.5$  nm which is in good agreement with the crystallite size obtained from XRD as discussed in our previous work [37]. The HRTEM images shown in **Figure 4-2 (b, d, f, h)** confirm the good crystallinity of the NPs, as indicated by the spacing of 0.36 nm which corresponds to the anatase plane (101) of TiO<sub>2</sub>. Small Pt NPs are observed on the TiO<sub>2</sub> and Co-TiO<sub>2</sub> surface as evidenced by the lattice spacing of 0.24 nm which corresponds to the Pt (111) lattice plane [45].

The optical properties of the prepared materials were investigated by means of UV-vis spectroscopy at room temperature. The diffuse reflectance spectra of all samples were converted into absorption spectra by using the Kubelka-Munk function as depicted in **Figure 4-3 (a)**. From these results, it can be seen that the platinized Degussa P25 and the platinized Hombikat UV100 only show optical absorptions within the UV region; with a band gap of 3.12 and 3.29 eV for Pt/P25 and Pt/UV100 respectively, as indicated in **Figure 4-3 (b)**. As it has been previously shown in our previous work and compared to the as-prepared pure TiO<sub>2</sub> [37], the optical absorption of Pt/TiO<sub>2</sub> is not affected by the 1.0 wt.% platinum loading even that the color of the sample turned from white to pale grey. On the other hand, the Pt/Co-TiO<sub>2</sub> catalysts compared to the Co-TiO<sub>2</sub>, show a blue-shifted absorption edge towards the UV region. Hence, the Co-TiO<sub>2</sub>-R and Co-TiO<sub>2</sub>-HT composites show broader absorption onsets at around 423 nm (2.93 eV) and 410 nm (3.03 eV), respectively [37]. These absorptions are slightly wider than those observed for Pt/Co-TiO<sub>2</sub>-R and Pt/Co-TiO<sub>2</sub>-HT NPs which are around  $\lambda = 404$  nm (3.11 eV) and  $\lambda = 401$  nm (3.14 eV), respectively. Similar behavior has been previously reported using Pt loaded N doped TiO<sub>2</sub> and explained by the loss of the cobalt from the photocatalyst during the Pt photodeposition. Since the photodeposition of Pt was prepared by dissolving Co-TiO<sub>2</sub> powders in the H<sub>2</sub>HPtCl<sub>6</sub> solution, the cobalt vanished from the TiO<sub>2</sub> lattice and dissolved into the solution. Furthermore, washing the photocatalyst after the photodeposition of Pt can also



contribute to the loss of cobalt ions from the photocatalyst [46]. From these results, it can be stated that despite the change in color and the slight shift in the bandgap, neither Pt/TiO<sub>2</sub> nor Pt/Co-TiO<sub>2</sub> catalysts are able to absorb significantly visible light.

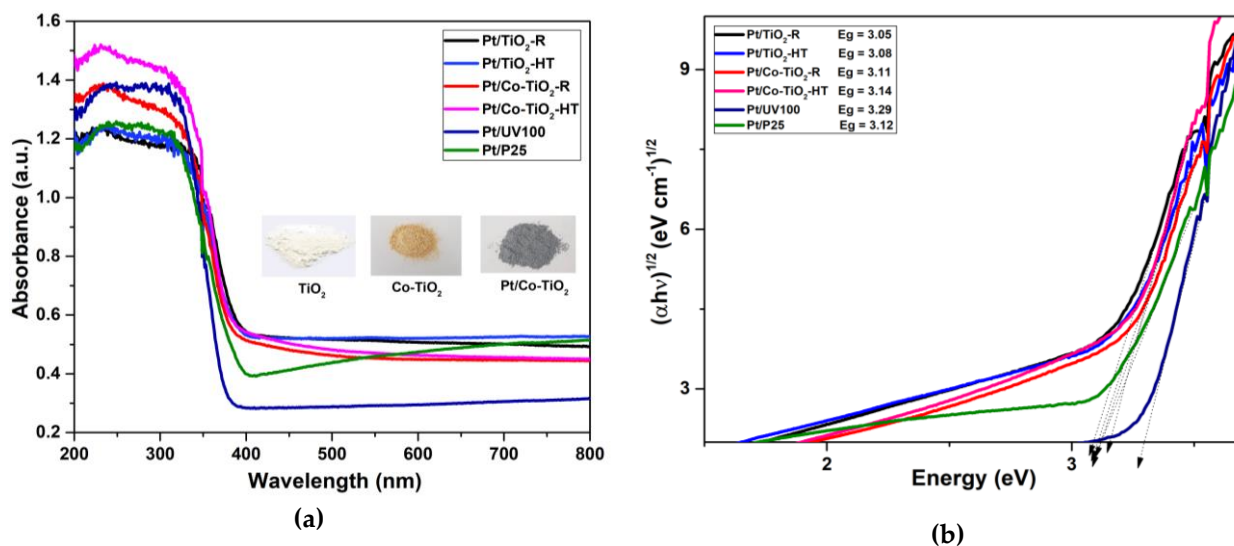


**Figure 4-3.** (a) UV-vis diffuse reflectance spectra, and (b) the corresponding indirect band gap energies of Pt/Co-TiO<sub>2</sub>-R, Pt/Co-TiO<sub>2</sub>-HT, Pt/TiO<sub>2</sub>-R, Pt/TiO<sub>2</sub>-HT, Pt/UV100, and Pt/P25.

#### 4.5.2. XPS Analysis of Co-TiO<sub>2</sub> and TiO<sub>2</sub> Photocatalysts

In order to investigate the oxidation states of the metal species present on the materials, X-ray photoelectron spectroscopy was performed. The XPS spectra of the bare TiO<sub>2</sub> and Co-TiO<sub>2</sub> composites are shown in **Figure 4-4**. The strong Ti 2p<sub>3/2</sub> and Ti 2p<sub>1/2</sub> XPS peaks at about 459.3 and 464.9 eV with a spin-orbital doublet splitting of 5.6 eV suggest that the Ti elements mainly existed as Ti<sup>4+</sup> in the TiO<sub>2</sub>-R sample. The deconvolution of the high-resolution spectra for O 1s XPS spectrum shows a strong peak at around 530.5 eV ascribed to the O<sup>2-</sup> in TiO<sub>2</sub>. In the presence of cobalt dopant, the Ti 2p<sub>3/2</sub>, Ti 2p<sub>1/2</sub> and O 1s peaks of the Co-TiO<sub>2</sub>-R catalyst are almost identical to those of the TiO<sub>2</sub>-R, except for a slight red-shift in the binding energy of about 0.2 eV, which is in agreement with previously reported results [47]. The characteristic peaks of Co 2p<sub>3/2</sub> and Co 2p<sub>1/2</sub> which have to be at around 781.0 and 797.2 eV [48] are not observed in this case (**Figure S4-4**), certainly because of the low amount of cobalt doping (ca 0.5 wt.%) [49]. Nevertheless, both Ti and O spectra have revealed the successful insertion of



cobalt within the TiO<sub>2</sub> matrix. Using the samples prepared within the hydrothermal methods, similar Ti 2p<sub>3/2</sub>, Ti 2p<sub>1/2</sub>, and O 1s XPS peaks were recorded for the bare TiO<sub>2</sub>-HT as shown in **Figure S4-4**, with a shift in the binding energy of the Ti and O spectra, which indicates that there were interactions between Ti-O-Co inside the TiO<sub>2</sub> framework. Similar results have been reported by Venturini *et al.* [50]. Unfortunately, the XPS measurements did not allow us to find out the cobalt spectra and, therefore, further investigations using EPR spectroscopy were carried out.

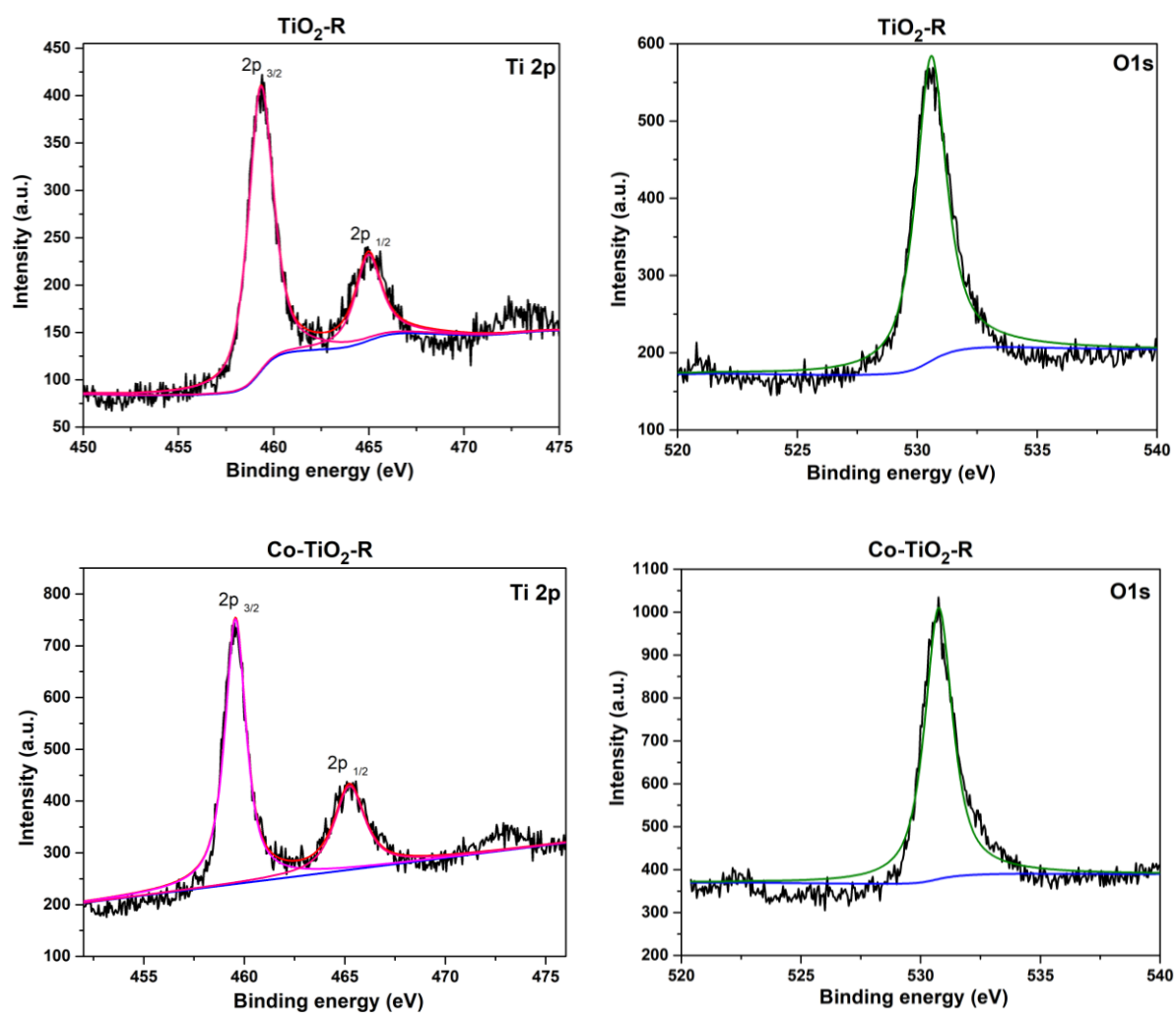


**Figure 4-4.** The XPS spectra of Ti 2p, and O 1s of TiO<sub>2</sub>-R and Co-TiO<sub>2</sub>-R.

### 4.5.3. EPR Analysis of Co-TiO<sub>2</sub> and TiO<sub>2</sub> Photocatalysts

Transition metal ions are usually paramagnetic because of their partially filled orbitals [51]. For the investigation of photogenerated electron and hole paramagnetic species, all the samples were studied in the dark and under illumination and the obtained results are depicted in **Figure 4-5**. The EPR spectrum of the as-synthesized TiO<sub>2</sub>-HT sample in the dark (**Figure 4-5 (a inset)**) exhibited mainly two sharp bands at around  $g = 1.997$  and  $g = 1.985$  which were assigned to the paramagnetic centres in the titanium dioxide crystal lattice, and which were earlier observed for bare TiO<sub>2</sub> before irradiation by Brezová *et al.* [52]. Upon continuous irradiation (**Figure 4-5 (a)**), changes in the EPR spectra were observed depicting an intensified broad band which was found to decrease with the irradiation time and characterized by  $g = 2.022$ ,  $g = 2.008$ , and  $g = 2.001$  assigned to a surface hole trapped radical  $\text{Ti}^{4+}\text{O}^{\bullet}-\text{Ti}^{4+}\text{OH}^-$  [53–56]. A sharp EPR signal (B) centered around  $g = 1.985$  increasing with irradiation time was detected and assigned to the trapped electron as a  $\text{Ti}^{3+}$  state in the TiO<sub>2</sub> matrix [55, 56]. The signal (C) induced at the region of 344.10 mT with  $g = 1.970$ ,  $g = 1.958$ , and  $g = 1.950$  which displayed an increase in intensity can be ascribed to the conduction band trapped electron which tend to reduce  $\text{Ti}^{4+}$  cations to the  $\text{Ti}^{3+}$  state [57], which is consistent with the XPS data shown above in which the  $\text{Ti}^{3+}$  were identified to be located at the surface. The EPR spectra of Co-TiO<sub>2</sub>-HT catalyst recorded in the dark (**Figure 4-5 (b inset)**) present two signals at around  $g = 1.997$  and  $g = 1.982$  which may also correspond to  $\text{Ti}^{3+}$  sites on TiO<sub>2</sub> as seen for the raw TiO<sub>2</sub>-HT. Under illumination (**Figure 4-5 (b)**), a large number of photoexcited electrons are formed, and the intensity of the signal (A) increased with the appearance of new signals (B) and (C) as observed for the bare TiO<sub>2</sub>-HT. However, in Co-TiO<sub>2</sub>-HT composite, the peak of  $\text{Ti}^{3+}$  at around  $g = 1.970$  disappeared in comparison with TiO<sub>2</sub> -HT, which proved that the photogenerated electrons are trapped in other sites than Ti in the presence of cobalt thus reducing the intensity of the  $\text{Ti}^{3+}$  signal. This can also be explained by the participation of  $\text{Ti}^{3+}$  to anchor the cobalt on TiO<sub>2</sub> support or with the fact that the cobalt ions are incorporated in the crystal lattice and appear as interstitial defects

rather than real substitutional dopants as reported in [58]. The oxidation state of cobalt after electron trapping cannot be determined from this EPR study. According to the literature [59–61], signals at around  $g = 4.200$  were previously observed and assigned to the high spin  $\text{Co}^{2+}$  in an octahedral environment, and a broad signal at  $g = 2.000$  was attributed to  $\text{Co}_3\text{O}_4$  [59]. Huang *et al.* have attributed a broad signal with  $g = 2.19$  to the high spin  $\text{Co}^{2+}$  in an octahedral environment [62]. Also, it has been reported that at low Co content, only hole defects are properly detected. Chao *et al.* have reported an EPR signal at  $g = 2.000$  which they have assigned to the paramagnetic adduct of oxygen and  $\text{Co}^{2+}$  on an oxide surface [63]. Other authors have stated that a fraction of cobalt ions can only be adsorbed on the nanocrystal surface and could not be seen in the EPR spectra but contribute to the magnetic susceptibility of a nanocrystal powder [59,64]. A close look at the Co-TiO<sub>2</sub>-HT spectra reveals a noticeable increase in the vacancy peak at around  $g = 2.001$  in comparison with that of TiO<sub>2</sub>-HT, indicating the introduction of Co species with a possible substitution of  $\text{Ti}^{4+}$  with  $\text{Co}^{2+}$ . This observation is consistent with a previous report in which Melanin and co-authors observed an increase in the oxygen vacancy peak with doping up to 2 wt.% of Co and attribute it to the  $\text{Co}^{2+}$  [48]. **Figure 4-5 (c)** shows the EPR spectra of the TiO<sub>2</sub>-R catalyst. The resonance at  $g = 1.985$  in the dark (**Figure 4-5 c inset**) is attributed to the  $\text{Ti}^{3+}$  site on TiO<sub>2</sub>. After irradiation, this peak intensified, and new signals were recorded; the peak with  $g = 2.020$ , and  $g = 2.002$  is assigned to the trapping hole at the surface, the signal B with  $g = 1.985$  is ascribed to  $\text{Ti}^{3+}$  surface electron trapping sites which improved with irradiation time. The signal C induced at  $g = 1.970$ ,  $g = 1.958$ , and  $g = 1.950$  is probably attributed to the conduction band electron trapped at the bulk as observed for the TiO<sub>2</sub>-HT. Similar spectra have been previously obtained [56]. With cobalt doping, changes in the EPR spectrum are observed for the Co-TiO<sub>2</sub>-R indicating that cobalt ions were successfully introduced into TiO<sub>2</sub>. Considering the dark spectra (**Figure 4-5 (d inset)**), new signals have been recorded under continuous illumination and were given as signals A, B and C (**Figure 4-5 d**). Signal A is attributed to the trapping hole at the surface which increases in intensity due to the  $\text{Co}^{2+}$  incorporation

as seen for the Co-TiO<sub>2</sub>-HT. The signal B with  $g = 1.985$  is induced due to the trapped electrons which belong to Ti<sup>3+</sup> as seen for the TiO<sub>2</sub>-R. The intensity of this peak decreased in compared with TiO<sub>2</sub>-R, which might be explicated by the electron trapped by cobalt ions inducing a decrease in Ti<sup>3+</sup> peak intensity as seen for the Co-TiO<sub>2</sub>-HT, and the broadband with  $g = 1.967$  can be assigned to the electron trapped at the surface of Ti<sup>4+</sup> site to form Ti<sup>3+</sup>. From these EPR results, it can be concluded that the overall mechanism is determined by either the competition between titania and cobalt to trap the photoinduced electrons or the increased recombination rate in the presence of Co inside the lattice thus reducing the Ti<sup>3+</sup> amount.

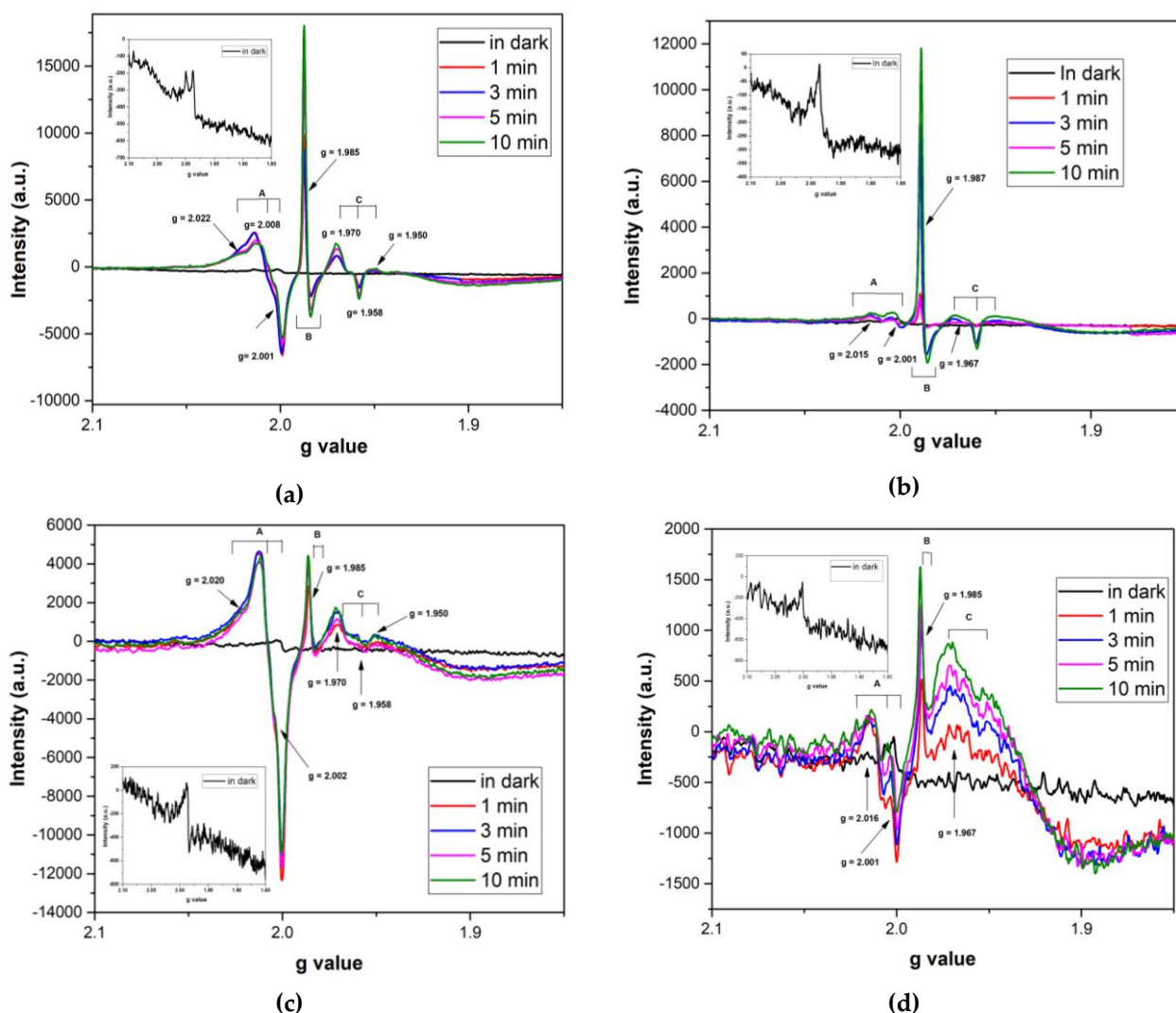


**Figure 4-5.** In situ EPR spectra at 77K of (a) TiO<sub>2</sub>-HT, (b) Co-TiO<sub>2</sub>-HT, (c) TiO<sub>2</sub>-R, (d) Co-TiO<sub>2</sub>-R in the dark and under 1, 3, 5, and 10 min of UV-vis-light irradiation (Xe lamp,  $\lambda = 300\text{--}450$  nm).

#### 4.5.4. Flatband Measurement of Co-TiO<sub>2</sub> and TiO<sub>2</sub> Photocatalysts

The flatband potential ( $E_{\text{FB}}$ ) of the synthesized materials were determined using Mott-Schottky plots. The measurements started at the potential of +0.20 V and finished at the potential of -0.8 V (vs Ag/AgCl) as illustrated in **Figure 4-6**. With an ideal semiconductor-solution interface, a plot of  $C^{-2}$  against V should yield a straight line and its intercept on the V axis corresponds to  $V_{\text{FB}}$ . As shown from the capacitance-voltage (CV) graph (**Figure 4-6**), three regions labeled as regions 1, 2, and 3 are observed. As previously interpreted by Xu *et al.* Region 1 could originate from the FTO film, region 2 is possibly due to the specific ion adsorption between the FTO surface and the NPs, and region 3 can be interpreted as the contribution of TiO<sub>2</sub> and Co-TiO<sub>2</sub> to the measured capacitance [65]. When the applied potential is more positive than  $\sim -0.33$  V (region 1 and 2), the space-charge region of the nanoparticle films is depleted. The resulting linear fitting of region 1 gives  $V_{\text{FB}}$  of the FTO glasses which are equal to -0.17, -0.22, -0.10, and -0.12V (vs. NHE) for TiO<sub>2</sub>-R, Co-TiO<sub>2</sub>-R, TiO<sub>2</sub>-HT, and Co-TiO<sub>2</sub>-HT, respectively. Once the applied potential is more negative than -0.33V (region 3), a drastic enhancement in the capacitance is seen. The linear fit of region 3 provides the  $V_{\text{FB}}$  of the NPs to be around -0.41, -0.45, -0.42, and -0.44V (vs. NHE) for TiO<sub>2</sub>-R, Co-TiO<sub>2</sub>-R, TiO<sub>2</sub>-HT, and Co-TiO<sub>2</sub>-HT, respectively. These values coincide well with those reported in the literature for the bare TiO<sub>2</sub> and the cobalt doped TiO<sub>2</sub> films [43,66]. Moreover, the flatbands potential of TiO<sub>2</sub> materials were shifted to the negative potential by doping with cobalt, as well as the n-type semiconducting nature of the NPs is also confirmed by the positive slopes of Mott-Schottky plots as indicated in **Table S4-1**.

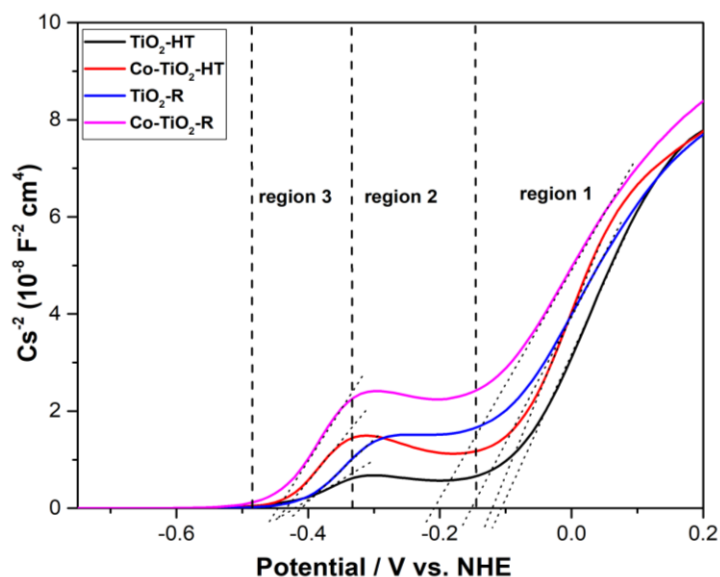


**Figure 4-6.** Mott-Schottky plots taken at room temperature and a probing frequency of 100 Hz of TiO<sub>2</sub>-R, Co-TiO<sub>2</sub>-R, TiO<sub>2</sub>-HT, and Co-TiO<sub>2</sub>-HT catalysts.

The energetic positions of the valence band and the conduction band of TiO<sub>2</sub> and Co-TiO<sub>2</sub> are shown in **Figure 4-7**. As the conduction band of the photocatalysts are estimated to be equal to the  $V_{FB}$  of region 3 for the n-type semiconductors, and the  $E_g$  values were calculated by extrapolating the linear area in the curve of  $(F(R\infty) h\nu)^{1/2}$  versus  $(h\nu)$  presented in our previous work [37], the valence band energies of TiO<sub>2</sub> and Co-TiO<sub>2</sub> powders can be estimated by adding the band gap energy ( $E_g$ ) to the flatband potential ( $E_{fb}$ ) of the composites:

$$E_{CB} = E_{fb}$$

$$E_{VB} = E_{fb} + E_g$$

Accordingly, the valence band energies of TiO<sub>2</sub>-R and TiO<sub>2</sub>-HT at pH 7 are 2.65 and 2.68 eV (vs. NHE), respectively. Owing to the additional intermediate energy states, the valence band energy values calculated for Co-TiO<sub>2</sub>-R and Co-TiO<sub>2</sub>-HT powders are 2.48 and 2.59 eV, respectively (**Figure 4-7**).

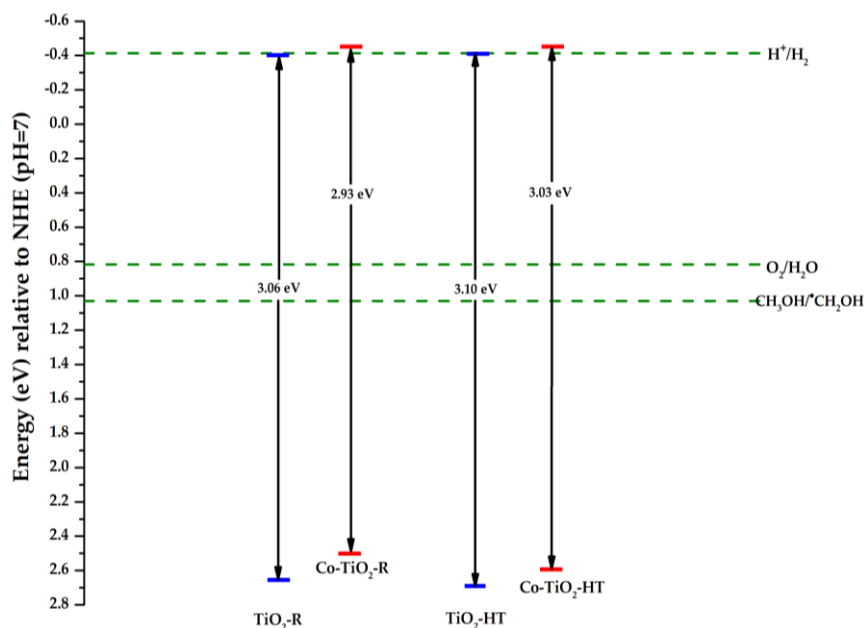


Figure 4-7. Electrochemical potentials (vs. NHE) of band edges of TiO<sub>2</sub> and Co-TiO<sub>2</sub> at pH7.

#### 4.5.5. Photocatalytic Hydrogen Generation of Pt/(Co-TiO<sub>2</sub>) and Pt/TiO<sub>2</sub> Composites

From the energetic viewpoint, bare TiO<sub>2</sub> could be considered as an active material for photocatalytic water splitting. However, kinetically when TiO<sub>2</sub> absorbs a photon the energy of which exceeds its band gap, an electron-hole pair is generated. In the presence of an electron acceptor and in the absence of molecular oxygen, the excess holes are consumed and photogenerated electrons are trapped in the surface forming Ti<sup>3+</sup> instead of reducing H<sup>+</sup> to molecular hydrogen [67]. To overcome this issue, Pt was loaded on the surface of the as-prepared photocatalysts to promote the formation of H<sub>2</sub> and aqueous methanol solution was used as a sacrificial reagent to control the undesired reaction of electron-hole recombination which is thermodynamically favored. As it can be seen from **Figure 4-8 (a, b, c, d)**, no significant reactivity for the photocatalytic hydrogen evolution under simulated solar light was detected neither for TiO<sub>2</sub>-R nor for TiO<sub>2</sub>-HT. This result suggests that the electrons are trapped as Ti<sup>3+</sup> species instead of reducing protons, which is consistent with the aforementioned EPR results. These data are in good agreement with previously published results [32, 68]. Co-TiO<sub>2</sub> -HT and Co-TiO<sub>2</sub> -R materials show also similar photocatalytic behavior as for bare TiO<sub>2</sub>-HT and TiO<sub>2</sub>-R, respectively. The formed amount of H<sub>2</sub> is still extremely low and close to the detection limit. These results

indicate that the reforming of aqueous methanol in the presence of the Co-TiO<sub>2</sub> composites under argon atmosphere is not an efficient chemical reaction. Similar findings have been reported by Hwang *et al.* who found that only Cr and Fe doped TiO<sub>2</sub> produce photocatalytically significant amounts of molecular hydrogen from aqueous methanol [69]. As can be seen from **Figure 4-7**, a small decrease in the band gap is observed upon Co doping. This decrease of the band gap energies enables the Co-doped photocatalysts to absorb more photons than the un-doped photocatalysts under the illumination conditions employed in this investigation. Considering only this, higher activity of the Co-doped titania samples is expected. However, according to **Figure 4-9**, the photocatalytic activity of Co-doped TiO<sub>2</sub> is not significantly enhanced. This result evinces that either the recombination rate is increased [35, 70] or that electrons are trapped more readily and are then not available for H<sup>+</sup> reduction via interfacial charge transfer.

In comparison with the unmodified TiO<sub>2</sub> and Co-TiO<sub>2</sub> samples, all Pt-loaded samples showed higher formation rates of H<sub>2</sub> as exhibited in **Figure 4-8 (a, b, c, d)**. Amounts of 2561, 1695, 2387, and 2203 μmol were evolved during 8 hours of reactions under simulated solar irradiation for Pt/Co-TiO<sub>2</sub>-HT, Pt/Co-TiO<sub>2</sub>-R, Pt/TiO<sub>2</sub>-HT, and Pt/TiO<sub>2</sub>-R, respectively. Also, it is noteworthy to mention that the photocatalytic hydrogen production activity from methanol reforming on the Pt/Co-TiO<sub>2</sub>-HT marginally outperforms that of the well-known platinized photocatalysts Pt/P25 and Pt/UV100 (**Figure 4-8 (e, f)**).



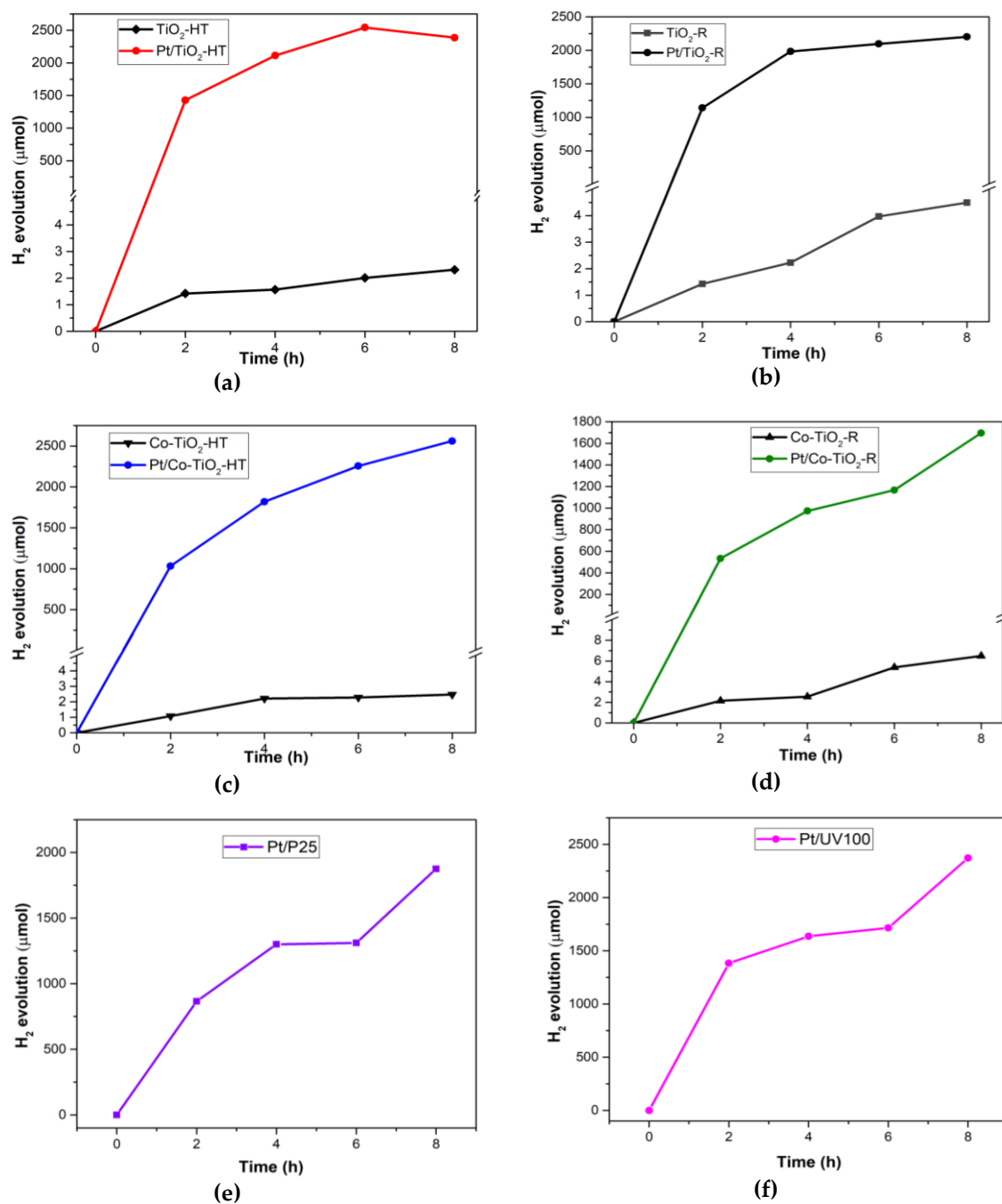


**Figure 4-8.** Time-course of the light-induced hydrogen evolution from aqueous CH<sub>3</sub>OH in the presence of some titania photocatalysts.

The calculated rates of the photocatalytic hydrogen evolution of all samples are shown in **Figure 4-9**. These reaction rates clearly evince that doping with Co ions alone does not significantly increase the photocatalytic activity of TiO<sub>2</sub> photocatalysts. In a study conducted by Wu *et al.*, 0.4 wt.% Co<sup>2+</sup> modified TiO<sub>2</sub> (P25) was found to decrease the photocatalytic hydrogen evolution activity from aqueous ethanol solution

[34]. On the contrary, Sadanandam *et al.* have observed an enhancement in the photocatalytic hydrogen evolution rate when using 1 wt.% Co<sup>2+</sup> doped TiO<sub>2</sub> in 5% glycerol aqueous solutions solution under solar light [32]. A maximum of 2499 μmol of molecular hydrogen, a value being almost six times higher than that of bare titania, has been also reported using 3 % of Co-TiO<sub>2</sub> [33].

All Pt-loaded titania samples employed in this study were found to be photocatalytically more active than the corresponding Pt-free photocatalysts. However, Pt/Co-TiO<sub>2</sub>-HT and Pt/Co-TiO<sub>2</sub>-R exhibit almost similar H<sub>2</sub> evolution rate as Pt/TiO<sub>2</sub>-HT and Pt/TiO<sub>2</sub>-R, respectively (within the limits of the experimental error). H<sub>2</sub> rates of 294, 317, 268, and 201 μmol h<sup>-1</sup> are recorded for Pt/TiO<sub>2</sub>-HT, Pt/Co-TiO<sub>2</sub>-HT, Pt/TiO<sub>2</sub>-R, and Pt/Co-TiO<sub>2</sub>-R, respectively. These results again suggest that the modification with cobalt species does not considerably improve the H<sub>2</sub> evolution activity over the platinized samples. Furthermore, the high photocatalytic activity obtained on all platinized samples was only due to the charge carrier separation caused by the Pt NPs deposited on the surface. It is worth noting that for each material, the H<sub>2</sub> evolution rate is decreasing with the irradiation time as depicted in **Figure 4-8**. This could be because all the methanol in the solution has been consumed within the first 2 or 4 h. The enhanced activity in the platinized samples is due to the presence of Pt co-catalyst which acts as an electron sink for efficient electron transfer to H<sup>+</sup>. Overall, it can be concluded that no significant impact of Co-doping on the photocatalytic activity of the platinized samples is recorded, suggesting that the cobalt doping does not affect significantly the photocatalytic H<sub>2</sub> evolution under these experimental conditions (**Figure 4-9**). This is in accordance with the flatband potential results where no significant impact of cobalt doping has been recorded within the limits of the experimental errors.

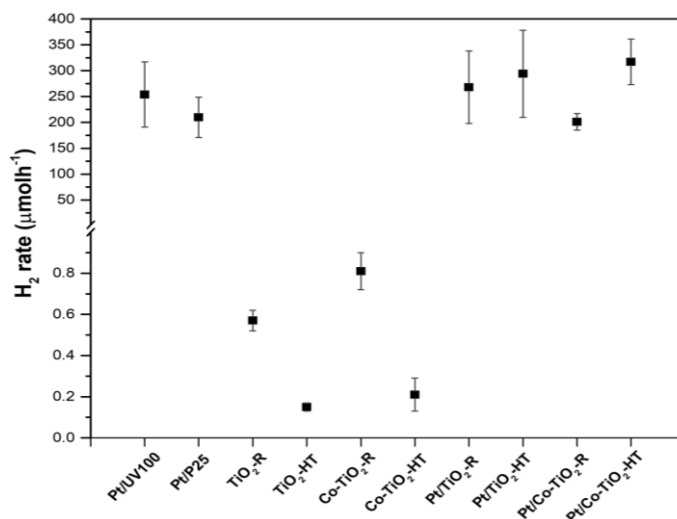


**Figure 4-9.** Hydrogen evolution rates from aqueous CH<sub>3</sub>OH of all prepared photocatalysts.

The observed increase of the hydrogen evolution rate by Pt loaded on TiO<sub>2</sub> photocatalysts corresponds to general experience. For example, Cigarillo *et al.* reported a significant increase in the hydrogen evolution rate of 1% Pt/TiO<sub>2</sub> by 52 times that of bare TiO<sub>2</sub> (P25) [71]. Pt photodeposited on TiO<sub>2</sub> has also been studied by Zou *et al.* The photocatalytic hydrogen evolution rate from methanol-water mixture was enhanced to 1920 μmol h<sup>-1</sup> [41]. Alcaide *et al.* have studied the catalytic activity of Pt deposited on Nb-doped titania support toward the hydrogen evolution reaction [72]. Pt supported on Nb-doped TiO<sub>2</sub> has shown better activity than Pt supported on bare TiO<sub>2</sub>, which was explained by the local increase of the electron density on Pt due to the strong metal-support interaction favored by the Nb doping. In another study, Pt loaded on N doped TiO<sub>2</sub> has shown upgraded hydrogen generation activity from aqueous methanol, which was higher than that of the N doped TiO<sub>2</sub> [73].

#### 4.5.6. Mechanism of Photocatalytic Hydrogen Evolution from Water/ Methanol using Pt/(Co-TiO<sub>2</sub>) and Pt/TiO<sub>2</sub> Catalysts

A schematic illustration of H<sub>2</sub> production via Co - TiO<sub>2</sub> and TiO<sub>2</sub> towards methanol reforming is shown in **Figure 4-10**. Under simulated solar light irradiation, TiO<sub>2</sub> absorbs a photon with energy equal to, or greater than, its bandgap energy (~ 3 eV). Electron and hole pairs are consequently generated in the CB and in the VB,

respectively. The photo-excited electron and hole could easily migrate to the TiO<sub>2</sub> surface, where the H<sup>+</sup> is reduced to molecular hydrogen by the conduction band electron, and methanol is oxidized by valence band holes. As confirmed by the flatband potential diagram shown in **Figure 4-7**, the as-prepared pure TiO<sub>2</sub> and Co-TiO<sub>2</sub> catalysts were found to be able to produce molecular hydrogen. However, the amount of the generated H<sub>2</sub> was very low and below the limits of quantification since the energy of the electrons in the conduction band of Co-TiO<sub>2</sub> and TiO<sub>2</sub> was insufficient to reduce a proton. This phenomenon was also observed by Bahnemann and co-authors reporting an amount of 41 μmol of H<sub>2</sub> over bare TiO<sub>2</sub> [68].

When Pt NPs are loaded on the TiO<sub>2</sub> surface, electrons tend to migrate from the TiO<sub>2</sub> conduction band to the Fermi level of Pt, as the Fermi level of platinum is lower than that of the n-type TiO<sub>2</sub> semiconductor. Therefore, Pt islands act as an electron sink and suppress the charge carrier recombination, whereas the holes left in the TiO<sub>2</sub> valence band oxidize aqueous methanol (**Figure 4-10**). Thus, Pt/TiO<sub>2</sub>-R and Pt/TiO<sub>2</sub>-HT samples exhibited higher photocatalytic hydrogen generation rates.

With cobalt doping, impurity levels create an energy band, which is a donor level in this case, above the valence band of the TiO<sub>2</sub> composites. This leads to a slight narrowing of the band gap of Co-TiO<sub>2</sub>-R and Co-TiO<sub>2</sub>-HT as described in the energetic diagram shown in **Figure 4-7**. After Pt loading, Co-TiO<sub>2</sub>-R and Co-TiO<sub>2</sub>-HT NPs show a drastic improvement in the photocatalytic activity. However, the hydrogen production rates were comparable with those obtained for the Pt/TiO<sub>2</sub>-R and Pt/TiO<sub>2</sub>-HT, presuming that cobalt doping does not significantly and positively affect the photocatalytic hydrogen evolution activity.

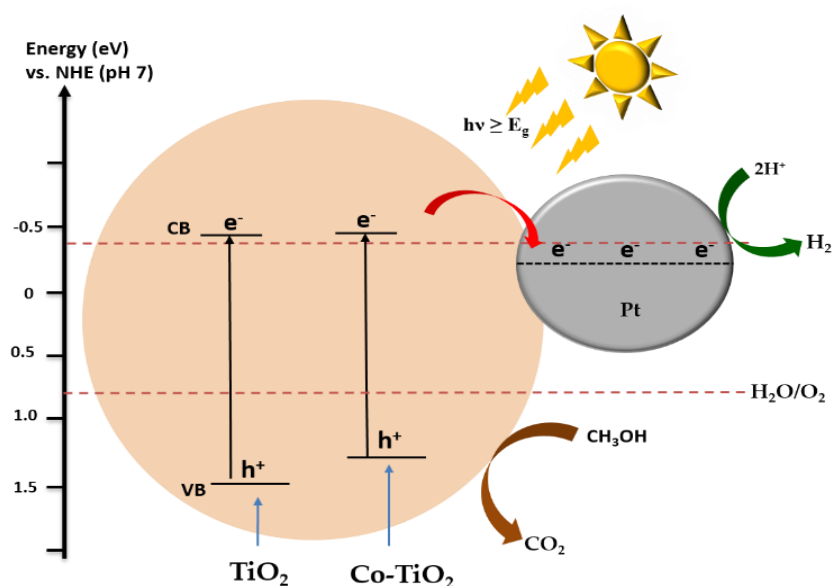


**Figure 4-10.** Schematic illustration of H<sub>2</sub> evolution over Pt/Co-TiO<sub>2</sub> photocatalysts.

## 4.6. Conclusions

In this work, Pt loaded on cobalt doped TiO<sub>2</sub> catalysts have been successfully synthesized by loading of 1 wt.% of Pt on 0.5 wt% Co-TiO<sub>2</sub> prepared through reflux and hydrothermal synthesis under different experimental conditions. The illumination of the bare TiO<sub>2</sub> and Co-TiO<sub>2</sub> powders using EPR resulted in the formation of trapped electrons (Ti<sup>3+</sup> centres) and holes (oxygen radicals covalently linked to surface Ti<sup>4+</sup>). Results of EPR measurements did not allow a conclusive statement. The number of Ti<sup>3+</sup> is reduced in Co-TiO<sub>2</sub> materials, however, this might be due to the increased charge carrier recombination as well as to the electron trapping by Co sites. The nature of semiconductor materials was explored through the determination of the flatband potential using the Mott–Schottky equation. The Mott–Schottky analysis of electrochemical impedance measurements showed that all semiconductors were n-type semiconductors and that cobalt doping induces small impurity levels within the band gap of TiO<sub>2</sub>. The experimental results of photocatalytic hydrogen generation from methanol-reforming showed that the Co -doping does not affect the photocatalytic activity of both Pt/Co-TiO<sub>2</sub> catalysts. Despite that, the Pt/Co-TiO<sub>2</sub>-HT was found to be the best photocatalyst under simulated solar light and show a maximum hydrogen evolution rate of  $317 \pm 44 \mu\text{mol h}^{-1}$ . The presence of Pt seems to

counteract the decrease of the photocatalytic activity due to Co-doping. However, technically usable hydrogen evolution rates were not achieved with the Co-doped titania photocatalysts presented here.

#### 4.7. Supplementary Material

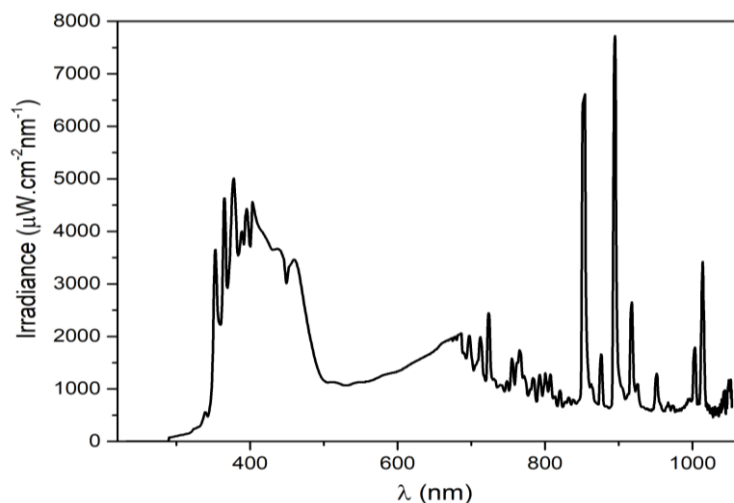


Figure S4-1. The emission spectrum of the used simulated solar light.

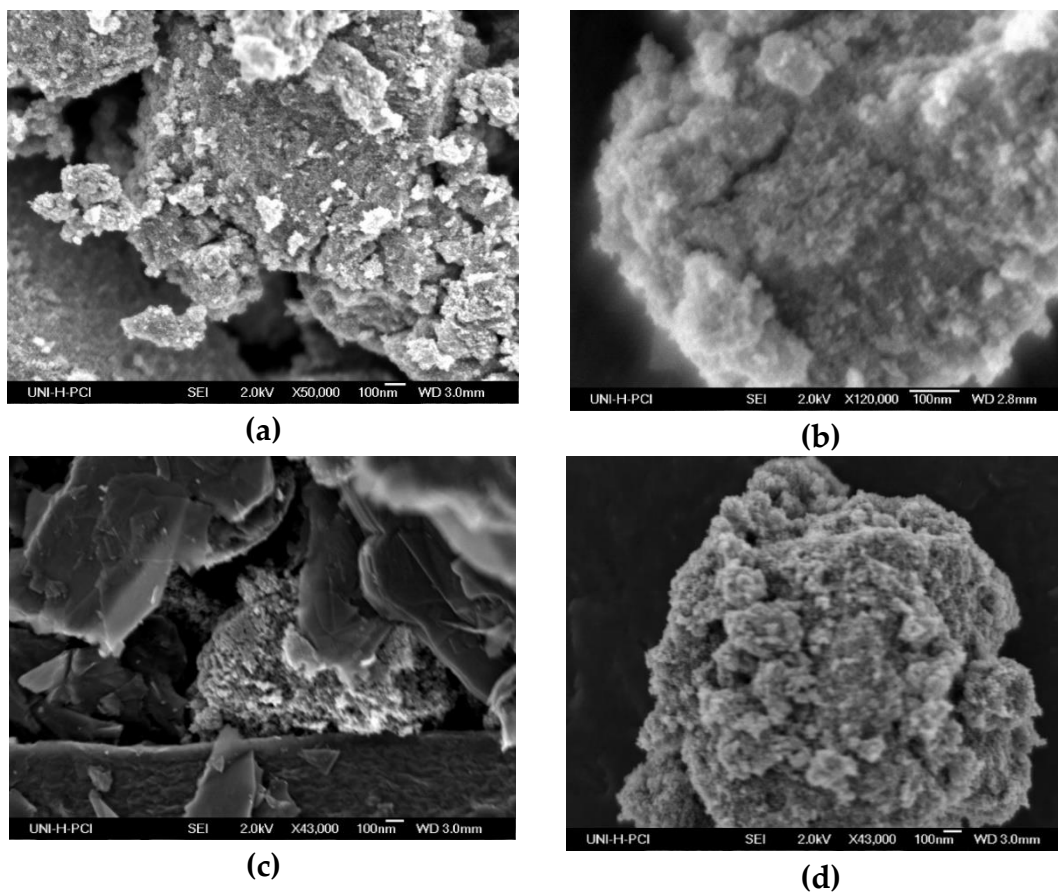
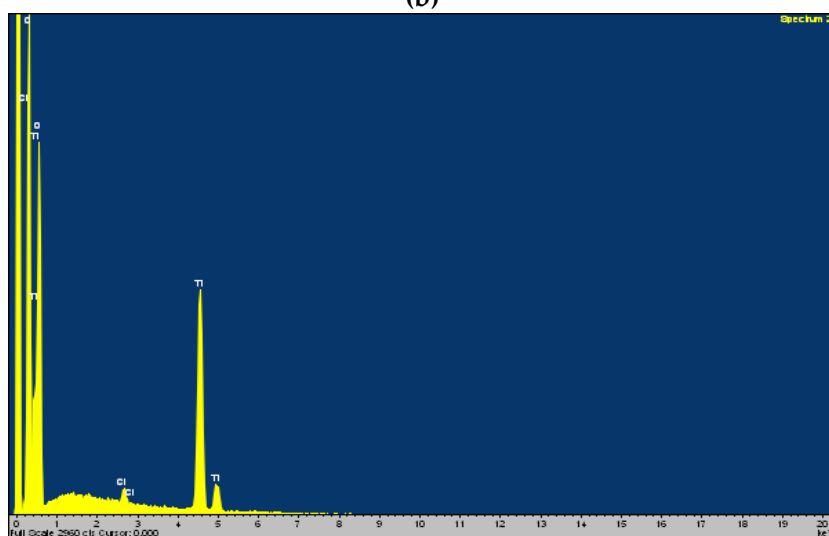
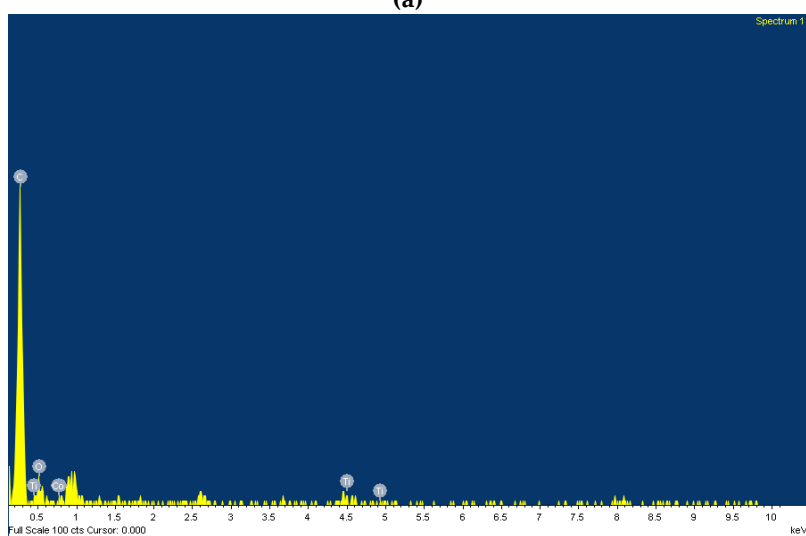
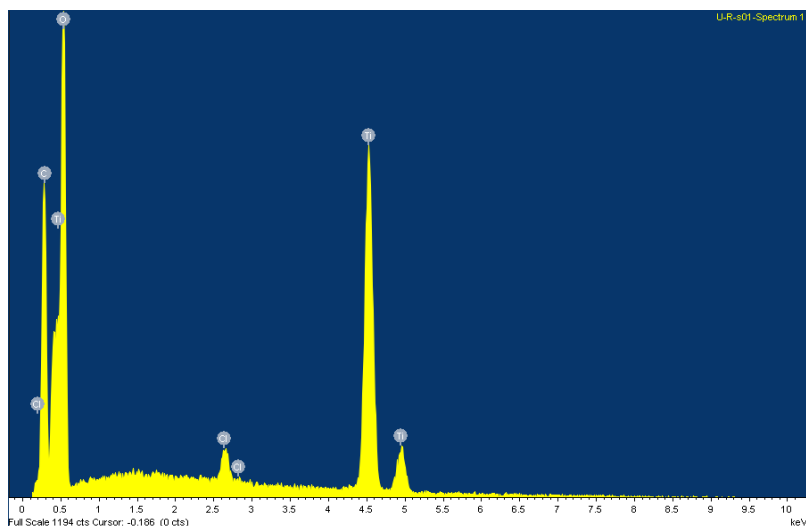
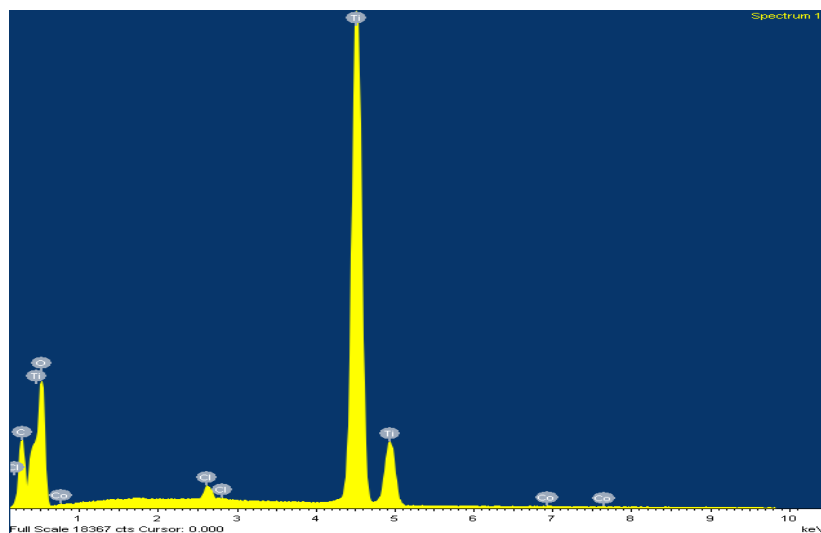


Figure S4-2. The SEM micrograph of (a) TiO<sub>2</sub>-R, (b) Co-TiO<sub>2</sub>-R, (c) TiO<sub>2</sub>-HT, (d) Co-TiO<sub>2</sub>-HT.





(d)

Figure S4-3. The EDX spectra of (a) TiO<sub>2</sub>-R, (b) Co-TiO<sub>2</sub>-R, (c) TiO<sub>2</sub>-HT, (d) Co-TiO<sub>2</sub>-HT.

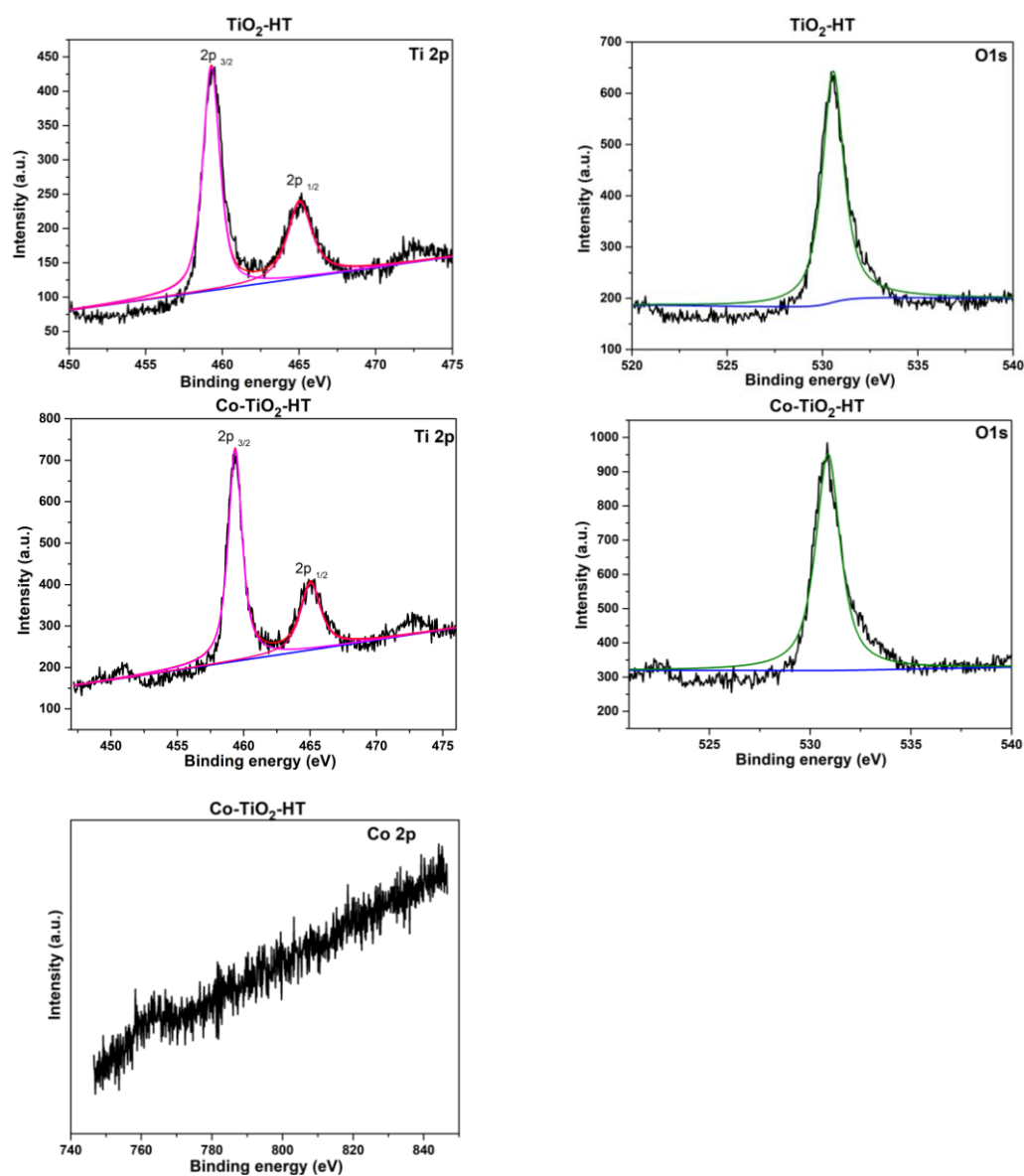


Figure S4-4. The XPS spectra of Ti 2p, Co 2p, and O 1s of TiO<sub>2</sub>-HT and Co-TiO<sub>2</sub>-HT.



**Table S4-1.** The flatband potentials and slopes calculated from the Mott–Schottky plots of all prepared catalysts.

Sample	E <sub>g</sub>	V <sub>fb</sub> (vs. NHE)	Slope
TiO <sub>2</sub> -R	3.06	-0.41	21.5 ± 0.3
Co-TiO <sub>2</sub> -R	2.93	-0.45	20.4 ± 0.3
TiO <sub>2</sub> -HT	3.10	-0.42	28.1 ± 0.4
Co-TiO <sub>2</sub> -HT	3.03	-0.44	27.5 ± 0.7

## 4.8. Acknowledgments

The authors wish to thank Dr. Redouan Boughaled and Narmina Balayeva for the valuable scientific discussions, Dr. Mariano Curti for the XRD measurement, Barbara Nunes for TEM images, Lucy Ombaka, and Abdalrahim Alahmad for SEM/EDX images, and Julian Koch for XPS measurements. Financial support from the Global Research Laboratory Program (2014K1A1A2041044), Korea government (MSIP) through NRF is gratefully acknowledged.

## 4.9. References

1. J.D. Holladay, J. Hu, D.L. King, Y. Wang. An Overview of Hydrogen Production Technologies. *Catal.Today* **2009**, 139 (4), 244–260.
2. A. Fujishima, K. Honda. Electrochemical Photolysis of Water at a Semiconductor Electrode. *Nature*. **1972**, 238 (5358), 37–38.
3. A.J. Bard. Photoelectrochemistry and Heterogeneous Photocatalysis at Semiconductors. *J. Photochem.* **1979**, 10, 59–75.
4. A. Kudo, Y. Miseki. Heterogeneous Photocatalyst Materials for Water Splitting. *Chem. Soc. Rev.* **2009**, 38(1), 253–278.
5. K. Maeda, K. Teramura, D. Lu, T. Takata, N. Saito, Y. Inoue, K. Domen. Photocatalyst Releasing Hydrogen from Water. *Nature* **2006**, 440(7082), 295.
6. T. Kawai, T. Sakata. Photocatalytic Hydrogen Production from Liquid Methanol and Water. *J. Chem. Soc. Chem. Commun.* **1980**, 694–695.

7. A. Mills, S.K. Lee. Platinum Group Metals and their Oxides in Semiconductor Photosensitisation. *Platinum Met. Rev.* **2003**, 47(1), 2–12.
8. N. Yamada, M. Suzumura, F. Koiwa, N. Negishi. Differences in Elimination Efficiencies of Escherichia coli in Freshwater and Seawater as a Result of TiO<sub>2</sub> Photocatalysis. *Water Res.* **2013**, 47(8), 2770–2776.
9. A. Kudo, A. Tanaka, K. Domen, K. Maruya, K. Aika and T. Onishi. Photocatalytic Decomposition of Water over NiO-K<sub>4</sub>NB<sub>6</sub>O<sub>17</sub> Catalyst. *J. Catal.* **1988**, 111(1), 67–76.
10. A. Galinska, J. Walendziewski. Photocatalytic Water Splitting over Pt-TiO<sub>2</sub> in the Presence of Sacrificial Reagents. *Energy Fuels* **2005**, 19(3), 1143–1147.
11. G.R. Bamwenda, S. Tsubota, T. Nakamura, M. Haruta. Photoassisted Hydrogen Production from a Water-ethanol Solution: A Comparison of Activities of Au-TiO<sub>2</sub> and Pt-TiO<sub>2</sub>. *J. Photochem. Photobiol. A: Chem.* **1995**, 89(2), 177–189.
12. E. Borgarello, N. Serpone, G. Emo, R. Harris, E. Pelizzetti, C. Minero. Light-induced Reduction of Rhodium (III) and Palladium (II) on Titanium Dioxide Dispersions and the Selective Photochemical Separation and Recovery of Gold (III), Platinum (IV), and Rhodium (III) in Chloride Media. *Inorg. Chem.* **1986**, 25, 4499–4503.
13. M.V. Daskalaki, D.I. Kondarides. Efficient Production of Hydrogen by Photo-induced Reforming of Glycerol at Ambient Conditions. *Catal. Today* **2009**, 144(1–2), 75–80.
14. P. D. Tran, L. Xi, S. K. Batabyal, L.H. Wong, J. Barber, J.S.C. Loo. Enhancing the Photocatalytic Efficiency of TiO<sub>2</sub> Nanopowders for H<sub>2</sub> Production by using Non-noble Transition Metal Co-catalysts. *Phys. Chem. Chem. Phys.* **2012**, 14(33), 11596–11599.
15. T. Kawai, T. Sakata. Conversion of Carbohydrate into Hydrogen Fuel by a Photocatalytic Process. *Nature* **1980**, 286, 474–476.
16. S. Bala, I. Mondal, A. Goswami, U. Pal, R. Mondal. Co-MOF as a Sacrificial Template: Manifesting a New Co<sub>3</sub>O<sub>4</sub>//TiO<sub>2</sub> System with a p–n Heterojunction for Photocatalytic Hydrogen Evolution. *J. Mater. Chem. A Mater. Energy Sustain.* **2015**, 3, 20288–20296.

17. Y. Qu, X. Duan. Progress, challenge and perspective of heterogeneous Photocatalysts. *Chem. Soc. Rev.* **2013**, 42(7), 2568–2580.
18. S.Y. Moon, B. Naik, K. An, S.M. Kim, J.Y. Park. Photocatalytic H<sub>2</sub> Generation on Macro-mesoporous Oxide-supported Pt Nanoparticles. *RSC Adv.* **2016**, 6, 18198–18203.
19. A.L. Linsebigler, G. Lu, J.T. Yates. Photocatalysis on TiO<sub>2</sub> Surfaces: Principles, Mechanisms, and Selected Results. *Chem. Rev.* **1995**, 95, 735–758.
20. E. Friehs, Y. AlSalka, R. Jonczyk, A. Lavrentieva, A. Jochums, V. Walter, F. Stahl, TC. Scheper, D. Bahnemann. Toxicity, Phototoxicity and Biocidal Activity of Nanoparticles Employed in Photocatalysis. *J. Photochem. Photobiol. C* **2016**, 29, 1–28.
21. H. Zhang, G. Chen, D.W. Bahnemann. Photoelectrocatalytic Materials for Environmental Applications. *J. Mater. Chem.* **2009**, 19(29), 5089–5121.
22. J. Schneider, M. Matsuoka, M. Takeuchi, J. Zhang, Y. Horiuchi, M. Anpo, D.W. Bahnemann. Understanding TiO<sub>2</sub> Photocatalysis: Mechanisms and Materials. *Chem. Rev.* **2014**, 114(19), 9919–9986.
23. V. Artero, M. Chavarot-Kerlidou, M. Fontecave. Splitting Water with Cobalt. *Angew. Chem. Int. Ed.* **2011**, 50(32), 7238–7266.
24. W.M. Singh, T. Baine, S. Kudo, S. Tian, X.A.N. Ma, H. Zhou, N.J. DeYonker, T.C. Pham, J.C. Bollinger, D.L. Baker, B. Yan, C.E. Webster, X. Zhao. Electrocatalytic and Photocatalytic Hydrogen Production in Aqueous Solution by a Molecular Cobalt Complex. *Angew. Chem. Int. Ed. Engl.* **2012**, 51(24), 5941–5944.
25. A. Rodenberg, M. Oraziotti, B. Probst, C. Bachmann, R. Alberto, K.K. Baldrige, P. Hamm. Mechanism of Photocatalytic Hydrogen Generation by a Polypyridyl-Based Cobalt Catalyst in Aqueous Solution. *Inorg. Chem.* **2015**, 54(2), 646–657.
26. W.R. McNamara, Z. Han, P.J. Alperin, W.W. Brennessel, P.L. Holland, R. Eisenberg. A Cobalt-dithiolene Complex for the Photocatalytic and Electrocatalytic Reduction of Protons. *J. Am. Chem. Soc.* **2011**, 133(39), 15368–15371.
27. S. Yusuf, F. Jiao. Effect of the Support on the Photocatalytic Water Oxidation Activity of Cobalt Oxide Nanoclusters. *ACS Catal.* **2012**, 2(12), 2753–2760.

28. M. Zhang, M. Respinis, H. Frei. Time-resolved Observations of Water Oxidation Intermediates on a Cobalt Oxide Nanoparticle Catalyst. *Nat. Chem.* **2014**, 6, 362–367.
29. Y. Wang, M. Hsieh, J. Lee, C. Yang. Nonaqueous Synthesis of CoO<sub>x</sub>/TiO<sub>2</sub> Nanocomposites Showing High Photocatalytic Activity of Hydrogen Generation. *Appl Catal B: Environ.* **2013**, 142–143, 626–632.
30. Z. Yan, H. Wu, A. Han, X. Yu, P. Du. Noble Metal-Free Cobalt Oxide (CoO<sub>x</sub>) Nanoparticles Loaded on Titanium Dioxide/Cadmium Sulfide Composite for Enhanced Photocatalytic Hydrogen Production from Water. *Int J. Hydrog. Energ.* **2014**, 39(25), 13353–13360.
31. L. Mahoney, R. Peng, C. Wu, J. Baltrusaitis, R.T. Koodali. Solar Simulated Hydrogen Evolution using Cobalt Oxide Nanoclusters Deposited on Titanium Dioxide Mesoporous Materials Prepared by Evaporation Induced Self-assembly Process. *Int J. Hydrog. Energ.* **2015**, 40(34), 10795–10806.
32. G. Sadanandam, K. Lalitha, V.D. Kumari, V.S. Muthukonda, M. Subrahmanyam. Cobalt Doped TiO<sub>2</sub>: A Stable and Efficient Photocatalyst for Continuous Hydrogen Production from Glycerol: Water Mixtures under Solar Light Irradiation. *Int J. Hydrog. Energ.* **2013**, 38(23), 9655–9664.
33. S. Yan, Q-D. Huang, Y-Z. Yuan, D-W. Liao. Photocatalytic Activity of Cobalt Doped Titania for H<sub>2</sub> Evolution. *Acta Phys.-Chim. Sin.* **2011**, 27(10), 2406–2410.
34. Y. Wu, G. Lu, S. J. Li. The Long-term Photocatalytic Stability of Co<sup>2+</sup> Modified P25-TiO<sub>2</sub> Powders for the H<sub>2</sub> Production from Aqueous Ethanol Solution. *Photochem. Photobiol. A: Chem.* **2006**, 181, 263–267.
35. W. Y. Choi, A. Termin, M. R. Hoffmann. The Role of Metal Ion Dopants in Quantum-Sized TiO<sub>2</sub>: Correlation between Photoreactivity and Charge Carrier Recombination Dynamics. *J. Phys. Chem.* **1994**, 98, 13669–13679.
36. J. Choi, H. Park, M.R. Hoffmann. Effects of Single Metal-ion Doping on the Visible-Light Photoreactivity of TiO<sub>2</sub>. *J. Phys. Chem. C* **2010**, 114(2), 783–792.

37. S. Akel, R. Boughaled, R. Dillert, M. El Azzouzi, D.W. Bahnemann. UV-vis Light Induced Degradation of Oxytetracycline Hydrochloride Mediated by Co - TiO<sub>2</sub> Nanoparticles. *Molecules* **2020**, 25(2), 249.
38. M. Nag, P. Basak, S.V. Manorama. Low-temperature Hydrothermal Synthesis of Phase-pure Rutile Titania Nanocrystals: Time Temperature Tuning of Morphology and Photocatalytic Activity. *Mater. Res. Bull.* **2007**, 42(9), 1691–1704.
39. A.L. Castro, M.R. Nunes, A.P. Carvalho, F.M. Costa, Florêncio, M.H. Synthesis of Anatase TiO<sub>2</sub> Nanoparticles with High Temperature Stability and Photocatalytic Activity. *Solid State Sci.* **2008**, 10(5), 602–606.
40. C. Zhao, X. Shu, D. Zhu, S. Wei, Y. Wang, M. Tu, W. Gao. High Visible Light Photocatalytic Property of Co<sup>2+</sup>-doped TiO<sub>2</sub> Nanoparticles with Mixed Phases. *Superlattices Microstruct.* **2015**, 88, 32–42.
41. J. Zou, C. Liu, K. Yu, D. Cheng, Y. Zhang, F. He, H. Du, L. Cui. Highly Efficient Pt/TiO<sub>2</sub> Photocatalyst Prepared by Plasma-enhanced Impregnation Method. *Chem. Phys. Lett.* **2004**, 400(4-6), 520–523.
42. J.F. Gomes, A. Lopes, K. Bednarczyk, M. Gmurek, M. Stelmachowski, A. Zaleska-Medynska, M.E. Quinta-Ferreira, R. Costa, R.M. Quinta-Ferreira, R.C. Martins. Effect of Noble Metals (Ag, Pd, Pt) Loading over the Efficiency of TiO<sub>2</sub> during Photocatalytic Ozonation on The Toxicity of Parabens. *ChemEngineering* **2018**, 2(1), 4.
43. I. Ganesh, A.K. Gupta, P.P. Kumar, P.S. Chandra Sekhar, K. Radha, G. Padmanabham, G. Sundararajan. Preparation and Characterization of Co-doped TiO<sub>2</sub> Materials for Solar Light Induced Current and Photocatalytic Applications. *Mater. Chem. Phys.* **2012**, 135(1), 220–234.
44. J. Yang, S. Cui, J. Qiao, H. Lian. The Photocatalytic Dehalogenation of Chlorophenols and Bromophenols by Cobalt Doped Nano TiO<sub>2</sub>. *J. Mol. Catal A: Chem.* **2014**, 395, 42–51.

45. L. Yu, Y. Shao, D. Li. Direct Combination of Hydrogen Evolution from Water and Methane Conversion in a Photocatalytic System over Pt/C. *Appl. Catal. B: Environ.* **2017**, 204, 216–223.
46. Slamet, Anny, Setiadi. Photocatalytic Hydrogen Generation from Glycerol and Water using Pt Loaded N-doped TiO<sub>2</sub> Nanotube. *Int. J. Eng.* **2011**, 11(3) 91–95.
47. M.S. Amer, M.A. Ghanem, P. Arunachalam, A.M. Al-Mayouf, S.M. Hadadi. Bifunctional Electrocatalyst of Low-symmetry Mesoporous Titanium Dioxide Modified with Cobalt Oxide for Oxygen Evolution and Reduction Reactions. *Catalysts* **2019**, 9(10), 836.
48. A. Ye. Yermakov, G.S. Zakharova, M. A. Uimin, M.V. Kuznetsov, L.S. Molochnikov, S.F. Konev, A.S. Konev, A.S. Minin, V. V. Mesilov, V.R. Galakhov, A.S. Volegov, A.V. Korolyov, A.F. Gubkin, A.M. Murzakayev, A.D. Svyazhin, K.V. Melanin. Surface Magnetism of Cobalt-doped Anatase TiO<sub>2</sub> Nanopowders. *J. Phys. Chem. C* **2016**, 120(50), 28857–28866.
49. S.H. Lim, C. Ferraris, M. Schreyer, K. Shih, J.O. Leckie, T.J. White. The Influence of Cobalt Doping on Photocatalytic Titania Crystal: Chemistry and Amorphicity. *J. Solid. State. Chem.* **2007**, 180(10), 2905–2915.
50. J. Venturini, F. Bonatto, W.C. Guaglianoni, T. Lemes, S. Arcaro, A.K. Alves, C.P. Bergmann. Cobalt-doped Titanium Oxide Nanotubes Grown via One-step Anodization for Water Splitting Applications. *Appl. Surf. Sci.* **2019**, 464, 351–359.
51. D. Dvoranova, V. Brezova, M. Mazur, M. Malati. Investigations of Metal-Doped Titanium Dioxide Photocatalysts. *Appl Catal B: Environ.* **2002**, 37(2), 91–105.
52. V. Brezová, A. Staško, L. Jr. Lapčík. Electron Paramagnetic Resonance Study of Photogenerated Radicals in Titanium Dioxide Powder and its Aqueous Suspensions. *J. Photochem. Photobiol. A: Chem.* **1991**, 59(1), 115–121.
53. L. Fan, J. Long, Q. Gu, H. Huang, H. Lin, X. Wang. Single-site Nickel-grafted Anatase TiO<sub>2</sub> for Hydrogen Production: Toward Understanding the Nature of Visible-light Photocatalysis. *J. Catal.* **2014**, 320, 147–159.

54. T. Petsi, G.D. Panagiotou, C.S. Garoufalis, C. Kordulis, P. Stathi, Y. Deligiannakis, A. Lycourghiotis, K. Bourikas. Interfacial Impregnation Chemistry in The Synthesis of Cobalt Catalysts Supported on Titania. *Chemistry* **2009**, 15(47), 13090–13104.
55. S. Dohshi, M. Anpo, S. Okuda, T. Kojima. Effect of  $\gamma$ -ray Irradiation on the Wettability of TiO<sub>2</sub> Single Crystals. *Top. Catal.* **2005**, 35(3-4), 327–330.
56. T. Berger, M. Sterrer, O. Diwald, E. Knözinger, D. Panayotov, T.L. Thompson, J.T. Yates. Light-induced Charge Separation in Anatase TiO<sub>2</sub> Particles. *J. Phys. Chem. B* **2005**, 109(13), 6061–6068.
57. Y. Nakaoka Y. Nosaka. ESR Investigation Into the Effects of Heat Treatment and Crystal Structure on Radicals Produced over Irradiated TiO<sub>2</sub> Powder. *J. Photochem. Photobiol. A.* **1997**, 110(3), 299–305.
58. K. Suriye, P. Praserttham, B. Jongsomjit. Effect of Surface Sites of TiO<sub>2</sub> Support on The Formation of Cobalt-support Compound in Co/TiO<sub>2</sub> Catalysts. *Catal. Commun.* **2007**, 8(11), 1772–1780.
59. P. Lommens, F. Loncke, P.F. Smet, F. Callens, D. Poelman, H. Vrielinck, Z. Hens. Dopant Incorporation in Colloidal Quantum Dots: A Case Study on Co<sup>2+</sup> Doped ZnO. *Chem. Mater.* **2007**, 19(23), 5576–5583.
60. Y. Yang, L.C. Kao, Y. Liu, K. Sun, H. Yu, J. Guo, S.Y.H. Liou, M.R. Hoffmann. Cobalt Doped Black TiO<sub>2</sub> Nanotube Array as a Stable Anode for Oxygen Evolution and Electrochemical Wastewater Treatment. *ACS Catal.* **2018**, 8(5), 4278–4287.
61. H.T. Langhammer, R. Böttcher, T. Müller, T. Walther, S.G. Ebbinghau. Defect Properties of Cobalt-doped Hexagonal Barium Titanate Ceramics. *J. Phys. Condens. Matter.* **2015**, 27(29), 295901–295912.
62. C. Huang, X. Liu, L. Kong, W. Lan, Q. Su, Y. Wang. The Structural and Magnetic Properties of Co-doped Titanate Nanotubes Synthesized under Hydrothermal Conditions. *Appl. Phys. A* **2007**, 87, 781–786.
63. K.J. Chao, S.P. Sheu, H.S. Sheu. Structure and Chemistry of Cobalt in CoAPO-5 Molecular Sieve. *J. Chem. Soci. Faraday Trans.* **1992**, 88, 2949–2954.

64. G. Mathies, R. M. Almeida, P. Gast, J.J.G. Moura, E.J.J. Groenen. Multifrequency EPR Study of Fe<sup>3+</sup> and Co<sup>2+</sup> in the Active Site of Desulforedoxin. *J. Phys. Chem. B* **2012**, 116(24), 7122–7128.
65. P. Xu, T.J. Milstein, T.E. Mallouk. Flat-band Potentials of Molecularly Thin Metal Oxide Nanosheets. *ACS Appl. Mater. Interfaces* **2016**, 8, 11539–11547.
66. M. Wang, J. Ioccozi, L. Sun, C. Lin, Z. Lin. Inorganic-modified Semiconductor TiO<sub>2</sub> Nanotube Arrays for Photocatalysis. *Environ. Sci.* **2014**, 7, 2182–2202.
67. D. Bahnemann, A. Henglein, J. Lilie, L. Spanhel. Flash Photolysis Observation of the Absorption Spectra of Trapped Positive Holes and Electrons in Colloidal TiO<sub>2</sub>. *J. Phys. Chem.* **1984**, 88, 709–711.
68. S. Hamid, R. Dillert, D.W. Bahnemann. Photocatalytic Reforming of Aqueous Acetic Acid into Molecular Hydrogen and Hydrocarbons over Co catalyst-loaded TiO<sub>2</sub>: Shifting the Product Distribution. *J. Phys. Chem. C* **2018**, 122(24), 12792–12809.
69. D.W. Hwang, H.G. Kim, J.S. Lee, J. Kim, W. Li, S.H. Oh. Photocatalytic Hydrogen Production from Water over M-doped La<sub>2</sub>Ti<sub>2</sub>O<sub>7</sub> (M) Cr, Fe) under Visible Light Irradiation ( $\lambda > 420$  nm). *J. Phys. Chem. B* **2005**, 109, 2093–2102.
70. P. Jiang, W. Xiang, J. Kuang, W. Liu, W. Cao. Effect of Cobalt Doping on the Electronic, Optical and Photocatalytic Properties of TiO<sub>2</sub>. *Solid State Sci.* **2015**, 46, 27–32.
71. G.L. Chiarello, M.H. Aguirre, E. Selli. Hydrogen Production by Photocatalytic Steam Reforming of Methanol on Noble Metal-modified TiO<sub>2</sub>. *J. Catal.* **2010**, 273(2), 182–190.
72. F. Alcaide, R.V. Genova, G. Alvarez, H. Grande, O. Miguel, P.L. Cabot. Platinum-catalyzed Nb -doped TiO<sub>2</sub> and Nb-doped TiO<sub>2</sub> Nanotubes for Hydrogen Generation in Proton Exchange Membrane Water Electrolyzers. *Int. J. Hydrog. Energy* **2020**, 45(40), 20605–20619.
73. M.Z. Selcuk, M.S. Boroglu, I. Boz. Hydrogen Production by Photocatalytic Water-Splitting using Nitrogen and Metal Co-doped TiO<sub>2</sub> Powder Photocatalyst. *React. Kinet. Mech. Catal.* **2012**, 106(2), 313–324.



## Chapter 5. Summarizing Discussion and Conclusions

This chapter provides a general overview of all experimental results of this doctoral study and affords a detailed discussion concerning the acquired observations.

At first, a summary of the different synthetic methods used within this study and the characterization analysis performed on (i) seven differently prepared photocatalysts of silver/silver oxide modified titanium dioxide ( $\text{Ag}/\text{Ag}_2\text{O} // \text{TiO}_2$ ) with different silver/silver oxide mass ratio, (ii) cobalt doped titanium dioxide photocatalysts ( $\text{Co-TiO}_2$ ), and (iii) platinum loaded on cobalt doped titanium dioxide ( $\text{Pt}/\text{Co-TiO}_2$ ) composites will be presented.

Subsequently, the photocatalytic activity of the  $\text{Ag}/\text{Ag}_2\text{O} // \text{TiO}_2$  photocatalysts assessed by the bleaching of methylene blue (MB) under UV-vis and vis-light illumination will be discussed. Hereby, the effect of the selected synthetic method, as well as of the  $\text{Ag}/\text{Ag}_2\text{O}$  mass ratio on the photocatalytic activity and the stability of  $\text{Ag}/\text{Ag}_2\text{O} // \text{TiO}_2$  samples, will be evaluated. Finally, the photocatalytic degradation of another pharmaceutical, i.e., oxytetracycline hydrochloride (OTC HCl), under UV-vis irradiation in the presence of  $\text{Co-TiO}_2$  photocatalysts has also been examined and will be discussed here.

As a second light-induced reaction, the evolution of molecular hydrogen from aqueous methanol in the presence of  $\text{Ag}/\text{Ag}_2\text{O}$ ,  $\text{Ag}/\text{Ag}_2\text{O} // \text{TiO}_2$  composites and mixtures,  $\text{Co-TiO}_2$ , and  $\text{Pt}/\text{Co-TiO}_2$  photocatalysts under simulated solar light irradiation will be discussed.

Based on the experimental results, a possible mechanistic explanation for the overall activities of all prepared materials will be proposed.

### 5.1. Synthesis and Characterization of Photocatalysts

#### 5.1.1. $\text{Ag}/\text{Ag}_2\text{O} // \text{TiO}_2$

As mentioned in **Chapter 1**,  $\text{TiO}_2$  can only harvest UV light, which constitutes only roughly 5% of the solar light reaching the earth's surface [1]. Furthermore, the fast recombination of photogenerated electron-hole pairs impedes its photocatalytic

applications [2]. Thus, the development of new photocatalytic materials with strong UV-vis-light absorbance ability and which can effectively suppress the undesired charge carrier recombination is one of the most promising strategies in photocatalysis that has attracted wide attention.

Silver/silver oxide (Ag/Ag<sub>2</sub>O) based photocatalysts constitute a very promising system amongst various types of semiconductors because of their surface plasmon resonance properties which can significantly improve the visible light photo-response and provide new opportunities to develop visible light driven photocatalysts [3]. More importantly, Ag/Ag<sub>2</sub>O based systems are very suitable for industrial applications because of their obviously simple preparation. They are inexpensive and have been shown to offer high photocatalytic efficiency. Ag<sub>2</sub>O is a p-type semiconductor with a reported band gap of  $\sim 1.2 - 1.46$  eV [3, 4] which has been widely employed as a photocatalyst in single, binary, or multiple composite systems [3, 5–8]. Upon UV illumination, Ag<sub>2</sub>O NPs were found to behave as effective electron accepting agents, while under visible light illumination they act as efficient photosensitizers [3, 5, 9, 10]. Nevertheless, the photosensitive and unstable properties of Ag<sub>2</sub>O ( $\text{Ag}_2\text{O} \rightarrow 2\text{Ag} + \frac{1}{2}\text{O}_2$ ) is the critical issue associated with its photocatalytic application.

A variety of synthetic approaches have been employed to synthesize Ag/Ag<sub>2</sub>O deposited titania materials with different morphologies and for various photocatalytic applications. Widely used methods include microwave-assisted procedures [8,11], a one-step solution reduction process in the presence of potassium borohydride [20], a simple mixing [12], a mechanical grinding [13], solvothermal methods [14, 15], a sol-gel technique [16], and simple pH-mediated precipitation [17].

In the present investigation, as described in detail in **Chapter 2**, self-prepared Ag/Ag<sub>2</sub>O, physical mixtures of Ag/Ag<sub>2</sub>O//TiO<sub>2</sub> (TM), and in situ prepared Ag/Ag<sub>2</sub>O//TiO<sub>2</sub> composites (TC) have been prepared. Ag/Ag<sub>2</sub>O is prepared by dissolving AgNO<sub>3</sub> in 50 mL distilled water, the solution is stirred for 30 min then 50 mL of 0.2 M NaOH is added dropwise and the mixture is stirred in the dark for another 30 min. The obtained suspension is centrifuged washed with distilled water and dried at 70 °C for 24 h. The

physical mixtures are synthesized by mixing the self-prepared Ag/Ag<sub>2</sub>O with TiO<sub>2</sub> at a mass ratio of 4:1 (20 mass% TiO<sub>2</sub>), 1:1 (50 mass% TiO<sub>2</sub>), and 1:4 (80 mass% TiO<sub>2</sub>) in an aqueous solution. The suspensions are sonicated for 1.5 h and dried at 70 °C for 24 h, and denoted as TM 41, TM 11, and TM 14, respectively. The in situ prepared Ag/Ag<sub>2</sub>O//TiO<sub>2</sub> composites are prepared by a published precipitation method [18, 19]. In brief, TiO<sub>2</sub> is suspended in distilled water. After that, a calculated amount of AgNO<sub>3</sub> corresponding to the desired mass ratio of Ag/Ag<sub>2</sub>O is added to the solution and stirred for 30 min. A volume of 50 mL of 0.2 M NaOH is added dropwise to the suspension and stirred for 30 min, then centrifuged, washed with distilled water, and dried at 70°C for 24 h. The resulting composites with a mass ratio of 4:1 (20 mass% TiO<sub>2</sub>), 1:1 (50 mass% TiO<sub>2</sub>), and 1:4 (80 mass% TiO<sub>2</sub>) are nominated as TC 41, TC 11, and TC 14, respectively.

The results of the characterization of the freshly synthesized Ag/Ag<sub>2</sub>O, Ag/Ag<sub>2</sub>O//TiO<sub>2</sub> mixtures, and Ag/Ag<sub>2</sub>O//TiO<sub>2</sub> composites by means of XRD are presented in **Chapter 2, Figure 2-1**. The results revealed the coexistence of Ag<sub>2</sub>O and Ag(0) in all synthesized samples except the TiO<sub>2</sub>-rich composites, i.e., TC 11 and TC 14, suggesting a complete reduction of Ag<sub>2</sub>O to Ag(0). This indicates that the small fraction of Ag<sub>2</sub>O present in these composites has thermally decomposed to Ag(0) during the drying process. A similar observation was reported by Hu *et al.* confirming that only at an air-drying temperature in the range between 70 °C and 100 °C, Ag<sub>2</sub>O starts to decompose to Ag(0) whereas pure Ag<sub>2</sub>O can only be obtained employing a vacuum freeze-drying process [20].

The electron binding energies of Ag 3d of all prepared photocatalysts using XPS analysis are presented in **Chapter 2, Figure S2-3**. The XPS results are consistent with those obtained from the XRD measurements of freshly prepared samples endorsing the presence of silver in the +1 oxidation state (Ag 3d<sub>5/2</sub> and Ag 3d<sub>3/2</sub>, at 367.5 and 373.5 eV, respectively) along with the silver in the Ag(0) state (Ag 3d<sub>5/2</sub> and Ag 3d<sub>3/2</sub>, at 368.3 and 374.3 eV, respectively). These results are in good agreement with those reported in the scientific literature [21–24].

In the current study, Ag/Ag<sub>2</sub>O exhibits a band gap energy of < 1.5 eV which agrees with the values reported in the literature (1.2 [4], 1.46 [25], and 1.3 ± 0.3 eV [26]). The scattering of the reported values may be due to different particle diameters as exhibited for TiO<sub>2</sub> [27]. To get a better understanding of the photogenerated charge carrier transfer within the Ag/Ag<sub>2</sub>O // TiO<sub>2</sub> materials, the flatbands potential are determined using Mott-Schottky plots yielding values of – 0.4 V and + 0.3 V vs. NHE at pH 7 for TiO<sub>2</sub> and Ag<sub>2</sub>O, respectively. The flatband potential of Ag<sub>2</sub>O measured here is in accordance with previous determinations of + 0.23 and + 0.37 V [28, 29]. The energetic positions of the VB of TiO<sub>2</sub> and Ag<sub>2</sub>O are then calculated by adding the band gap energy (E<sub>g</sub>) of each composite to its flatband potential (E<sub>fb</sub>) according to:

$$E_{CB} = E_{fb}$$

$$E_{VB} = E_{fb} + E_g$$

As mentioned in **Chapter 1**, Ag<sub>2</sub>O/TiO<sub>2</sub> materials belong to the straddling gap (type I) semiconductor heterojunction. In this type of heterojunction and as shown in **Figure 5-1**, the CB of TiO<sub>2</sub> is higher than the CB of Ag<sub>2</sub>O and the VB of TiO<sub>2</sub> is lower than the VB of Ag<sub>2</sub>O. Thus, under UV irradiation, the photogenerated electrons of TiO<sub>2</sub> can migrate to the CB of Ag<sub>2</sub>O which acts as an absorbing material under UV light irradiation or can reduce the O<sub>2</sub> adsorbed on its surface, since E(O<sub>2</sub>/O<sub>2</sub><sup>•-</sup>) = – 0.33 V vs. NHE [30] is more positive than the energetic position of the conduction band of TiO<sub>2</sub> (– 0.4 V vs. NHE at pH 7). Besides, the TiO<sub>2</sub> VB holes are either transferred to the VB of Ag<sub>2</sub>O or they are forming •OH through water oxidation, as the energetic position of the valence band of TiO<sub>2</sub> is more positive than E(H<sub>2</sub>O/•OH) = 2.8 V vs. NHE at pH 0. Upon vis-light irradiation, only Ag<sub>2</sub>O is active for the degradation of organic pollutants and in most cases, Ag(0) is formed and contributes to the increased lifetime and mobility of the charge carriers retarding their recombination.

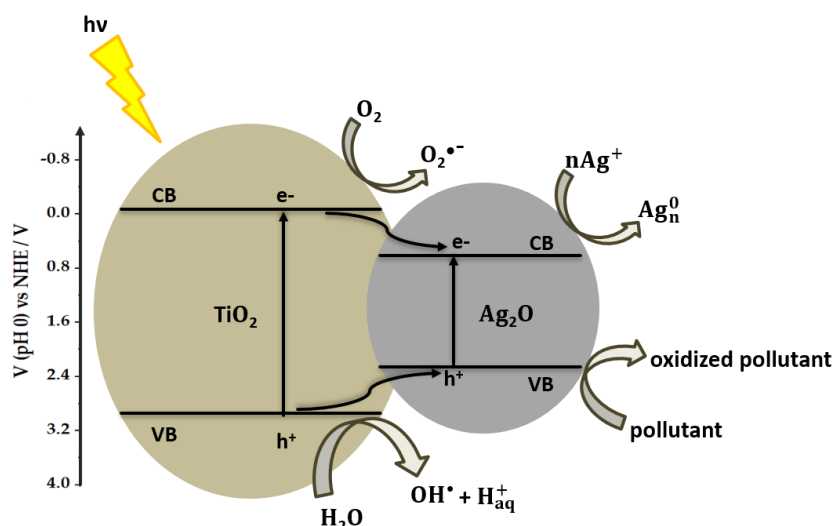


**Figure 5-1.** Electrochemical potentials (vs. NHE) of the valence and conduction bands of  $\text{TiO}_2$  and  $\text{Ag}_2\text{O}$ .

### 5.1.2. Co-doped $\text{TiO}_2$

In the scientific literature, Co- $\text{TiO}_2$  photocatalysts have been synthesized with different preparation approaches, such as the sol/gel technique [31–41], hydrothermal treatment [42–45], impregnation method [46,47], and precipitation process [48]. Herein, as described in detail in **Chapter 3**, 0.5 wt.% Co- $\text{TiO}_2$  photocatalysts have been prepared through two different synthetic processes, namely, a reflux synthesis (R) and a hydrothermal method (HT). Pure  $\text{TiO}_2$  powders have been also prepared using the same procedures without adding the cobalt precursor. The preparation methods are illustrated in **Figure 5-2**.

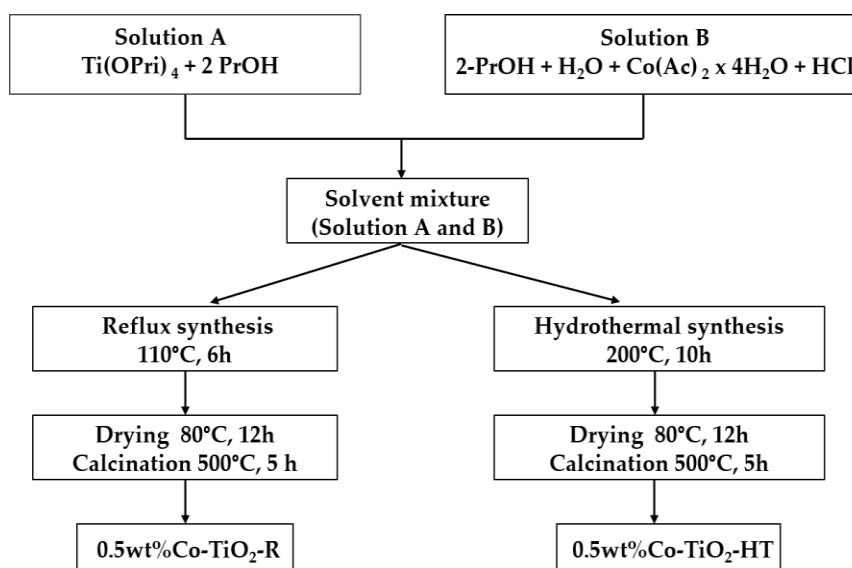


**Figure 5-2.** Flow chart of preparation of 0.5 wt.% Co- $\text{TiO}_2$  by hydrothermal and reflux synthesis.

After the synthesis, a primary characterization of Co-TiO<sub>2</sub>-HT, Co-TiO<sub>2</sub>-R, TiO<sub>2</sub>-HT, and TiO<sub>2</sub>-R has been carried out using XRD, Raman, TEM, BET, and UV-vis spectroscopy and presented in **Chapter 3**. **Table 5-1** summarize the physico-chemical properties of the prepared materials.

**Table 5-1.** Properties of the synthesized TiO<sub>2</sub>-R, Co-TiO<sub>2</sub>-R, TiO<sub>2</sub>-HT, and Co-TiO<sub>2</sub>-HT composites.

Catalysts	XRD Size (nm)	TEM Size (nm)	SSA (m <sup>2</sup> g <sup>-1</sup> )	Band Gap (eV)
TiO <sub>2</sub> -R	9.5	9.8 ± 0.2	160 ± 5	3.06
Co-TiO <sub>2</sub> -R	9.2	9.5 ± 0.2	153 ± 5	2.93
TiO <sub>2</sub> -HT	9.9	10.5 ± 0.2	109 ± 5	3.10
Co-TiO <sub>2</sub> -HT	8.4	9.7 ± 0.2	126 ± 5	3.03
P25	21	20.0 ± 0.2	50 ± 5	3.06

The average particle sizes of the as-synthesized NPs are estimated by the Debye–Scherrer formula and from the TEM images shown in **Chapter 3**, **Figure 3-2**. The Co-TiO<sub>2</sub> NPs are found to have a particle size between 8.4 ± 0.2 and 9.8 ± 0.2 indicating that the particle size is not excessively changed by the different synthetic approaches. In the literature, Co-TiO<sub>2</sub> prepared by hydrothermal treatment show a grain size that ranges between 8.4 and 10.5 nm [49], which is in accordance with the values found in this study. However, the particle sizes of Co-TiO<sub>2</sub> prepared with different methods are found to have a size range between 8.4 and 29 nm [50, 51, 52]. According to the XRD results presented in **Chapter 3**, **Figure 3-1 (a)**, the anatase phase of TiO<sub>2</sub> dominated in all samples with some brookite impurities observed at 2θ = 30.83°. XRD patterns of TiO<sub>2</sub>-HT sample showed a small contamination of rutile phase. The anatase to rutile phase transformation can lead to the assumption that the Co ions are in some way stabilizing the anatase crystalline structure of titania, which was previously observed with Co-TiO<sub>2</sub> prepared via a sol-gel route [24]. According to Nag *et al.*, anatase to rutile transformation in titania occurs above 450 °C [53]. Evidence for brookite formation has been previously reported and was attributed to the acidic milieu of the Co-TiO<sub>2</sub> synthesis [54]. In another investigation, it has been proven that

the synthesis in ammonia limits the brookite phase formation [55]. Moreover, Zhao *et al.* demonstrated the presence of three titania polymorphs in Co-doped TiO<sub>2</sub> prepared with combined sol-gel and hydrothermal methods [54]. The XRD patterns of the Co-TiO<sub>2</sub> did not show any peaks of Co clusters or metal oxides, indicating that most of the Co ions are substituted into the Ti lattice site. This cobalt substitution has been also reported elsewhere [50]. The results of Raman spectroscopy presented in **Chapter 3, Figure 3-1 (b)** are found to be consistent with the above results of XRD and are in good agreement with those reported for anatase and brookite phases of titania [56].

In comparison with bare TiO<sub>2</sub>, Co-TiO<sub>2</sub> samples reveal absorption edge shifting toward higher wavelengths as depicted in **Figure 5-3 (a)**. Two additional regions are observed in the visible range and assigned to the <sup>4</sup>T<sub>1g</sub>-to-<sup>4</sup>T<sub>1g</sub> (P) transition and the <sup>4</sup>T<sub>1g</sub>-to-<sup>4</sup>A<sub>2g</sub> transition of high spin Co<sup>2+</sup> (3d<sup>7</sup>) substituted to the TiO<sub>2</sub> lattice. These types of d-d electronic transition are shown by Co<sup>2+</sup> when it substitutes Ti<sup>4+</sup> resulting in the splitting of d-orbital of Co<sup>2+</sup>. This observation has been previously reported in the scientific literature [49, 57, 58]. The corresponding band gaps of all composites using the Tauc plot method are estimated to be equal to 3.06, 3.10, 2.93, 3.03 eV for TiO<sub>2</sub>-R, TiO<sub>2</sub>-HT, Co-TiO<sub>2</sub>-R, and TiO<sub>2</sub>-HT, respectively as shown in **Figure 5-3 (b)**. This energy band gap narrowing of Co-TiO<sub>2</sub> has been also observed previously and explained by the introduction of new energy states above the TiO<sub>2</sub> valence band edge [39,40,49].

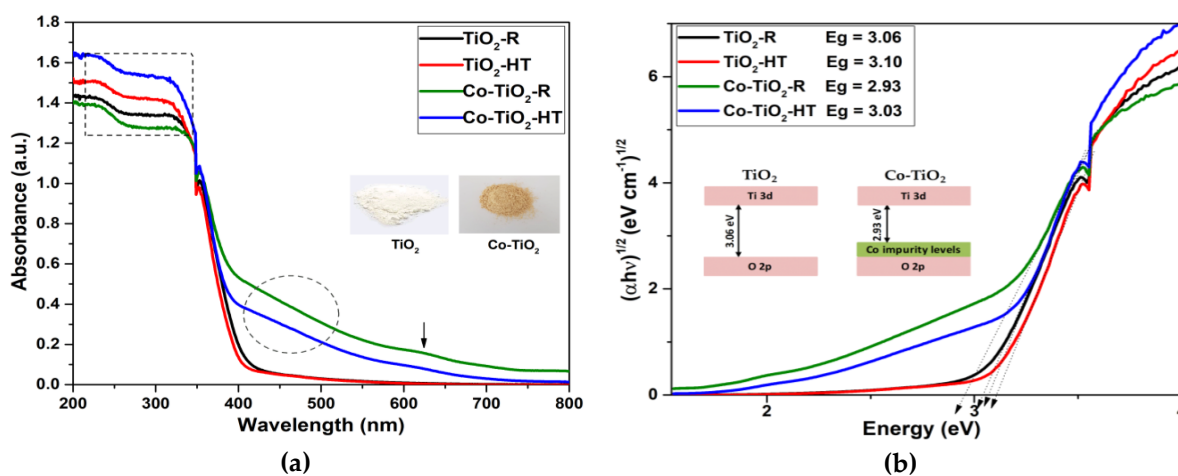


**Figure 5-3.** (a) UV-vis DRS and (b) the corresponding band gap energies of TiO<sub>2</sub>-R, Co-TiO<sub>2</sub>-R, TiO<sub>2</sub>-HT, and Co-TiO<sub>2</sub>-HT NPs. This figure is a reprint of Figure 3-3 in Chapter 3 (page 90).

Electrochemical measurements in the presence of Co-TiO<sub>2</sub> and plain TiO<sub>2</sub> are performed. Therefore, the energetic positions of the conduction bands of Co-TiO<sub>2</sub> and TiO<sub>2</sub> are calculated (within the limit of the experimental error) assuming that the flatband potential ( $E_{fb}$ ) of each composite is equal to the potential of its conduction band ( $E_{CB} = E_{fb}$ ) so that the valence band energy ( $E_{VB} = E_{fb} + E_g$ ) can be estimated by adding the band gap energy ( $E_g$ ) to the flatband potential of the composites.

Accordingly, the valence band energies of TiO<sub>2</sub>-R and TiO<sub>2</sub>-HT at pH 7 are calculated to be 2.65 and 2.68 eV (vs. NHE), respectively. Owing to the additional intermediate energy states, the valence band energies determined for Co-TiO<sub>2</sub>-R and Co-TiO<sub>2</sub>-HT are 2.48 and 2.59 eV, respectively (**Figure 5-4**).

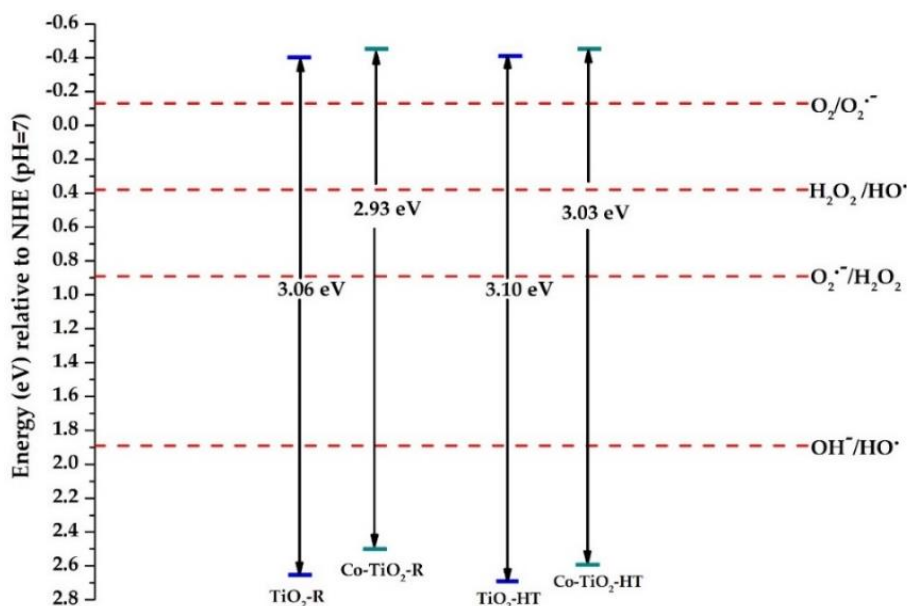


**Figure 5-4.** Energetic positions of the valence and the conduction band of Co-TiO<sub>2</sub> and TiO<sub>2</sub> composites at pH 7. This figure is a reprint of Figure 4-7 from in Chapter 4 (page 135).

### 5.1.3. Pt/Co-doped TiO<sub>2</sub>

As mentioned in **Chapter 1**, higher photocatalytic hydrogen evolution activities were observed when noble metals such as Pt were used as co-catalysts in TiO<sub>2</sub> photocatalysis [59-61]. For this purpose, the previously prepared Co-TiO<sub>2</sub>-HT, Co-TiO<sub>2</sub>-R, TiO<sub>2</sub>-HT, and TiO<sub>2</sub>-R composites are loaded with 1 wt.% Pt. The Pt deposition is performed by a simple photoplatinization method and described in **Chapter 4**. The



synthesized photocatalysts are denoted as Pt/ Co-TiO<sub>2</sub>-HT, Pt/ Co-TiO<sub>2</sub>-R, Pt/TiO<sub>2</sub>-HT, and Pt/TiO<sub>2</sub>-R. For comparison, titanium dioxide Evonik P25 and Hombikat UV100 are also modified with 1 wt.% Pt using the same method. The synthesis principle is illustrated in **Figure 5-5**.

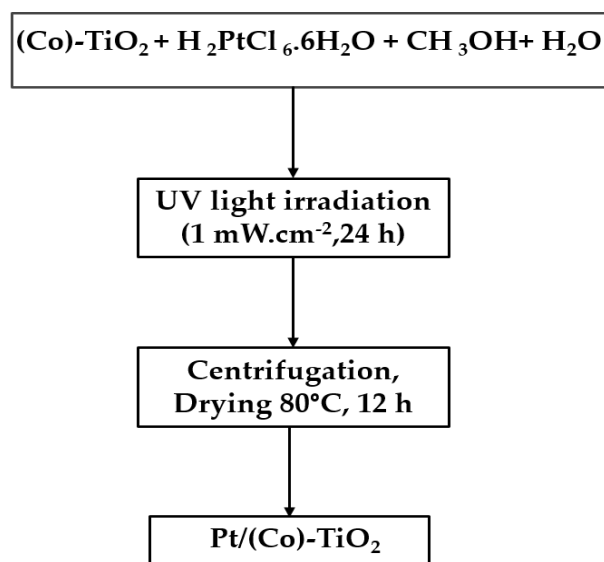


**Figure 5-5.** Typical procedure of Pt/Co-TiO<sub>2</sub> and Pt/TiO<sub>2</sub> preparation by photoplatinization method.

Characterization of the prepared Pt/ Co - TiO<sub>2</sub> photocatalysts through XRD shown in **Chapter 4, Figure 4-1**, revealed the presence of a very small characteristic Pt diffraction at around  $2\theta = 39.6^\circ$ , which corresponds to Pt (111) [62]. Other characteristic peaks of Pt are not detected, reasonably because of the low amount of loading (1 wt.%). In a study conducted by Chen *et al.*, no diffraction peaks were observed for Pt in the diffraction patterns of the 2 wt.% Pt deposited TiO<sub>2</sub>, which was due to the small Pt NPs sizes and the low nominal metal loadings [63]. In another study, Wang *et al.*, have interpreted the absence of Pt signals in the XRD spectra by the well-dispersion of Pt particles in TiO<sub>2</sub> [64]. As reported by Yu *et al.*, increasing the Pt proportion from 0.1% until 2% resulted in the appearance of a weak peak at  $39.8^\circ$  [65]. TEM/HRTEM images presented in **Chapter 4, Figure 4-2** clearly confirm the presence of spherical Pt NPs on the surface of Co-TiO<sub>2</sub> and TiO<sub>2</sub> support by the lattice fringe of 0.24 nm which is indexed as the (111) crystal plane of Pt [66].

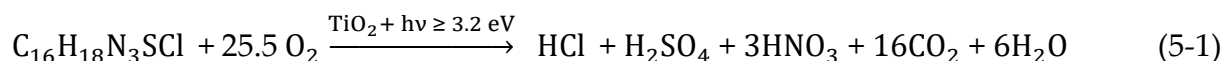
The comparison between the optical response of bare TiO<sub>2</sub> with Pt-loaded TiO<sub>2</sub> and of Co-TiO<sub>2</sub> with Pt-loaded Co-TiO<sub>2</sub> shown in **Chapter 3, Figure 3-3**, and in **Chapter 4, Figure 4-3**, leads to the conclusion that Pt loading did not affect significantly the optical absorption of the TiO<sub>2</sub>. However, for Co-TiO<sub>2</sub> materials, the absorption in the visible range which was due to the Co-doping is not any longer observed when Pt islands are deposited on the surface. This result suggests that the surface of the Co-TiO<sub>2</sub> catalysts is totally covered by the Pt NPs.

## 5.2. Photocatalytic Oxidation of Organic Compounds

### 5.2.1. Methylene Blue Bleaching in the Presence of Ag/Ag<sub>2</sub>O // TiO<sub>2</sub>

In the present study, methylene blue (C<sub>16</sub>H<sub>18</sub>ClN<sub>3</sub>S) has been chosen as a model compound to study the photocatalytic performance of the Ag / Ag<sub>2</sub>O // TiO<sub>2</sub> photocatalysts. Among the published standards from ISO/TC206 in the area of water purification, methylene blue degradation was introduced as a reference method namely, the "ISO 10678; 2010, Fine ceramics (advanced ceramics, advanced technical ceramics)-Determination of photocatalytic activity of surfaces in an aqueous medium by degradation of methylene blue" [67]. Therefore, MB was extensively used as a model contaminant for photocatalytic studies [68–71]. In the scientific literature, several papers have been published reporting the photocatalytic activity of Ag<sub>2</sub>O/semiconductors, and Ag/Ag<sub>2</sub>O/semiconductor composites for photocatalytic degradation of MB [72, 73].

According to Mills [74], the complete mineralization of MB by a semiconductor photocatalyst can be achieved by the following **Equation 5-1**:



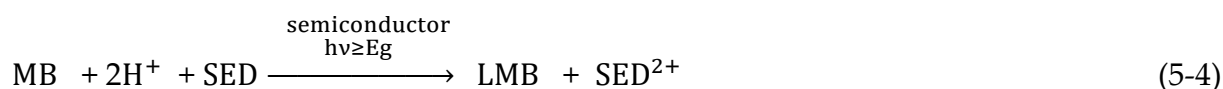
In this reaction, it is assumed that the photogenerated electron on the semiconductor photocatalyst is scavenged by dissolved oxygen, i.e. (**Equation 5-2**):



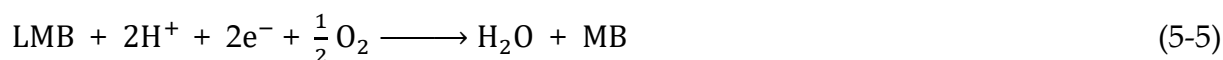
And the photogenerated hole oxidizes the dye molecule (either directly or indirectly) to eventually produce permanently bleached products, i.e. (**Equation 5-3**):



However, it is worth to mention that using an organic dye such as MB may often not be an appropriate choice for the assessment of the photocatalytic activity of a photocatalyst, since MB undergo a photocatalytic reduction reaction leading to its photobleaching as discussed in detail by Mills *et al.* [75]. Under anaerobic conditions, and in the presence of a sacrificial electron acceptor (SED), MB will be reduced to leuco-methylene blue (LMB), a colorless, reduced form of MB upon irradiation in the presence of a semiconductor following **Equation 5-4**:



However, LMB is known to be oxidized back to MB very rapidly by oxygen, i.e. **Equation 5-5**:



Both reactions (5-1) and (5-4) appears to give the same superficial result, which is bleaching of the MB dye over ultra-band gap irradiation of a semiconductor, the difference being that in reaction (5-4) the process is reversible, but in reaction (5-1) it is irreversible. Thus, the initial observed photobleaching of MB is not necessarily due to its oxidation. This misidentification between the two systems happens especially when the reaction conditions favor the LMB formation such as a low, easily depleted dissolved oxygen level and a low pH [75].

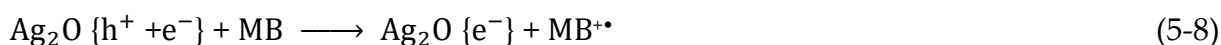
Furthermore, upon visible light irradiation, MB itself acts as a photosensitive material that a dye photosensitized process can also occur. in which the electronically excited state of the dye,  $\text{MB}^*$ , injects an electron into the conduction band of the semiconductor to produce an oxidized dye radical,  $\text{MB}^{*\bullet}$ , which is unstable and easily

reduced back to MB in acidic milieu [76], and able to decompose in slightly alkaline (pH = 9.1) solution to form bleached products [77], i.e. (**Equation 5-6**):



Hence, the similarity of the MB absorption spectra under visible light and the subsequent reactions of the excited MB molecule is usually misinterpreted as a visible-light activity of the scrutinized semiconductor [78].

In the current study, photocatalytic experiments for MB bleaching in the presence of Ag/Ag<sub>2</sub>O, Ag/Ag<sub>2</sub>O//TiO<sub>2</sub> mixtures, and Ag/Ag<sub>2</sub>O//TiO<sub>2</sub> composites under UV-vis and vis illumination are carried out. Under both illumination conditions, and in the presence only of Ag/Ag<sub>2</sub>O, it is observed that the MB conversion is attained rapidly (**Chapter 2, Figure 2-4**). As shown in **Figure 5-6**, in the presence of Ag/Ag<sub>2</sub>O, the bleaching of MB cannot occur between photocatalytically generated reactive oxygen species such as  $\cdot\text{OH}$  or  $\text{O}_2^{\bullet-}$  and the probe compound, since the energetic position of the CB of Ag<sub>2</sub>O is less negative than  $E(\text{O}_2/\text{O}_2^{\bullet-}) = -0.33 \text{ V vs. NHE}$  [30] and the energetic position of its VB is less positive than  $E(\text{H}_2\text{O}/\cdot\text{OH}) = 2.8 \text{ V vs. NHE}$ . However, the standard reduction potential for  $\text{MB}^{\bullet+}/\text{MB}$  (1.08 V vs. NHE [75]) is located within the bandgap of Ag<sub>2</sub>O indicating that the light-induced valence band holes can oxidize the adsorbed MB molecule (**Equations (5-7) and (5-8)**).



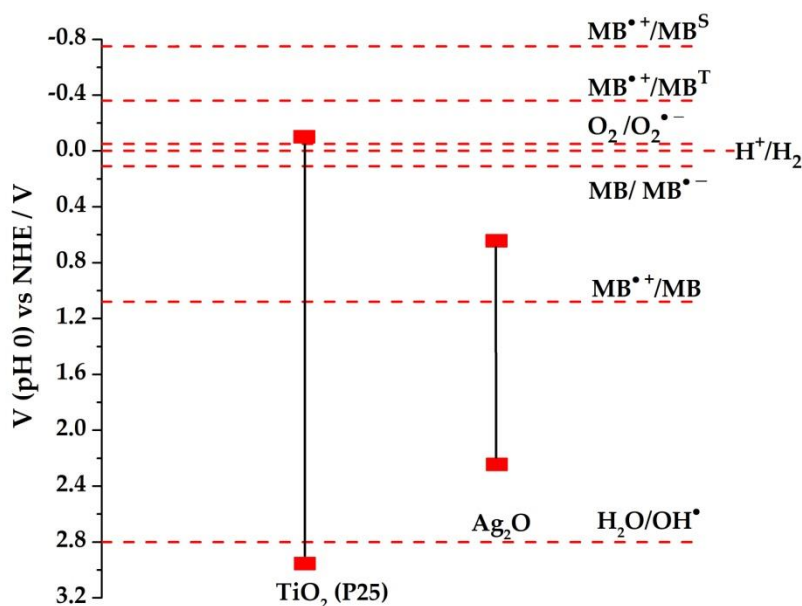


**Figure 5-6.** The electrochemical potentials (vs. NHE) of the valence and conduction bands of  $\text{TiO}_2$  and  $\text{Ag}_2\text{O}$ , and the reduction potentials of some species (possibly) present in the surrounding electrolyte. This figure is a reprint of Figure 2-6 in Chapter 2 (page 52).

Alternatively, MB bleaching in the presence of  $\text{Ag}/\text{Ag}_2\text{O}$  can be explained as well by the excitation of MB by a suitable wavelength resulting in the formation of its singlet excited state ( $\text{MB}^{\text{S}}$ ). This state has a short lifetime (nanoseconds) and a fraction of these  $\text{MB}^{\text{S}}$  molecules can undergo an intersystem crossing process forming the relatively long-lived triplet excited state ( $\text{MB}^{\text{T}}$ ) (**Equation (5-9)**,  $\text{MB}^* = \text{MB}^{\text{S}}$  and/or  $\text{MB}^{\text{T}}$ ) [75]. Due to the adsorption of the excited MB molecules on the surface of the  $\text{Ag}/\text{Ag}_2\text{O}$ , an interfacial electron transfer is occurring between the  $\text{MB}^*$  and  $\text{Ag}_2\text{O}$  (**Equation (5-10)**). Thus, this electron injection into the conduction band of  $\text{Ag}_2\text{O}$  can be considered similar to a dye-sensitized process, which has been previously reported [75, 78].



Both mechanisms necessitate an electron transfer between  $\text{Ag}_2\text{O}$  and MB. Even with the low surface area available for this reaction (*cf.* **Chapter 2, Table 2-1**), the electron transfer between the solid and the dye molecule seems to be very efficient.

According to Takizawa *et al.* [79], and taking into consideration the relative positions of the redox potentials  $E(O_2/O_2^{\bullet-}) = -0.33$  V,  $E(MB^{+\bullet}/MB^S) = -0.75$  V, and  $E(MB^{+\bullet}/MB^T) = -0.36$  V vs. NHE, the one-electron oxidation of  $MB^*$  by  $O_2$  might be possible (**Equation (5-11)**). However, the backward electron transfer yielding MB has to be considered since the relative positions of the redox potentials of the two radicals are close to each other's (**Equation (5-12)**).



As beforementioned,  $Ag_2O$  is very sensitive to light and undergoes decomposition under illumination to  $Ag(0)$ . Nevertheless, it has been claimed that  $Ag(0)$  formed in  $Ag/Ag_2O$  behaves as an electron scavenger for the conduction band electron of  $Ag_2O$ , hence preventing the reduction of  $Ag^+$  and stabilizing  $Ag_2O$  [3, 80, 81–83]. However, the possible reduction of  $Ag^+$  might happen during the processes given in the **Equations (5-7) - (5-10)**, yielding  $Ag(0)$ , since no other suitable electron acceptor is available.

In this context, Wang and co-worker have studied the photoreduction of  $Ag^+$  and the stability of  $Ag_2O$  under visible light irradiation. They have ascribed the high stability of  $Ag_2O$  NPs to the  $Ag-Ag_2O$  structure formed during the photodegradation process of organic substances [3]. This was clarified by the partial in-situ reduction of  $Ag^+$  on the  $Ag_2O$  by photogenerated electrons forming metallic Ag in the first cycle of photocatalytic runs as depicted in **Figure 5-5 (a)**. After a certain amount of  $Ag(0)$  was formed on the  $Ag_2O$  surface, the ensuing photogenerated electrons are transferred through  $Ag(0)$  which acts as an electron pool to  $O_2$  as schematically shown in **Figure 5-7. (b)**.

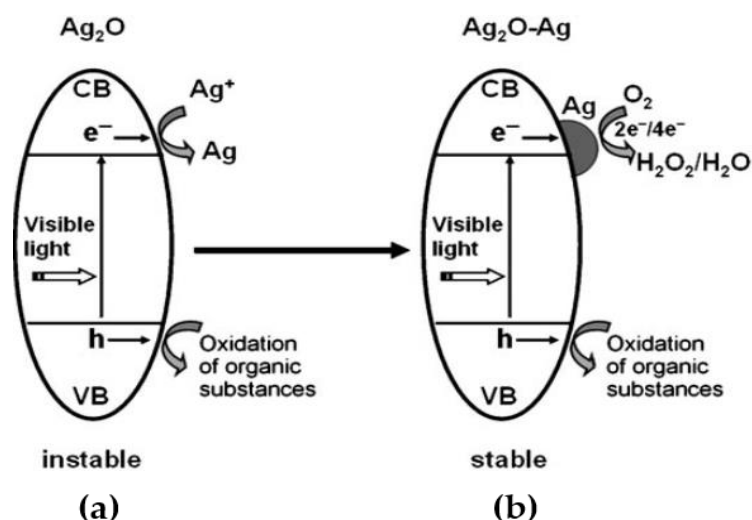
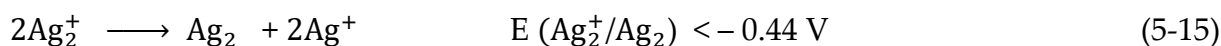
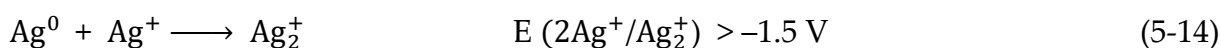
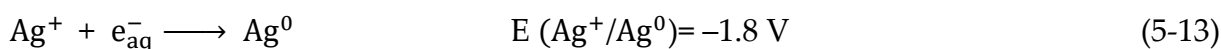


**Figure 5-7.** Self-stabilizing process of  $\text{Ag}_2\text{O}$  photocatalyst under visible light irradiation; **(a)** photogenerated electrons are captured by  $\text{Ag}^+$  on the as-prepared  $\text{Ag}_2\text{O}$ , and **(b)** photogenerated electrons are captured by  $\text{O}_2$  through  $\text{Ag}(0)$  formed during the initial light irradiation of fresh  $\text{Ag}_2\text{O}$ . Reprinted with permission from ref. [3].

According to the literature [84, 85], the silver ions have been reduced to silver colloids by the hydrated electrons in homogeneous solutions involving a series of reactions. The mechanism can be proposed as an initial rapid reduction of a fraction of  $\text{Ag}^+$  to form silver atoms (**Equation (5-13)**), followed by the growth of these atoms forming silver particles. These silver particles contain both reduced silver atoms as well as silver ions. i.e. **Equation (5-14) and (5-15)**. These processes will be accompanied by shifts of the redox potential towards higher values.



This multielectron transfer has also been proved later by Bahnemann and co-workers who have studied the primary processes of the light-induced deposition of silver particles on  $\text{TiO}_2$  in the presence of polyvinyl alcohol (PVA) using a nanosecond XeF laser. They detected the photodeposition of metallic silver cluster containing  $\geq 12$

silver atoms on  $\text{TiO}_2$  by detecting their absorption spectra with a maximum at 380 nm [86].

In the presence of  $\text{Ag}/\text{Ag}_2\text{O} // \text{TiO}_2$  mixtures under UV-vis-light irradiation, the TM 41 (with 20%  $\text{TiO}_2$ ), and TM 11 (with 50%  $\text{TiO}_2$ ) were not significantly able to bleach MB suspension. However, MB bleaching using TM 14 (with 80%  $\text{TiO}_2$ ) was relatively faster (**Chapter 2, Figure 2-4 (a)**) indicating that the rate of MB degradation increased with increasing the amount of  $\text{TiO}_2$  in the prepared  $\text{Ag}/\text{Ag}_2\text{O} // \text{TiO}_2$  mixtures. Nevertheless, the corresponding calculated rates for these composites were lower than those obtained for MB suspensions containing the single components ( $\text{Ag}/\text{Ag}_2\text{O}$  or bare  $\text{TiO}_2$ ) as depicted in **Figure 5-8**.

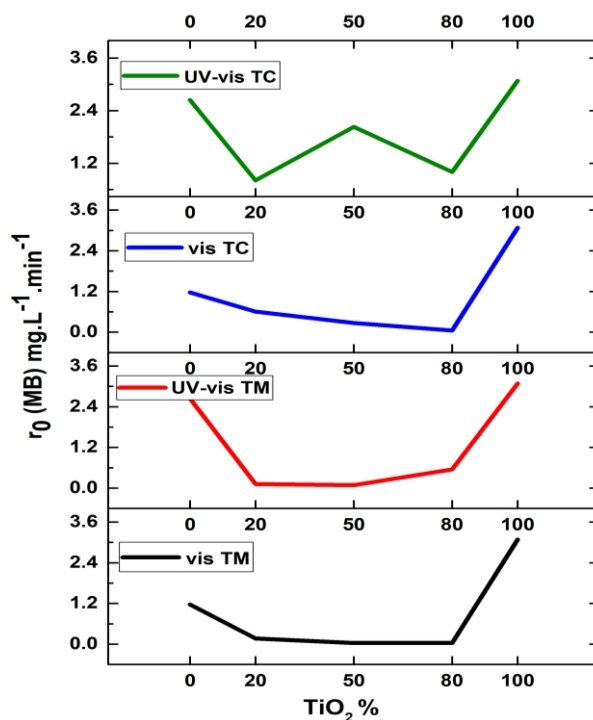


**Figure 5-8.** Initial rates ( $r_0$ ) of MB bleaching using TM mixtures and TC composites with different mass ratio of  $\text{TiO}_2$  under UV-vis-light and only vis-light. The samples with 0 % of  $\text{TiO}_2$  refer to 100 % of  $\text{Ag}/\text{Ag}_2\text{O}$ , the 20 % of  $\text{TiO}_2$  to 80 % of  $\text{Ag}/\text{Ag}_2\text{O}$ , the 50 % of  $\text{TiO}_2$  to 50 % of  $\text{Ag}/\text{Ag}_2\text{O}$ , and 80 % of  $\text{TiO}_2$  to 20 % of  $\text{Ag}/\text{Ag}_2\text{O}$ .

These results correlate well with the optical properties of the catalysts presented in **Chapter 2, Figure 2-3 (a)**. However, the optical properties of the samples are not the only criterion to explain these reaction rates. The specific surface area (SSA) decreased



with increasing Ag/Ag<sub>2</sub>O loadings (**Chapter 2, Table 2-1**). Assuming that the TiO<sub>2</sub> does not change during the synthesis process of the composites, the decrease of the SSA suggests that the growth of Ag/Ag<sub>2</sub>O has blocked a fraction of available surface sites on the TiO<sub>2</sub> surface. Therefore, as the loading of Ag/Ag<sub>2</sub>O in the mixtures increased, more UV photons can be absorbed by Ag<sub>2</sub>O leading to the decrease of the light absorption ability of TiO<sub>2</sub>. The generation of charge carriers is then decreasing in the TiO<sub>2</sub> and, consequently, the rates of MB bleaching decreased. Nonetheless, the rate of MB bleaching determined for the TiO<sub>2</sub>-rich mixture TM 14 suggests that some of the photogenerated charge carriers were not used for MB degradation but contribute to the undesired reactions between excited TiO<sub>2</sub> and Ag/Ag<sub>2</sub>O, reducing Ag<sup>+</sup> to Ag(0).

To confirm this hypothesis, XRD and XPS measurements have been performed after two experimental runs of MB bleaching. The XRD results of the TC 41 composite are depicted in **Figure 5-9**. As revealed by XRD results, the intensities of Ag(0) peaks are increased when those of Ag<sub>2</sub>O disappeared confirming the reduction of Ag<sup>+</sup> during the light-induced bleaching of MB under UV-vis illumination. These experimental XRD findings proved that Ag/Ag<sub>2</sub>O as a co-catalyst is not stable even when Ag(0) was formed on its surface.

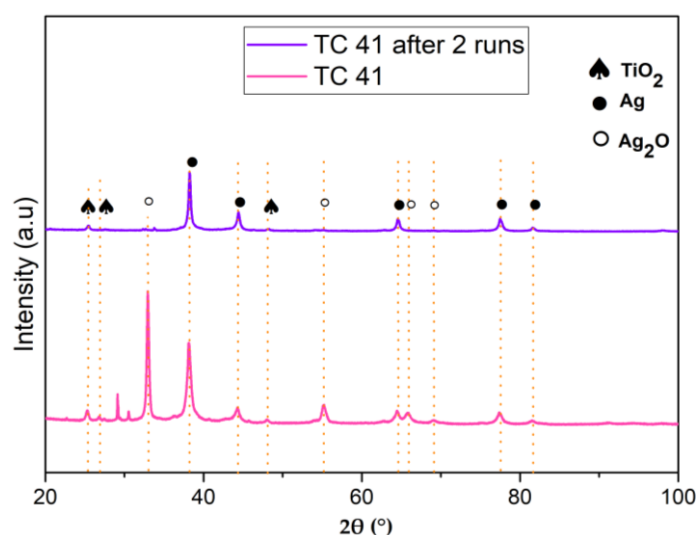


**Figure 5-9.** XRD patterns of TC 41 after two experimental runs of MB bleaching under UV-vis light.

The XPS results are presented in **Chapter 2, Figure 2-9**, and confirm similarly the light-induced reduction of  $\text{Ag}^+$  yielding  $\text{Ag}(0)$ , since the intensities of the  $\text{Ag } 3d_{5/2}$  and  $\text{Ag } 3d_{3/2}$  peaks decrease and those of the  $\text{Ag}(0) 3d_{5/2}$  and  $\text{Ag}(0) 3d_{3/2}$  peaks increase after two photocatalytic runs of MB bleaching under UV-vis light.

Similar to the current study, Hu *et al.* have also observed the formation of  $\text{Ag}(0)$  in both  $\text{Ag}_2\text{O}$  and  $\text{Ag}_2\text{O}/\text{TiO}_2$  after four cycles of tetracycline degradation [17]. Zanella and co-workers have also reported the photo-transformation of  $\text{Ag}_2\text{O}$  to  $\text{Ag}(0)$  in  $\text{Ag}_2\text{O}$  deposited on  $\text{TiO}_2$  [87]. In another study conducted by Ren *et al.*, the light-induced decomposition of  $\text{Ag}_2\text{O}$  in  $\text{Ag}_2\text{O}/\text{TiO}_2$  suspensions has been observed. The authors suggested that the formation of  $\text{Ag}(0)$  contributes to stabilizing the  $\text{Ag}_2\text{O}/\text{TiO}_2$  photocatalyst [18]. Chen *et al.* have as well reported the stabilization of  $\text{Ag}_2\text{O}/\text{TiO}_2$  photocatalysts by the  $\text{Ag}(0)$  formed at the initial stage of the photocatalytic experiment [72]. Mandari *et al.* have synthesized plasmonic  $\text{Ag}_2\text{O}/\text{TiO}_2$  photocatalysts and observed the formation of  $\text{Ag}(0)$  by light-induced reduction of  $\text{Ag}_2\text{O}$  [88]. The photoreduction of  $\text{Ag}(I)$  to  $\text{Ag}(0)$  has also been reported for simultaneously  $\text{Ag}(0)$  deposited and  $\text{Ag}(I)$  co-doped  $\text{TiO}_2$  photocatalyst [89]. Moreover, the formed  $\text{Ag}(0)$  has been proven to act as an electron sink for the photogenerated electrons demonstrating strong visible-light absorption ability owing to its surface plasmon resonance (SPR) [3, 10, 14, 80]. Considering this, the deposition of  $\text{Ag}$  on the surface of  $\text{Ag}_2\text{O}$  has been recognized as an effective way of suppressing the photocorrosion of  $\text{Ag}_2\text{O}$ . [20, 73, 90, 91]. However, once all  $\text{Ag}_2\text{O}$  has been reduced, the photocorrosion has also been completed.

Under visible light irradiation, the situation is, however, completely different and the rate of MB bleaching is found to decrease with increasing amounts of  $\text{TiO}_2$  as shown in **Figure 5-8** and in the graphs given in **Chapter 2, Figure 2-4 (c)**.  $\text{Ag}/\text{Ag}_2\text{O}$  shows high photoactivity of MB bleaching, although it remains below the photoactivity observed for  $\text{Ag}/\text{Ag}_2\text{O}$  under UV-vis-light. The MB degradation using a suspension containing only  $\text{TiO}_2$  is very low, which is expected considering that the latter cannot be excited under vis-light due to its large band gap (3.06 eV). Moreover,

the interfacial electron transfer from excited MB to  $\text{TiO}_2$  which is thermodynamically possible (cf. **Figure 5-6**) obviously did not contribute significantly since no MB bleaching was observed in the presence of bare  $\text{TiO}_2$  under vis-light illumination. Among all mixtures, TM 41 shows a very slight significant conversion during vis-light irradiation implying that the vis-light absorption of the  $\text{Ag}_2\text{O}$ -rich mixture increases with the increasing amount of  $\text{Ag}_2\text{O}$ , while the other mixtures, namely, TM 11 and TM 14 are completely inactive under these illumination conditions. As discussed before, the limited photocatalytic activities of the mixtures under vis-light illumination can be explained based on the interfacial electron transfer between  $\text{Ag}_2\text{O}$  and MB inhibited by the  $\text{TiO}_2$  layer. With increasing  $\text{TiO}_2$  content, the  $\text{Ag}_2\text{O}$  surface is increasingly covered with  $\text{TiO}_2$  as displayed in the SEM images given in **Chapter 2, Figure 2-2**. Thus, the interfacial electron transfer is hindered by  $\text{TiO}_2$  NPs, and the  $\text{TiO}_2$ -rich mixtures (TM 11 and TM 14) exhibit rates of bleaching almost the same as the rate of MB photolysis.

Previous investigation of MB degradation under vis-light using  $\text{TiO}_2/\text{Ag}_2\text{O}$  showed that the MB degradation efficiency increased with the increasing amount of  $\text{Ag}_2\text{O}$ . However, an optimum degradation efficiency existed in the  $\text{Ag}_2\text{O}$  amount present in the  $\text{TiO}_2/\text{Ag}_2\text{O}$  catalyst. Moreover, and after conducting successive photocatalyst tests under vis-light illumination, the formation of  $\text{Ag}(0)$  has been observed [93]. Many authors have reported that when silver oxides are supported on  $\text{TiO}_2$ , the photoreduction of  $\text{Ag}_2\text{O}$  to  $\text{Ag}(0)$  limits the photocatalytic performance of the composite by increasing the recombination rate of the electron-hole pairs [73, 88, 93]. On the other hand, other researchers stated that the photo-reduced  $\text{Ag}(0)$  increased the photoactivity of the composite by capturing photoelectrons and thus impeding the charge carrier recombination [94–96].

In the presence of  $\text{Ag}/\text{Ag}_2\text{O} // \text{TiO}_2$  composites, the rate of MB bleaching is significantly higher in comparison with that of  $\text{Ag}/\text{Ag}_2\text{O} // \text{TiO}_2$  mixtures under UV-vis-light and only vis-light irradiation as evidenced in **Figure 5-8** and **Chapter 2, Figure 2-4**. Considering the  $\text{Ag}/\text{Ag}_2\text{O} // \text{TiO}_2$  composites, the bleaching of MB is found to be higher under UV-vis-light than under vis-light irradiation which has been also

observed previously by Kumar *et al.* [73]. Moreover, and as observed and extensively discussed for the TM samples, the rates of MB bleaching using the composites are lower than in suspensions containing only Ag / Ag<sub>2</sub>O or TiO<sub>2</sub>. XRD and XPS measurements carried out after two experimental runs of MB bleaching over TC 41 (Figure 5-9 and in Chapter 2, Figure 2-9 (c, d)), also confirm the photoreduction of Ag<sub>2</sub>O forming Ag(0) which has been also previously observed [94]. These results prove that Ag<sub>2</sub>O is not stabilized by Ag(0) as claimed by several authors [3, 18, 20, 72, 81, 82].

Under vis-light irradiation, all TC composites exhibit higher activity than the corresponding TM mixtures. As seen for TM materials, the rates of MB bleaching decrease with increasing amounts of TiO<sub>2</sub>. In the presence of Ag<sub>2</sub>O-rich composites, the reaction rates for MB bleaching are increasing compared to the rate of photolysis under visible light illumination. This is explained with an interfacial electron transfer from excited MB to Ag<sub>2</sub>O as widely discussed before. However, the experimental result is astonishing when considering that the surfaces of the composites are smaller than the surfaces of the corresponding TM mixtures. A possible explanation may be that in the TC materials, the Ag/Ag<sub>2</sub>O was prepared in-situ in a TiO<sub>2</sub> suspension. Therefore, the Ag/Ag<sub>2</sub>O was attached to the surface of the TiO<sub>2</sub> particles. In contrast, in the TM mixtures, large Ag/Ag<sub>2</sub>O particles were covered by TiO<sub>2</sub>, hindering the electron transfer from excited MB to the Ag<sub>2</sub>O, as discussed above.

According to the above-mentioned experimental results, a plausible schematic illustration for the photocatalytic degradation of MB by Ag<sub>2</sub>O, Ag/Ag<sub>2</sub>O//TiO<sub>2</sub> mixtures, and Ag/Ag<sub>2</sub>O//TiO<sub>2</sub> composites under vis-light irradiation is shown in Figure 5-10.



**Figure 5-10.** Proposed mechanism for MB bleaching over Ag<sub>2</sub>O, Ag<sub>2</sub>O-containing mixtures, and composites under vis-light illumination. This figure is a reprint of Figure 2-7 in Chapter 2 (page 54).

After all, and regardless of whether the photogenerated electrons reduce  $\text{Ag}^+$  or become stored in  $\text{Ag}(0)$ ,  $\text{Ag}/\text{Ag}_2\text{O} // \text{TiO}_2$  is not performing as a photocatalyst, because the material changes irreversibly during the photocatalytic reaction of MB as confirmed by XRD and XPS data. Therefore, it was decided not to do any further investigation on  $\text{Ag}/\text{Ag}_2\text{O} // \text{TiO}_2$  materials, and the subsequent work will focus on another transition metal modified  $\text{TiO}_2$ , which is Co-doped  $\text{TiO}_2$ .

### 5.2.2. Oxytetracycline Hydrochloride Oxidation in the presence of Co-doped $\text{TiO}_2$

In this section, another pharmaceutical compound that belongs to the tetracycline group of antibiotics, namely oxytetracycline hydrochloride (OTC HCl), has been chosen as a model compound to study the photocatalytic performance of cobalt-doped  $\text{TiO}_2$  ( $\text{Co-TiO}_2$ ) photocatalysts.

Under the identical experimental conditions employed for MB bleaching, the photolytic and the photocatalytic degradation of OTC HCl upon UV-vis-light irradiation in the presence of  $\text{Co-TiO}_2$  as well as bare of  $\text{TiO}_2$  are compared with each other.

OTC HCl (**Figure 5-11**) is the most important pharmaceutical among the broad-spectrum antibiotics belonging to the tetracyclines class and frequently detected in different environmental compartments such as waste, surface, ground, seawater, sediments, and soil around the world. Because of its high stability, OTC cannot be degraded biologically or using conventional treatment processes. Thus, AOPs have been proposed as promising alternative approaches to eliminate this contaminant of emerging concern (CEC) from the aquatic environment [97]. Nevertheless, and due to the various limitations including the formation of byproducts, the selective functional, photosensitive groups, and contact time, heterogeneous photocatalysis using  $\text{TiO}_2$  [98, 99–103], and modified  $\text{TiO}_2$  [104, 105] have been attracting considerable attention in the recent years and have been considered as a promising process for the mineralization of tetracyclines present in the aquatic environment.

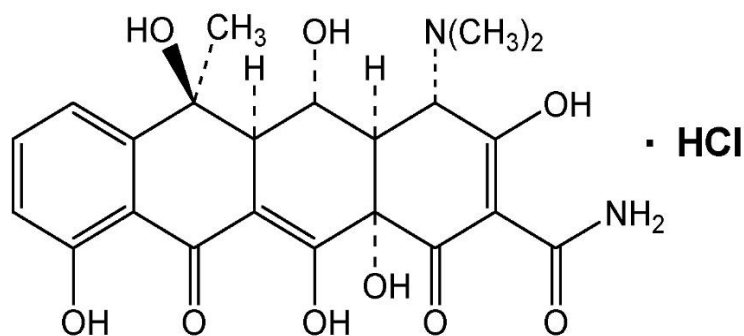


**Figure 5-11:** The chemical structure of oxytetracycline hydrochloride.

After the characterization of the synthesized Co-TiO<sub>2</sub> samples (**Section 5.1.2**), photocatalytic experiments for OTC HCl degradation under UV-vis-light irradiation have been carried out using Co - TiO<sub>2</sub> -HT, Co - TiO<sub>2</sub> -R, TiO<sub>2</sub> -HT, TiO<sub>2</sub> -R, and commercial Degussa P25 as benchmark materials. The initial rates of the OTC HCl degradation reactions are shown in **Table 5-2**.

**Table 5-2.** Initial rates ( $r_0$ ) of OTC HCl degradation in the presence of TiO<sub>2</sub>-R, Co-TiO<sub>2</sub>-R, TiO<sub>2</sub>-HT, Co-TiO<sub>2</sub>-HT, and commercial P25.

Catalysts	$r_0$ [OTC HCl] UV-vis (mg L <sup>-1</sup> min <sup>-1</sup> )
TiO <sub>2</sub> -R	3.45
Co-TiO <sub>2</sub> -R	8.83
TiO <sub>2</sub> -HT	3.87
Co-TiO <sub>2</sub> -HT	4.05
P25	3.34
Photolysis	1.26

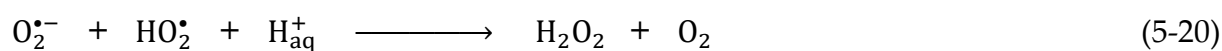
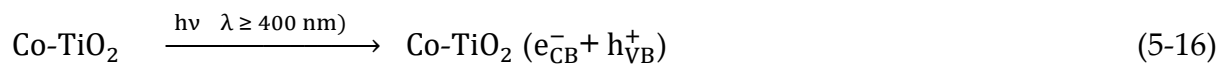
The initial reaction rates of the light-induced degradation of OTC HCl as shown in **Table 5-2** is considerably increased when cobalt was doped in TiO<sub>2</sub>. For the Co-TiO<sub>2</sub>-R composite, the rate was found to be almost 2.5 times higher than the rate obtained with pure TiO<sub>2</sub>-R. On the other hand, the Co-TiO<sub>2</sub>-HT shows an increase up to 4.05 mg L<sup>-1</sup>min<sup>-1</sup>. These results correlate very well with the UV-vis absorption data and the SSA reported in **Section 5.1.2**, since the catalyst which has higher SSA and lower band gap energy, namely, Co - TiO<sub>2</sub> -R, exhibits better photocatalytic activity. This

enhancement is attributed in part to the high SSA, which allows adsorbing more substrate (OTC HCl) on the surface of the catalyst, and in another part to the high ability of this catalyst to absorb UV-vis-light, which facilitates the electron-hole pair generation. Nonetheless, a complete conversion of OTC HCl is observed in the presence of all prepared catalysts, even bare TiO<sub>2</sub>. Notably, the initial reaction rates observed for Co-TiO<sub>2</sub> and TiO<sub>2</sub> composites are greater than those for Degussa P25.

Iwasaki *et al.* have reported the reflux synthesis of Co-TiO<sub>2</sub> for the photocatalytic degradation of CH<sub>3</sub>CHO under UV-vis-light irradiation. They concluded that Co-doped TiO<sub>2</sub> has a higher photocatalytic activity under vis-light as well as under UV-vis-light irradiation than bare TiO<sub>2</sub>. Furthermore, the photoactivity under vis light irradiation was found to strongly depend on the valence state of Co ions in the dopant and to its concentration rather than to the specific surface area and the crystallinity of anatase [106]. Moreover, the visible response completely vanished when Co (III) was used as a dopant instead of Co (II). In another study conducted by Hamadani *et al.*, Co-TiO<sub>2</sub> NPs were prepared by sol/gel method using methyl orange as the probe compound. Among the Co-doped samples, the 0.5% Co/TiO<sub>2</sub> catalyst exhibited the highest photocatalytic activity under visible light irradiation suggesting that the factors responsible for the activity were the surface area and the light absorption of the photocatalysts [41].

In the presence of Co-TiO<sub>2</sub> catalysts, the cobalt doping introduces new energy levels (3d orbital) just above the VB of TiO<sub>2</sub> thus decreasing the band gap energy of the photocatalyst, as shown in **Figure 5-4, Section 5.1.2**. Hence, more photons from the visible range can be employed for the excitation of the doped photocatalyst and consequently more charge carriers are available to initiate the photocatalytic reaction. The photogenerated electrons in the CB of Co-TiO<sub>2</sub> are easily transferred to adsorbed molecular oxygen (O<sub>2</sub>), forming a superoxide radical anion O<sub>2</sub><sup>•-</sup> (-0.33 V vs. NHE). This O<sub>2</sub><sup>•-</sup> combines later with protons forming hydrogen peroxide H<sub>2</sub>O<sub>2</sub> (0.89 V vs. NHE). Subsequently H<sub>2</sub>O<sub>2</sub> is further reduced by e<sub>CB</sub><sup>-</sup> generating •OH (0.38 V vs. NHE), which further converts OTC HCl to mineralized products. On the other hand, the

photogenerated holes accumulate in the VB of Co-TiO<sub>2</sub> and either directly oxidize the pollutant, or they are consumed by water oxidation reaction yielding •OH (1.89 V vs. NHE). This hydroxyl radical further oxidizes OTC HCl. (**Equations 5-16 to 5-23**).



On the other hand, OTC HCl might be converted indirectly using the  $e_{\text{CB}}^-$  of Co-TiO<sub>2</sub>. In this case, OTC HCl might act as an electron scavenger on the surface of TiO<sub>2</sub> (**Equations 5-24 and 5-25**). It should be considered that OTC is pH dependent and has four species at different pH ranges and each species has a distinctive electric charge state (**Figure 5-12**), which may affect the photocatalytic and photolytic degradation at different wavelengths, and at pH 5 the OTC changed to its zwitterionic form H<sub>2</sub>OTC<sup>±</sup> [107].





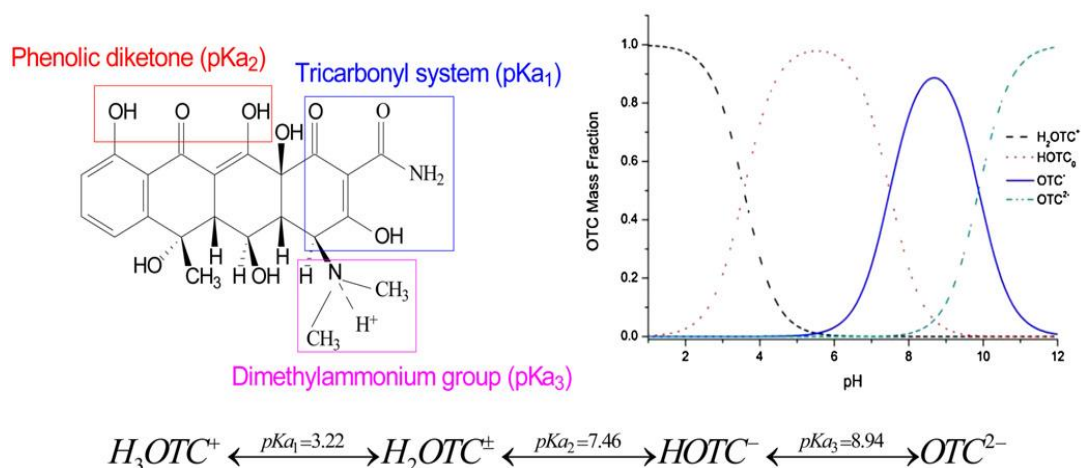
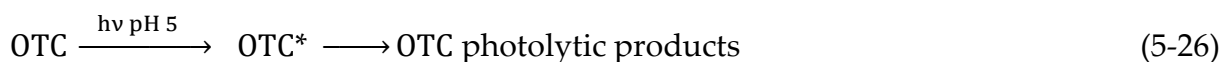
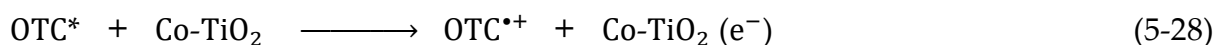


**Figure 5-12.** Molecular structure of OTC with the different pH-dependent species. Reproduced with permission from ref. [108].

In parallel to the photocatalytic degradation of OTC by Co-TiO<sub>2</sub> and TiO<sub>2</sub> under UV-vis-light a direct photolysis mechanism is also involved by the excitation of the OTC molecule to its excited state (OTC\*) (**Equation 5-26**), since around 38% of OTC was decayed without a photocatalyst within 30 min with an initial rate of 1.26 mg L<sup>-1</sup>min<sup>-1</sup> as shown in **Table 5-2**.



It is assumed that the excited OTC HCl molecule injects an electron into the conduction band of the Co-TiO<sub>2</sub>, resulting in the formation of the OTC radical cation (OTC<sup>•+</sup>) which readily undergoes degradation yielding degradation products (**Equations 5-27 and 5-28**).



It is well known that OTC is sensitive to UV [109] and solar light [110] in aqueous solutions. OTC has been proposed to be a potential photosensitizer generating reactive oxygen species (ROS) depending on the solution pH and the wavelengths of irradiation [108, 111]. For instance, Zhao *et al.* have observed that at pH 5.5, at which the OTC changed to its zwitterionic form H<sub>2</sub>OTC<sup>±</sup> (**Figure 5-12**), the photolysis of OTC

cannot occur under visible light irradiation due to the poor visible light absorption, while only minor photolysis of OTC was observed under solar light. In contrast, a self-photosensitization pathway with the detection of singlet oxygen during the photolysis of OTC at high pH has been observed. At pH 8.5 which represents the fraction of  $\text{HOTC}^-$ , and at pH 11.0 in which the OTC mainly exists as  $\text{OTC}^{2-}$  (**Figure 5-12**), the OTC photolysis was enhanced under visible and solar light. Thus, it has been concluded that the self-photosensitized reactions only take place with the negatively charged states ( $\text{HOTC}^-$  and  $\text{OTC}^{2-}$ ) [108].

This was explained by the change of the internal electrostatic force in the OTC molecule as a function of the solution pH. For instance, at pH 5 the positively charged dimethylammonium group for  $\text{H}_3\text{OTC}^+$ ,  $\text{HOTC}^\pm$ , and  $\text{OTC}^-$ , might slow down the electron transfer from the tricarbonyl group to an excited state by electrostatic forces for  $\text{HOTC}^\pm$  under solar/visible light irradiation. On the other hand, at pH 8.5 ( $\text{OTC}^-$ ) the phenolic diketone loses a proton thus "activating" the electron transfer from the excited state due to electrostatic forces from the positively charged dimethylammonium group. Moreover, at pH 11.0 ( $\text{OTC}^{2-}$ ), the dimethylammonium loses another proton to become neutrally charged. In this case, the electrostatic force is entirely removed from the system thus the electrons from tricarbonyl and phenolic diketone can be more easily activated to excited states, leading to a fast OTC photolysis rate. As evidenced by the experimental results of Zhao *et al.*, the photolytic mechanism of OTC at  $\text{pH} > 5$  might involve the combined paths (1) and (2), while the mechanism for OTC photolysis at pH 5.5 may involve path (1) only, as shown in **Figure 5-13** [108]. At pH 8.5 and 11.0, 4-benzoquinone and tert-butyl alcohol or methanol were used to scavenge  $\text{O}_2^{\bullet-}$  and  $\bullet\text{OH}$ , respectively. However, OTC photolysis was found not to be affected in the presence of these quenchers, suggesting that path (3) does not contribute to the OTC photolytic mechanism [105]. This mechanism including the formation of  $^1\text{O}_2$  and  $\text{O}_2^{\bullet-}$  has been earlier proposed in the literature by Seto *et al.* [112]. Based on these results, one concludes that the self-photosensitized reactions mainly occur with negatively charged states, that is  $\text{OTC}^-$  and  $\text{OTC}^{2-}$ .

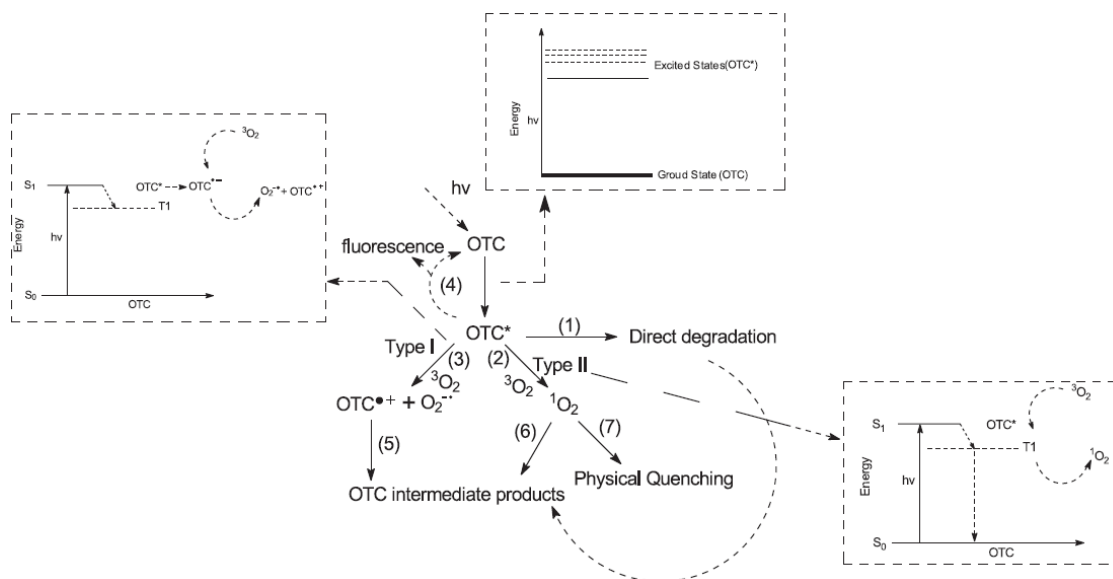


Figure 5-13. Photolytic degradation of OTC. Reprinted with permission from ref [108].

After all, based on the experimental results of the current study, the mechanism given in Figure 5-14 is proposed for the OTC HCl degradation under UV-vis irradiation. As explained before Co-TiO<sub>2</sub> composites enhance the light-induced degradation rate of OTC HCl under UV-vis irradiation due to their high SSA and strong light absorption. However, direct photolytic degradation can still take part in the overall process.

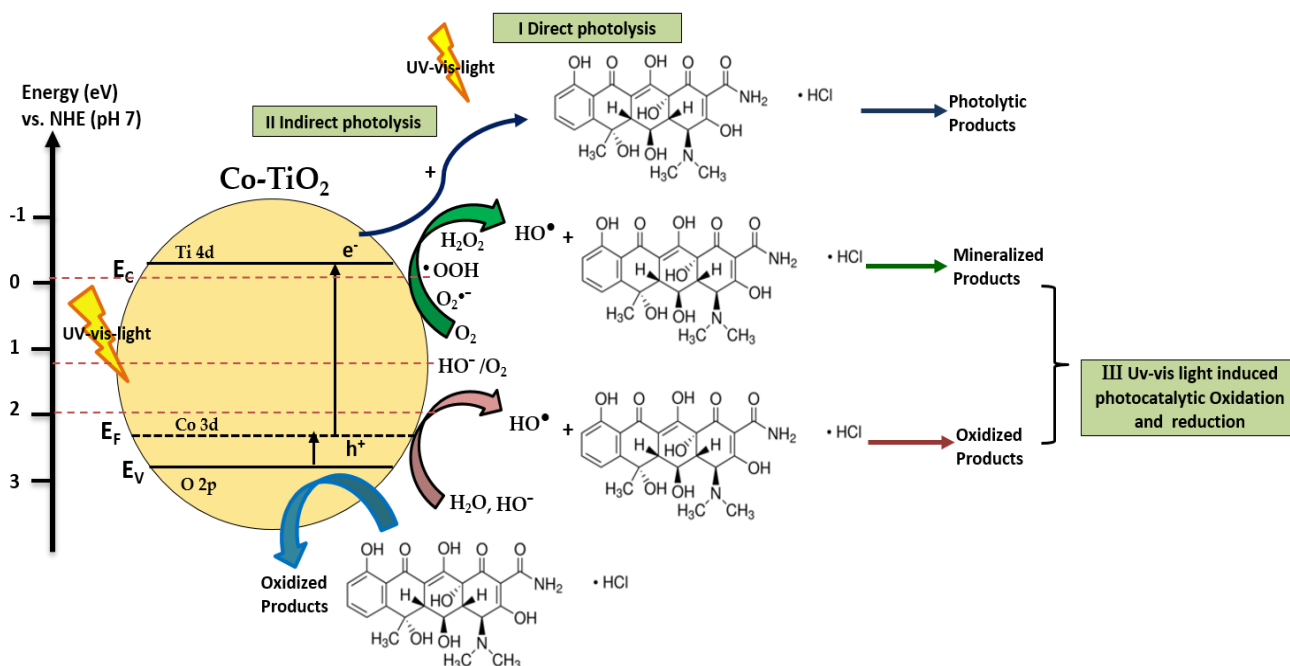


Figure 5-14. Schematic illustration of the photolytic and photocatalytic mechanism of OTC HCl upon UV-vis-light using Co-TiO<sub>2</sub> NPs. This figure is a reprint of Figure 3-5 in Chapter 3 (page 100).

## 5.3. Photocatalytic Reforming of Methanol Yielding H<sub>2</sub>

### 5.3.1. H<sub>2</sub> Evolution in the Presence of Ag/Ag<sub>2</sub>O, Ag/Ag<sub>2</sub>O // TiO<sub>2</sub> Mixtures, and Ag/Ag<sub>2</sub>O // TiO<sub>2</sub> Composites

As mentioned in **Chapter 1**, photocatalytic fuel synthesis by converting wastewater using sunlight is a promising alternative to provide clean energy. For this purpose, the Ag/Ag<sub>2</sub>O and Ag/Ag<sub>2</sub>O // TiO<sub>2</sub> systems prepared in **Section 5.1.1** have been investigated for the photocatalytic hydrogen evolution from aqueous methanol under UV-vis-light irradiation. The photocatalytic experiments have been conducted under solar illumination as described in detail in **Section 2.6.4.2** in **Chapter 2**. The results are shown in **Chapter 2, Figure 2-5**.

Ag<sub>2</sub>O / TiO<sub>2</sub> systems have been well investigated in great detail for the photocatalytic H<sub>2</sub> formation [88, 113–117]. From a thermodynamic point of view, Ag/Ag<sub>2</sub>O is completely inactive for the proton reduction reaction since the CB potential of Ag<sub>2</sub>O (+ 0.3 V vs. NHE at pH 7) does not meet the requirements for H<sub>2</sub> formation (– 0.41 V vs. NHE at pH 7) as depicted in **Figure 5-6**, and as reported in the literature [118]. Therefore, the excitation of TiO<sub>2</sub> is a prerequisite for the photocatalytic H<sub>2</sub> evolution. However, TiO<sub>2</sub> is a relatively inactive material for the photocatalytic reduction of protons and high evolution rates of H<sub>2</sub> are obtained only in the presence of a suitable co-catalyst [119, 120]. As can be seen from **Figure 2-5 (a)** in **Chapter 2**, pure TiO<sub>2</sub> shows an extremely low photocatalytic activity with regard to H<sub>2</sub> evolution from aqueous methanol. Thus, the deposition of Ag/Ag<sub>2</sub>O as an electrocatalyst at the TiO<sub>2</sub> surface to accelerate the interfacial electron transfer is likely to be beneficial. A significant increase in the amount of H<sub>2</sub> evolved during six hours of illumination is observed when using TiO<sub>2</sub>-rich mixtures (TM 14) which consequently correspond to an increase in the reaction rates. This enhancement can be explained by presuming that Ag<sub>2</sub>O absorbs a significant portion of the photons being inactive under these illumination condition, and thus no more photons are available for the H<sub>2</sub> evolution reaction. However, this portion is decreasing with increasing TiO<sub>2</sub> amount in the mixture. Instead, the electron transfer from the conduction band of TiO<sub>2</sub> to the Ag<sub>2</sub>O

conduction band is thermodynamically favorable, resulting in the reduction of  $\text{Ag}^+$  to  $\text{Ag}(0)$ . These electrons are thus not available for the desired  $\text{H}_2$  evolution reaction. Obviously, the higher the mass fraction of  $\text{TiO}_2$  in the physical mixture the lower these undesired electron losses, resulting in increasing the rates of  $\text{H}_2$  evolution.

Very recently,  $\text{Ag}_2\text{O}/\text{TiO}_2$  prepared by a simple mechanical grinding for the photocatalytic methanol dehydrogenation under UV-vis irradiation has been reported. It has been observed that the addition of inactive  $\text{Ag}_2\text{O}$  to titania caused a significant increase in  $\text{H}_2$  formation for almost all samples except  $\text{Ag}_2\text{O}/\text{P25}$ . Hence, it has been concluded that the Z-scheme mechanism was responsible for this enhancement in which the photo-reduced  $\text{Ag}(0)$  on the  $\text{Ag}_2\text{O}$  surface acts as a sink for the photogenerated electrons resulting in  $\text{H}_2$  formation, and methanol works as a hole scavenger at the  $\text{TiO}_2$  surface to hinder the hole-electron recombination [117]. In a study conducted by Lalitha *et al.*, bare  $\text{Ag}_2\text{O}$  was found to be active for the photocatalytic  $\text{H}_2$  production from aqueous methanol under solar light illumination with a maximum amount of  $140 \mu\text{mol h}^{-1}$ . A mechanical mixture of 1 wt.%  $\text{Ag}_2\text{O}/\text{TiO}_2$  has also been prepared and an amount of  $760 \mu\text{mol h}^{-1}$  has been reported. According to these results, a synergistic activity has been observed when  $\text{Ag}^+$  interacted with  $\text{TiO}_2$ . These authors have concluded that a structure-activity correlation has been established in which  $\text{Ag}^+$  interacting with the surface layers of  $\text{TiO}_2$  plays an important role in maintaining the continuous hydrogen production activity under solar irradiation rather than  $\text{Ag}(0)$  [114].

As compared to the  $\text{Ag}/\text{Ag}_2\text{O} // \text{TiO}_2$  mixtures (TM),  $\text{Ag}/\text{Ag}_2\text{O} // \text{TiO}_2$  composites (TC) are found to be more active for promoting the light-induced  $\text{H}_2$  evolution, and almost all TC composites exhibit higher  $\text{H}_2$  evolution activity. In term of  $\text{H}_2$  formation rates, the order of the photocatalytic activity is  $\text{TC 11} > \text{TC 14} > \text{TiO}_2 > \text{TC 41} > \text{Ag}/\text{Ag}_2\text{O}$ . Among all composites, TC 11 was the most active system demonstrating a higher evolution rate than all other samples (**Chapter 2, Figure 2-5 (b)**). In the current study, this composite has also shown the highest photocatalytic activity for MB bleaching under UV-vis illumination (**section 5.2.1**). This can be explained by the synergetic

effects present between Ag(0), Ag<sub>2</sub>O, and TiO<sub>2</sub> as illustrated in **Figure 5-15**. Under solar irradiation, TiO<sub>2</sub> is excited by UV photons resulting in the formation of electron-hole pairs in this semiconductor. The photogenerated e<sub>CB</sub><sup>-</sup> migrate to the Ag(0) attached to the surface of TiO<sub>2</sub>. As known, the metal co-catalyst is acting as an electron pool since its Fermi level is lower than the TiO<sub>2</sub> CB, moreover, Ag(0) has a low overpotential for the reduction of water [120]. An interfacial electron transfer from Ag(0) to protons is occurring yielding H<sub>2</sub>. The VB hole of the TiO<sub>2</sub> particle is then filled by an electron from an attached Ag<sub>2</sub>O particle. Methanol is subsequently oxidized by the thus formed hole in the valence band of Ag<sub>2</sub>O. According to this mechanism, Ag(0) acts as an electrocatalyst for the hydrogen evolution reaction, while Ag<sub>2</sub>O is an electrocatalyst for the methanol oxidation.

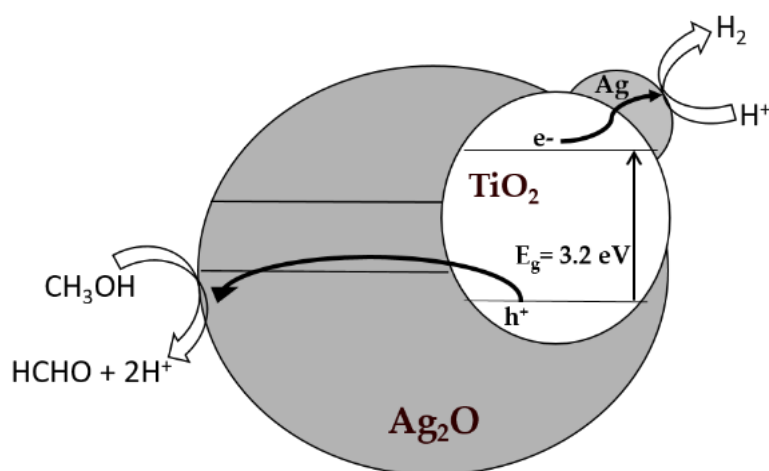


**Figure 5-15.** Proposed mechanism of H<sub>2</sub> evolution from aqueous CH<sub>3</sub>OH under UV-vis illumination. This figure is a reprint of Figure 2-10 in Chapter 2 (page 61).

Mandari *et al.* have reported that in-situ formed Ag(0) islands may also transfer electrons to TiO<sub>2</sub> through surface plasmon resonance (SPR) excitation thus improving the photocatalytic H<sub>2</sub> production on Ag<sub>2</sub>O // TiO<sub>2</sub> photocatalysts [88]. The same mechanism is proposed in this study, involving the oxidation of methanol at the Ag<sub>2</sub>O surface through an electron transfer to the valence band of the excited TiO<sub>2</sub>, as stated before [17, 21, 94]. Nevertheless, the mechanism proposed here in the presence of the TM mixtures and TC composites does not contradict the mechanism discussed for

Ag/Ag<sub>2</sub>O//TiO<sub>2</sub> materials, with a significantly more negative conduction band energy of Ag<sub>2</sub>O than that of TiO<sub>2</sub> [88, 121, 122].

The photocatalytic activities of the TC and TM discussed here are therefore determined to a large extent by the competition between interfacial electron transfer to protons, and to Ag<sup>+</sup> in Ag<sub>2</sub>O. Variations in the TiO<sub>2</sub>, Ag, and Ag<sub>2</sub>O mass fractions may impact the hydrogen evolution rate. Increasing the mass fractions of Ag and Ag<sub>2</sub>O reduces the number of photons to be absorbed by TiO<sub>2</sub>, hence the H<sub>2</sub> evolution rate decreases, and, on the other hand, decreasing the mass fractions of metallic Ag and Ag<sub>2</sub>O may slow down the interfacial electron transfer to the proton thus negatively affecting the oxidation reaction, respectively. These opposing effects could be the main reason for the differences observed here in the H<sub>2</sub> evolution rates in the presence of TC composites and TM mixtures.

### 5.3.2. H<sub>2</sub> Evolution in the Presence of Co-TiO<sub>2</sub>

The Co-TiO<sub>2</sub> photocatalysts prepared in **Section 5.1.2** have also been further examined for the photocatalytic H<sub>2</sub> evolution from aqueous methanol under UV-vis-light irradiation. The results are presented in **Figure 5-16 (a, b)**. As can be seen, neither pure TiO<sub>2</sub>-R nor TiO<sub>2</sub>-HT show a significant photocatalytic activity for the hydrogen evolution reaction. Using Co-TiO<sub>2</sub>-R and Co-TiO<sub>2</sub>-HT composites, the formed amount of H<sub>2</sub> still extremely low and close to the detection limit. To understand the reaction pathways of Co-TiO<sub>2</sub> electrons and holes produced under illumination and to examine the effect of Co-doping on the behavior of these electron-hole pairs, EPR study of Co-TiO<sub>2</sub> and bare TiO<sub>2</sub> have been conducted and are displayed in **Figure 5-17**.

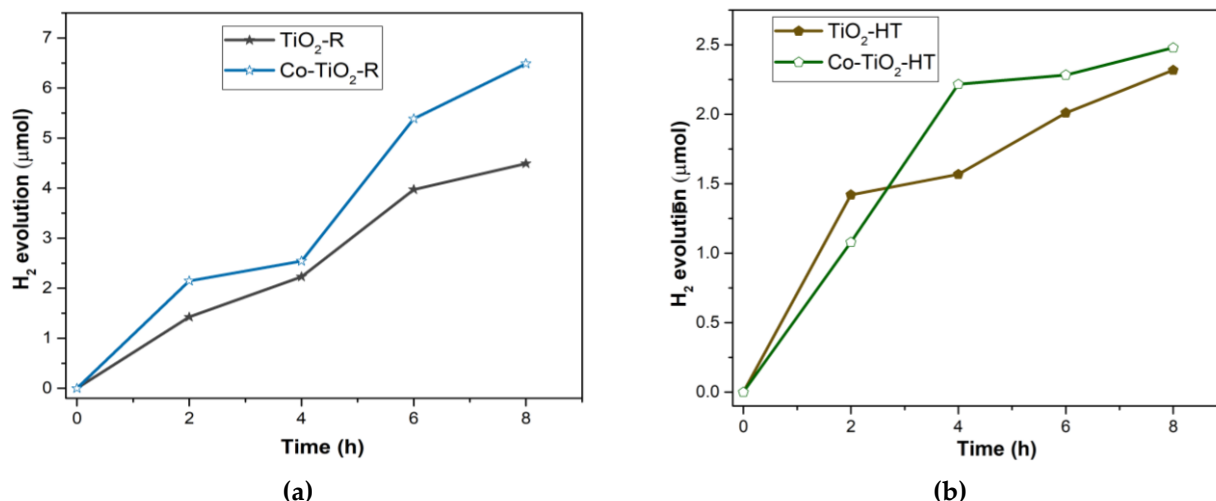


**Figure 5-16.** Light-induced hydrogen evolution from aqueous CH<sub>3</sub>OH in the presence of (a) TiO<sub>2</sub>-HT and Co-TiO<sub>2</sub>-R, (b) TiO<sub>2</sub>-HT and Co-TiO<sub>2</sub>-HT.

According to the EPR results (**Figure 5-17**), bare and Co-doped TiO<sub>2</sub> show the same characteristic peaks in the dark which is assigned to the paramagnetic centers in the TiO<sub>2</sub> crystal lattice [123]. Upon UV-vis illumination of bare TiO<sub>2</sub> samples, three signals are observed. Signal (A) is assigned to the surface trapped hole, that is the radical Ti<sup>4+</sup>O<sup>•</sup>-Ti<sup>4+</sup>OH<sup>-</sup> [124, 125], signal (B) is attributed to the Ti<sup>3+</sup> formed by trapping the photogenerated electrons [126, 127], and signal C is ascribed to the trapped conduction band electrons [127, 128]. When Cobalt is introduced to the TiO<sub>2</sub> crystal lattice, a decrease in the vacancy peaks is observed. Such a trend has also been observed for Co and has been explained as a detrimental effect on the formation of oxygen vacancy defects [129]. The intensity of signal (B) is also reduced indicating that the cobalt ions are trapping the electrons instead of Ti<sup>4+</sup>. Moreover, signal (C) is vanishing suggesting that the photogenerated electrons are trapped in sites other than Ti, thus reducing the intensity of the Ti<sup>3+</sup> signal. These EPR results lead to the conclusion that in the Co-TiO<sub>2</sub> composites part of the photoinduced electrons are trapped by cobalt which might also work as a recombination center for the electron-hole pairs.



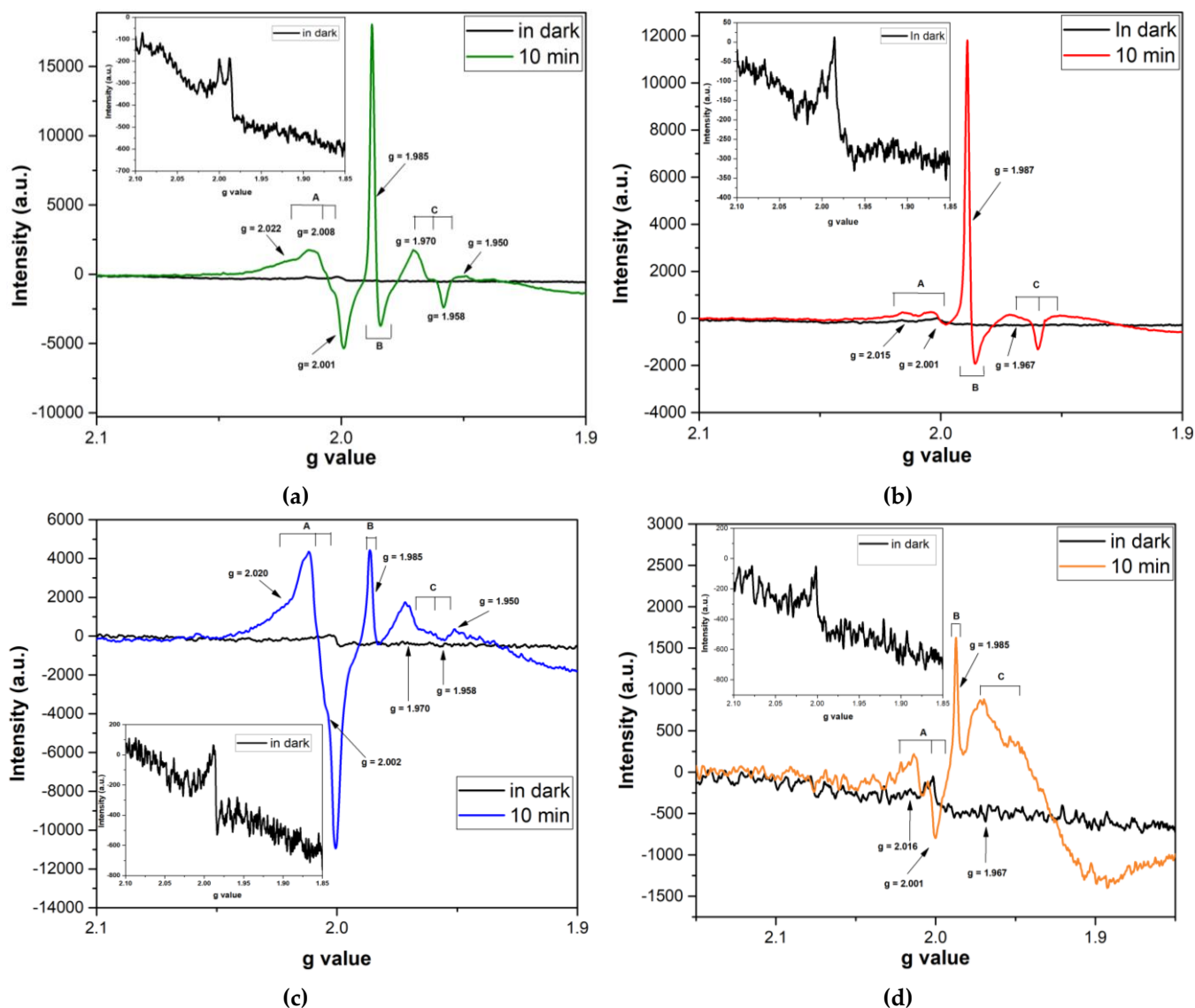


**Figure 5-17.** In situ EPR spectra at 77K of (a)  $\text{TiO}_2\text{-HT}$ , (b)  $\text{Co-TiO}_2\text{-HT}$ , (c)  $\text{TiO}_2\text{-R}$ , (d)  $\text{Co-TiO}_2\text{-R}$  in the dark and after 10 min of UV-vis-light irradiation (Xe lamp,  $\lambda = 300 - 450$  nm).

Accordingly, the low photocatalytic activity observed for bare materials (**Figure 5-16**), suggests that the electrons could be trapped as  $\text{Ti}^{3+}$  species instead of reducing protons, which is consistent with the above EPR results. This observation is in good agreement with published studies [130, 131]. In the presence of  $\text{Co-TiO}_2\text{-HT}$  and  $\text{Co-TiO}_2\text{-R}$  composites, the evolved amount of  $\text{H}_2$  is remaining low and close to the detection limit of the equipment employed here. Considering **Figure 5-4**, a significant decrease of the band gap is observed in dark for the  $\text{Co-TiO}_2$  samples which allows more photons to be absorbed as compared with bare  $\text{TiO}_2$  under the illumination conditions employed in this investigation. Considering this, higher activity of the  $\text{Co-TiO}_2$

samples is expected. However, the photocatalytic activity of Co-TiO<sub>2</sub> is not enhanced. These results suggest that the recombination rate is increased in these composites [49, 132]. This can be explained by a decreased number of oxygen vacancy defects since these defects act as active sites on the photocatalyst surface thus delaying the recombination of photogenerated electrons and holes. The other possibility is that the electrons can be trapped rapidly and are then not available for H<sup>+</sup> reduction via interfacial charge transfer, which is in accordance with the EPR data. Similar findings have been reported by Hwang *et al.* who found that only Cr and Fe doped TiO<sub>2</sub> can generate significant amounts of molecular hydrogen from aqueous methanol [133]. In another study conducted by Wu *et al.*, 0.4 wt.% Co<sup>2+</sup> modified TiO<sub>2</sub> (P25) was found to decrease the photocatalytic hydrogen evolution activity from aqueous ethanol [134].

After all, and as the evolved amount of hydrogen in the presence of both Co-TiO<sub>2</sub> photocatalysts is extremely low with no significant effect of Co-doping on the photocatalytic H<sub>2</sub> formation, deposition of Pt on the surface of these composites has also been performed here to study same photocatalytic reactions under identical experimental conditions.

### 5.3.3. H<sub>2</sub> Evolution in the Presence of Pt loaded Co-TiO<sub>2</sub>

The photocatalytic hydrogen production from aqueous methanol has been investigated for platinized Co-TiO<sub>2</sub> and TiO<sub>2</sub> samples, and the continuous hydrogen production profile of all samples is depicted in **Figure 5-18**. The improved hydrogen evolution activity by Pt loading onto TiO<sub>2</sub> corresponds to general experience [120, 135]. The platinized Co-TiO<sub>2</sub> photocatalysts show a drastic enhancement of the photocatalytic H<sub>2</sub> evolution in comparison with Co-TiO<sub>2</sub> and pure TiO<sub>2</sub> materials and even outperforms that of the well-known platinized photocatalysts Pt/P25 and Pt/UV100.

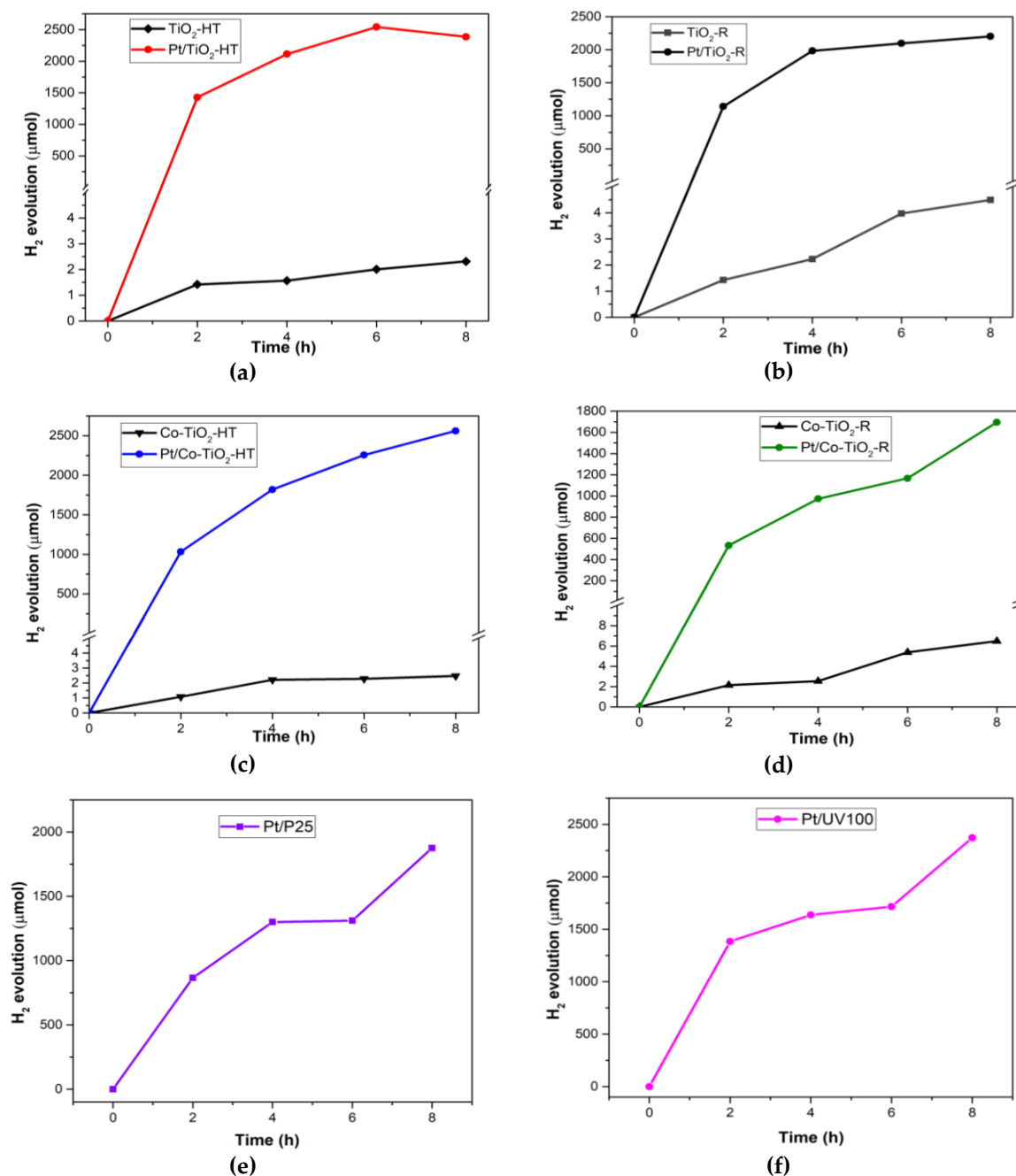


**Figure 5-18.** Light-induced hydrogen evolution from aqueous CH<sub>3</sub>OH in the presence of all prepared photocatalysts. This figure is a reprint of Figure 4-8 in Chapter 4 (page 137).

The rate of H<sub>2</sub> production is found to greatly improve for all platinumized samples, and a maximum of  $317 \pm 44 \mu\text{mol h}^{-1}$  is observed for Pt/Co-TiO<sub>2</sub>-HT. However, Pt/Co-TiO<sub>2</sub>-HT and Pt/Co-TiO<sub>2</sub>TiO<sub>2</sub>-R exhibit almost similar H<sub>2</sub> production rates as Pt/TiO<sub>2</sub>-HT and Pt/TiO<sub>2</sub>-R, respectively (within the limits of the experimental error). These results confirm again that cobalt species do not improve the H<sub>2</sub> evolution activity. Accordingly, the high photocatalytic activity obtained with all platinumized samples can

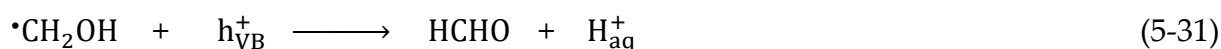
only be attributed to the improved charge carrier separation by the Pt NPs deposited on the surface of the photocatalysts.

It is worth mentioning that the H<sub>2</sub> evolution rate in all prepared catalysts is decreasing with the irradiation time (**Figure 5-18**). To explain this, the possible mechanism of the photocatalytic degradation of methanol has to be taken into consideration. Reaction pathways for photocatalytic reforming of methanol on Pt/(Co)-TiO<sub>2</sub> may involve the following reaction equations (**Equation (5-29) – (5-35)**).

Upon solar simulated irradiation, electron-hole pairs are generated:



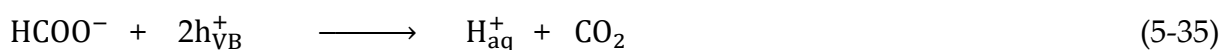
The photogenerated holes oxidize methanol yielding formaldehyde (HCHO) according to [136]:

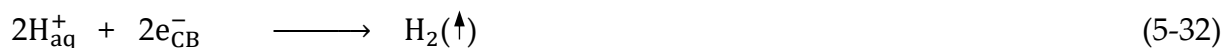


The H<sub>aq</sub><sup>+</sup> generated during the total process are transferred to the metal loaded semiconductor photocatalyst where they are reduced by the photogenerated electrons to molecular hydrogen [136].



The primary product, formaldehyde, could be further oxidized to methanoic (formic) acid (HCOOH) and subsequently to CO<sub>2</sub> together with hydrogen generation via the following equations [136]:





Chiarello *et al.* have also examined the photocatalytic hydrogen production from methanol oxidation over Pt deposited on  $\text{TiO}_2$ . In their study, they demonstrated that methanol undergoes oxidation up to  $\text{CO}_2$  via the formation of formaldehyde and formic acid. They concluded that the amount of methanol in the feed gas mixture should be kept low (0.1–0.7) because complete methanol oxidation to  $\text{CO}_2$  decreases quickly with increasing the amount of methanol producing carbon monoxide from formic acid [120].

Overall, one can conclude that no significant impact of Co-doping on the photocatalytic  $\text{H}_2$  activity of the platinized samples is observed under the experimental conditions used in the current study. This result is in accordance with the flatband potential results (**Figure 5-4**) where no significant impact of cobalt doping has been recorded within the limits of the experimental errors. After all, the obtained results can be summarized as illustrated in **Figure 5-19**. Under simulated solar light irradiation, electron/hole pairs are produced in the CB and the VB of Co- $\text{TiO}_2$ , respectively. Subsequently, the electrons migrate from the  $\text{TiO}_2$  CB to Pt. Thus, Pt islands act as electron sinks decreasing the charge carrier recombination, whereas the holes left in the  $\text{TiO}_2$  valence band oxidize aqueous methanol. Hence, the presence of Pt seems to counteract the decrease of the photocatalytic activity due to Co-doping.

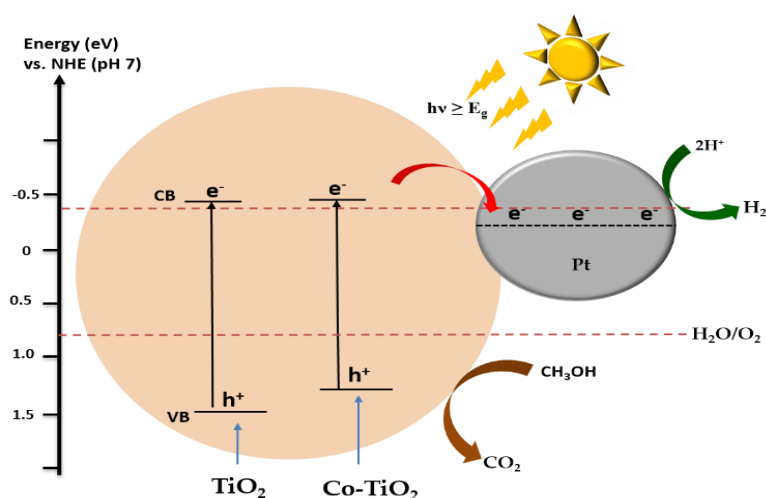


**Figure 5-19.** Schematic illustration of  $\text{H}_2$  evolution over Pt/Co- $\text{TiO}_2$  photocatalysts. This figure is a reprint of Figure 4-10 in Chapter 4 (page 141).

## 5.4. Conclusions

This study aims to combine the removal of organic pollutants from water and the production of molecular hydrogen as a renewable fuel by the investigation of  $\text{TiO}_2$  modified with transition metals, which are  $\text{Ag}/\text{Ag}_2\text{O} // \text{TiO}_2$  and  $\text{Co-TiO}_2$ .

In conclusion, the experimental results of the first part of this study show that the synthesized  $\text{Ag}/\text{Ag}_2\text{O} // \text{TiO}_2$  mixtures (formed by mechanical grinding) and  $\text{Ag}/\text{Ag}_2\text{O} // \text{TiO}_2$  composites (in situ-prepared) enhance the rate of the light-induced bleaching of aqueous methylene blue (MB) under both UV-vis and visible illumination, in comparison to the bleaching in homogeneous solution. However, bare  $\text{Ag}/\text{Ag}_2\text{O}$  remained the most active material under both illumination conditions. This result leads to the conclusion that the bleaching of MB is initiated by an interfacial electron transfer from the photo-excited organic compound adsorbed on the  $\text{Ag}_2\text{O}$  surface to the conduction band of this semiconductor. This electron transfer seems to be inhibited by increasing the amount of  $\text{TiO}_2$  layers covering the  $\text{Ag}_2\text{O}$  in the  $\text{Ag}/\text{Ag}_2\text{O} // \text{TiO}_2$  mixtures and composites. Irrespective whether MB undergoes a photocatalytic reduction reaction leading to its photobleaching or acts as a sensitizer,  $\text{Ag}^+$  present in  $\text{Ag}/\text{Ag}_2\text{O}$  is confirmed to be reduced yielding  $\text{Ag}(0)$ .

For thermodynamic reasons,  $\text{Ag}_2\text{O}$  cannot transfer an electron to a proton at the experimental conditions used in this study. With increasing the mass fraction of  $\text{TiO}_2$  in  $\text{Ag}/\text{Ag}_2\text{O} // \text{TiO}_2$ , electron transfer from the  $\text{TiO}_2$  conduction band to the  $\text{Ag}_2\text{O}$  conduction band (which is thermodynamically favorable) is used to reduce  $\text{Ag}^+$  to  $\text{Ag}(0)$  and therefore is not available for the  $\text{H}_2$  evolution reaction. However, an increase in the rates of  $\text{H}_2$  formation has been identified at increasing amounts of  $\text{TiO}_2$  in the  $\text{Ag}/\text{Ag}_2\text{O} // \text{TiO}_2$  mixtures suggesting that the fraction of photons absorbed by  $\text{Ag}_2\text{O}$  where they are being inactivated decreases. Consequently, it can be concluded that  $\text{Ag}/\text{Ag}_2\text{O}$  is not a (photo)stable material since it is reduced yielding metallic  $\text{Ag}$ .

Since  $\text{Ag}/\text{Ag}_2\text{O}$  containing photocatalysts were found to be unstable the focus of the subsequent work was shifted to  $\text{Co-TiO}_2$  photocatalysts.

The experimental results of the second part of this study demonstrated that both photocatalysts, namely Co-TiO<sub>2</sub>-R (reflux synthesis) and Co-TiO<sub>2</sub>-HT (hydrothermal synthesis) enhance the degradation rate of oxytetracycline hydrochloride (OTC HCl) under UV-vis irradiation. These results are found to agree well with the SSA and the UV-vis-light absorption data, indicating that the high SSA along with the decreased band gap have a major influence on the photocatalytic performance of the photocatalyst. On the other hand, the homogeneous photolysis of OTC HCl was found to occur with over 30%. Therefore, and despite the observed complete degradation of OTC HCl in the presence of Co-TiO<sub>2</sub> photocatalysts, the use of such complex organic molecules can be assumed to be unsuitable for the evaluation of the photocatalytic activity of semiconducting materials.

As a second test reaction for the photocatalytic activity of the Co-TiO<sub>2</sub> materials, the UV-vis-light-induced evolution of H<sub>2</sub> by the reforming of aqueous methanol has been investigated evincing that no significant impact of Co -doping on the photocatalytic H<sub>2</sub> generation can be detected with the evolved amounts of H<sub>2</sub> being close to the detection limit. Therefore, and in order to obtain significant amounts of future renewable energy fuels (i.e., H<sub>2</sub>), Pt is chosen as a co-catalyst loaded on Co-TiO<sub>2</sub> composites.

The third part of this study focuses on the photocatalytic H<sub>2</sub> activity over Pt/Co-TiO<sub>2</sub> photocatalysts. Higher H<sub>2</sub> formation rates are observed and related to the Pt NPs which act to improve the separation of photogenerated charge carriers ( $e_{CB}^-$  and  $h_{VB}^+$ ) thus enhancing the methanol oxidation at the same time. Accordingly, it can be concluded that Pt apparently offsets the decrease of the photocatalytic activity due to Co-doping.

In summary, the obtained experimental results within the frame of this doctoral thesis contribute to the evaluation of the photoactivity of the investigated semiconducting materials in both water treatment and fuel synthesis. Despite the increased photocatalytic activity, limitations, and challenges concerning the stability of the used semiconductor need to be overcome. Furthermore, attention should be

focused on the selected organic contaminants to ensure that the photolytic mechanism will not be confused with the photocatalytic degradation. Organic contaminants such as methanol can perform the role of electron donors, thereby reducing the hydrogen generation costs whereas at the same time serving the dual role of hydrogen production as well as organic pollutant degradation.

## 5.5. References

1. M. Grätzel, F.P. Rotzinger. The Influence of the Crystal Lattice Structure on the Conduction Band Energy of Oxides of Titanium (IV). *Chem. Phys. Lett.* **1985**, 118, 474–477.
2. D.W. Bahnemann, M. Hilgendorff, R. Memming. Charge Carrier Dynamics at TiO<sub>2</sub> Particles: Reactivity of Free and Trapped Holes. *J. Phys. Chem. B* **1997**, 101, 4265–4275.
3. X. Wang, S. Li, H. Yu, J. Yu, S. Liu. Ag<sub>2</sub>O as a New Visible-light Photocatalyst: Self-stability and High Photocatalytic Activity. *Chem. Eur. J.* **2011**, 17, 7777–7780.
4. Y. Ida, S. Watase, T. Shinagawa, M. Watanabe, M. Chigane, M. Inaba, A. Tasaka, M. Izaki. Direct Electrodeposition of 1.46 eV Bandgap Silver(I) Oxide Semiconductor Films by Electrogenenerated Acid. *Chem. Mater.* **2008**, 20, 1254–1256.
5. W. Zhou, H. Liu, J. Wang, D. Liu, G. Du, J. Cui. Ag<sub>2</sub>O / TiO<sub>2</sub> Nanobelts Heterostructure with Enhanced Ultraviolet and Visible Photocatalytic Activity. *ACS Appl. Mater. Interfaces* **2010**, 2(8), 2385–2392.
6. D. Sarkar, C.K. Ghosh, S. Mukherjee, K.K. Chattopadhyay. Three Dimensional Ag<sub>2</sub>O / TiO<sub>2</sub> Type-II (p–n) Nanoheterojunctions for Superior Photocatalytic Activity. *ACS Appl. Mater. Interfaces* **2013**, 5, 331–337.
7. W. Zhou, H. Liu, J. Wang, D. Liu, G. Du, S. Han, J. Lin, R. Wang. Interface Dominated High Photocatalytic Properties of Electrostatic Self-assembled Ag<sub>2</sub>O/TiO<sub>2</sub> Heterostructure. *Phys. Chem. Chem. Phys.* **2010**, 12, 15119–15123.



8. S.P. Prakoso, A. Taufik, R. Saleh. Ag/Ag<sub>2</sub>O/TiO<sub>2</sub> Nanocomposites: Microwave Assisted Synthesis, Characterization, and Photosonocatalytic Activities. *IOP Conf. Ser., Mater. Sci. Eng.* **2017**, 188, 012029.
9. W.J. Zhou, Y.H. Leng, D.M. Hou, H.D. Li, L.G. Li, G.Q. Li, H. Liu, S.W. Chen. Phase Transformation and Enhanced Photocatalytic Activity of S-doped Ag<sub>2</sub>O/TiO<sub>2</sub> Heterostructured Nanobelts. *Nanoscale* **2014**, 6, 4698–4704.
10. H. G. Yu, R. Liu, X. F. Wang, P. Wang, J. G. Yu. Enhanced Visible-light Photocatalytic Activity of Bi<sub>2</sub>WO<sub>6</sub> Nanoparticles by Ag<sub>2</sub>O Cocatalyst. *Appl. Catal. B: Environ.* **2012**, 111–112, 326–333.
11. A. Taufik, S.P. Prakoso, R. Saleh. The Synthesis and Characterization of Ag / Ag<sub>2</sub>O / TiO<sub>2</sub> /NGP Composites as Adsorbents and Photocatalysts for Wastewater Removal. *J. Phys. Conf. Ser.* **2017**, 820, 012018.
12. R. El-Shabasy, N. Yosri, H. El-Seedi, K. Shoueir, M. El-Kemary. A Green Synthetic Approach using Chili Plant Supported Ag/Ag<sub>2</sub>O @P25 Heterostructure with Enhanced Photocatalytic Properties under Solar Irradiation. *Optik* **2019**, 192, 162943.
13. S. Kohtani, K. Yoshid, T.Maekaw, A. Iwase, A. Kudo, H. Miyabe, R. Nakagaki. Loading Effects of Silver Oxides upon Generation of Reactive Oxygen Species in Semiconductor Photocatalysis. *Phys. Chem. Chem. Phys.* **2008**, 10, 2986–2992.
14. M. Zou, H. Liu, L. Feng, F. Xiong, T. Thomas, M. Yang. Effect of Nitridation on Visible Light Photocatalytic Behavior of Microporous (Ag, Ag<sub>2</sub>O) Co-loaded TiO<sub>2</sub>. *Microporous Mesoporous Mater.* **2017**, 240, 137–144.
15. A. Deng, Y. Zhu. Synthesis of TiO<sub>2</sub> / SiO<sub>2</sub> / Ag / Ag<sub>2</sub>O and TiO<sub>2</sub> / Ag / Ag<sub>2</sub>O Nanocomposite Spheres with Photocatalytic Performance. *Res. Chem. Intermed.* **2018**, 44, 4227–4243.
16. M.E. Olya, M. Vafaei, M. Jahangiri. Modeling of Acid Dye Decolorization by TiO<sub>2</sub>-Ag<sub>2</sub>O Nano-photocatalytic Process using Response Surface Methodology. *J. Saudi Chem. Soc.* **2017**, 21, 633–642.

17. X. Hu, X. Liu, J. Tian, Y. Li, H. Cui. Towards Full-Spectrum (UV, Visible, and Near-infrared) Photocatalysis: Achieving an All-solid-state Z-scheme Between  $\text{Ag}_2\text{O}$  and  $\text{TiO}_2$  using Reduced Graphene Oxide as the Electron Mediator. *Catal. Sci. Technol.* **2017**, 7, 4193–4205.
18. H.T. Ren, Q. Yang. Fabrication of  $\text{Ag}_2\text{O}/\text{TiO}_2$  with Enhanced Photocatalytic Performances for Dye Pollutants Degradation by a pH-induced Method. *Appl. Surf. Sci.* **2017**, 396, 530–538.
19. B. Liu, L. Mu, B. Han, J. Zhang, H. Shi. Fabrication of  $\text{TiO}_2/\text{Ag}_2\text{O}$  Heterostructure with Enhanced Photocatalytic and Antibacterial Activities under Visible Light Irradiation. *Appl. Surf. Sci.* **2017**, 396, 1596–1603.
20. X. Hu, C. Hu, R. Wang. Enhanced Solar Photodegradation of Toxic Pollutants by Long-lived Electrons in  $\text{Ag}-\text{Ag}_2\text{O}$  Nanocomposites. *Appl. Catal. B: Environ.* **2015**, 176, 637–645.
21. H.-T. Ren, S.-Y. Jia, J.-J. Zou, S.-H. Wu, X. Han. A Facile Preparation of  $\text{Ag}_2\text{O}/\text{P25}$  Photocatalyst for Selective Reduction of Nitrate. *Appl. Catal. B: Environ.* **2015**, 176–177, 53–61.
22. J.S. Hammond, S.W. Gaarenstroom, N. Winograd. X-ray Photoelectron Spectroscopic Studies of Cadmium and Silver-oxygen Surfaces. *Anal. Chem.* **1975**, 47, 2193–2199.
23. B.A. Zacheo, R.M. Crooks. Stabilization of Alkaline Phosphatase with  $\text{Au}@\text{Ag}_2\text{O}$  Nanoparticles. *Langmuir* **2011**, 27, 11591–11596.
24. G. Schön. ESCA Studies of  $\text{Ag}$ ,  $\text{Ag}_2\text{O}$  and  $\text{AgO}$ . *Act. Chem. Scand.* **1973**, 27(7).
25. Y. Xu, M. Schoonen. The Absolute Energy Positions of Conduction and Valence Bands of Selected Semiconducting Minerals. *Am. Mineral.* **2000**, 85, 543.
26. L.H. Tjeng, M.B.J. Meinders, J. van Elp, J. Ghijsen, G.A. Sawatzky, R.L. Johnson. Electronic Structure of  $\text{Ag}_2\text{O}$ . *Phys. Rev. B* **1990**, 41, 3190–3199.
27. J.J. Reinoso, P. Leret, C.M. Álvarez-Docio, A. Del Campo, J.F. Fernández. Enhancement of UV Absorption Behavior in  $\text{ZnO}-\text{TiO}_2$  Composites. *Bol. Soc. Esp. Ceram. Vidr.* **2016**, 55, 55–62.

28. Z. Jiang, S. Huang, B. Quian. Semiconductor Properties of Ag<sub>2</sub>O Film Formed on the Silver Electrode in 1 M NaOH Solution. *Electrochim. Acta* **1994**, 39, 2465–2470.
29. A. Vvedenskii, S. Grushevskaya, D. Kudryashov, S. Ganzha. The Influence of the Conditions of the Anodic Formation and the Thickness of Ag(I) Oxide Nanofilm on its Semiconductor Properties. *J. Solid State Electrochem.* **2010**, 14, 1401–1413.
30. P.M. Wood. The Potential Diagram for Oxygen at pH 7. *Biochem. J.* **1988**, 253, 287–289.
31. Alamgir, W. Khan, S. Ahmad, M.M. Hassan, A.H. Naqvi. Structural Phase Analysis, Band Gap Tuning and Fluorescence Properties of Co Doped TiO<sub>2</sub> Nanoparticles. *Opt. Mater.* **2014**, 38, 278–285.
32. A. Siddiqa, D. Masih, D. Anjum, M. Siddiq. Cobalt and Sulfur Co-doped Nano-Size TiO<sub>2</sub> for Photodegradation of Various Dyes and Phenol. *J. Environ. Sci.* **2015**, 37, 100–109.
33. M.A. Barakat, H. Schaeffer, G. Hayes, S. Ismat-Shah. Photocatalytic Degradation of 2-Chlorophenol by Co-doped TiO<sub>2</sub> Nanoparticles. *Appl. Catal. B: Environ.* **2005**, 57, 23–30.
34. J. Choi, H. Park, M. Hoffman. Effects of Single Metal-ion Doping on the Visible-light Photoreactivity of TiO<sub>2</sub>. *J. Phys. Chem. C* **2010**, 114, 2, 783–792.
35. P. Bouras, E. Stathatos, P. Lianos. Pure Versus Metal-ion-doped Nanocrystalline Titania for Photocatalysis. *Appl. Catal. B: Environ.* **2007**, 73, 51–59.
36. K. Karthik, P.S. Kesava, K. Suresh Kumar, N. Victor Jaya. Influence of Dopant Level on Structural, Optical and Magnetic Properties of Co-doped Anatase TiO<sub>2</sub> Nanoparticles. *Appl. Surf. Sci.* **2010**, 256, 4757.
37. L. Samet, J.B. Nasseur, R. Chtourou, K. March, O. Stephan. Heat Treatment Effect on the Physical Properties of Cobalt Doped TiO<sub>2</sub> Sol-gel Materials. *Mater. Charact.* **2013**, 85, 1–12.
38. C. Huang, X. Liu, Y. Liu, Y. Wang. Room Temperature Ferromagnetism of Co-doped TiO<sub>2</sub> Nanotube Arrays Prepared by Sol-gel Template Synthesis. *Chem. Phys. Lett.* **2006**, 432, 468–472.

39. B. Choudhury, A. Choudhury. Luminescence Characteristics of Cobalt Doped TiO<sub>2</sub> Nanoparticles. *J. Lumin.* **2012**, 132, 178–184.
40. C. Khurana, O.P. Pandey, B. Chudasama. Synthesis of Visible Light-responsive Cobalt-doped TiO<sub>2</sub> Nanoparticles with Tunable Optical Band Gap. *J. Sol.-Gel Sci. Technol.* **2015**, 75, 424–435.
41. A. Hamadian, A. Reisi-Vanani, A. Majedi. Sol-gel Preparation and Characterization of Co/TiO<sub>2</sub> Nanoparticles: Application to the Degradation of Methyl Orange. *J. Iran. Chem. Soc.* **2010**, 7, 52–58.
42. A.L. Castro, M.R. Nunes, M.D. Carvalho, L.P. Ferreira, J.-C. Jumes, F.M. Costa, M.H. Florencio. Doped Titanium Dioxide Nanocrystalline Powders with High Photocatalytic Activity. *J. Solid State Chem.* **2009**, 182, 1838–1845.
43. H. Zhang, T. Ji, Y. Liu, J. Cai. Preparation and Characterization of Room Temperature Ferromagnetic Co-doped Anatase TiO<sub>2</sub> Nanobelts. *J. Phys. Chem. C* **2008**, 112, 8604–8608.
44. A.Y. Yermakov, G.S. Zakharova, M.A. Uimin, M.V. Kuznetsov, L.S. Molochnikov, S.F. Konev, A.S. Konev, A.S. Minin, V.V. Mesilov, V.R. Galakhov. Surface Magnetism of Cobalt-doped Anatase TiO<sub>2</sub> Nanopowders. *J. Phys. Chem. C* **2016**, 120, 28857–28866.
45. V.V. Mesilov, V.R. Galakhov, A.F. Gubkin, E.A. Sherstobitova, G.S. Zakharova, M.A. Uimin, A.Y.e. Yermakov, K.O. Kvashnina, D.A. Smirnov. X-ray Diffraction and X-ray Spectroscopy Studies of Cobalt-doped Anatase TiO<sub>2</sub> : Co Nanopowders. *J. Phys. Chem. C* **2017**, 121, 24235–24244.
46. R.J. Tayade, R.G. Kulkarni, R.V. Jasra. Transition metal Ion Impregnated Mesoporous TiO<sub>2</sub> for Photocatalytic Degradation of Organic Contaminants in Water. *Ind. Eng. Chem. Res.* **2006**, 45, 5231–5238.
47. A. Di Paola, E. García-López, S. Ikeda, G. Marci, B. Ohtani, L. Palmisano. Photocatalytic Degradation of Organic Compounds in Aqueous Systems by Transition Metal Doped Polycrystalline TiO<sub>2</sub>. *Catal. Today* **2002**, 75, 87–93.

48. Ö. Kerkez-Kuyumcu, E. Kibar, K. Dayıoglu, F. Gedik, A.N. Akın, S. Özkara-Aydınoglu. A Comparative Study for Removal of Different Dyes over M/TiO<sub>2</sub> (M = Cu, Ni, Co, Fe, Mn, and Cr) Photocatalysts under Visible Light Irradiation. *J. Photochem. Photobiol. A: Chem.* **2015**, 311, 176–185.
49. P. Jiang, W. Xiang, J. Kuang, W. Liu, W. Cao. Effect of Cobalt Doping on the Electronic, Optical and Photocatalytic Properties of TiO<sub>2</sub>. *Solid State Sci.* **2015**, 46, 27–32.
50. T.T. Le, M.S. Akhtar, D.M. Park, J.C. Lee, O.B. Yang. Water Splitting on Rhodamine-B Dye-sensitized Co-doped TiO<sub>2</sub> Catalyst under Visible Light. *Appl. Catal. B: Environ.* **2012**, 111–112, 397–401.
51. C.-T. Hsieh, W.-S. Fan, W.-Y. Chen, J.-Y. Lin. Adsorption and Visible-light-derived Photocatalytic Kinetics of Organic Dye on Co-doped Titania Nanotubes Prepared by Hydrothermal Synthesis. *Sep. Purif. Technol.* **2009**, 67, 312–318.
52. C. M. Whang, J. G. Kim, E. Y. Kim, Y. H. Kim, W. I. Lee. Effect of Co, Ga, and Nd Additions on the Photocatalytic Properties of TiO<sub>2</sub> Nanopowders. *Sov. J. Glass Phys. Chem.* **2005**, 31(3), 390–395.
53. M. Nag, P. Basak. S.V. Manorama. Low-temperature Hydrothermal Synthesis of Phase-pure Rutile Titania Nanocrystals: Time Temperature Tuning of Morphology and Photocatalytic Activity. *Mater. Res. Bull.* **2007**, 42, 1691–1704.
54. C. Zhao, X. Shu, D. Zhu, S. Wei, Y. Wang, M. Tu, W. Gao. High Visible Light Photocatalytic Property of Co<sup>2+</sup>-doped TiO<sub>2</sub> Nanoparticles with Mixed Phases. *Superlattices Microstruct.* **2015**, 88, 32–42.
55. A. Martinelli, S. Alberti, V. Caratto, P. Lova, F. Locardi, G. Pampararo, S. Villa, M. Ferretti. Structural Studies on Copper and Nitrogen-doped Nanosized Anatase. *Z. Kristallogr.* **2018**, 233, 867–876.
56. M. Qiu, Y. Tian, Z. Chen, Z. Yang, W. Li, K. Wang, L. Wang, K. Wang, W. Zhang. Synthesis of Ti<sup>3+</sup> Self-doped TiO<sub>2</sub> Nanocrystals Based on Le Chatelier's Principle and their Application in solar light photocatalysis. *RSC Adv.* **2016**, 6, 74376–74383.

57. N. Dubey, K. Labhsetwar, S. Devotta, S. Rayalu. Hydrogen Evolution by Water Splitting using Novel Composite Zeolite-based Photocatalyst. *Catal. Today* **2007**, 129, 428–434.
58. Y. Lu, Y. Lin, D. Wang, L. Wang, T. Xie, T. Jiang. A High Performance Cobalt-doped ZnO Visible Light Photocatalyst and its Photogenerated Charge Transfer Properties. *Nano Res.* **2011**, 4, 1144–1152.
59. C.-H.L. Feng-Chieh Wang, Chih-Wei Liu, Jiunn-Hsing Chao, C.-H. Lin. Effect of Pt Loading Order on Photocatalytic Activity of Pt-TiO<sub>2</sub> Nanofiber in Generation of H<sub>2</sub> from Net Ethanol. *J. Phys. Chem. C* **2009**, 113, 13832–13840.
60. GR. Bamwenda, S. Tsubota, T. Nakamura, M. Haruta. Photoassisted Hydrogen Production from a Water Ethanol Solution: A Comparison of Activities of Au-TiO<sub>2</sub> and Pt-TiO<sub>2</sub>. *J. Photochem. Photobiol. A: Chem.* **1995**, 89, 177–189.
61. D. Eastman. Photoelectric Work Functions of Transition, Rare-earth, and Noble Metals. *Phys. Rev. B* **1970**, 2, 1.
62. L.M. Ahmed, I. Ivanova, F.H. Hussein, D.W. Bahnemann. Role of Platinum Deposited on TiO<sub>2</sub> in Photocatalytic Methanol Oxidation and Dehydrogenation Reactions. *Int. J. Photoenergy* **2014**, 503516.
63. Y. Chen, Y. Wang, W. Li, Q. Yang, Q. Hou, L. Wei, L. Liu, F. Huang, M. Ju. Enhancement of Photocatalytic Performance with the Use of Noble-metal-Decorated TiO<sub>2</sub> Nanocrystals as Highly Active Catalysts for Aerobic Oxidation under Visible-light Irradiation. *Appl. Catal. B: Environ.* **2017**, 210, 352–367
64. F-C. Wang, C-H. Liu, C-W. Liu, J-H. Chao, C-H. Lin. Effect of Pt Loading Order on Photocatalytic Activity of Pt/TiO<sub>2</sub> Nanofiber in Generation of H<sub>2</sub> from Neat Ethanol. *J. Phys. Chem. C* **2009**, 113, 13832–13840.
65. L. Yu, Y. Shao, D. Li. Direct Combination of Hydrogen Evolution from Water and Methane Conversion in a Photocatalytic System over Pt/TiO<sub>2</sub>. *Appl. Catal. B: Environ.* **2017**, 204, 216–223.

66. C. Lia, Y. Yamauchi. Facile Solution Synthesis of Ag @ Pt Core-shell Nanoparticles with Dendritic Pt shells. *Phys. Chem. Chem. Phys.* **2013**, 15, 3490–3496
67. ISO 10678:2010 - Fine Ceramics (Advanced Ceramics, Advanced Technical Ceramics)- Determination of Photocatalytic Activity of Surfaces in an Aqueous Medium by Degradation of Methylene Blue; Geneva, **2010**.
68. J. Tschirch, R. Dillert, D. Bahnemann. Photocatalytic Degradation of Methylene Blue on Fixed Powder Layers: Which Limitations are to be Considered? *J. Adv. Oxid. Technol.* **2008**, 11, 193–198.
69. S. Lakshmi, R. Renganathan, S. Fujita. Study on TiO<sub>2</sub>-mediated Photocatalytic Degradation of Methylene Blue. *J. Photochem. Photobiol. A: Chem.* **1995**, 88, 163–167.
70. M.K. Nowotny, D.W. Bahnemann. Improved Photocatalytic Performance of Rutile TiO<sub>2</sub>. *Phys. status solidi.* **2011**, 5, 92–94.
71. B.O. Burek, A. Sutor, D.W. Bahnemann, J.Z. Bloh. Completely Integrated Wirelessly-powered Photocatalyst-coated Spheres as A Novel Means to Perform Heterogeneous Photocatalytic Reactions. *Catal. Sci. Technol.* **2017**, 7, 4977–4983.
72. F. Chen, Z. Liu, Y. Liu, P. Fang, Y. Dai. Enhanced Adsorption and Photocatalytic Degradation of High-concentration Methylene Blue on Ag<sub>2</sub>O-modified TiO<sub>2</sub>-based Nanosheet. *Chem. Eng. J.* **2013**, 221, 283–291.
73. R. Kumar, R. M. El-Shishtawy, M. A. Barakat. Synthesis and Characterization of Ag - Ag<sub>2</sub>O / TiO<sub>2</sub> @polypyrrole Heterojunction for Enhanced Photocatalytic Degradation of Methylene Blue. *Catalysts* **2016**, 6, 76.
74. A. Mills. An overview of the methylene blue ISO test for assessing the activities of photocatalytic films. *Appl. Catal. B: Environ.* **2012**, 128, 144–149.
75. A. Mills, J. Wang. Photobleaching of Methylene Blue Sensitised by TiO<sub>2</sub>: An Ambiguous System? *J. Photochem. Photobiol. A: Chem.* **1999**, 127, 123–134.
76. J.M. Bauldrey, M.D. Archer. Dye-modified electrodes for photogalvanic cells. *Electrochim. Acta* **1983**, 28, 1515–1522.

77. A.A. Karyakin, A.K. Strakhova, E.E. Karyakina, S.D. Varfolomeyev, A.K. Yatsimirsky. The electrochemical polymerization of methylene blue and bioelectrochemical activity of the resulting film. *Bioelectrochemistry Bioenerg.* **1993**, 32, 35–43.
78. X. Yan, T. Ohno, K. Nishijima, R. Abe, B. Ohtani. Is methylene Blue an Appropriate Substrate for a Photocatalytic Activity Test? A Study with Visible-light Responsive Titania. *Chem. Phys. Lett.* **2006**, 429, 606–610.
79. T. Takizawa, T. Watanabe, K. Honda. Photocatalysis Through Excitation of Adsorbates. 2. A Comparative Study of Rhodamine B and Methylene Blue on Cadmium Sulfide. *J. Phys. Chem.* **1978**, 82, 1391–1396.
80. M.P. Villavicencio, A.E. Morales, M.L.R. Peralta, M. Sanchez-Cantu, L.R. Blanco, E.C. Anota, J.H.C. García, F. Tzompantzi. Ibuprofen Photodegradation by Ag<sub>2</sub>O and Ag/Ag<sub>2</sub>O Composites under Simulated Visible Light Irradiation. *Catal. Lett.* **2020**, 150, 2385–2399.
81. G. Wang, X. Ma, B. Huang, H. Cheng, Z. Wang, J. Zhan, X. Qin, X. Zhang, Y. Dai. Controlled Synthesis of Ag<sub>2</sub>O Microcrystals with Facet-dependent Photocatalytic Activities. *J. Mater. Chem.* **2012**, 22, 21189.
82. H. Yang, J. Tian, T. Li, H. Cui. Synthesis of Novel Ag/Ag<sub>2</sub>O Heterostructures with Solar Full Spectrum (UV, Visible and Near-infrared) Light-driven Photocatalytic Activity and Enhanced Photoelectrochemical Performance. *Catal. Commun.* **2016**, 87, 82–85.
83. M.O. Ansari, M.M. Khan, S.A. Ansari, K. Raju, J. Lee, M.H. Cho. Enhanced Thermal Stability under DC Electrical Conductivity Retention and Visible Light Activity of Ag / TiO<sub>2</sub> @Polyaniline Nanocomposite Film. *ACS Appl. Mater. Interfaces* **2014**, 6, 8124–8133.
84. A. Henglein. The Reactivity of Silver Atoms in Aqueous Solutions (A  $\gamma$ -Radiolysis Study) *Ber. Bunsenges. Phys. Chem.* **1977**, 81, 556–561.



85. T. Linnert, P. Mulvaney, A. Henglein, H. Weller. Long-Lived Nonmetallic Silver Clusters in Aqueous Solution: Preparation and Photolysis. *J. Am. Chem. Soc.* **1990**, 112, 4657–4664.
86. D. Friedmann, H. Hansing, D. W. Bahnemann. Primary Processes During the Photodeposition of Ag Clusters on TiO<sub>2</sub> Nanoparticles. *Z. Phys. Chem.* **2007**, 221, 329–348.
87. J.C. Durán-Álvarez, V.A. Hernández-Morales, M. Rodríguez-Varela, D. Guerrero-Araque, D. Ramirez-Ortega, F. Castellón, P. Acevedo-Peña, R. Zanella. Ag<sub>2</sub>O/TiO<sub>2</sub> Nanostructures for the Photocatalytic Mineralization of the Highly Recalcitrant Pollutant Iopromide in Pure and Tap Water. *Catal. Today* **2020**, 341, 71–81.
88. K.K. Mandari, B.S. Kwak, A.K.R. Police, M. Kang. In-situ Photo-reduction of Silver Particles and their SPR Effect in Enhancing the Photocatalytic Water Splitting of Ag<sub>2</sub>O/TiO<sub>2</sub> Photocatalysts under Solar Light Irradiation: A Case Study. *Mater. Res. Bull.* **2017**, 95, 515–524.
89. R. Liu, P. Wang, X. Wang, H. Yu, J. Yu. UV- and Visible-light Photocatalytic Activity of Simultaneously Deposited and Doped Ag/Ag(I)- TiO<sub>2</sub> Photocatalyst. *J. Phys. Chem. C* **2012**, 116, 17721–17728.
90. H. Xu, J. Xie, W. Jia, G. Yu, Y. Cao. The Formation of Visible light-driven Ag/Ag<sub>2</sub>O Photocatalyst with Excellent Property of Photocatalytic Activity and Photocorrosion Inhibition. *J. Colloid Interface Sci.* **2018**, 516, 511-521.
91. Y. Cui, Q. Ma, X. Deng, Q. Meng, X. Cheng, M. Xie, X. Li, Q. Cheng, H. Liu. Fabrication of Ag - Ag<sub>2</sub>O /reduced TiO<sub>2</sub> Nanophotocatalyst and its Enhanced Visible Light Driven Photocatalytic Performance for Degradation of Diclofenac Solution. *Appl. Catal. B: Environ.* **2017**, 206, 136–145.
92. O. Kerkez, İ. Boz. Photodegradation of Methylene Blue with Ag<sub>2</sub>O/TiO<sub>2</sub> under Visible Light: Operational Parameters. *Chem. Eng. Commun.* **2015**, 202, 534–541.

93. P. Chen. A Novel Synthesis of  $\text{Ti}^{3+}$  Self-doped  $\text{Ag}_2\text{O} / \text{TiO}_2$  (p-n) Nanoheterojunctions for Enhanced Visible Photocatalytic Activity. *Mater. Lett.* **2016**, 163, 130–133.
94. N. Wie, H. Cui, Q. Song, L. Zhang, X. Song, K. Wang, Y. Zhang, J. Li, J. Wen, J. Tian.  $\text{Ag}_2\text{O}$  Nanoparticle/ $\text{TiO}_2$  Nanobelt Heterostructures with Remarkable Photo-response and Photocatalytic Properties under UV, Visible and Near-infrared Irradiation. *Appl. Catal. B: Environ.* **2016**, 198, 83–90.
95. J. Gou, Q. Ma, X. Deng, Y. Cui, H. Zhang, X. Cheng, X. Li, M. Xie, Q. Cheng. Fabrication of  $\text{Ag}_2\text{O}/\text{TiO}_2$ -Zeolite Composite and its Enhanced Solar Light Photocatalytic Performance and Mechanism for Degradation of Norfloxacin. *Chem. Eng. J.* **2017**, 308, 818–826.
96. C. Liu, C. Cao, X. Luo, S. Luo. Ag-bridged  $\text{Ag}_2\text{O}$  Nanowire Network/ $\text{TiO}_2$  Nanotube Array p-n Heterojunction as a Highly Efficient and Stable Visible Light Photocatalyst. *J. Hazard. Mater.* **2015**, 285, 319–324.
97. M.M. Huber, S. Canonica, G. Park, U. Gunten. Oxidation of Pharmaceuticals during Ozonation and Advanced Oxidation Processes. *Environ. Sci. Technol.* **2003**, 37, 1016–1024.
98. C. Reyes, J. Fernandez, J. Freer, M.A. Mondaca, C. Zaror, S. Malato, H.D. Mansilla. Degradation and Inactivation of Tetracycline by  $\text{TiO}_2$  Photocatalysis. *J. Photochem. Photobiol. A: Chem.* **2006**, 184, 141–146.
99. R.A. Palominos, M.A. Mondaca, A. Giraldo, G. Penuela, M. Pérez-Moya, H.D. Mansilla. Photocatalytic Oxidation of the Antibiotic Tetracycline on  $\text{TiO}_2$  and  $\text{ZnO}$  Suspensions. *Catal. Today* **2009**, 144, 100–105.
100. J.H.O.S. Pereira, A.C. Reis, D. Queirós, O.C. Nunes, M.T. Borges, V.J.P. Vilar, R.A.R. Boaventura. Insights into Solar  $\text{TiO}_2$ -assisted Photocatalytic Oxidation of Two Antibiotics Employed in Aquatic Animal Production, Oxolinic Acid and Oxytetracycline. *Sci. Total Environ.* **2013**, 463–464, 274–283.

- 101.L. Rimoldi, D. Meroni, G. Cappelletti, S. Ardizzone. Green and Low Cost Tetracycline Degradation Processes by Nanometric and Immobilized TiO<sub>2</sub> Systems. *Catal. Today* **2017**, 281, 38–44.
- 102.S. Yahiat, F. Fourcade, S. Brosillon, A. Amrane. Removal of Antibiotics by An Integrated Process Coupling Photocatalysis and Biological Treatment-case of Tetracycline and Tylosin. *Int. Biodeterior. Biodegrad.* **2011**, 65, 997–1003.
- 103.X.-D. Zhu, Y.-J. Wang, R.-J. Sun, D.-M. Zhou. Photocatalytic Degradation of Tetracycline in Aqueous Solution by Nanosized TiO<sub>2</sub>. *Chemosphere* **2013**, 92, 925–932.
- 104.Q. Chen, S. Wu, Y. Xin. Synthesis of Au–CuS–TiO<sub>2</sub> Nanobelts Photocatalyst for Efficient Photocatalytic Degradation of Antibiotic Oxytetracycline. *Chem. Eng. J.* **2016**, 302, 377–387.
- 105.R. Li, Y. Jia, J. Wu, Q. Zhen. Photocatalytic Degradation and Pathway of Oxytetracycline in Aqueous Solution by Fe<sub>2</sub>O<sub>3</sub>–TiO<sub>2</sub> Nanopowder. *RSC Adv.* **2015**, 5, 40764–40771.
- 106.M. Iwasaki, M. Hara, H. Kawada, H. Taday, S. Ito. Cobalt Ion-doped TiO<sub>2</sub> Photocatalyst Response to Visible Light. *J. Colloid Interface Sci.* **2000**, 224, 202–204.
- 107.P. Kulshrestha, R.F. Giese, D.S. Aga. Investigating the Molecular Interactions of Oxytetracycline in Clay and Organic Matter: Insights on Factors Affecting its Mobility in Soil. *Environ. Sci. Technol.* **2004**, 38, 4097–4105.
- 108.C. Zhao, M. Pelaez, X. Duan, H. Deng, K. O'Shead, D. Fatta-Kassinose, D.D. Dionysiou. Role of pH on Photolytic and Photocatalytic Degradation of Antibiotic Oxytetracycline in Aqueous Solution under Visible/solar Light: Kinetics and Mechanism Studies. *Appl. Catal. B: Environ.* **2013**, 134–135, 83–92.
- 109.I. Kim, N. Yamashita, H. Tanaka. Performance of UV and UV/H<sub>2</sub>O<sub>2</sub> Processes for the Removal of Pharmaceuticals Detected in Secondary Effluent of a Sewage Treatment Plant in Japan. *J. Hazard. Mater.* **2009**, 166, 1134–1140.

- 110.S. Jiao, S. Zheng, D. Yin, L. Wang, L. Chen. Aqueous Oxytetracycline Degradation and the Toxicity Change of Degradation Compounds in Photoirradiation Process. *J. Environ. Sci.* **2008**, 20, 806–813.
- 111.Y. Chen, C. Hu, J. Qu, M. Yang. Photodegradation of Tetracycline and Formation of Reactive Oxygen Species in Aqueous Tetracycline Solution under Simulated Sunlight Irradiation. *J. Photochem. Photobiol. A: Chem.* **2008**, 197, 81–87.
- 112.Y. Seto, M. Ochi, S. Onoue, S. Yamada. High-throughput Screening Strategy for Photogenotoxic Potential of Pharmaceutical Substances using Fluorescent Intercalating Dye. *J. Pharmaceut. Biomed.* **2010**, 52, 781–786.
- 113.Z. Yang, W. Zhong, Y. Chen, Ch. Wang, S. Mo, J. Zhang, R. Shu, Q. Song. Improving Glycerol Photoreforming Hydrogen Production Over  $\text{Ag}_2\text{O}$ - $\text{TiO}_2$  Catalysts by Enhanced Colloidal Dispersion Stability. *Front. Chem.* **2020**, 8, 342.
- 114.K. Lalitha, J.K. Reddy, M.V. Phanikrishna Sharma, V.D. Kumari, M. Subrahmanyam. Continuous Hydrogen Production Activity Over Finely Dispersed  $\text{Ag}_2\text{O}/\text{TiO}_2$  Catalysts from Methanol: Water Mixtures under Solar Irradiation: A Structure-Activity Correlation. *Int. J. Hydrog. Energy* **2010**, 35, 3991–4001.
- 115.MS. Park, M. Kang. The Preparation of the Anatase and Rutile Forms of  $\text{Ag}-\text{TiO}_2$  and Hydrogen Production from Methanol/Water Decomposition. *Mater Lett.* **2008**, 62, 183.
- 116.J-W. Park, M. Kang. Synthesis and Characterization of  $\text{Ag}_x\text{O}$ , and Hydrogen Production from Methanol Photodecomposition over the Mixture of  $\text{Ag}_x\text{O}$  and  $\text{TiO}_2$ . *Int. J. Hydrog. Energy* **2007**, 32, 4840–4846.
- 117.M. Endo-Kimura, M. Janczarek, Z. Bielan, D. Zhang, K. Wang, A. Markowska-Szczupak, E. Kowalska. Photocatalytic and Antimicrobial Properties of  $\text{Ag}_2\text{O}/\text{TiO}_2$  Heterojunction. *ChemEngineering* **2019**, 3, 3.
- 118.D.P. Kumar, N.L. Reddy, M. Karthik, B. Neppolian, J. Madhavan, M.V. Shankar, Solar Light Sensitized  $p\text{-Ag}_2\text{O}/n\text{-TiO}_2$  Nanotubes Heterojunction Photocatalysts

- for Enhanced Hydrogen Production in Aqueous-glycerol Solution. *Sol. Energy Mater. Sol. Cells* **2016**, 154, 78–87.
119. U. Siemon, D. Bahnemann, J.J. Testa, D. Rodríguez, M.I. Litter, N. Bruno. Heterogeneous Photocatalytic Reactions Comparing TiO<sub>2</sub> and Pt / TiO<sub>2</sub>. *J. Photochem. Photobiol. A: Chem.* **2002**, 148, 247–255.
120. G.L. Chiarello, M.H. Aguirre, E. Selli. Hydrogen Production by Photocatalytic Steam Reforming of Methanol on Noble Metal-modified TiO<sub>2</sub>. *J. Catal.* **2010**, 273, 182–190.
121. A. Kaur, D.B. Salunke, A. Umar, S.K. Mehta, A.S.K. Sinha, S.K. Kansal. Visible Light Driven Photocatalytic Degradation of Fluoroquinolone Levofloxacin Drug using Ag<sub>2</sub>O / TiO<sub>2</sub> Quantum Dots: A Mechanistic Study and Degradation Pathway. *New J. Chem.* **2017**, 41, 12079–12090.
122. C. Hao, W. Wang, R. Zhang, B. Zou, H. Shi. Enhanced Photoelectrochemical Water Splitting with TiO<sub>2</sub> @ Ag<sub>2</sub>O Nanowire Arrays via p-n Heterojunction Formation. *Sol. Energy Mater. Sol. Cells* **2018**, 174, 132–139.
123. V. Brezová, A. Staško, L. Jr. Lapčík. Electron Paramagnetic Resonance Study of Photogenerated Radicals in Titanium Dioxide Powder and its Aqueous Suspensions. *J. Photochem. Photobiol. A: Chem.* **1991**, 59, 115–121.
124. L. Fan, J. Long, Q. Gu, H. Huang, H. Lin, X. Wang. Single-site Nickel-grafted Anatase TiO<sub>2</sub> for Hydrogen Production: Toward Understanding the Nature of Visible-light Photocatalysis. *J. Catal.* **2014**, 320, 147–159.
125. J.B. Priebe, M. Karnahl, H. Junge, M. Beller, D. Hollmann, A. Brückner. Angewandte Water Reduction with Visible Light: Synergy between Optical Transitions and Electron Transfer in Au-TiO<sub>2</sub> Catalysts Visualized by In Situ EPR Spectroscopy. *Angew. Chem. Int. Ed.* **2013**, 52, 11420–11424.
126. S. Dohshi, M. Anpo, S. Okuda, T. Kojima. Effect of  $\gamma$ -ray Irradiation on the Wettability of TiO<sub>2</sub> Single Crystals. *Top. Catal.* **2005**, 35(3-4), 327–330.

127. T. Berger, M. Sterrer, O. Diwald, E. Knözinger, D. Panayotov, T.L. Thompson, J.T. Yates. Light-induced Charge Separation in Anatase TiO<sub>2</sub> Particles. *J. Phys. Chem. B* **2005**, 109(13), 6061–6068.
128. Y. Nakaoka, Y. Nosaka. ESR Investigation Into the Effects of Heat Treatment and Crystal Structure on Radicals Produced Over Irradiated TiO<sub>2</sub> Powder. *J. Photochem. Photobiol. A: Chem.* **1997**, 110, 3, 299–305.
129. S. Roy, A.G. Joshi, S. Chatterjee, A.K. Ghosh. Local Symmetry Breaking in SnO<sub>2</sub> Nanocrystals with Cobalt Doping and its Effect on Optical Properties. *Nanoscale* **2018**, 10, 10664–10682.
130. G. Sadanandam, K. Lalitha, V.D. Kumari, V.S. Muthukonda, M. Subrahmanyam. Cobalt doped TiO<sub>2</sub>: A stable and Efficient Photocatalyst for Continuous Hydrogen Production from Glycerol: Water Mixtures under Solar Light Irradiation. *Int. J. Hydrog. Energy* **2013**, 38(23), 9655–9664.
131. S. Hamid, R. Dillert, D.W. Bahnemann. Photocatalytic Reforming of Aqueous Acetic Acid into Molecular Hydrogen and Hydrocarbons over Co Catalyst-loaded TiO<sub>2</sub>: Shifting the Product Distribution. *J. Phys. Chem. C* **2018**, 122, 12792–12809.
132. W. Choi, A. Termin, M. R. Hoffmann. Effects of Metal Ion Dopants on the Photocatalytic Reactivity of Quantum Sized TiO<sub>2</sub> Particles. *Angew. Chem. Int. Ed.* **1994**, 33(10), 1091–1092.
133. D.W. Hwang, H.G. Kim, J.S. Lee, J. Kim, W. Li, S.H. Oh. Photocatalytic Hydrogen Production from Water over M-doped La<sub>2</sub>Ti<sub>2</sub>O<sub>7</sub> (M = Cr, Fe) under Visible Light Irradiation ( $\lambda > 420$  nm). *J. Phys. Chem. B* **2005**, 109(6), 2093–2102.
134. Y. Wu, G. Lu, S.J. Li. The Long-term Photocatalytic Stability of Co<sup>2+</sup>-modified P25 -TiO<sub>2</sub> Powders for the H<sub>2</sub> Production from Aqueous Ethanol Solution. *Photochem. Photobiol. A: Chem.* **2006**, 181(2-3), 263–267.
135. J. Zou, C. Liu, K. Yu, D. Cheng, Y. Zhang, F. He, H. Du, L. Cui. Highly Efficient Pt/TiO<sub>2</sub> Photocatalyst Prepared by Plasmaenhanced Impregnation Method. *Chem. Phys. Lett.* **2004**, 400(4-6), 520–523.

136. T. Miwa, S. Kaneco, H. Katsumata, T. Suzuki, K. Ohta, S. Chand Verma, K. Sugihara. Photocatalytic Hydrogen Production from Aqueous Methanol Solution with CuO/Al<sub>2</sub>O<sub>3</sub>/TiO<sub>2</sub> Nanocomposite. *Int. J. Hydrog. Energy* **2010**, 35, 6554–6560.

## Publications

### Journal Publication:

S. Akel, R. Dillert, D.W. Bahnemann. Photocatalytic Hydrogen Evolution over Pt/Co-TiO<sub>2</sub> Photocatalysts. *J. Photocatalysis*. **2021**, 2(1), 35–48.

(doi: 10.2174/2665976x01999200718010443).

Own participation: 90%

S. Akel, R. Boughaled, R. Dillert, M. El Azzouzi, D.W. Bahnemann. UV-vis Light Induced Degradation of Oxytetracycline Hydrochloride Mediated by Co-TiO<sub>2</sub> Nanoparticles. *Molecules*. **2020**, 25(2), 249.

(doi: 10.3390/molecules25020249).

Own participation: 90%

S. Akel, R. Dillert, N. Balayeva, R. Boughaled, J. Koch, M. El Azzouzi, D.W. Bahnemann. Ag/Ag<sub>2</sub>O as a Co-Catalyst in TiO<sub>2</sub> Photocatalysis: Effect of the Co-Catalyst/Photocatalyst Mass Ratio. *Catalysts*. **2018**, 8(12), 647.

(doi: 10.3390/catal8120647).

Own participation: 80%

S. Bougarrani, L. El Azzouzi, S. Akel, L. Latrach, A. Bouziani, M. El Azzouzi. Factors Influencing Imazapyr Herbicide Removal from Wastewater Using Photocatalytic Ozonation, *Acta Chim. Slov.* **2018**, 65 (2), 470–474.

(doi: 10.17344/acsi.2018.4297).

Own participation: 20%

S. Bougarrani, L. El Azzouzi, A. Bouziani, S. Akel, L. Latrach, Z. Baicha, M. El Azzouzi. The Influence of Humic Acids Extracted from Chaouia Soil on the Behavior of Transition Metal Ions and Pesticides. *Mor. J. Chem.* 5 N°3, **2017**, 446–452.

(doi: 10.48317/imist.prsm/morjchem-v5i3.8560).

Own participation: 10%



## Oral Presentations

S. Akel. Photocatalytic Degradation of Oxytetracycline Chloride and Simultaneous Hydrogen Evolution by Co-TiO<sub>2</sub> and Pt@Co-TiO<sub>2</sub>. 6th Russian - German Workshop, 26–29 November, 2018. Hannover, Germany.

S. Akel, R. Dillert, D.W. Bahnemann. TiO<sub>2</sub>/Ag<sub>2</sub>O Photocatalysts for H<sub>2</sub> Generation and Methylene Blue Degradation. 5th Russian - German Workshop, 16–20 October, 2017. National University of Saint Petersburg, Russia.

## Poster Presentations

S. Akel, R. Boughaled, D.W. Bahnemann. Photocatalytic Degradation of Oxytetracycline Hydrochloride over Co-TiO<sub>2</sub> Photocatalysts under Simulated Solar Light. 6th International Conference on Semiconductor Photochemistry (SP6), Carl von Ossietzky University, 11–14 September, 2017. Oldenburg, Germany.

S. Akel, R. Boughaled, D.W. Bahnemann. Cobalt- TiO<sub>2</sub> Photocatalysts for Photocatalytic Degradation of Antibiotic Oxytetracycline Hydrochloride in Aqueous Solution: Kinetics and Mechanism Studies. NanoDay, Laboratorium für Nano- und Quantenengineering (LNQE), Leibniz University Hannover, 28 September, 2017. Hannover, Germany.

# Curriculum Vitae

## Personal Data

**Name** Boughaled El Lakhmissi, geb. Akel, Soukaina  
**Date of Birth** 06.11.1990  
**Place of Birth** Rabat, Morocco

## Education

Since 06.2016 **Ph.D. Student** at Institute of Technical Chemistry, Leibniz University of Hannover, Germany  
Ph.D. Thesis: "Combining Photocatalysis Water Treatment and Fuel Synthesis: Improving the Activity of TiO<sub>2</sub> by Cobalt - Doping and Ag/Ag<sub>2</sub>O- Deposition"

09.2012 – 07.2014 **Master of Science in Chemistry**, specialized in Analytical Sciences and Environment (achieved with distinction), Department of Chemistry, Faculty of Sciences, Mohammed V University Rabat, Morocco

09.2009 – 07.2012 **Bachelor of Science** in Analytical Sciences, Quality, and Environment (achieved with distinction), Department of Chemistry, Faculty of Sciences, Mohammed V University Rabat, Morocco

09.1997 – 07.2009 **Diploma and Pre-University** in Physical Sciences (achieved with distinction) at Hassan II High School, Rabat, Morocco

## Work Experience/ Internship

11.2015 The Use of Photolysis and Photocatalysis Technology to remove Veterinary Drugs from Water  
*Scientific and Technological Research Council of Turkey (TUBITAK), İnönü University, Malatya, Turkey*

02.2014 – 06.2014 Retrospective and Prospective Study of Cholinesterase Activity by Test-Mate in Emergency Toxicology  
*Centre Anti Poison et de Pharmacovigilance du Maroc (CAPM), Rabat, Morocco*

09.2014 – 12.2014 Wastewater treatment plants  
*Conseil, Ingenierie et Developpement (CID), Rabat, Morocco*

08.2011 – 09.2011 Treatment of Surface Water  
*Office National de l'Eau Potable (ONEP), Rabat, Morocco*